

Dissertation zur Erlangung des Doktorgrades
der Fakultät für Chemie und Pharmazie
der Ludwig-Maximilians-Universität München

**Mechanistic investigations
on various carbon-nucleophiles**

Artem Leonov

aus

Moskau, Russland

2018

Erklärung

Diese Dissertation wurde im Sinne von § 7 der Promotionsordnung vom 28. November 2011 von Herrn PD Dr. Armin R. Ofial betreut.

Eidesstattliche Versicherung

Diese Dissertation wurde eigenständig und ohne unerlaubte Hilfe erarbeitet.

München, 15.06.2018

.....

(Artem Leonov)

Dissertation eingereicht am	15.06.2018
1. Gutachter	PD Dr. Armin R. Ofial
2. Gutachter	Professor Dr. Paul Knochel
Mündliche Prüfung am	17.07.2018

For Daria

Acknowledgement

First, I would like to sincerely thank my supervisor, Dr. Armin R. Ofial for offering me an opportunity to work in his group and enjoy exploring chemistry. I am very grateful for his guidance, critical comments and useful suggestions at all stages of my PhD studies. I greatly appreciate Professor Dr. Herbert Mayr for his constant support, motivational and valuable discussions.

Furthermore, I would like to thank Professor Dr. Paul Knochel for reviewing my thesis and also the board of examiners for their participation in my defense examination.

I am also thankful to my past and present group mates, Dr. Alexander Wagner, Elija Wiedemann, Dr. Ángel Puente, Dr. Francisco Corral, Dr. Johannes Ammer, Katharina Böck, Dr. Quan Chen, Prof. Dr. Shinjiro Kobayashi, Zhen Li, Robert Mayer, Patrick Jüstel, Le Li. Special thanks to Dr. Guillaume Berionni, Elsa Follet, Ieva Teikmane and Feng An for all the time spent together in the lab and beyond. It has been a great pleasure to work with you.

Many thanks to Frau Hildegard Lipfert for her kind help and making my stay in Munich a lot easier. I thank Nathalie Hampel for solving all organizational problems in the lab and especially for synthesizing reference electrophiles, and Brigitte Janker for ordering chemicals.

Огромное спасибо завсегдаааа русскому ланча, Оле, Глебу, Наташе, Ире и Игорю за весёлые встречи, интересные беседы и поддержку. Отдельная благодарность Вале и Илье за позитивное настроение, помощь и отзывчивость. Большое спасибо моим друзьям в Москве, Вале, Роме, Саше, Ксюше, Джанине и Игорю, а также Мише и Маше в Праге. Особенная благодарность Паше и Ксюше за их доброту и гостеприимство.

Отдельное спасибо Максиму и Лёше за подготовку в химии.

Больше всего я хочу выразить благодарность своим родителям за их бесконечную поддержку и любовь, и моей любимой Даше за терпение, веру в меня, и за то, что была рядом.

Publications

Fine-Tuning the Nucleophilic Reactivities of Boron Ate Complexes Derived from Aryl and Heteroaryl Boronic Esters

G. Berionni, A. I. Leonov, P. Mayer, A. R. Ofial, H. Mayr, *Angew. Chem.* **2015**, 127, 2820-2824; *Angew. Chem. Int. Ed.* **2015**, 54, 2780-2783.

Contributions to Conferences

Electrophilicities and Nucleophilicities of Grignard Reagents

A. I. Leonov, S. Minegishi, H. Mayr, A. R. Ofial, *GDCh-Wissenschaftsforum Chemie*, Berlin (Germany) 2017

Table of Contents

A. Summary	1
B. Introduction	9
Chapter 1. Fine-Tuning the Nucleophilic Reactivities of Boron Ate Complexes Derived from Aryl and Heteroaryl Boronic Esters	14
Chapter 2. Transition Metal-Free C-H Activation of Tertiary Amines: Diisopropyl Azodicarboxylate Mediated α -Functionalization	66
Chapter 3. Reactivity Studies of Alkynyl-Stabilized Carbanions	90
Chapter 4. Lewis Acidic and Nucleophilic Properties of Grignard Reagents	124
Chapter 5. Reactivity Comparison of Structurally Related Enamines and Silyl Enol Ethers	168

A. Summary

General

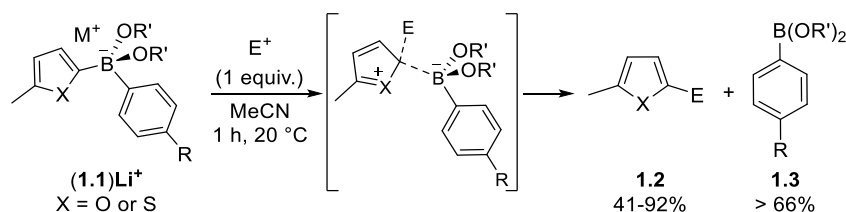
It has been shown previously that second-order rate constants k of polar reactions of nucleophiles with electrophiles at 20 °C follow the linear free energy relationship given in Equation (1), where nucleophilic reactivity is expressed by the solvent-dependent parameters N (nucleophilicity) and s_N (sensitivity) and electrophiles are characterized by the solvent independent parameter E (electrophilicity).

$$\lg k (20\text{ }^{\circ}\text{C}) = s_N(N + E) \quad (1)$$

The purpose of this work was to examine the applicability of this relationship to reactions of benzhydrylium ions with carbon nucleophiles of different nature. This allowed the inclusion of these nucleophiles in the most comprehensive reactivity scale presently available, which currently covers a range of over 30 orders of magnitude. In consequence, it was possible to compare the nucleophilic reactivities found for different carbon nucleophiles with those of previously studied structurally related compounds and to gain insight in the mechanistic aspects of C-C bond forming reactions.

Chapter 1. Fine-Tuning the Nucleophilic Reactivities of Boron Ate Complexes Derived from Aryl and Heteroaryl Boronic Esters

Diaryl boronate complexes (BACs) with a number of structural variations were synthesized, isolated and fully characterized by the NMR spectroscopy and X-ray analysis for selected examples. Product studies indicated exclusive attack of the electrophile at the more electron-rich aromatic ring of the BACs (Scheme A.1).



Scheme A.1. Reactions of BACs with various electrophiles in CH_3CN .

Kinetics and mechanisms of the reactions of the BACs with several diarylcarbenium ions have been investigated by UV-Vis and NMR spectroscopy in CH_3CN at 20 °C. We have found that the nucleophilic reactivity of the furylboronate **1.4** ($N = 2.90$) is increased by a factor $> 10^5$ by the addition of 4- CF_3 -phenyllithium to give **1.1a-Li⁺** (Figure A.1). A somewhat stronger

activation can be achieved with aryllithium compounds carrying electron donor substituents, but the loss of the selectivity in such cases should be taken into account.

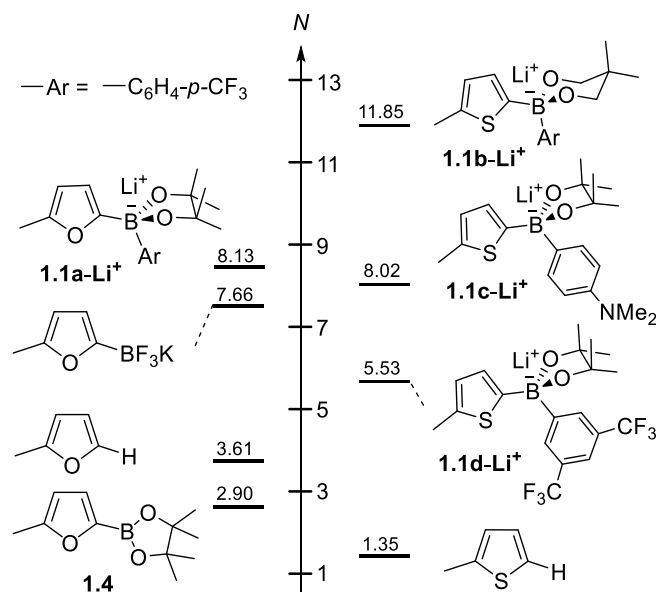


Figure A.1. Comparison of the nucleophilicities of BACs with those of other borylated and π -excessive heteroarenes.

While the nucleophilic reactivities of the BACs depend only slightly on their counterions, the nature of the diol ligand has a profound effect on their nucleophilicities. Thus, the $-B(gly)$ and $-B(neo)$ derivatives are 10^4 times more reactive than the $-B(pin)$ derivatives (Figure A.2). With these data in hand, we now have a quantitative basis for the fine-tuning of the nucleophilic reactivities of boron-ate complexes for synthetic applications.

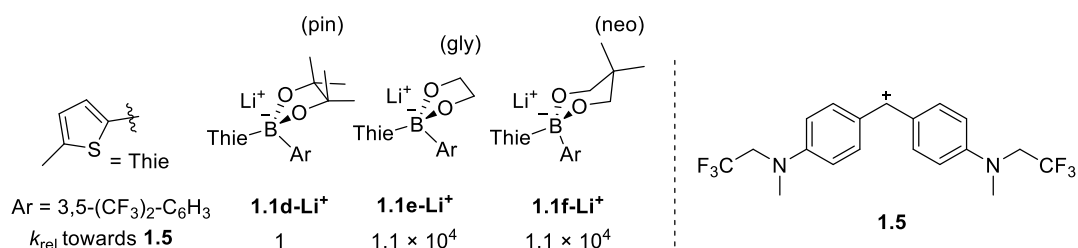
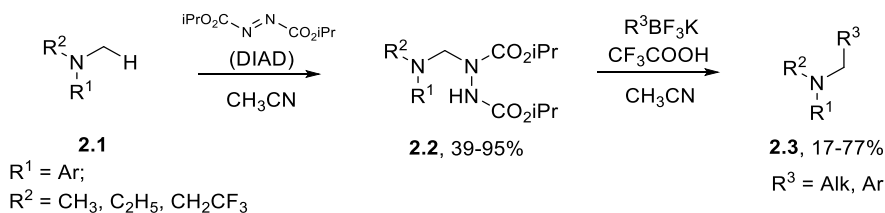


Figure A.2. Relative reactivities of the thienyl BACs **1.1d-f** derived from $B(pin)$, $B(gly)$ and $B(neo)$ toward carbenium ion **1.5** in CH_3CN at 20 °C.

Chapter 2. Transition Metal-Free C-H Activation of Tertiary Amines: Diisopropyl Azodicarboxylate Mediated α -Functionalization

Combination of the electrophilic and oxidative properties of diisopropylazodicarboxylate (DIAD) have been utilized for C-H activation at the α -position of tertiary amines (Scheme 2). Thus obtained aminals were reacted with various scope of aryl-, alkyl- and unsaturated

organotrifluoroborates to achieve α -functionalized *N*-methylanilines under mild conditions without any use of transition-metal catalysis.



Scheme A.2. α -Functionalization of *N*-methylanilines with DIAD.

DIAD demonstrated exclusive attack on the α -CH₃ group in *N*-alkyl-*N*-methylanilines with subsequent substitution of hydrazine moiety with potassium trifluoroborates (selected examples are shown in Figure A.3). Furthermore, this method was shown to successfully introduce functional group at the α -methyl position in a series of aliphatic amines.

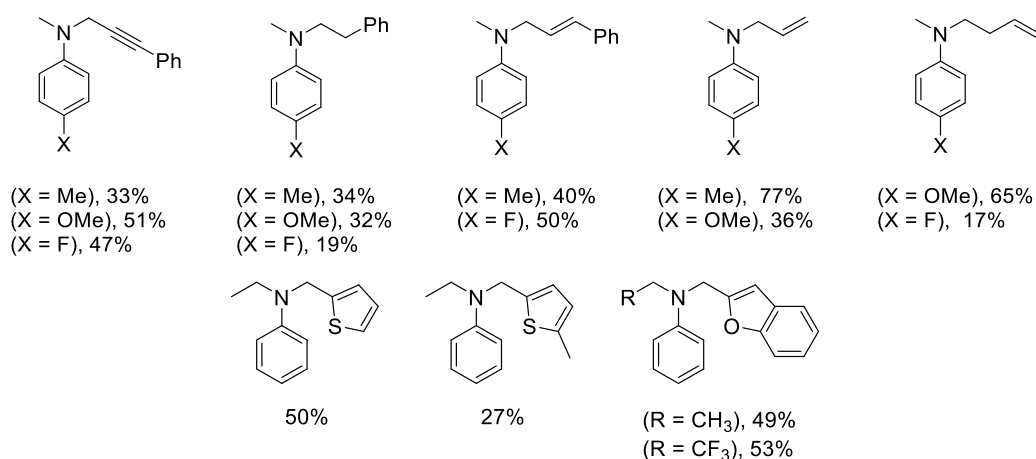
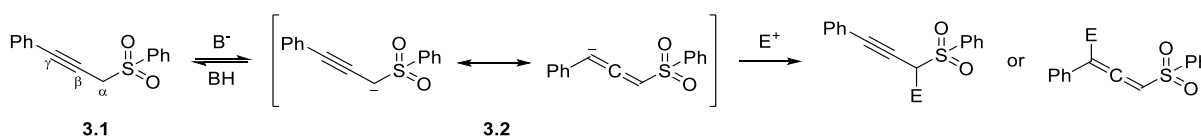


Figure A.3. Selected examples of substituted anilines obtained from amins **2.2** and organotrifluoroborates. Yields refer to isolated products after purification by column chromatography.

Chapter 3. Reactivities Studies of Alkynyl-Stabilized Carbanions

It has been demonstrated that addition of base to phenyl-propargyl sulfones **3.1** form nucleophilic species that react with standard electrophiles (Scheme A.3). These reactions have been investigated photometrically and obtained rate constants were used to calculate the nucleophilicity parameters for sulfonyl-stabilized carbanions **3.2**.



Scheme A.3. Formation of sulfonyl-stabilized carbanion **3.2** from the corresponding sulfones **3.1** and subsequent electrophilic attack at the α - and γ -positions.

The suggested carbanionic structures **3.2** showed reactivity similar to previously studied sulfonyl carbanions, decreased by a factor of 70 with the quinone methide **3.3** due to resonance stabilization of the anion by the neighboring triple bond (Figure A.4).

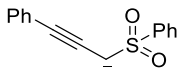
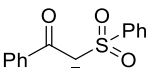
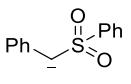
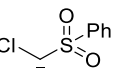
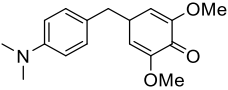
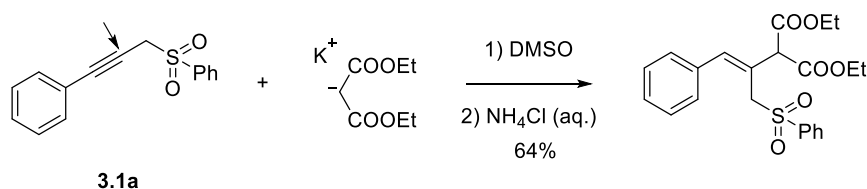
					
	3.2a	3.4a	3.4b	3.4c	
k_2 (3.3)	9.07×10^2	$1.01^{[a]}$	6.46×10^4 [a]	4.55×10^4 [a]	
k_{rel}	1	0.001	71	50	3.3

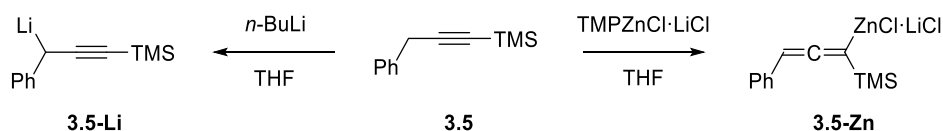
Figure A.4. Comparison of absolute (in $\text{L mol}^{-1} \text{s}^{-1}$) and relative rate constants for the reaction of sulfonyl stabilized carbanions **3.2a** and **3.4a-c** with quinone methide **3.3** in DMSO at 20 °C. [a] Calculated using equation (1).

The reaction of propargyl sulfone with potassium diethylmalonate demonstrated high reactivity of such structural motifs towards nucleophiles (Scheme A.4). Furthermore, compounds with propargyl skeleton may isomerize in the presence of base to its corresponding allenic form that is known for its electrophilic activity. Taking the possible oligomerization reactions, i.e. between carbanion and its protonated allenic form, into account, one could not correctly identify the reactive intermediate in studied reactions.



Scheme A.4. Nucleophilic attack of the potassium diethyl malonate on the sulfone **3.1a**.

To overcome those difficulties propargyl and allenic organometallic species **3.5-Li** and **3.5-Zn** were used for quantitative kinetic studies (Scheme A.5). The covalent character of the carbon-metal bonds in these structures should reduce the reactivity towards electrophiles and thus neglect possible side processes.

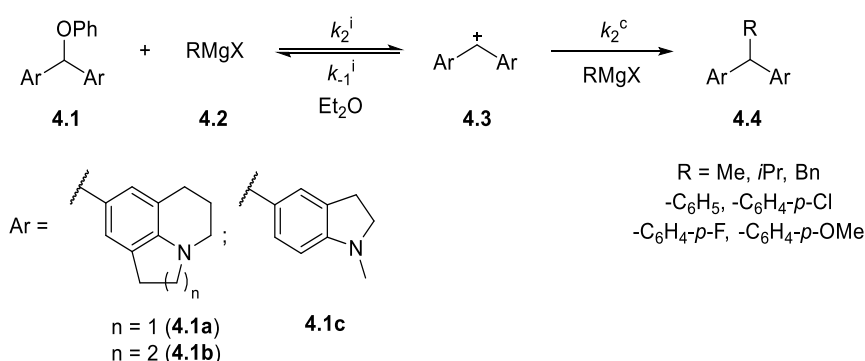


Scheme A.5. Metallation of **3.5** with *n*-BuLi and TMPZnClLiCl to form **3.5-Li** and **3.5-Zn** respectively.

However, the observed first-order rate constants of the reaction of an excess of **3.5-Zn** with bis-(*p*-(dimethylamino)phenyl)methylmethyl tetrafluoroborate did not linearly correlate with the nucleophile concentration. Thus, the nucleophilicity of these species could not be established.

Chapter 4. Lewis Acidic and Nucleophilic Properties of Grignard Reagents

The reaction of benzhydryl phenyl ethers with various Grignard reagents was found to proceed through formation of an intermediate carbocation as it is described by the S_N1 mechanism (Scheme A.6). The time-dependent concentration of the intermediate **4.3** could be followed photometrically, and quantitative analysis of the kinetic plots allowed us to calculate the rates of the involved reactions for ionization of the benzhydryl phenyl ethers and the subsequent nucleophilic trapping of the intermediate carbocations (Figure A.5).



Scheme A.6. S_N1-type reaction between benzhydryl phenyl ethers **4.1** and the Grignard reagents **4.2** in diethyl ether.

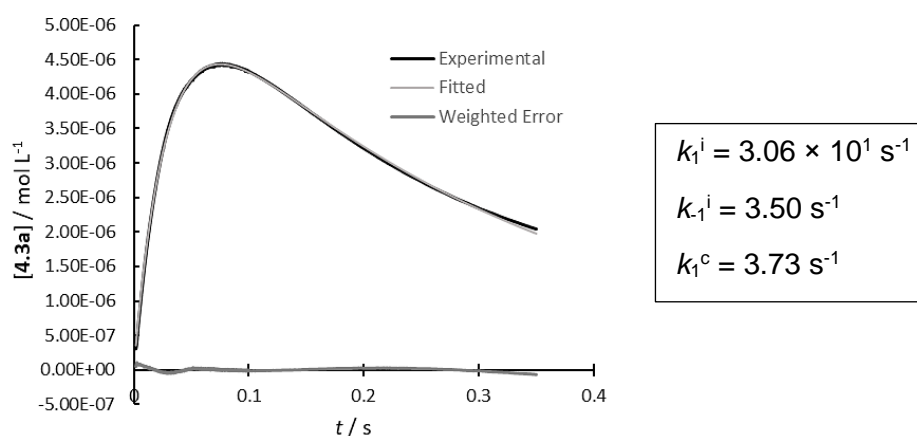


Figure A.5. Experimental plot of the concentration of the corresponding carbocation **4.3a** (black) in the reaction of **4.1a** ($2.18 \times 10^{-5} \text{ mol L}^{-1}$) with MeMgBr ($1.96 \times 10^{-2} \text{ mol L}^{-1}$) in Et₂O at 20 °C; calculated plot of the concentration (light grey) and weighted error (dark grey) found with COPASI software for a standard consecutive reversible reaction. Calculated first-order rate constants for the individual steps (right).

Comparison of the obtained rates of the ionization of the benzhydryl phenyl ether (k_2^i) showed that the ionization power of 4-substituted arylmagnesiumbromides increases in the range: 4-F < 4-Cl < 4-H with an exception of 4-MeO due to its possible intermolecular dimerization that may result in a reduced experimental rate constant (Figure A.6). The Grignard reagent with a relatively strong C-Mg bond, such as MeMgBr, differs by less than one order of magnitude from PhMgBr with respect to ionization of certain benzhydryl phenyl ether.

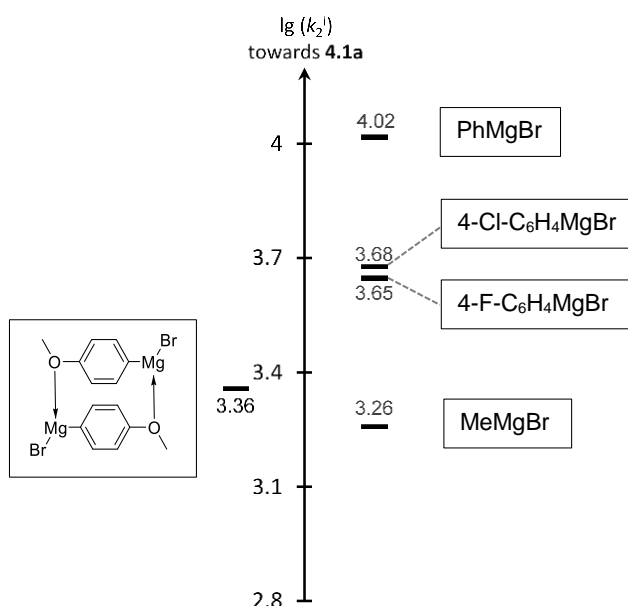


Figure A.6. Comparison of logarithms of rate constants for ionization of substrate **4.1a** with Grignard reagents.

Figure A.7 shows that the reactivities of the Grignard reagents towards carbocations in the S_N1 reaction are in the same range as enamines, highly reactive silyl enol ethers and highly stabilized carbanions.

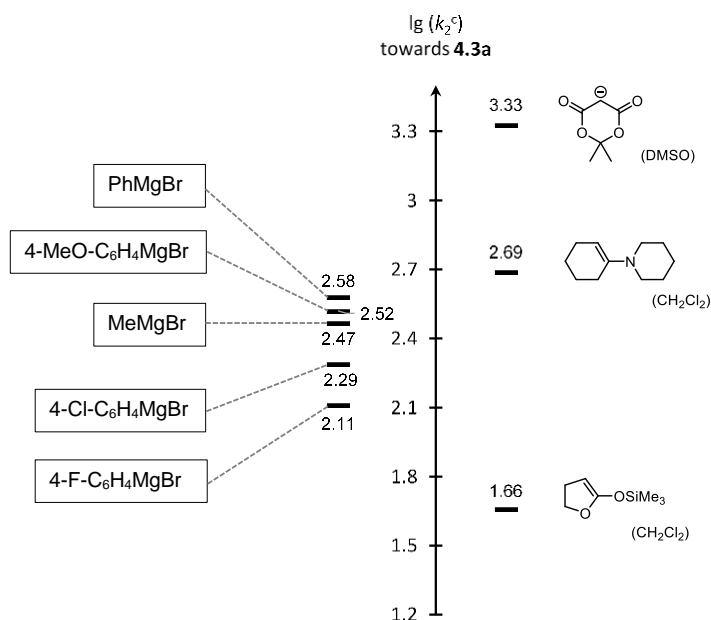


Figure A.7. Reactivity comparison between studied Grignard reagents and several reference nucleophiles towards **4.3a**.

Organomagnesium bromides in diethyl ether have shown the ability to shift the coordination equilibrium and substitute the solvent molecules with the substrate (benzhydryl phenyl ether)

with following formation of the benzhydrylium ion. In contrast, with the stronger solvating THF or weaker Lewis acidic organomagnesium chlorides the intermediate carbocation is not observed, which may indicate a different mechanism for the nucleophilic substitution, though the corresponding products **4.4** were isolated.

Chapter 5. Reactivity Comparison of Structurally Related Enamines and Silyl Enol Ethers

The second-order rate constants for the reaction of C-nucleophiles, such as silyl enol ethers and enamines, with reference electrophiles, either indolylmethyl cation or benzhydrylium ions **5.3**, in CH₂Cl₂ and CH₃CN followed the linear free-energy relationship (1) (Figure A.8).

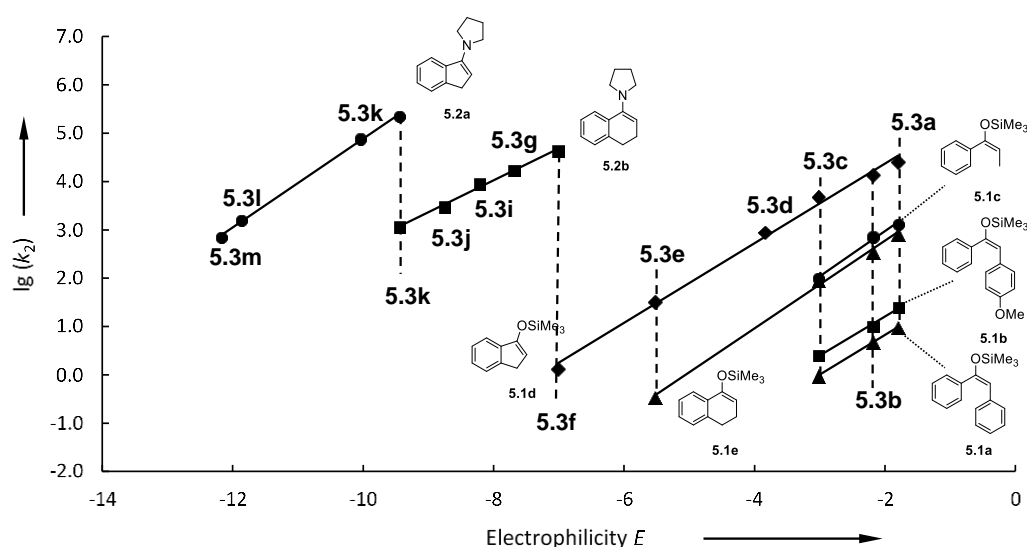


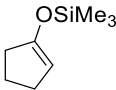
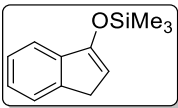
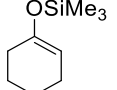
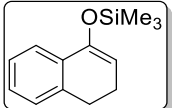
Figure A.8. Correlations of the second-order rate constants $\lg(k_2)$ for the reactions of C-nucleophiles **5.1** and **5.2** with the electrophiles **5.3** in CH₃CN at 20 °C with the electrophilicity parameters E of **5.3**.

With the obtained data it is possible to compare the reactivities of deoxybenzoin derived enolates, enamines and silyl enol ethers (Figure A.9). In terms of nucleophilicity the reactivity of the silyl enol ethers is 9 and 20 orders of magnitude lower than those of their structurally related enamines and enolates respectively. For the synthetic use of these species, the change in the reactivity should be considered: the high reaction rates with the electrophiles will increase the number of side-product and lead to loss of stereoselectivity.

N	3.00	11.66	23.15
s_N	0.82	0.82	0.60

Figure A.9. Comparison of the nucleophilicities of structurally related silyl enol ethers, enamines and enolates in CH₃CN at 20 °C.

Annulation of a planar aromatic moiety to cyclopentanone- and cyclohexanone-derived enamines and silyl enol ethers, while influencing the nucleophilicity only slightly, shows significant effects on the sensitivity parameter s_N making these substrates less sensitive towards changes in the nature of the electrophile (Figure A.10).

				
5.4a (CH_2Cl_2)	5.1d (CH_3CN)	5.4b (CH_2Cl_2)	5.1e (CH_3CN)	
N	6.57	7.32	5.21	5.06
(s_N)	(0.93)	(0.82)	(1.00)	(0.91)

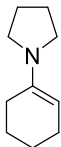
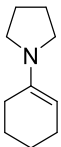
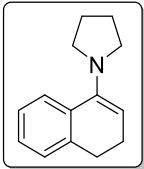
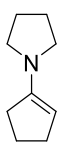
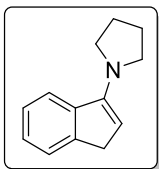
					
5.5a (CH_2Cl_2)	5.5a (CH_3CN)	5.2b (CH_3CN)	5.5b (CH_2Cl_2)	5.2a (CH_3CN)	
N	14.91	16.42	14.10	15.91	15.28
(s_N)	(0.86)	(0.70)	(0.66)	0.86	0.93

Figure A.10. Comparison of the nucleophilicity N and sensitivity s_N parameters for various silyl enol ethers and enamines.

B. Introduction

Since Ingold introduced^[1] the concept of “nucleophiles” (as electron-rich molecules) and “electrophiles” (as electron-deficient molecules) the task of systematic quantification of the reactivities of organic compounds became crucial for physical organic chemistry.^[2] Early efforts by Swain and Scott resulted in equation (1) that describes the nucleophilic parameter n as a ratio of the rate constants of the specific nucleophile and water.^[3]

$$\lg (k/k_{\text{H}_2\text{O}}) = s'n \quad (1)$$

n = nucleophilicity constant ($n_{\text{H}_2\text{O}} = 0$)

s' = sensitivity of electrophile ($s'_{\text{CH}_3\text{Br}} = 1$)

In 1972 Ritchie demonstrated^[4] that the rates of the reactions of carbocations and diazonium ions with various nucleophiles follow the simple two-parameter correlation in equation 2. Therefore, nucleophilicity is described by a single, solvent specific and electrophile-independent parameter N_+ , and the reactivities of the electrophiles are quantified by the rates k_0 of their reaction with water. From these two parameters, the rate constant k for the reaction of the corresponding reactants in a specific solvent can be obtained.

$$\lg (k/k_0) = N_+ \quad (2)$$

So-called “Constant Selectivity Relationships” were confirmed further for numerous nucleophiles in reactions with transition-metal π -complexes^[5] and for various hydride donors towards benzhydrylium ions.^[6] However, with more and more kinetic data available it was realized that Ritchie’s principle was not generally applicable and better correlations were obtained when different classes of electrophiles were treated separately.^[7] As a consequence, a nucleophile-specific sensitivity parameter was included in the arithmetic expression that describes different reaction series. In 1994 Mayr and Patz reported^[8] the modified linear free energy relationship equation (3) which characterizes electrophiles by one solvent-independent parameter E and nucleophiles by two solvent-dependent parameters, s_N (nucleophiles-specific sensitivity) and N (nucleophilicity).

$$\lg (k_2) = s_N(N + E) \quad (3)$$

Benzhydrylium ions and structurally related quinone methides were chosen as reference electrophiles as they exhibit similar steric surroundings at the reaction centers, while their reactivities can be varied widely by substituents at the aromatic rings. On this basis it was possible to construct the most comprehensive reactivity scale presently available, covering a

reactivity range of over 30 orders of magnitude. It has been shown that such scale can be employed for predicting rates of reactions of the corresponding nucleophiles with carbocations,^[9] cationic metal- π -complexes^[9] as well as electron deficient alkenes^[10] and arenes.^[11]

The formation of new carbon-carbon bonds is one of the central aims in organic chemistry. Organoboronates and boronic esters widely known for their transition metal catalyzed cross-coupling transformation^[12] can also undergo various uncatalyzed reactions with electrophiles, e.g. Michael additions^[13] and Friedel-Crafts reactions.^[14] However, most of the reported reactions require an activation of the boronic group for subsequent electrophilic attack. Addition of an organometallic species to form a boron “ate” complex and thus increase the reactivity of the substrate was exploited by Aggarwal^[15] and Morken^[16] for various stereoselective transformations. The quantitative influence of such activation on nucleophilicity of organoboronic esters is discussed in Chapter 1.

Oxidative functionalization of tertiary amines at the sp^3 -hybridized α -carbon traditionally relies on the use of stoichiometric or catalytic amounts of metal salts.^[17] In this context, dialkyl azodicarboxylates (DAADs) that are known to form reactive ainals with tertiary amines^[18] are particularly attractive for subsequent transformations. A number of publications has shown that oxidative properties of DAADs are suitable for C-H functionalization with various nucleophiles.^[19] However, the substrates scope was limited to mostly organometallic reagents. Chapter 2 describes the application of diisopropyl azodicarboxylate in combination with organotrifluoroborates for the α -functionalization of tertiary amines.

Carbanions belong to the most useful nucleophiles in synthetic organic chemistry, which undergo numerous substitutions or additions reactions.^[20] In context of further transformations carbanions bearing sulfone and acetylenic fragments are of particular interest.^[21] Kishida et al. demonstrated in the early 1970s the use of propargyl sulfur ylides^[22] and sulfonic carbanions^[23] as intermediates in reactions with aldehydes and Michael acceptors to form synthetically valuable substrates such as conjugated enones and substituted oxiranes. However, a strong electron-withdrawing group such as sulfonyl may serve as an activator for the nucleophilic attack at the unsaturated C-C bond.^[21c, 24] This makes acetylenic and propargyl sulfones versatile electrophiles for their potential transformations.^[21a] Mechanistic investigations on the reactions of the propargyl sulfonyl carbanions and corresponding C-H acids are discussed in Chapter 3.

Enamines and silyl enol ethers are typically serve as noncharged equivalents of highly reactive enolates. These electron-rich alkenes are widely used for synthesis of enantioenriched α - functionalized ketones. Selected examples of electrophilic fluorinations,^[25] thiolations^[26] and

trifluoromethylations^[27] demonstrate the loss of stereoselectivity and increased number of by-products when more reactive enamines (including generated *in situ*) are employed. The detailed analysis of nucleophilic reactivity differences between enamines and silyl enol ethers is discussed in Chapter 4.

Since their discovery more than hundred years ago^[28] Grignard reagents became an important tool in organic chemistry. While their synthetic applications have been extensively developed, relatively few investigations on their reactivities have so far been reported. It is well-understood that Grignard reagents behave both as nucleophiles attacking carbonyl groups and as Lewis acids, activating the carbonyl group by coordination to oxygen atom.^[29] A few examples have shown that these two functions can be separated, i.e. substrate ionization towards a stable carbocation with successful nucleophilic attack by the organomagnesium species.^[30] A detailed description and mechanistic insights of the S_N1-type reaction of benzhydryl phenyl ethers with various organomagnesium species is provided in Chapter 5.

References

- [1] a) K. C. Ingold, *Recl. Trav. Chim. Pays-Bas* **1929**, *48*, 797-812; b) C. K. Ingold, *J. Chem. Soc. (Resumed)* **1933**, 1120-1127; c) C. K. Ingold, *Chem. Rev.* **1934**, *15*, 225-274.
- [2] J. M. Harris, S. P. McManus, *Nucleophilicity*, American Chemical Society, Washington, DC, **1987**, p. 494.
- [3] C. G. Swain, C. B. Scott, *J. Am. Chem. Soc.* **1953**, *75*, 141-147.
- [4] a) C. D. Ritchie, *Acc. Chem. Res.* **1972**, *5*, 348-354; b) C. D. Ritchie, P. O. I. Virtanen, *J. Am. Chem. Soc.* **1972**, *94*, 4966-4971.
- [5] L. A. P. Kane-Maguire, E. D. Honig, D. A. Sweigart, *Chem. Rev.* **1984**, *84*, 525-543.
- [6] H. Mayr, N. Basso, *Angew. Chem. Int. Ed. Engl.* **1992**, *31*, 1046-1048.
- [7] C. D. Ritchie, *Can. J. Chem.* **1986**, *64*, 2239-2250.
- [8] H. Mayr, M. Patz, *Angew. Chem. Int. Ed. Engl.* **1994**, *33*, 938-957.
- [9] a) H. Mayr, T. Bug, M. F. Gotta, N. Hering, B. Irrgang, B. Janker, B. Kempf, R. Loos, A. R. Ofial, G. Remennikov, H. Schimmel, *J. Am. Chem. Soc.* **2001**, *123*, 9500-9512; b) H. Mayr, B. Kempf, A. R. Ofial, *Acc. Chem. Res.* **2003**, *36*, 66-77; c) H. Mayr, A. R. Ofial, *Pure Appl. Chem.* **2005**, 1807-1821.
- [10] T. Lemek, H. Mayr, *J. Org. Chem.* **2003**, *68*, 6880-6886.
- [11] a) F. Terrier, S. Lakhdar, R. Goumont, T. Boubaker, E. Buncel, *Chem. Commun.* **2004**, 2586-2587; b) F. Terrier, S. Lakhdar, T. Boubaker, R. Goumont, *J. Org. Chem.* **2005**, *70*, 6242-6253; c) G. Ya. Remennikov, B. Kempf, A. R. Ofial, K. Polborn, H. Mayr, *J. Phys. Org. Chem.* **2003**, *16*, 431-437.

- [12] a) A. Suzuki, *Angew. Chem. Int. Ed.* **2011**, *50*, 6722-6737; b) G. A. Molander, N. Ellis, *Acc. Chem. Res.* **2007**, *40*, 275-286; c) S. Darses, J.-P. Genet, *Chem. Rev.* **2008**, *108*, 288-325.
- [13] a) H. Wu, S. Radomkit, J. M. O'Brien, A. H. Hoveyda, *J. Am. Chem. Soc.* **2012**, *134*, 8277-8285; b) C. Pubill-Ulldemolins, A. Bonet, C. Bo, H. Gulyás, E. Fernández, *Chem. Eur. J.* **2012**, *18*, 1121-1126.
- [14] a) S. Lee, D. W. C. MacMillan, *J. Am. Chem. Soc.* **2007**, *129*, 15438-15439; b) E.-i. Negishi, A. Abramovitch, R. E. Merrill, *Chem. Commun.* **1975**, 138-139.
- [15] a) M. Mohiti, C. Rampalakos, K. Feeney, D. Leonori, V. K. Aggarwal, *Chem. Sci.* **2014**, *5*, 602-607; b) A. Bonet, M. Odachowski, D. Leonori, S. Essafi, V. K. Aggarwal, *Nat. Chem.* **2014**, *6*, 584-589; c) R. Larouche-Gauthier, T. G. Elford, V. K. Aggarwal, *J. Am. Chem. Soc.* **2011**, *133*, 16794-16797.
- [16] L. Zhang, G. J. Lovinger, E. K. Edelstein, A. A. Szymaniak, M. P. Chierchia, J. P. Morken, *Science* **2016**, *351*, 70.
- [17] a) S. A. Girard, T. Knauber, C. J. Li, *Angew. Chem. Int. Ed. Engl.* **2014**, *53*, 74-100; b) C. J. Li, *Acc. Chem. Res.* **2009**, *42*, 335-344; c) Z. Li, D. S. Bohle, C. J. Li, *Proc. Natl. Acad. Sci. USA* **2006**, *103*, 8928-8933; d) X. Zheng, Z. Li in *From C-H to CC-bonds: Cross-Dehydrogenative-Couplings* (Ed. C. J. Li), RSC Green Chemistry Series, Royal Society of Chemistry: Cambridge, UK, **2015**, pp. 55-66; e) A. McNally, C. K. Prier, D. W. MacMillan, *Science* **2011**, *334*, 1114-1117; f) C. K. Prier, D. W. MacMillan, *Chem. Sci.* **2014**, *5*, 4173-4178; g) N. M. Reid, D. A. Proestou, B. W. Clark, W. C. Warren, J. K. Colbourne, J. R. Shaw, S. I. Karchner, M. E. Hahn, D. Nacci, M. F. Oleksiak, D. L. Crawford, A. Whitehead, *Science* **2016**, *354*, 1305-1308; h) Q. Li, C. W. Liskey, J. F. Hartwig, *J. Am. Chem. Soc.* **2014**, *136*, 8755-8765; i) W. Muramatsu, K. Nakano, C. J. Li, *Org. Biomol. Chem.* **2014**, *12*, 2189-2192.
- [18] a) O. Diels, M. Paquin, *Ber. Dtsch. Chem. Ges.* **1913**, *46*, 2000-2013; b) R. Huisgen, F. Jakob, *Liebigs Ann. Chem.* **1954**, *590*, 37-54.
- [19] a) X. Xu, X. Li, *Org. Lett.* **2009**, *11*, 1027-1029; b) K. Singh, P. Singh, A. Kaur, P. Singh, *Synlett* **2012**, *23*, 760-764; c) Y. Miyake, K. Nakajima, Y. Nishibayashi, *Chem. Eur. J.* **2012**, *18*, 16473-16477; d) K. Singh, S. Kessar, P. Singh, P. Singh, M. Kaur, A. Batra, *Synthesis* **2014**, *46*, 2644-2650; e) W. Huang, C. Ni, Y. Zhao, J. Hu, *New J. Chem.* **2013**, *37*, 1684-1687; f) T. Suga, S. Iizuka, T. Akiyama, *Org. Chem. Front.* **2016**, *3*, 1259-1264.
- [20] a) R. B. Bates, C. A. Ogle, *Carbanion Chemistry*, Springer, Berlin, **1983**; b) L. Brandsma, *Preparative Polar Organometallic Chemistry 2*, Springer, Berlin, **1990**; c) V. Snieckus, *Advances in Carbanion Chemistry*, JAI Press, Greenwich, CT, **1992**; d) M. B. Smith in *March's Advanced Organic Chemistry*, Wiley, Hoboken, **2013**, pp. 221-234.
- [21] a) T. G. Back, *Tetrahedron* **2001**, *57*, 5263-5301; b) S. Patai, Z. Rappoport, C. J. M. Stirling, *The Chemistry of Sulphones and Sulphoxides*, Wiley, Chichester, **1988**; c) N. S. Simpkins, *Sulphones in Organic Synthesis*, Pergamon, Oxford, **1993**.
- [22] A. Terada, Y. Kishida, *Chem. Pharm. Bull.* **1970**, *18*, 505-510.
- [23] a) M. Yoshimoto, N. Ishida, Y. Kishida, *Chem. Pharm. Bull.* **1972**, *20*, 2137-2142; b) M. Yoshimoto, Y. Kishida, *Chem. Pharm. Bull.* **1970**, *18*, 2528-2534.
- [24] N. S. Simpkins, *Tetrahedron* **1990**, *46*, 6951-6984.

- [25] J. Baudoux, D. Cahard in *Electrophilic Fluorination with N-F Reagents*, (Ed. S. E. Denmark), Wiley, Hoboken, **2007**, pp. 347-672.
- [26] a) W. Wang, H. Li, J. Wang, L. Liao, *Tetrahedron Lett.* **2004**, *45*, 8229-8231; b) S. E. Denmark, S. Rossi, M. P. Webster, H. Wang, *J. Am. Chem. Soc.* **2014**, *136*, 13016-13028; c) S. Arimori, M. Takada, N. Shibata, *Org. Lett.* **2015**, *17*, 1063-1065; d) Y. D. Yang, A. Azuma, E. Tokunaga, M. Yamasaki, M. Shiro, N. Shibata, *J. Am. Chem. Soc.* **2013**, *135*, 8782-8785; e) R. Sergio, P. Alessandra, R. Laura, B. Maurizio, *ChemCatChem* doi:10.1002/cctc.201800170
- [27] a) A. Prieto, O. Baudoin, D. Bouyssi, N. Monteiro, *Chem. Commun.* **2016**, *52*, 869-881; b) T. Umemoto, S. Ishihara, *J. Am. Chem. Soc.* **1993**, *115*, 2156-2164.
- [28] V. Grignard, *Compt. Rend. Acad. Sci.* **1900**, *130*, 1322-1324.
- [29] E. C. Ashby, J. Laemmle, H. M. Neumann, *Acc. Chem. Res.* **1974**, *7*, 272-280.
- [30] a) F. G. Mann, F. H. C. Stewart, *J. Chem. Soc. (Resumed)* **1954**, 4127-4134; b) J. P. Mason, M. Zief, *J. Am. Chem. Soc.* **1940**, *62*, 1450-1452; c) A. T. Stewart, C. R. Hauser, *J. Am. Chem. Soc.* **1955**, *77*, 1098-1103.

Chapter 1

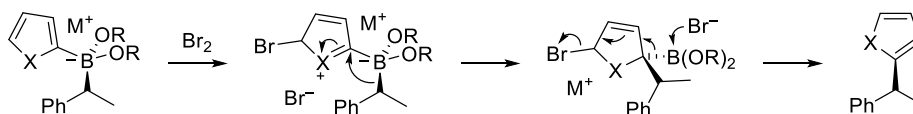
Fine-Tuning the Nucleophilic Reactivities of Boron Ate Complexes Derived from Aryl and Heteroaryl Boronic Esters

G. Berionni, A. I. Leonov, P. Mayer, A. R. Ofial, H. Mayr

Angew. Chem. **2015**, 127, 2820-2824; *Angew. Chem. Int. Ed.* **2015**, 54, 2780-2783.

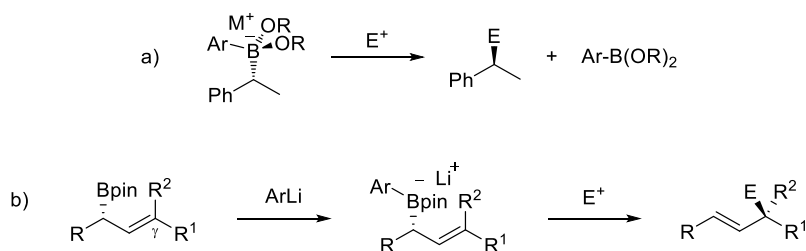
1.1 Introduction

Boron “ate” complexes (BAC) that are readily available by treatment of boronic esters $R-B(OR)_2$ with organometallic compounds are air-stable, functional-group-tolerant nucleophiles.^[1] Following the principle of the Zweifel olefination,^[2] Aggarwal et al. reported^[3] that treatment of BACs with suitable electrophiles led to the stereospecific coupling of arenes with secondary alkyl groups (e.g. Scheme 1.1).



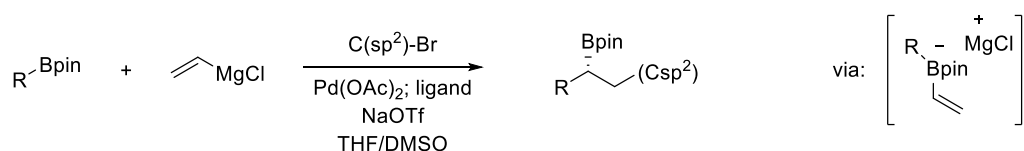
Scheme 1.1. Reaction of metal boronate complexes with electrophiles (e.g. bromine) and successive stereospecific elimination.

In contrast, BACs with less electron-rich arenes (Scheme 1.2a) were attacked by electrophiles at the boron substituted sp^3 -hybridized carbon, and the coupling products $R-E$ were formed with high degree of inversion.^[4] Chiral BACs, derived from secondary boronic esters, reacted in this way with a broad range of carbon-, oxygen- and nitrogen-centered electrophiles, including carbenium and iminium ions.^[4] In similar manner, formation of BACs from allylborons were employed for their activation towards weak carbon- and heteroatom-based electrophiles with very high γ -selectivity (Scheme 1.2b).^[5]



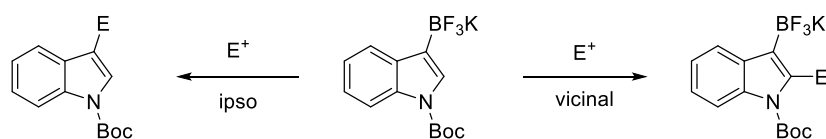
Scheme 1.2. Electrophilic attack at the C_{sp^3} carbon of boronate complex.

Recent work by Morken et al. demonstrated the preparation of the chiral organoboronic esters via Pd-catalyzed cross-coupling reaction of an in situ formed vinylic boronate complexes.^[6] Furthermore they have shown that the same type of the reaction may utilize simple and commercially available Grignard reagents in the presence of sodium triflate (Scheme 1.3).^[7]



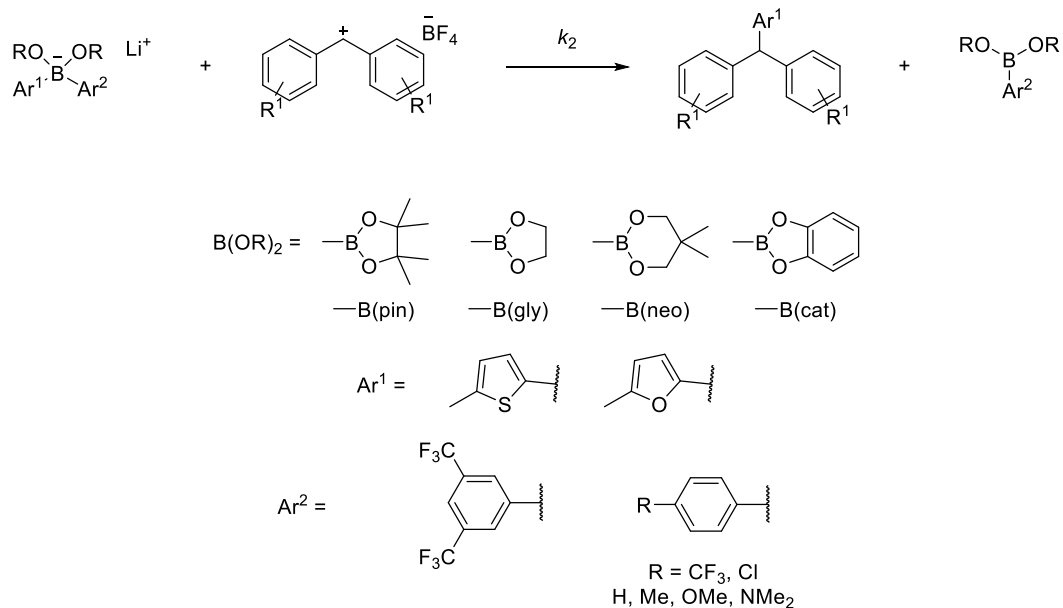
Scheme 1.3. Pd-catalyzed conjunctive cross-coupling of Grignard-derived boronate complexes.

Borate salts M^+ Aryl- BX_3^- with electron-rich arene rings, on the other hand, are known to react with electrophiles at the *ipso* position of the aryl ring.^[8] Recently it was demonstrated^[9] that the borate or boronate groups, such as $-B(OR)_3^-$, $-BF_3^-$, $-B(pin)$, and $-B(MIDA)$ ($MIDA = N$ -methyliminodiacetate), raises the nucleophilicity of the carbon directly attached to the boron atom (*ipso*-activation) by a factor of approximately 10^3 - 10^4 , although the activation of the vicinal or more remote position of the π -system is even greater (Scheme 1.4).



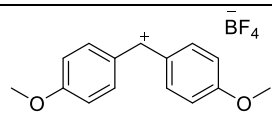
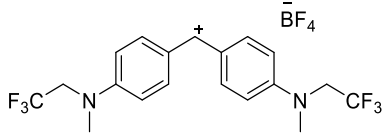
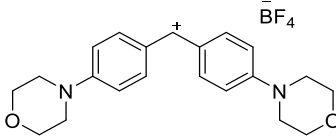
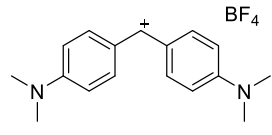
Scheme 1.4. Ipso and vicinal activation of the trifluoroborate group in the indolyl system.

To quantify the effect of the boronate complex formation on the nucleophilic reactivity of the aryl systems, we have prepared BACs with two aryl rings (Scheme 1.5) and utilized the benzhydrylium methodology^[10] to determine their nucleophilic parameters using reference electrophiles listed in Table 1.1.



Scheme 1.5. General scheme of the reaction of BAC with benzhydrylium tetrafluoroborates.

Table 1.1. Electrophiles used in the kinetic study of BACs.

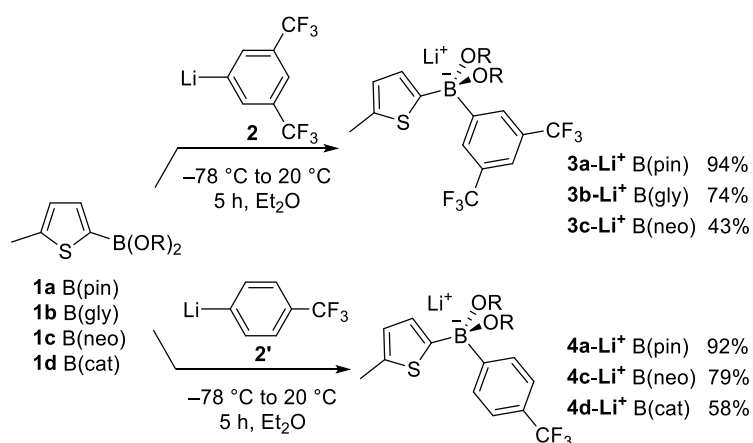
Electrophile	$\lambda_{\text{max}} / \text{nm}^{[a]}$	$E^{[b]}$
 15a	500	0
 15b	586	-3.85
 15c	611	-5.53
 15d	605	-7.02

[a] Measured in acetonitrile. [b] From ref. ^[10]

1.2 Results and Discussion

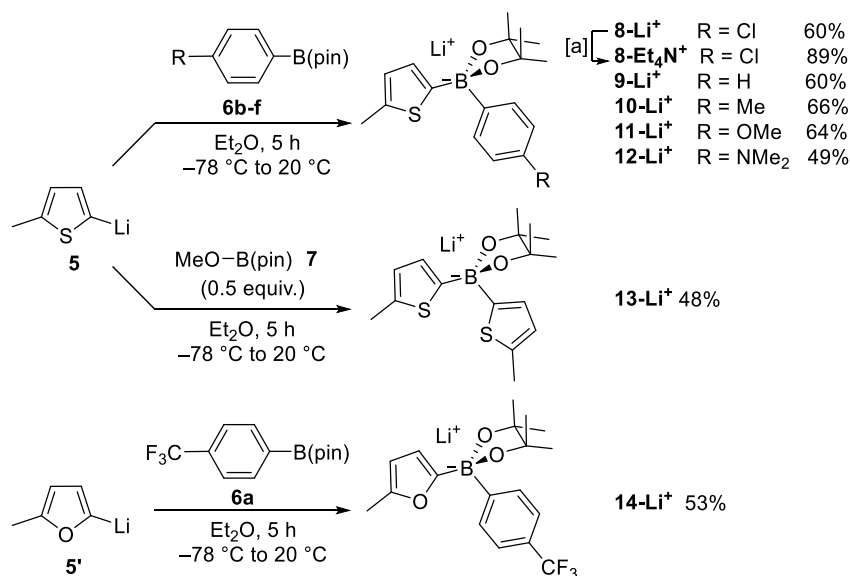
1.2.1 Synthesis of the Boronate Complexes

Following a procedure by Brown^[1] addition of the thienyl boronic esters **1a–d** to ethereal solutions of the trifluoromethylated aryl-lithium compounds **2** and **2'** followed by evaporation of the solvent produced the lithium BACs (**3–4**)-Li⁺ as colorless crystalline solids (Scheme 1.6). The ¹¹B NMR spectra of all BACs show a sharp resonance at δ +2 to +10 ppm that is characteristic for an anionic tetra-coordinated boron atom derived from boronic esters.^[1] No decomposition of these BACs in CD₃CN solutions was observed by ¹H NMR spectroscopy within several days at 20 °C.



Scheme 1.6. Synthesis and isolated yields of the lithium BACs (**3–4**)-Li⁺.

As shown in Scheme 1.7, addition of thienyl- and furyl-lithium derivatives **5** and **5'** to the pinacol boronates **6** or **7** produced the BACs (**8–14**)-Li⁺ in good yields. The tetraethylammonium salt **8-Et₄N⁺** was obtained by cation metathesis from **8-Li⁺** with Et₄N⁺Cl⁻.



Scheme 1.7. Synthesis of the BACs **8-14** and isolated yields after crystallization from THF/Et₂O or CH₃CN/Et₂O mixtures (see the Experimental section for details). [a] Reaction conditions: Et₄N⁺Cl⁻ (1 equiv.), THF, 20 °C.

Crystals of **3a-Li⁺·(MeCN)₃** suitable for X-ray analysis were grown by storing a concentrated CH₃CN solution of **3a-Li⁺** at 0 °C for one week. Its solid-state structure (Figure 1.1a) shows that the lithium cation is coordinated to one oxygen of the pinacol moiety (Li–O1 = 1.924 Å) as well as to three CH₃CN molecules (Li–N = 2.070 Å in average). Single crystals of the catechol borate **4d-Li⁺·(THF)₃** were obtained by vapour diffusion of *n*-pentane into its solution in THF. Figure 1.1b shows that Li⁺ is coordinated to a catechol oxygen and to three THF molecules. The quaternary boron atoms in both BACs are in perfect tetrahedral environments (tetrahedral character > 99.9 %).^[11]

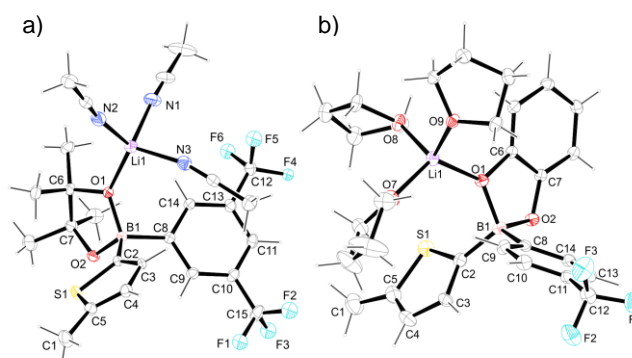


Figure 1.1. ORTEP view of the BACs **3a-Li⁺·(CH₃CN)₃** (a) and of **4d-Li⁺·(THF)₃** (b) with thermal ellipsoids on a 30% probability level. For bond lengths and angles see the Experimental Section.

1.2.2 Kinetic Investigation

The kinetics of the reactions of the BACs **3-4** and **8-14** with the benzhydrylium ions **15a-d** have been monitored by time-resolved UV-Vis spectroscopy in CH₃CN at λ_{max} of **15** (Table 1.1). In the presence of more than ten equivalents of the BACs, mono-exponential decays of the benzhydrylium ions' absorbances were observed, indicating pseudo-first-order kinetics. The second-order rate constants k_2 reported in Table 1.2 were derived from the slopes of the plots of k_{obs} (s⁻¹) against the concentration of the BACs (see Section 1.4).

$$\lg k_2 (20\text{ }^\circ\text{C}) = s_N (N + E) \quad (1)$$

Substitution of the determined second-order rate constants k_2 into equation (1)^[12] allows us to calculate the nucleophile specific parameters for BACs **3-4** and **8-14**: the nucleophilicity parameter N and the sensitivity parameter s_N .

Table 1.2. Second-order rate constants k_2 for the reactions of lithium BACs with electrophiles **15b-d** in CH₃CN at 20 °C and the resulting nucleophilicity parameters.

Lithium BAC	N (s_N)	Electrophile	k_2 / L mol ⁻¹ s ⁻¹
3a	5.53 (1.00) ^[a]	15b	4.84×10^1
		15c	< 1 ^[b]
3b	11.23 (0.77)	15b	5.22×10^5
		15c	2.24×10^4
		15d	1.88×10^3
3c	10.13 (0.91)	15b	5.36×10^5
		15c	1.57×10^4
4a	6.24 (1.00)	15b	2.40×10^2
		15c	5.06
4c	11.85 (0.72)	15b	$> 10^6$
		15c	3.73×10^4
		15d	3.12×10^3
4d	6.50 (0.77)	15b	1.10×10^2
		15c	5.57
8	6.77 (0.88)	15b	3.68×10^2
		15c	1.23×10^1
9	7.24 (0.83)	15b	6.82×10^2
		15c	2.70×10^1

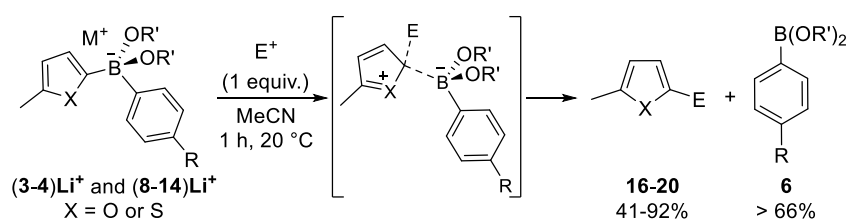
Table 1.2. Continued.

Lithium BAC	<i>N</i> (<i>s_N</i>)	Electrophile	<i>k₂</i> / L mol ⁻¹ s ⁻¹
10	6.98 (0.93)	15b	8.12×10^2
		15c	2.22×10^1
11	7.51 (0.87)	15b	1.49×10^3 [c]
		15c	5.20×10^1 [c]
12	8.02 (0.89)	15b	5.14×10^3
		15c	1.65×10^2
13	7.67 (0.87)	15b	2.08×10^3
		15c	7.19×10^1
14	8.13 (0.85)	15b	4.38×10^3
		15c	1.63×10^2

[a] Derived from a single k_2 value assuming $s_N = 1$ as for **4a**. [b] Not accessible due to high reversibility of the reaction and the non-linearity of the plot of k_{obs} vs **[3a]**. [c] Partial attack (< 5%) of the **15b-c** at the anisole ring of **11**.

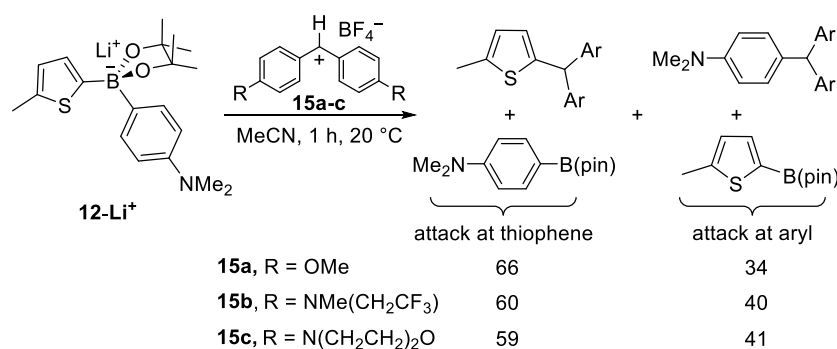
1.2.3 Product Studies

A general mechanism for the electrophilic attack at the aromatic ring of the BACs (**3-4**)-Li⁺ is shown on the Scheme 1.8. In all the studied substances (with exception of **12-Li**⁺ that will be discussed below) the exclusive attack at the more electron-rich thiophenyl- or furanyl-aromatic system was observed.



Scheme 1.8. Reactions of the BACs (**3-14**)-Li⁺ with various electrophiles at 20 °C in CH₃CN. Yields and structures of **16-20** are given in the Experimental section.

As shown in Scheme 1.9, the reaction of the NMe₂ derivative **12-Li**⁺ with electrophiles is not regioselective, and the thiophene ring of **12-Li**⁺ is only slightly faster attacked than the dimethylanilino ring. As electrophilic attack at the aryl group is least likely when these are carrying electron-withdrawing substituents, the aryl lithium compounds **2** and **2'** are often used for the activation of boronic esters in synthetic applications.^[3a, 4]



Scheme 1.9. Unselective reactions of **12-Li⁺** with Ar₂CH⁺BF₄⁻ **15a-c**. Product ratios determined by ¹H-NMR spectroscopy and GC-MS of the crude reaction mixtures.

1.2.4 Structure-Reactivity Relationship

Kinetic experiments revealed that **8-Li⁺** was three times less reactive than its sodium analogue **8-Na⁺** (Figure 1.2), in line with the coordination of the Li⁺ cation to an oxygen atom of the pinacol ligand, which decreases the electron density of the thiophene-boron bond. The reactivity of **8-Et₄N⁺** is in between that of **8-Na⁺** and **8-Li⁺**, indicating that Et₄N⁺ slightly reduces the nucleophilicity of **8**, probably by the formation of a C-H...O hydrogen bond with the oxygen atoms of the pinacol ligand.^[13] Nevertheless, the kinetic data show that counterions have only a small effect on the nucleophilicities of BACs in CH₃CN.

	8-M⁺	8-Li⁺	8-Na⁺	8-Et₄N⁺
<i>k</i> ₂ with 15b [M ⁻¹ s ⁻¹]		3.68 × 10 ²	1.26 × 10 ³	6.77 × 10 ²
<i>k</i> _{rel}		1	3.4	1.8

Figure 1.2. Influence of the counterions on the reactivity of **8** toward the benzhydrylium ion **15b** in CH₃CN at 20 °C.

The small Hammett reaction constants ($\rho \approx -1$), derived from the correlations in Figure 1.3, indicate a transition state resembling a σ -adduct (Scheme 1.8), in which breaking of the C-B bond is not far advanced.

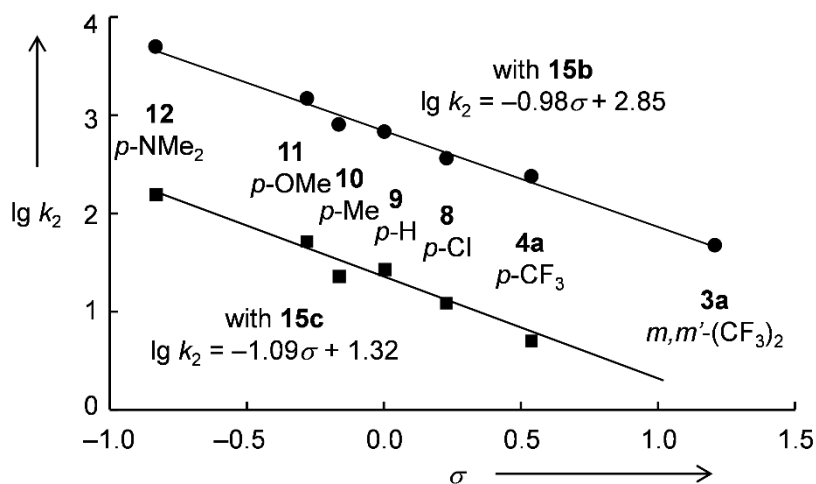


Figure 1.3. Correlation of the second-order rate constants $\lg k_2$ for the reactions of the lithium thienyl pinacol BACs **3a**, **4a**, and **8-12** with the benzhydrylium ions **15b** (black dots) and **15c** (black squares) with Hammett's σ parameters.

Figure 1.4 shows that the ethylene glycol and neopentyl glycol derived BACs **3b**, **3c** and **4c** are $\approx 10^4$ times more reactive than the pinacol and catechol BACs **3a**, **4a** and **4d**, in line with previous qualitative observations.^[14] The origin of these differences is revealed by quantum chemical calculations. It has already been reported that catechol boronates are significantly stronger Lewis acids than ethylene glycol and neopentyl glycol-derived boronates because a phenolate oxygen exerts a weaker +M effect than an alkoxide oxygen.^[15]

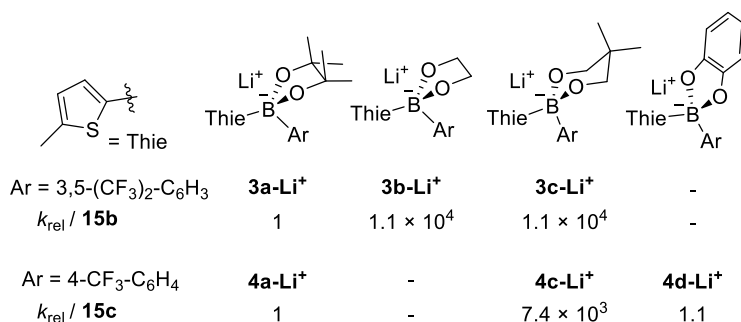
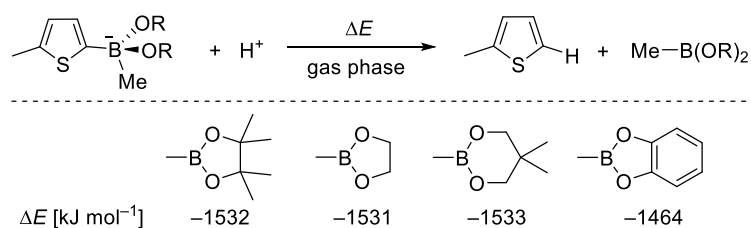


Figure 1.4. Relative reactivities of the thienyl BACs **3-4** derived from B(pin), B(gly), B(neo) and B(cat) toward carbenium ions **15b-c** in CH₃CN at 20 °C.

In line with these findings we calculated that the protodeborylation of a catechol-derived BAC is significantly less exothermic than that of the analogous reaction of the other BACs (Scheme 1.11). The 10^4 -fold lower nucleophilicity of the catechol-derived BAC **4d** (compared with **4c**, Scheme 1.10) shows that a fraction of this difference in reaction energies is already observed in the transition states of the reactions with benzhydrylium ions.



Scheme 1.10. Protodeborylation energies in the gas phase (B3LYP/6–31G(d)).

On the other hand, similar exothermicities are calculated for the protodeborylations of the B(pin), B(gly), and B(neo) derivatives (Scheme 1.10). For that reason, we can conclude that the difference in nucleophilicities of the BACs **3a** and **3b** is exclusively due to steric effects. The identical nucleophilicities of **3b** and **3c**, in line with the comparable reaction energies of the corresponding protodeborylations shown in Scheme 1.11, furthermore show that conceivable stereoelectronic effects (ideal overlap of the empty p-orbital at boron with the oxygen lone pair) do not increase the reactivity of the neopentyl derivatives **3c** and **4c**.

1.3 Conclusion

In conclusion, we have found that the nucleophilic reactivity of the furylboronate **1'** ($N = 2.90$) is increased by a factor $> 10^5$ by the addition of 4- CF_3 -phenyllithium (**2'**) to give **14** (Figure 1.5). A somewhat stronger activation can be achieved with aryllithium compounds carrying electron donor substituents, but the loss of the selectivity in such cases should be taken into account (Scheme 1.9).

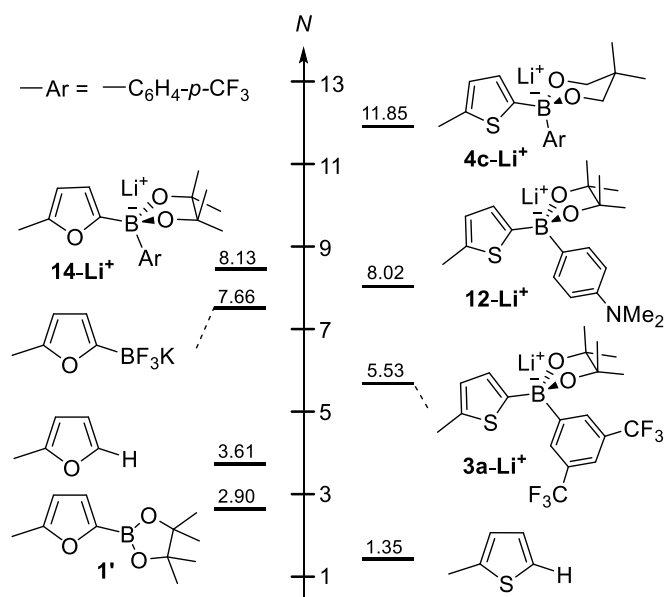


Figure 1.5. Comparison of the nucleophilic reactivities of BACs with those of other borylated and electron-rich heteroarenes. N parameters from Table 1.2 and ref. [9]

While the nucleophilic reactivities of the BACs depend only slightly on their counterions, the nature of the diol ligand has a profound effect on its nucleophilicity. Thus, the $-\text{B}(\text{gly})$ and $-\text{B}(\text{neo})$ derivatives are 10^4 times more reactive than the $-\text{B}(\text{pin})$ and $-\text{B}(\text{cat})$ derivatives. With these data in hand, we now have a quantitative basis for the fine-tuning of the nucleophilic reactivities of boron-ate complexes for synthetic applications.

1.4 Experimental section

1.4.1 General

All reactions were performed in carefully dried Schlenk glassware in an atmosphere of dry nitrogen. The reactions were not optimized for high yields.

^1H NMR (400 MHz), ^{13}C NMR (100 MHz), and ^{19}F NMR spectra (376 MHz) were recorded on Varian NMR spectrometers in CD_3CN or CDCl_3 . Chemical shifts in ppm refer to the solvent residual signal in CD_3CN (δ_{H} 1.94, δ_{C} 118.7 ppm) or CDCl_3 (δ_{H} 7.24, δ_{C} 77.2 ppm) as internal standard or to external CFCl_3 (δ_{F} 0.0 ppm), respectively. ^{11}B NMR spectra (128 MHz) were obtained by using a JEOL ECX-400 spectrometer and referenced to external $\text{BF}_3\cdot\text{OEt}_2$ (0.0 ppm). The following abbreviations were used to describe the multiplicities of resonances: br s = broad singlet, s = singlet, d = doublet, t = triplet, q = quartet, sept = septet, m = multiplet. NMR signal assignments are based on additional 2D-NMR experiments (COSY, HSQC, HMBC, and NOESY). HRMS was performed on a Finnigan MAT 95 (EI) or a Thermo Finnigan LTQ FT (ESI) mass spectrometer. Melting points were determined on a Büchi B-540 device and are not corrected. An IR spectrometer (Spectrum BX from Perkin Elmer) with an ATR unit (attenuated total reflection; Dura Sampler Diamond ATR from Smiths Detection) was used to record the IR spectra of neat compounds.

Solvents. For the kinetic experiments commercially available acetonitrile (Acros, 99.9%, Extra Dry, AcroSeal) was used as received. Commercially available Et_2O (p.a.) was dried for 24 hours over CaCl_2 and distilled over Na/benzophenone prior to use.

Chemicals. 2-Methoxy-4,4,5,5-tetramethyl-1,3,2-dioxaborolane **7** (96%), triisopropyl borate (> 98%) and *N,N*-dimethylmethyleiminium iodide **15e** (98%) were purchased from Aldrich used as received. Commercially available *n*-butyl lithium (Chemetall GmbH, 15% in *n*-hexane) was titrated before each use.

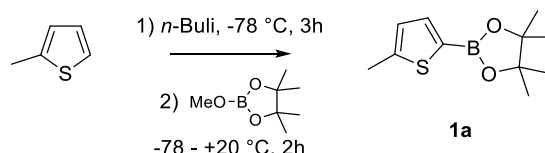
Kinetics. The rates of all investigated reactions were determined spectrophotometrically (UV-Vis). The temperature of the solutions during all kinetic studies was kept constant ($20.0 \pm 0.1^\circ\text{C}$) by using a circulating bath thermostat. The kinetic experiments were carried out with freshly prepared stock solutions of the boron-ate complexes **3**, **4**, and **8-14** in CH_3CN under nitrogen. The benzhydrylium tetrafluoroborates **15b-d**, also prepared as stock solutions in CH_3CN under nitrogen, were always employed as minor component in the reactions with the BACs **3**, **4** and **8-14**, resulting in pseudo first-order kinetics. The rates of the reactions were determined by using a stopped-flow spectrophotometer system Applied Photophysics SX.18MV-R. Rate constants k_{obs} (s^{-1}) were obtained by fitting the single exponential decay A_t

$= A_0 \exp(-k_{\text{obs}}t) + C$ (exponential decrease) to the observed time-dependent absorbance (averaged from at least 5 kinetic runs for each nucleophile concentration). Second-order rate constants k_2 ($\text{M}^{-1} \text{s}^{-1}$) were derived from the slopes of the linear correlations of k_{obs} with nucleophile concentrations, as shown in the main text. The slightly positive intercepts of some plots of k_{obs} (s^{-1}) against the BACs concentrations (for example in the correlations related to Tables 1.16, 1.22, and 1.24), which were used for determining the second-order rate constants k_2 reported in Table 2, may be explained by the fact that triarylmethanes such as **16-20** are easily cleaved by weak Brønsted acids (traces of $\text{H}_2\text{O} + \mathbf{6}$), which results in the regeneration of the benzhydrylium ions **15**.

DFT calculations were carried out by Dr. Guillaume Berionni.

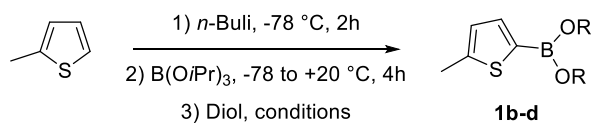
1.4.2 Synthesis and characterization of the thiophenyl-boronates **1a-d**

Synthesis of 4,4,5,5-tetramethyl-2-(5-methylthiophen-2-yl)-1,3,2-dioxaborolane (**1a**)



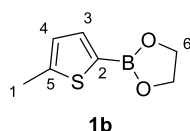
To a solution of 2-methylthiophene (2.0 mL, 21 mmol) in THF (40 mL) cooled at $-78\text{ }^{\circ}\text{C}$ was slowly added *n*-butyl lithium (2.2 M in *n*-hexane, 9.6 mL, 21 mmol) under N_2 . After 3 h, neat 2-methoxy-4,4,5,5-tetramethyl-1,3,2-dioxaborolane (3.6 mL, 22 mmol) was added slowly under N_2 and the mixture was allowed to warm to $20\text{ }^{\circ}\text{C}$ within ca. 2 h. Subsequently, a saturated NH_4Cl solution (2 mL) was poured into the reaction mixture, followed by distilled water (20 mL). The mixture was then extracted with EtOAc ($3 \times 25\text{ mL}$) and the organic layer was washed with water and brine. After removal of the organic solvents under vacuum, a yellow oil was obtained and distilled ($90\text{-}100\text{ }^{\circ}\text{C} / 0.1\text{-}0.3\text{ mbar}$) to give **1a** as a colorless oil (2.36 g, 10.5 mmol, 50 %). NMR data agree with those in the literature.^[16]

General procedure for the synthesis of **1b-d**



To a solution of 2-methylthiophene (2.0 mL, 21 mmol, 1 eq.) in THF (40 mL) cooled at $-78\text{ }^\circ\text{C}$ was slowly added *n*-butyl lithium (2.45 M in *n*-hexane, 8.6 mL, 21 mmol, 1 eq.) under N_2 . The mixture was then allowed to warm progressively to $0\text{ }^\circ\text{C}$ within 2 h. After re-cooling at $-78\text{ }^\circ\text{C}$, neat triisopropyl borate (7.5 g, 40 mmol) was added slowly under N_2 and the mixture was allowed to warm to room temperature within 4 h to give a white suspension. Subsequently, the diol (40 mmol of neopentyl glycol, ethylene glycol or catechol) dissolved in distilled Et_2O (10 mL) was added dropwise into the reaction mixture to give a clear yellowish solution, and the reaction was stirred overnight at the ambient temperature.

2-(5-Methylthiophen-2-yl)-1,3,2-dioxaborolane (**1b**)



Following the general procedure from ethylene glycol (2.23 mL, 40 mmol, 1.90 eq.), after stirring overnight, the solvent was removed under vacuum and toluene (200 mL) was added to the brown residue. The suspension was filtered over celite, and the toluene phase was dried over MgSO_4 and concentrated in vacuum to give a yellow oil. The oil was distilled ($64\text{--}65\text{ }^\circ\text{C}$, 5×10^{-3} mbar) to give **1b** as a pale yellowish solid (1.85 g, 11.0 mmol, 52 %).

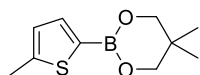
M.p.: $31\text{--}35\text{ }^\circ\text{C}$.

^1H NMR (400 MHz, CD_3CN): δ = 2.52 (s, 3H, 1-H), 4.30 (br s, 4H, 6-H), 6.90 (dq, $^3J_{\text{H4-H3}} = 3.4$ Hz, $^4J_{\text{H4-H1}} = 1.0$ Hz, 1H, 4-H), 7.41 (d, $^3J_{\text{H3-H4}} = 3.4$ Hz, 1H, 3-H) ppm.

^{13}C NMR (100 MHz, CD_3CN): δ = 15.7 (C-1), 67.4 (C-6), 128.7 (C-4), 139.3 (C-3), 149.3 (C-5) ppm. C-2 not detected.

^{11}B NMR (128 MHz, CD_3CN): δ = 29.4 (s) ppm.

5,5-Dimethyl-2-(5-methylthiophen-2-yl)-1,3,2-dioxaborinane (**1c**)

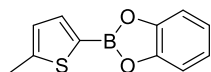


1c

Following the general procedure from neopentyl glycol (4.17 g, 40 mmol, 1.90 eq.). After stirring overnight, the reaction was hydrolyzed with water (20 mL) and extracted with EtOAc (3 × 50 mL). The organic phase was washed with brine (2 × 25 mL), dried over MgSO₄, and evaporated to give a light yellow/orange oil that solidified upon standing. Recrystallization from *n*-pentane gave **1c** (2.70 g, 12.9 mmol, 61 %).

NMR data agree with those in the literature.^[17]

2-(5-Methylthiophen-2-yl)benzo[d][1,3,2]dioxaborole (**1d**)



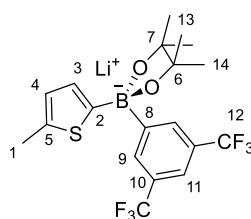
1d

Following the general procedure from catechol (3.29 mL, 40 mmol, 1.90 eq.). After stirring overnight, the reaction was hydrolyzed with water (20 mL) and extracted with EtOAc (3 × 50 mL). The organic phase was washed with brine (2 × 25 mL), dried over MgSO₄, and evaporated to give a light yellow/orange oil that solidified upon standing. Recrystallization from *n*-pentane gave **1d** (3.90 g, 18 mmol, 86 %).

NMR data agree with those in the literature.^[18]

1.4.3 Synthesis of the trifluoromethylated BACs 3-4

Synthesis of 3a-Li⁺



3a-Li⁺

A flame-dried Schlenk flask flushed with nitrogen was charged with distilled Et₂O (7.5 mL) and with 1-bromo-3,5-bis(trifluoromethyl)benzene (0.65 g, 2.2 mmol). After cooling at –78 °C, *n*-butyl lithium (2.5 M in *n*-hexane, 0.94 mL, 2.4 mmol) was added dropwise. The mixture was then allowed to warm progressively to 0 °C within 2 h and the lithium reagent **2** was formed in situ (brown-yellow solution). After re-cooling at –78 °C, neat **1a** (0.50 g, 2.2 mmol) was added dropwise under fast stirring and the pale-yellow solution was then allowed to warm to 20 °C within 4 h whilst a white solid precipitated. The solid was filtrated under nitrogen and washed three times with distilled Et₂O (3 × 20 mL). After drying overnight under high-vacuum (10^{–3} mbar) the borate **3a-Li⁺** was obtained as a colorless powder (922 mg, 2.07 mmol, 94 %).

Mp: > 220 °C (from Et₂O, dec.).

¹H NMR (400 MHz, CD₃CN): δ = 0.92 and 1.16 (2 × s, 2 × 6H, 13-H and 14-H), 2.37 (s, 3H, 1-H), 6.37 (d, ³J_{H3-H4} = 3.1 Hz, 1H, 3-H), 6.48-6.49 (m, 1H, 4-H), 7.56 (br s, 1H, 11-H), 8.07 (br s, 2H, 9-H) ppm.

¹³C NMR (100 MHz, CD₃CN): δ = 15.6 (C-1), 26.8 and 27.1 (C-13 and C-14), 80.1 (C-6 and C-7), 118.3 (sept, ³J_{C,F} = 4.1 Hz, C-11), 126.4 (q, ¹J_{C,F} = 271.6 Hz, C-12), 126.5 (C-4), 129.0 (q, ²J_{C,F} = 31.1 Hz, C-10), 129.2 (C-3), 133.4 (q, ³J_{C,F} = 1.6 Hz, C-9), 139.1 (C-5) ppm. C-2 and C-8 were not detected.^[19]

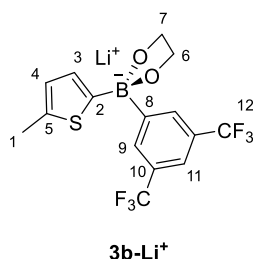
¹⁹F NMR (376 MHz, CD₃CN): δ = –62.7 (s) ppm.

¹¹B NMR (128 MHz, CD₃CN): δ = 4.6 (s) ppm.

HRMS (ESI[–]) *m/z* calcd. for C₁₉H₂₀BF₆O₂S[–] (M – Li⁺): 437.1187; found: 437.1191.

IR (ATR): $\tilde{\nu}$ 2978, 1613, 1461, 1369, 1276, 1161, 1144, 1124, 1103, 1004, 991, 917, 887, 840, 806, 769, 681 cm^{–1}.

Synthesis of **3b-Li⁺**



A flame-dried Schlenk flask flushed with nitrogen was charged with distilled Et₂O (8.0 mL) and with 1-bromo-3,5-bis(trifluoromethyl)benzene (0.70 g, 2.4 mmol). After cooling at $-78\text{ }^{\circ}\text{C}$, *n*-butyl lithium (2.5 M in *n*-hexane, 0.95 mL, 2.4 mmol) was added dropwise over 5 min. The mixture was then allowed to warm progressively to $0\text{ }^{\circ}\text{C}$ within 2 h and **2** was formed in situ. After re-cooling at $-78\text{ }^{\circ}\text{C}$, an ethereal solution (5 mL) of **1b** (0.40 g, 2.4 mmol) was added dropwise under fast stirring and the orange solution was allowed to warm to $20\text{ }^{\circ}\text{C}$ within 5 h whilst a beige suspension was formed. Subsequently, half of the solvent was removed under vacuum. The white solid which precipitated was filtrated under nitrogen and washed three times with distilled Et₂O ($3 \times 25\text{ mL}$). After drying overnight under high vacuum (10^{-3} mbar) the borate (**3b-Li⁺**)·(Et₂O)_{0.75} was obtained as a colorless powder (780 mg, 74 %).

¹H NMR (400 MHz, CD₃CN): δ = 1.13 (t, J = 7.0 Hz, $0.75 \times 6\text{H}$, Et₂O), 2.41 (d, J = 1.1 Hz, 3H, 1-H), 3.42 (q, J = 7.0 Hz, $0.75 \times 4\text{H}$, Et₂O), 3.58-3.59 and 3.68-3.70 (2 m, $2 \times 2\text{H}$, 6- H), 6.45 (d, $^3J_{\text{H3-H4}}$ = 3.1 Hz, 1H, 3-H), 6.55-6.56 (m, 1H, 4-H), 7.64 (br s, 1H, 11-H), 8.03 (br s, 2H, 9-H) ppm.

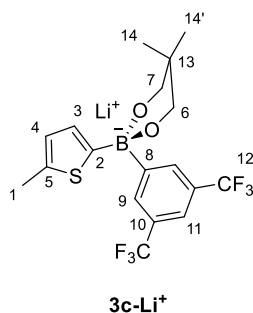
¹³C NMR (100 MHz, CD₃CN): δ = 15.7 (C-1), 16.0 (Et₂O), 65.1 (C-6), 66.7 (Et₂O), 119.4 (sept, $^3J_{\text{C,F}}$ = 4.0 Hz, C-11), 126.3 (q, $^1J_{\text{C,F}}$ = 271.7 Hz, C-12), 126.7 (C-4), 129.5 (q, $^2J_{\text{C,F}}$ = 31.4 Hz, C-10), 129.6 (C-3), 134.0 (q, $^3J_{\text{C,F}}$ = 1.6 Hz, C-9), 139.7 (C-5) ppm. C-2 and C-8 were not detected.

¹⁹F NMR (376 MHz, CD₃CN): δ = -62.8 (s) ppm.

¹¹B NMR (128 MHz, CD₃CN): δ = 5.4 (s) ppm.

IR (ATR): $\tilde{\nu}$ 2975, 2924, 2870, 1611, 1468, 1449, 1365, 1273, 1218, 1149, 1114, 1049, 938, 898, 891, 834, 803, 759, 709, 680 cm⁻¹.

Synthesis of 3c-Li⁺



A flame-dried Schlenk flask flushed with nitrogen was charged with distilled Et₂O (8 mL) and with 1-bromo-3,5-bis(trifluoromethyl)benzene (0.59 g, 2.0 mmol). After cooling at $-78\text{ }^{\circ}\text{C}$, *n*-butyl lithium (2.4 M in hexane, 0.83 mL, 2.0 mmol) was added dropwise over 5 min. The mixture was then allowed to warm progressively to $0\text{ }^{\circ}\text{C}$ within 2 h to form **2** in situ. After re-cooling at $-78\text{ }^{\circ}\text{C}$, an ethereal solution (5 mL) of 5-methylthiophen-2-yl neopentyl boronic ester **1c** (0.42 g, 2.0 mmol) was added under stirring and the yellowish solution was then allowed to warm to $20\text{ }^{\circ}\text{C}$ within 4 h whilst a white solid was formed. The solid was filtrated under nitrogen and washed with distilled Et₂O ($3 \times 25\text{ mL}$). After drying overnight under high-vacuum (10^{-3} mbar) the borate **3c-Li⁺** was obtained as a colorless powder (372 mg, 0.865 mmol, 43 %).

Mp: 258-260 $^{\circ}\text{C}$ (from Et₂O, dec.).

¹H NMR (400 MHz, CD₃CN): δ = 0.73 and 0.83 (2 s, $2 \times 3\text{H}$, 14-H and 14'-H), 2.36 (s, 3H, 1-H), 3.18 and 3.44 (2 d, each 2J = 9.9 Hz, $2 \times 2\text{H}$, 6-H and 7-H), 6.46 (d, $^3J_{\text{H3-H4}}$ = 3.0 Hz, 1H, 3-H), 6.50-6.51 (m, 1H, 4-H), 7.51 (br s, 1H, 11-H), 7.97 (br s, 2H, 9-H) ppm.

¹³C NMR (100 MHz, CD₃CN): δ = 15.8 (C-1), 23.6 and 23.7 (C-14 and C-14'), 34.0 (C-13), 73.5 (C-6 and C-7), 119.2 (sept, $^3J_{\text{C,F}}$ = 3.7 Hz, C-11), 126.3 (q, $^1J_{\text{C,F}}$ = 271.8 Hz, C-12), 126.8 (C-4), 129.4 (C-3), 129.7 (q, $^2J_{\text{C,F}}$ = 31.3 Hz, C-10), 134.2 (q, $^3J_{\text{C,F}}$ = 1.6 Hz, C-9), 139.8 (C-5) ppm. C-2 and C-8 were not detected.

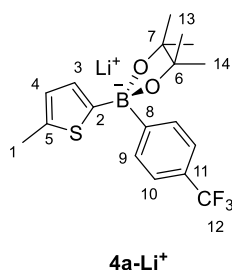
¹⁹F NMR (376 MHz, CD₃CN): δ = -62.7 (s) ppm.

¹¹B NMR (128 MHz, CD₃CN): δ = 2.0 (s) ppm.

HRMS (ESI⁻) m/z calcd. for C₁₈H₁₈BF₆O₂S⁻ (M – Li⁺): 423.1030; found: 423.1026.

IR (ATR): $\tilde{\nu}$ 2952, 2864, 1612, 1470, 1399, 1367, 1276, 1218, 1158, 1124, 1092, 1042, 953, 857, 899, 818, 760 cm⁻¹.

Synthesis of 4a-Li⁺



In a flame-dried Schlenk flask flushed under nitrogen, *n*-butyl lithium (2.45 M in hexane, 1.9 mL, 4.7 mmol) was added dropwise to a solution of 1-bromo-4-(trifluoromethyl)benzene (1.0 g, 4.4 mmol) in distilled Et₂O (20 mL) at $-78\text{ }^{\circ}\text{C}$. The mixture was then allowed to warm progressively to $0\text{ }^{\circ}\text{C}$ within 3 h and the lithium reagent **2'** was formed in situ (yellow solution). After re-cooling at $-78\text{ }^{\circ}\text{C}$, neat **1a** (1.0 g, 4.5 mmol) was added and the solution was stirred for 5 h (temperature gradually increased to $20\text{ }^{\circ}\text{C}$). Half of the solvent was removed under a flow of nitrogen and a heterogeneous orange suspension was obtained and filtered under nitrogen. The white powder was washed with an Et₂O/CH₃CN (9/1) mixture (3 × 30 mL) and dried overnight at a vacuum of 10^{-3} mbar, affording **4a-Li⁺** as a colorless solid (1.53 g, 4.07 mmol, 92 %).

Mp: $> 230\text{ }^{\circ}\text{C}$ (from Et₂O/MeCN, dec.)

¹H NMR (400 MHz, CD₃CN + 1 drop of DMSO-*d*₆): δ = 0.89 and 1.07 (2 × s, 2 × 6H, 13-H and 14-H), 2.34 (d, $^4J_{\text{H1-H4}}$ = 1.0 Hz, 3H, 1-H), 6.41 (d, $^3J_{\text{H3-H4}}$ = 3.0 Hz, 1H, 3-H), 6.45 (dq, $^3J_{\text{H4-H3}}$ = 3.0 Hz, $^4J_{\text{H4-H1}}$ = 1.0 Hz, 1H, 4-H), 7.30 (d, J = 7.9 Hz, 2H, 10-H), 7.64 (d, J = 7.8 Hz, 2H, 9-H) ppm.

¹³C NMR (100 MHz, CD₃CN + 1 drop of DMSO-*d*₆): δ = 15.7 (C-1), 27.2 and 27.3 (2 × s, C-13 and C-14), 79.3 (C-6 and C-7), 123.3 (q, $^3J_{\text{C,F}}$ = 3.9 Hz, C-10), 125.5 (q, $^2J_{\text{C,F}}$ = 30.7 Hz, C-11), 126.2 (C-4), 127.1 (q, $^1J_{\text{C,F}}$ = 270.3 Hz, C-12), 127.2 (C-3), 133.2 (C-9), 137.8 (C-5), 164.8 (C-2), 169.7 (C-8) ppm.

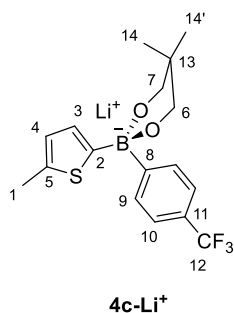
¹⁹F NMR (376 MHz, CD₃CN + 1 drop of DMSO-*d*₆): δ = -62.0 (s) ppm.

¹¹B NMR (128 MHz, CD₃CN + 1 drop of DMSO-*d*₆): δ = 4.6 (s) ppm.

HRMS (ESI⁻) *m/z* calcd. for C₁₈H₂₁BF₃O₂S⁻ (M – Li⁺): 369.1313; found: 369.1306.

IR (ATR): $\tilde{\nu}$ 2985, 1578, 1491, 1480, 1440, 1388, 1375, 1367, 1213, 1150, 1080, 1025, 1003, 981, 938, 902, 872, 825, 812, 791, 690 cm⁻¹.

Synthesis of 4c-Li⁺



In a flame-dried Schlenk flask flushed under nitrogen, *n*-butyl lithium (2.45 M in hexane, 1.5 mL, 3.8 mmol) was added dropwise to a solution of 1-bromo-4- trifluoromethylbenzene (0.80 g, 3.6 mmol) in distilled Et₂O (10 mL) at -78°C . The mixture was allowed to warm to -30°C within 2 h and **2'** was formed in situ. After re-cooling at -78°C , an ethereal solution (10 mL) of 5-methylthiophen-2-yl neopentyl boronic ester **1c** (0.75 g, 3.6 mmol) was added dropwise and the mixture was stirred for 2 h at -78°C and allowed to warm to 0°C within 5 h, yielding a pale-yellow suspension with a white precipitate. Filtration under nitrogen, and washing of the solid with 50 mL of Et₂O/CH₃CN (1/1) mixtures (5×10 mL) and drying overnight (under vacuum, 10^{-3} mbar) afforded (**4c-Li⁺**)·(CH₃CN)_{0.6} as a colorless solid (1.09 g, 79%).

¹H NMR (400 MHz, CD₃CN + 1 drop of DMSO-*d*₆): δ = 0.74 and 0.80 (2 s, $2 \times 3\text{H}$, 14-H and 14'-H), 1.96 (s, $0.6 \times 6\text{H}$, CH₃CN), 2.34 (d, $^4J_{\text{H1-H4}} = 1.0$ Hz, 3H, 1-H), 3.18 and 3.39 (2 d, each $^2J = 9.9$ Hz, $2 \times 2\text{H}$, 6-H and 7-H), 6.41 (d, $^3J_{\text{H3-H4}} = 3.1$ Hz, 1H, 3-H), 6.46-6.48 (m, 1H, 4-H), 7.31 (d, $J = 8.1$ Hz, 2H, 10-H), 7.60 (d, $J = 8.1$ Hz, 2H, 9-H) ppm.

¹³C NMR (100 MHz, CD₃CN + 1 drop of DMSO-*d*₆): δ = 15.8 (C-1), 24.0 and 24.2 (C-14 and C-14'), 34.0 (C-13), 73.8 (C-6 and C-7), 118.7 (CH₃CN), 123.5 (q, $^3J_{\text{C,F}} = 4.0$ Hz, C-10), 125.8 (q, $^2J_{\text{C,F}} = 30.6$ Hz, C-11), 126.3 (C-4), 127.2 (q, $^1J_{\text{C,F}} = 270.5$ Hz, C-12), 127.5 (C-3), 133.7 (C-9), 138.2 (C-4), 163.7 (C-8, detected by HMBC) ppm. C-2 was not detected.

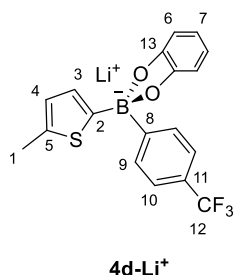
¹⁹F NMR (376 MHz, CD₃CN + 1 drop of DMSO-*d*₆): δ = -61.1 (s) ppm.

¹¹B NMR (128 MHz, CD₃CN + 1 drop of DMSO-*d*₆): δ = 2.4 (s) ppm.

HRMS (ESI⁻) *m/z* calcd. for C₁₇H₁₉BF₃O₂S⁻ (M – Li⁺): 355.1156; found: 355.1158.

IR (ATR): $\tilde{\nu}$ 2905, 2853, 1455, 1398, 1359, 1325, 1211, 1151, 1114, 1102, 1083, 1061, 1038, 1021, 955, 909, 888, 871, 822, 805 cm⁻¹.

Synthesis of 4d-Li⁺



A flame-dried Schlenk flask flushed with nitrogen was charged with 1-bromo-4-trifluoromethylbenzene (0.78 g, 3.5 mmol) and distilled Et₂O (10 mL) and cooled to $-78\text{ }^{\circ}\text{C}$. *n*-Butyl lithium (2.45 M in hexane, 1.4 mL, 3.5 mmol) was added dropwise to this solution and the mixture was then allowed to warm progressively to $-30\text{ }^{\circ}\text{C}$ within 2 h and **2'** was formed in situ. After re-cooling at $-78\text{ }^{\circ}\text{C}$, 5-methylthiophen-2-yl catechol boronic ester **1d** (0.75 g, 3.5 mmol) dissolved in 10 mL of distilled Et₂O was added dropwise and the solution was stirred for 2 h at $-78\text{ }^{\circ}\text{C}$ and then allowed to warm to $20\text{ }^{\circ}\text{C}$ within 3 h. A colorless solid precipitated, was filtrated under nitrogen, washed with distilled Et₂O ($3 \times 25\text{ mL}$) and dried overnight under vacuum (10^{-3} mbar) to afford (**4d-Li⁺**)·(OEt₂)_{0.6} as a colorless crystalline solid (823 mg, 58 %).

¹H NMR (400 MHz, CD₃CN): δ = 1.13 (t, J = 7.0 Hz, $0.6 \times 6\text{ H}$, Et₂O), 2.41 (s, 3H, 1-H), 3.41 (q, J = 7.0 Hz, $0.6 \times 4\text{ H}$, Et₂O), 6.41-6.47 (m, 4H, 6-H, 7-H), 6.58-6.60 (m, 2H, 3-H and 4-H), 7.47 (d, J = 7.5 Hz, 2H, 10-H), 7.69 (d, J = 7.5 Hz, 2H, 9-H) ppm.

¹³C NMR (100 MHz, CD₃CN): δ = 15.6 (C-1), 16.0 (Et₂O), 66.7 (Et₂O), 109.4 and 118.4 (C-6 and C-7), 124.2 (q, $^3J_{\text{C,F}}$ = 3.9 Hz, C-10), 126.7 (C-4), 126.8 (q, $^1J_{\text{C,F}}$ = 270.5 Hz, C-12), 127.8 (q, $^2J_{\text{C,F}}$ = 31.1 Hz, C-11), 129.4 (C-3), 133.5 (C-9), 140.2 (C-5), 155.5 (C-13), 160.6 (C-8, detected by HMBC) ppm. C-2 was not detected.

¹⁹F NMR (376 MHz, CD₃CN): δ = -62.4 (s) ppm.

¹¹B NMR (128 MHz, CD₃CN): δ = 9.9 (s) ppm.

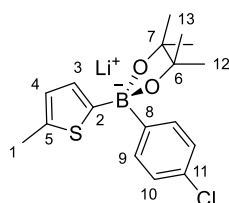
HRMS (ESI⁻) m/z calcd. for C₁₈H₁₃BF₃O₂S⁻ (M – Li⁺): 361.0687; found: 361.0653.

IR (ATR) $\tilde{\nu}$ 2976, 1609, 1486, 1394, 1360, 1322, 1239, 1216, 1158, 1114, 1096, 1061, 1017, 922, 818, 734 cm⁻¹.

General procedure for synthesis of boronate complex 8-12

To a solution of 2-methylthiophene (1.0 equiv.) in dry Et₂O (10 mL) was added *n*-butyllithium (2.35 M in *n*-hexane) dropwise at -78 °C under N₂. The reaction mixture was allowed to warm slowly to -20 °C within 2 h. Subsequently an ethereal solution (5 mL) of the aryl pinacol ester **6b-f** was added dropwise. The clear solution was then allowed to warm progressively to 20 °C within 5 h whilst a solid precipitated. If precipitation did not take place spontaneously, the solvent was slowly evaporated under the vacuum until the precipitation commenced. The solid was filtrated under N₂, washed with Et₂O or CH₃CN and recrystallized from CH₃CN, THF or Et₂O.

Synthesis of 8-Li⁺



8-Li⁺

According to GP from 2-methylthiophene (0.75 mL, 7.7 mmol), *n*-butyl lithium (3.3 mL, 7.7 mmol) and 4-(4,4,5,5-tetramethyl-1,3,2-dioxaborolan-2-yl)chlorobenzene **6b** (1.9 g, 7.7 mmol). The solid was filtrated under N₂, washed with Et₂O (3 × 10 mL) and with THF (5 mL) to give **8-Li⁺** as a colorless powder (1.59 g, 4.64 mmol, 60%). Even after drying the solid under a vacuum of 10⁻³ mbar for 24 h, traces of THF (< 5%) could not be removed.

¹H NMR (400 MHz, CD₃CN + 1 drop of DMSO-*d*₆): δ = 0.89 and 1.05 (2 s, 2 × 6H, 12-H and 13-H), 2.33 (d, ⁴J_{H1-H4} = 1.0 Hz, 3H, 1-H), 6.40 (d, ³J_{H3-H4} = 3.0 Hz, 1H, 3-H), 6.42-6.44 (m, 1H, 4-H), 6.97-7.00 (m, 2H, 9-H), 7.44 (d, *J* = 8.1 Hz, 2H, 10-H) ppm.

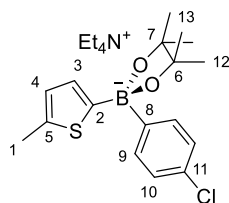
¹³C NMR (100 MHz, CD₃CN + 1 drop of DMSO-*d*₆): δ = 15.7 (C-1), 26.6 and 27.4 (C-12 and C-13), 79.2 (C-6 and C-7), 126.2 (C-4), 126.6 (C-9), 127.1 (C-3), 129.3 (C-11), 134.8 (C-10), 137.6 (C-5), 161.7 (br s, C-8, detected by HMBC), 164.7 (br s, C-2, detected by HMBC) ppm.

¹¹B NMR (128 MHz, CD₃CN + 1 drop of DMSO-*d*₆): δ = 4.9 (s) ppm.

HRMS (ESI⁻): *m/z* calc. for C₁₇H₂₁BClO₂S⁻ (M – Li⁺): 335.1049; found: 335.1044.

IR (ATR): ν̃ 2985, 1578, 1491, 1480, 1440, 1388, 1375, 1367, 1213, 1150, 1080, 1025, 1003, 981, 902, 825, 812, 786 cm⁻¹.

Synthesis of 8-Et₄N⁺



8-Et₄N⁺

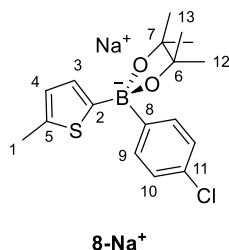
To a solution of **8-Li⁺** (0.20 g, 0.58 mmol) in dry THF (15 mL) at 20 °C under N₂ was added solid tetraethylammonium chloride (0.13 g, 0.60 mmol). After 1 h, Et₂O (10 mL) was added, and a colorless solid precipitated. The solid was filtrated under N₂ and washed with Et₂O (5 × 20 mL) to give a colorless powder (242 mg, 0.520 mmol, 89%).

¹H NMR (400 MHz, CD₃CN): δ = 0.92 and 1.09 (2 × s, 2 × 6H, 12-H and 13-H), 1.20 (tt, $J_{\text{H,H}} = 7.3$ Hz, $J_{\text{H,N}} = 1.9$ Hz, 12H, N⁺CH₂CH₃), 2.35 (d, $^4J_{\text{H1-H4}} = 1.1$ Hz, 3H, 1-H), 3.15-3.21 (q, $J_{\text{H,H}} = 7.3$ Hz, 8H, N⁺CH₂CH₃), 6.41 (d, $^3J_{\text{H3-H4}} = 3.1$ Hz, 1H, 3-H), 6.45 (dd, $^3J_{\text{H4-H3}} = 3.1$ Hz, $^4J_{\text{H4-H1}} = 1.1$ Hz, 1H, 4-H), 7.02 (d, $J = 8.3$ Hz, 2H, 9-H), 7.45 (d, $J = 8.2$ Hz, 2H, 10-H) ppm.

¹³C NMR (100 MHz, CD₃CN): δ = 8.2 (s, N⁺CH₂CH₃), 15.6 (C-1), 27.1 and 27.2 (C-12 and C-13), 53.5 (t, $J_{\text{C,N}} = 3.1$ Hz, N⁺CH₂CH₃), 79.6 (C-6 and C-7), 126.3 (C-4), 126.7 (C-9), 128.2 (C-3), 129.7 (C-11), 135.1 (C-10), 138.3 (C-5) ppm (C-2 and C-8 not detected).

¹¹B NMR (128 MHz, CD₃CN): δ = 4.6 (s) ppm.

Synthesis of 8-Na⁺



To a solution of *n*-butyl sodium^[20] (0.25 g, 3.1 mmol) in dry THF (15 mL) at -78 °C under N₂ was added neat 2-methylthiophene (0.30 mL, 3.1 mmol) dropwise. After 2 h at this temperature, the color of the solution turned light red (formation of **5''**) and an ethereal solution (10 mL) of 4-(4,4,5,5-tetramethyl-1,3,2-dioxaborolan-2-yl)chlorobenzene **6b** (745 mg, 3.12 mmol) was added dropwise. The pale orange solution was then allowed to warm progressively to 20 °C within 5 h whilst an orange solid precipitated. The solid was filtrated under N₂, washed with Et₂O and *n*-pentane to give (**8-Na⁺**)·(Et₂O)_{0.67} as a light orange powder (532 mg, 42%). Even after drying the solid under a vacuum of 10⁻³ mbar for 24 h, traces of Et₂O could not be removed.

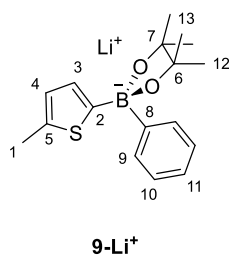
¹H NMR (400 MHz, CD₃CN): δ = 0.89 and 1.05 (2 × s, 2 × 6H, 12-H and 13-H), 1.12 (t, *J* = 7.0 Hz, 0.67 × 6H, Et₂O), 2.34 (s, 3H, 1-H), 3.42 (q, *J* = 7.0 Hz, 0.67 × 4H, Et₂O), 6.37 and 6.44 (2 × br s, 2H, 3-H and 4-H), 6.99-7.01 (m, 2H, 9-H), 7.42 (d, *J* = 8.0 Hz, 2H, 10-H) ppm.

¹³C NMR (100 MHz, CD₃CN): δ = 15.7 (C-1), 27.4 and 27.5 (C-12 and C-13), 79.2 (C-6 and C-7), 126.3 (C-4), 126.8 (C-9), 127.3 (C-3), 129.3 (C-11), 134.8 (C-10) ppm (C-2, C-5 and C-8 not detected).

¹¹B NMR (128 MHz, CD₃CN): δ = 4.6 (s) ppm.

IR (ATR): $\tilde{\nu}$ 2980, 2956, 2871, 1575, 1481, 1446, 1383, 1373, 1361, 1213, 1158, 1146, 1081, 1076, 1042, 1021, 979, 948, 903, 863, 832, 806, 788, 701, 690 cm⁻¹.

Synthesis of 9-Li⁺



According to GP from 2-methylthiophene (0.50 mL, 5.2 mmol), *n*-butyl lithium (2.3 mL, 5.3 mmol) and phenyl pinacol boronic ester **6c** (1.0 g, 5.0 mmol). The borate **9-Li⁺** was obtained as a colorless solid (928 mg, 3.01 mmol, 60%) after recrystallization from THF/Et₂O (1/1) mixtures and CH₃CN/Et₂O (1/1) mixtures (10 mL each).

Mp: 180-190°C (from THF/Et₂O/CH₃CN, dec.)

¹H NMR (400 MHz, CD₃CN + 1 drop of DMSO-*d*₆): δ = 0.91, 1.05 (2 s, 2 × 6H, 12-H and 13-H), 2.33 (d, ⁴J_{H1-H4} = 0.7 Hz, 3H, 1-H), 6.41-6.43 (m, 2H, 3-H and 4-H), 6.83-6.86 (m, 1H, 11-H), 6.97-7.01 (m, 2H, 10-H), 7.45 (d, *J* = 6.5 Hz, 2H, 9-H) ppm.

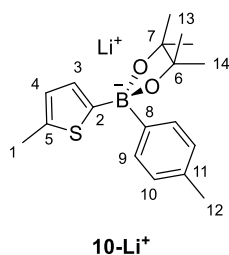
¹³C NMR (100 MHz, CD₃CN + 1 drop of DMSO-*d*₆): δ = 15.7 (C-1), 27.4 (C-12 and C-13), 79.1 (C-6 and C-7), 124.0 (C-10), 126.1 (C-4), 126.8 (C-3), 126.9 (C-9), 133.1 (C-8), 137.3 (C-5), 162.8 (br s, C-8, detected by HMBC), 166.0 (br s, C-2, detected by HMBC) ppm.

¹¹B NMR (128 MHz, CD₃CN + 1 drop of DMSO-*d*₆): δ = 4.7 (s) ppm.

HRMS (ESI⁻): *m/z* calc. for C₁₇H₂₂BO₂S⁻ (M – Li⁺): 301.1439, found: 301.1449.

IR (ATR): $\tilde{\nu}$ 2968, 1599, 1386, 1363, 1214, 1147, 1085, 1023, 976, 942, 892, 861, 797, 751, 712, 701 cm⁻¹.

Synthesis of **10-Li⁺**



According to GP from 2-methylthiophene (0.50 mL, 5.2 mmol), *n*-butyl lithium (2.3 mL, 5.3 mmol) and **6d** (1.1 g, 5.1 mmol): The compound **10-Li⁺** was obtained as a white powder (1.09 g, 3.38 mmol, 66%) after recrystallization from THF/Et₂O (1/1) mixtures and CH₃CN/Et₂O (1/1) mixtures (10 mL each).

Mp: > 230 °C (from THF/Et₂O/CH₃CN, dec.)

¹H NMR (400 MHz, CD₃CN): δ = 0.96 and 1.12 (2 s, 2 × 6H, 13-H and 14-H), 2.23 (s, 3H, 12-H), 2.37 (d, ⁴J_{H1-H4} = 1.2 Hz, 3H, 1-H), 6.44 (d, ³J_{H3-H4} = 3.1 Hz, 1H, 3-H), 6.47-6.48 (m, 1H, 4-H), 6.87-6.89 (m, 2H, 9-H), 7.36 (d, *J* = 7.8 Hz, 2H, 10-H) ppm.

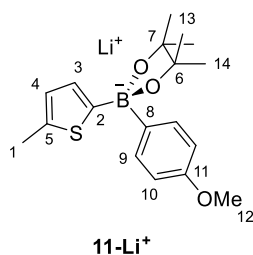
¹³C NMR (100 MHz, CD₃CN): δ = 15.7 (C-1), 21.7 (C-12), 27.1 and 27.2 (C-13 and C-14), 79.7 (C-6 and C-7), 126.3 (C-4), 127.8 (C-9), 128.8 (C-3), 133.4 (C-11), 133.7 (C-10), 138.5 (C-5), 157.1 (C-8, detected by HMBC) ppm. C-2 was not detected.

¹¹B NMR (128 MHz, CD₃CN): δ = 5.1 (s) ppm.

HRMS (ESI⁻): *m/z* calc. for C₁₈H₂₄BO₂S⁻ (M – Li⁺): 315.1596; found: 315.1587.

IR (ATR): $\tilde{\nu}$ 3062, 2965, 2919, 1445, 1429, 1384, 1372, 1362, 1212, 1153, 1086, 1026, 1002, 980, 940, 887, 817, 798, 753, 710 cm⁻¹.

Synthesis of 11-Li⁺



According to GP from 2-methylthiophene (0.40 mL, 4.1 mmol), *n*-butyl lithium (1.7 mL, 4.0 mmol) and **6e** (0.94 g, 4.0 mmol). The solid was recrystallized from CH₃CN/Et₂O (1/1) mixtures (2 × 5 mL) to give **11-Li⁺** as a colorless solid (884 mg, 2.61 mmol, 64%).

Mp: 235-240 °C (from CH₃CN/Et₂O, dec.)

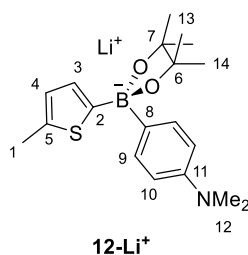
¹H NMR (400 MHz, CD₃CN): δ = 0.93 and 1.06 (2 s, 2 × 6H, 13-H and 14-H), 2.35 (s, 3 H, 1-H), 3.69 (s, 3H, 12-H), 6.44 (br s, 2H, 3-H, 4-H), 6.60-6.63 (m, 2H, 9-H), 7.36 (d, J = 8.4 Hz, 2H, 10-H) ppm.

¹³C NMR (100 MHz, CD₃CN): δ = 15.7 (C-1), 27.36 and 27.40 (C-13 and C-14), 55.7 (C-12), 79.2 (C-6 and C-7), 112.6 (C-9), 126.1 (C-4), 127.0 (C-3), 134.0 (C-10), 137.5 (C-5), 153.5 (C-8, detected by HMBC), 157.7 (C-11), 166.2 (C-2, detected by HMBC) ppm.

¹¹B NMR (128 MHz, CD₃CN): δ = 4.9 (s) ppm.

IR (ATR): $\tilde{\nu}$ 2987, 1594, 1503, 1460, 1440, 1386, 1364, 1278, 1242, 1212, 1147, 1074, 1014, 980, 943, 898, 869, 831, 800, 776, 704 cm⁻¹.

Synthesis of 12-Li⁺



According to GP from 2-methylthiophene (0.40 mL, 4.1 mmol), *n*-butyl lithium (1.8 mL, 4.2 mmol) and *N,N*-dimethyl-4-aniline pinacol boronic ester **6f** (1.0 g, 4.1 mmol). The product **12-Li⁺** was obtained as a pale grey solid (711 mg, 2.02 mmol, 49%) after recrystallization from THF/Et₂O (1/1) mixtures (2 × 10 mL).

Mp: 235-240°C (Et₂O, decomp.)

¹H NMR (400 MHz, CD₃CN): δ = 0.98 and 1.10 (2 s, 2 × 6H, 13-H and 14-H), 2.37 (br s, 3H, 1-H), 2.81 (s, 6H, 12-H), 6.46-6.49 (m, 2H, 3-H and 4-H), 6.58 (d, *J* = 8.6 Hz, 2H, 9-H), 7.31 (d, *J* = 8.6 Hz, 2H, 10-H) ppm.

¹³C NMR (100 MHz, CD₃CN): δ = 15.7 (C-1), 27.2 and 27.3 (C-13 and C-14), 42.1 (C-12), 79.7 (C-6 and C-7), 113.4 (C-9), 126.3 (C-4), 128.5 (C-3), 134.4 (C-10), 138.3 (C-5), 149.7 (C-11) ppm; C-2 and C-8 were not detected.

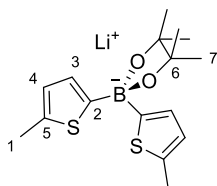
¹¹B NMR (128 MHz, CD₃CN): δ = 5.2 ppm.

HRMS (FAB⁻) *m/z* calcd. for C₁₉H₂₇BNO₂S⁻ (M – Li⁺): 344.1859; found: 344.1854.

IR (ATR): $\tilde{\nu}$ 2984, 2965, 2919, 1602, 1513, 1444, 1363, 1341, 1213, 1156, 1146, 1079, 1013, 983, 940, 817, 797 cm⁻¹.

Synthesis of boronate complexes 13-14

Synthesis of 13-Li⁺



13-Li⁺

A flame-dried Schlenk flask flushed with nitrogen was charged with 2-methylthiophene (2.00 g, 20.4 mmol) and distilled Et₂O (50 mL) and cooled to $-78\text{ }^{\circ}\text{C}$. *n*-Butyl lithium (9.50 mL, 2.15 M in hexane, 20.4 mmol) was added dropwise to this solution and the mixture was then allowed to warm progressively to $0\text{ }^{\circ}\text{C}$ within 3 h to form **5**. After re-cooling at $-78\text{ }^{\circ}\text{C}$, neat 2-methoxy-4,4,5,5-tetramethyl-1,3,2-dioxaborolane **7** (1.61 g, 10.2 mmol) was added dropwise and the orange solution was stirred for 5 h (temperature increased to $20\text{ }^{\circ}\text{C}$). A white-orange solid precipitated, was filtrated under nitrogen and washed with distilled Et₂O ($3 \times 30\text{ mL}$). The product was recrystallized from a Et₂O/CH₃CN (1:1) mixture (40 mL), again filtrated under nitrogen, washed with distilled Et₂O ($2 \times 30\text{ mL}$) and dried overnight (at 10^{-3} mbar) to afford **13-Li⁺** as a colorless crystalline solid (1.60 g, 4.90 mmol, 48%).

Mp: (Et₂O/CH₃CN): $197\text{--}199\text{ }^{\circ}\text{C}$

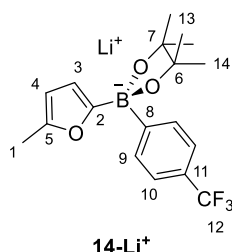
¹H NMR (400 MHz, CD₃CN): $\delta = 1.07$ (s, 12H, 7-H), 2.38 (s, 6H, 1-H), $6.50\text{--}6.51$ (m, 2H, 4-H), 6.58 (d, $^3J_{\text{H3-H4}} = 3.1\text{ Hz}$, 2H, 3-H) ppm.

¹³C NMR (100 MHz, CD₃CN): $\delta = 15.7$ (C-1), 27.2 (C-7), 79.9 (C-6), 126.2 (C-3), 128.4 (C-4), 138.3 (C-5) ppm. C-2 not detected.

¹¹B NMR (128 MHz, CD₃CN): $\delta = 4.1$ (s) ppm.

HRMS (ESI⁻): m/z calcd. for C₁₆H₂₂BO₂S₂⁻ (M – Li⁺): 321.1160; found: 321.1159.

Synthesis of **14-Li⁺**



A flame-dried Schlenk flask flushed with nitrogen was charged with 2-methylfuran (0.30 g, 3.7 mmol) and Et₂O (10 mL) and then cooled to −78 °C. *n*-Butyl lithium (1.8 mL, 2.15 M in hexane, 3.9 mmol, 1.1 equiv.) was added dropwise to this solution and the mixture was then allowed to warm progressively to 0 °C within 2 h to form **5'**. After re-cooling at −78 °C, an ethereal solution (10 mL) of 4-(trifluoromethyl)phenyl pinacol boronic ester **6a** (1.0 g, 3.7 mmol) was added dropwise and the bright orange solution was stirred for 2 h at −78 °C and then allowed to warm to 20 °C within 3 h. A colorless solid precipitated, was filtrated under nitrogen and washed with distilled Et₂O (3 × 25 mL). The product was recrystallized in a Et₂O/THF (1:1) mixture (2.5 mL), again filtrated under nitrogen, washed with distilled Et₂O (2 × 10 mL) and dried overnight (at 10^{−3} mbar) to afford **14-Li⁺** as a colorless crystalline solid (702 mg, 1.95 mmol, 53%).

Mp: 215-220 °C (from Et₂O/THF)

¹H NMR (400 MHz, CD₃CN): δ = 0.97 and 1.05 (2 s, 2 × 6H, 13-H and 14-H), 2.17 (d, ⁴J_{H1-H4} = 1.0 Hz, 3H, 1-H), 5.76-5.79 (m, 2H, 3-H and 4-H), 7.37 (d, *J* = 7.8 Hz, 2H, 10-H), 7.68 (d, *J* = 7.7 Hz, 2H, 9-H) ppm.

¹³C NMR (100 MHz, CD₃CN): δ = 13.9 (C-1), 26.3 and 26.7 (C-13 and C-14), 80.1 (C-6 and C-7), 107.5 (C-4), 111.0 (C-3), 123.8 (q, 3*J*_{C,F} = 4.0 Hz, C-10), 126.3 (q, 2*J*_{C,F} = 30.6 Hz, C-11), 127.0 (q, 1*J*_{C,F} = 270.0 Hz, C-12), 133.1 (C-9), 150.6 (C-5) ppm. C-2 and C-8 not detected. Additional resonances in the ¹³C NMR spectrum are caused by slow decomposition of **14-Li⁺** in CD₃CN during the time required for the data acquisition.

¹⁹F NMR (376 MHz, CD₃CN): δ = −62.2 (s) ppm.

¹¹B NMR (128 MHz, CD₃CN): δ = 3.6 (s) ppm.

HRMS (FAB[−]) *m/z* calcd. for C₁₈H₂₁BF₃O₃[−] (M − Li⁺): 353.1539; found: 353.1533.

IR (ATR): ν̃ 2981, 1607, 1388, 1366, 1323, 1154, 1111, 1062, 995, 977, 908, 812, 792 cm^{−1}.

1.4.4 Reactions of the boronate complexes with various electrophiles

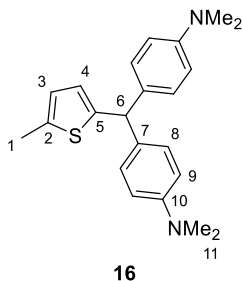
Reaction of **3a-Li⁺** and **15d-BF₄⁻**

The benzhydrylium tetrafluoroborate **15d-BF₄⁻** (0.17 mg, 0.50 mmol) was dissolved in CH₃CN (5 mL) and added dropwise into a CH₃CN solution (5 mL) of **3a-Li⁺** (0.22 g, 0.50 mmol) at 20 °C. After 1 h the solvent was removed under vacuum and the ¹H NMR spectrum was recorded. Only the starting materials were detected.

Reaction of **4c-Li⁺** and **15d-BF₄⁻**

The benzhydrylium tetrafluoroborate **15d-BF₄⁻** (150 mg, 0.441 mmol) was dissolved in CH₃CN (5 mL) and added dropwise into a CH₃CN solution (5 mL) of **4c-Li⁺** (175 mg, 0.483 mmol) at 20 °C. After 1 h, the solvent was removed and the ¹H NMR spectrum of the crude material showed the formation of **16** and **6e**. Attempts to separate the mixture by flash chromatography on silica gel (deactivated by NEt₃), with an *n*-pentane/EtOAc eluent (9/1) gave the 4-(trifluoromethyl)phenyl neopentyl boronic ester **6e** as a brownish solid (75 mg, 0.29 mmol, 66%), but **16** decomposed and could not be isolated.

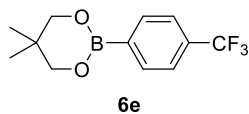
4,4'-((5-Methylthiophen-2-yl)methylene)bis(N,N-dimethylaniline) (**16**)



¹H NMR (400 MHz, CD₃CN, from the crude material): δ = 2.39 (d, ⁴*J*_{H1-H3} = 1.0 Hz, 3H, 1-H), 2.87 (s, 12H, 11-H), 5.19 (s, 1H, 6-H), 6.52-6.54 (m, 2H, 3-H and 4-H), 6.66-6.70 (m, 4H, 9-H), 6.96-6.99 (m, 4H, 8-H) ppm.

¹³C NMR (100 MHz, CD₃CN, from the crude material): δ = 15.8 (C-1), 40.9 (C-11), 52.1 (C-6), 113.9 (C-9), 120.8 (C3 or C4), 128.4 (C3 or C4), 131.9 (C-8), 134.1 (C-7), 140.9 (C-2 or C-5), 147.9 (C-10) ppm.

5,5-Dimethyl-2-(4-(trifluoromethyl)phenyl)-1,3,2-dioxaborinane (**6e**)



R_f (*n*-pentane/EtOAc: 9/1) = 0.41.

^1H NMR (400 MHz, CDCl_3): δ = 1.01 (s, 6H, 8-H), 3.77 (s, 4H, 7-H), 7.58 (d, $^3J_{\text{H3,H4}}$ = 8.3 Hz, 2H, 3-H), 7.89 (d, $^3J_{\text{H4,H3}}$ = 8.3 Hz, 2H, 4-H) ppm.

^{13}C NMR (100 MHz, CDCl_3): δ = 22.1 (C-8), 32.1 (C-6), 72.6 (C-7), 124.4 (q, $^3J_{\text{C,F}}$ = 3.8 Hz, C-3), 124.5 (q, $^1J_{\text{C,F}}$ = 272.3 Hz, C-1), 132.5 (q, $^2J_{\text{C,F}}$ = 32.0 Hz, C-3), 134.3 (C-5) ppm.

^{19}F NMR (376 MHz, CDCl_3): δ = -63.0 (s) ppm.

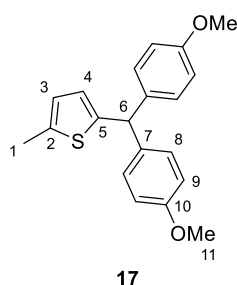
^{11}B NMR (128 MHz, CDCl_3): δ = 26.3 (s) ppm.

NMR data were in agreement with those reported in the literature.^[21]

Reaction of **4a-Li⁺** and **15a-BF₄⁻**

The benzhydrylium tetrafluoroborate **15a-BF₄⁻** (80 mg, 0.25 mmol) was dissolved in CH₃CN (5 mL) and added slowly into a CH₃CN solution (5 mL) of **4a-Li⁺** (96 mg, 0.26 mmol) at 20 °C. The reaction mixture was stirred for 30 min, quenched with water and extracted with EtOAc (3 × 15 mL). The organic phase was washed with brine, dried over MgSO₄ and concentrated in the vacuum. The crude product was purified with column chromatography, using a mixture of *n*-pentane/EtOAc (10/1) as eluent to give **17** as a colorless solid (29 mg, 0.089 mmol, 36%). The 4-(trifluoromethyl)phenyl pinacol boronic ester **6a** (*R_f* = 0.85) was characterized by ¹H NMR spectroscopy (data in agreement with those in the literature)^[22] and GC-MS but its isolation was not attempted.

2-(Bis(4-methoxyphenyl)methyl)-5-methylthiophene (**17**)



R_f (*n*-pentane/EtOAc: 10/1) = 0.35.

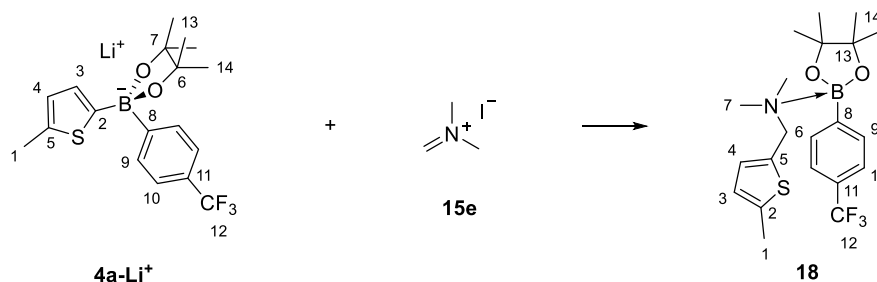
Mp: 75-76 °C (from *n*-pentane/EtOAc, 10/1).

¹H NMR (300 MHz, CDCl₃): δ = 2.40 (d, ⁴*J*_{H1-H3} = 1.1 Hz, 3H, 1-H), 3.76 (s, 6H, 11-H), 5.28 (s, 1H, 6-H), 6.41-6.42 (m, 1H, 4-H), 6.49-6.50 (m, 1H, 3-H), 6.78-6.83 (m, 4H, 9-H), 7.01-7.06 (m, 4H, 8-H) ppm.

¹³C NMR (75 MHz, CDCl₃): δ = 15.6 (C-1), 51.4 (C-6), 55.5 (C-11), 113.9 (C-9), 120.4 (C-4), 127.2 (C-3), 130.0 (C-8), 136.6 (C-7), 139.9 (C-2), 145.6 (C-5), 158.2 (C-10) ppm.

The data for compound **17** agree with those previously reported in the literature.^[23]

Reaction of **4a-Li⁺** and **15e**



The BAC **4a-Li⁺** (250 mg, 0.665 mmol) was dissolved in CH₃CN (5 mL) and added dropwise into a CH₃CN solution (10 mL) of the Eschenmoser salt **15e** (123 mg, 0.665 mmol) at 20 °C. After 1 h, half of the solvent was removed under vacuum and *n*-pentane was added until **18** precipitated as a white powder (219 mg, 0.513 mmol, 77%).

N,N-Dimethyl-1-(5-methylthiophen-2-yl)methanamine/*p*-trifluoromethyl phenyl pinacol boronic ester complex (**18**)

¹H NMR (400 MHz, CD₃CN): δ = 1.34 (s, 12H, 14-H), 2.17 (s, 6H, 7-H), 2.42 (s, 3H, 1-H), 3.50 (s, 2H, 6-H), 6.58 (dq, ³J_{H3-H4} = 3.4 Hz, ⁴J_{H3-H1} = 1.1 Hz, 1H, 3-H), 6.66 (d, ³J_{H4-H3} = 3.4 Hz, 1H, 4-H), 7.68 (d, *J* = 7.6 Hz, 2H, 9-H), 7.88 (d, *J* = 7.6 Hz, 2H, 10-H) ppm.

¹³C NMR (100 MHz, CD₃CN): δ = 15.8 (C-1), 25.6 (C-14), 45.6 (C-7), 59.5 (C-6), 85.8 (C-13), 125.8 (q, ¹J_{C,F} = 271.5 Hz, C-12), 125.8 (q, ⁴J_{C,F} = 4.8 Hz, C-10), 125.8 (C-4), 127.0 (C-3), 133.5 (q, ²J_{C,F} = 31.8 Hz, C-11), 136.3 (C-9), 140.6 (C-2), 142.2 (C-5) ppm. C-8 not detected.

¹⁹F NMR (376 MHz, CD₃CN): δ = −63.6 (s) ppm.

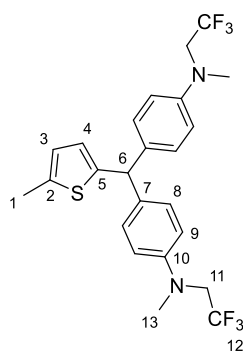
¹¹B NMR (128 MHz, CD₃CN): δ = 30.5 (s) ppm.

Reaction of **8-Li⁺** and **15b-BF₄⁻**

The benzhydrylium tetrafluoroborate **15b-BF₄⁻** (60 mg, 0.13 mmol) was dissolved in CH₃CN (3 mL) and added dropwise into a CH₃CN solution (2 mL) of **8-Li⁺** (37 mg, 0.11 mmol) at 20 °C. The reaction mixture was stirred for 30 min, quenched with water and extracted with EtOAc (3 × 15 mL). Organic phase was washed with brine, dried over MgSO₄ and concentrated in vacuum. Crude product was purified with column chromatography on silica gel, using *n*-pentane/EtOAc: 10/1 mixtures as eluent, to give **19** as a colorless solid (23 mg, 0.047 mmol, 43%).

4,4'-((5-Methylthiophen-2-yl)methylene)bis(N-methyl-N-(2,2,2-trifluoroethyl)aniline)

(19)



19

R_f (*n*-pentane/EtOAc: 10/1): 0.25

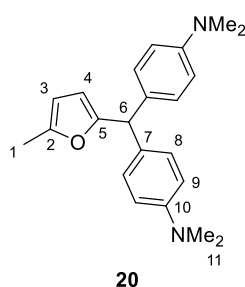
¹H NMR (300 MHz, CDCl₃): δ = 2.39 (d, ⁴J_{H1-H3} = 1.1 Hz, 3H, 1-H), 3.01 (s, 6H, 13-H), 3.80 (q, ³J_{H,F} = 9.0 Hz, 4H, 11-H), 5.22 (s, 1H, 6-H), 6.43-6.44 (m, 1H, 4-H), 6.51-6.54 (m, 1H, 3-H), 6.69-6.73 (m, 4H, 9-H), 7.00-7.05 (m, 4H, 8-H) ppm.

¹³C NMR (75 MHz, CDCl₃): δ = 15.4 (C-1), 39.2 (C-13), 50.9 (C-6), 54.7 (q, ²J_{C,F} = 32.6 Hz, C-11), 112.6 (C-9), 120.0 (C-4), 125.6 (q, ¹J_{C,F} = 282.3 Hz, C-12), 127.0 (C-3), 129.6 (C-8), 134.2 (C-7), 139.5 (C-2), 145.7 (C-5), 147.1 (C-10) ppm.

Reaction of **14**-Li⁺ and **15d**-BF₄⁻

The benzhydrylium tetrafluoroborate **15d**-BF₄⁻ (95 mg, 0.28 mmol) was dissolved in CH₃CN (5 mL) and added dropwise into a CH₃CN solution (5 mL) of **14**-Li⁺ (0.11 g, 0.31 mmol) at 20 °C. After 1 h the deep blue color completely decolorized and the solvent was removed. After purification by flash chromatography on silica gel (*n*-pentane/EtOAc: 9/1) the product **20** was obtained as a colorless oil (86 mg, 0.26 mmol, 92%) and separate from the boronic ester **6a** (63 mg, 0.23 mmol, 82%).

4,4'-((5-Methylfuran-2-yl)methylene)bis(N,N-dimethylaniline) (**20**)



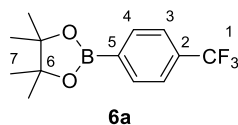
The compound **20** was obtained as a colorless oil, as reported in the literature, but solidified after standing for several weeks to give a pale-yellow solid. The NMR data of **20** agreed with those reported previously.^[9a]

R_f = 0.60 (*n*-pentane/EtOAc: 9/1)

Mp (*n*-pentane/EtOAc: 9/1): 107-108 °C.

¹H NMR (400 MHz, CDCl₃): δ = 2.22 (s, 3H, 1-H), 2.90 (s, 12H, 11-H), 5.21 (s, 1H, 6-H), 5.71 (d, *J* = 1.8 Hz, 1H, 3-H), 5.83 (d, *J* = 1.8 Hz, 1H, 4-H), 6.68 (d, *J* = 8.4 Hz, 4H, 8-H), 7.02 (d, *J* = 8.6 Hz, 4H, 9-H) ppm.

4-(Trifluoromethyl) phenyl pinacol boronic ester (6a)



The ^1H NMR data for the 4-(trifluoromethyl) phenyl pinacol boronic ester **6a** agreed with those in the literature.^[22]

$R_f = 0.70$ (*n*-pentane/EtOAc: 9/1)

^1H NMR (300 MHz, CDCl_3): $\delta = 1.34$ (s, 12H, 7-H), 7.59 (d, $J = 8.5$ Hz, 2H), 7.89 (d, $J = 8.5$ Hz, 2H) ppm.

Reactions of 12-Li^+ with benzhydrylium tetrafluoroborates 15-BF_4^- (Scheme 1.9)

In an NMR tube, the BAC **12-Li⁺** (15.0 mg, 0.043 mmol) and 1 equivalent of the benzhydrylium tetrafluoroborate **15a-BF₄⁻** (13.5 mg, 0.043 mmol), **15b-BF₄⁻** (20.3 mg, 0.043 mmol) or **15c-BF₄⁻** (18.1 mg, 0.043 mmol) were mixed in CD_3CN (0.6 mL) at room temperature. After 1 h, the ^1H NMR spectra were recorded. The ratio of the Friedel-Crafts products was calculated by comparing the integrals of the ^1H NMR signal of their $\text{Ar}_3\text{C-H}$ proton (in the range of $\delta = 4.6$ to 5.5 ppm) or by GC-MS.

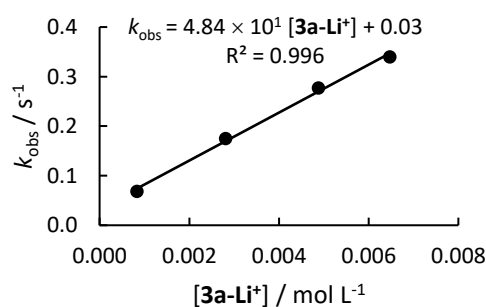
1.4.5 Kinetic experiments

1.4.5.1 Reactions of 3a-Li^+

Table 1.3. Kinetics of the reaction of **3a-Li⁺** with **15b** in CH_3CN (20 °C, at 586 nm)

[15b] / mol L ⁻¹	[3a-Li⁺] / mol L ⁻¹	k_{obs} / s ⁻¹
5.40×10^{-6}	8.35×10^{-4}	6.88×10^{-2}
5.40×10^{-6}	2.81×10^{-3}	1.75×10^{-1}
5.40×10^{-6}	4.88×10^{-3}	2.77×10^{-1}
5.40×10^{-6}	6.47×10^{-3}	3.40×10^{-1}

$$k_2 = 4.84 \times 10^1 \text{ L mol}^{-1} \text{ s}^{-1}$$



1.4.5.2 Reactions of **3b-Li⁺**

Table 1.4. Kinetics of the reaction of **3b-Li⁺** with **15b** in CH₃CN (20 °C, at 586 nm)

[15b] / mol L ⁻¹	[3b-Li⁺] / mol L ⁻¹	<i>k</i> _{obs} / s ⁻¹
6.50 × 10 ⁻⁶	1.41 × 10 ⁻⁴	1.06 × 10 ²
6.50 × 10 ⁻⁶	3.54 × 10 ⁻⁴	2.33 × 10 ²
6.50 × 10 ⁻⁶	7.08 × 10 ⁻⁴	4.04 × 10 ²
6.50 × 10 ⁻⁶	1.41 × 10 ⁻³	7.75 × 10 ²

$$k_2 = 5.22 \times 10^5 \text{ L mol}^{-1} \text{ s}^{-1}$$

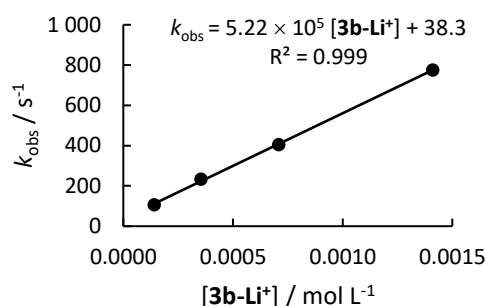


Table 1.5. Kinetics of the reaction of **3b-Li⁺** with **15c** in CH₃CN (20 °C, at 611 nm)

[15c] / mol L ⁻¹	[3b-Li⁺] / mol L ⁻¹	<i>k</i> _{obs} / s ⁻¹
6.90 × 10 ⁻⁶	2.43 × 10 ⁻⁴	8.17
6.90 × 10 ⁻⁶	3.54 × 10 ⁻⁴	1.18 × 10 ¹
6.90 × 10 ⁻⁶	4.86 × 10 ⁻⁴	1.46 × 10 ¹
6.90 × 10 ⁻⁶	7.08 × 10 ⁻⁴	2.10 × 10 ¹
6.90 × 10 ⁻⁶	9.72 × 10 ⁻⁴	2.62 × 10 ¹
6.90 × 10 ⁻⁶	1.42 × 10 ⁻³	3.59 × 10 ¹
6.90 × 10 ⁻⁶	2.12 × 10 ⁻³	5.07 × 10 ¹
6.90 × 10 ⁻⁶	2.92 × 10 ⁻³	6.91 × 10 ¹
6.90 × 10 ⁻⁶	3.89 × 10 ⁻³	9.10 × 10 ¹

$$k_2 = 2.24 \times 10^4 \text{ L mol}^{-1} \text{ s}^{-1}$$

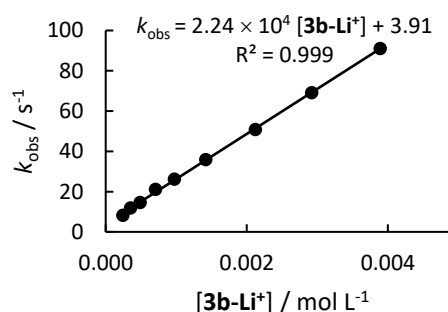
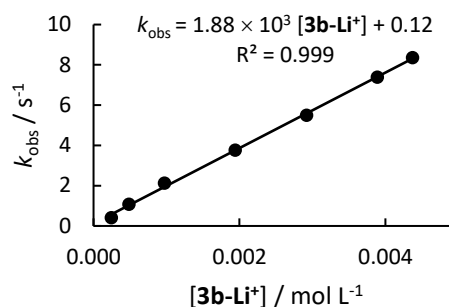


Table 1.6. Kinetics of the reaction of **3b-Li⁺** with **15d** in CH₃CN (20 °C, at 605 nm)

[15d] / mol L ⁻¹	[3b-Li⁺] / mol L ⁻¹	<i>k</i> _{obs} / s ⁻¹
5.30 × 10 ⁻⁶	2.43 × 10 ⁻⁴	4.14 × 10 ⁻¹
5.30 × 10 ⁻⁶	4.86 × 10 ⁻⁴	1.07
5.30 × 10 ⁻⁶	9.72 × 10 ⁻⁴	2.13
5.30 × 10 ⁻⁶	1.94 × 10 ⁻³	3.76
5.30 × 10 ⁻⁶	2.92 × 10 ⁻³	5.49
5.30 × 10 ⁻⁶	3.89 × 10 ⁻³	7.38
5.30 × 10 ⁻⁶	4.37 × 10 ⁻³	8.36

$$k_2 = 1.88 \times 10^3 \text{ L mol}^{-1} \text{ s}^{-1}$$



1.4.5.3 Reactions of **3c-Li⁺**

Table 1.7. Kinetics of the reaction of **3c-Li⁺** with **15b** in CH₃CN (20 °C, at 586 nm)

[15b] / mol L ⁻¹	[3c-Li⁺] / mol L ⁻¹	<i>k</i> _{obs} / s ⁻¹
6.50 × 10 ⁻⁶	1.05 × 10 ⁻⁴	1.10 × 10 ²
6.50 × 10 ⁻⁶	2.11 × 10 ⁻⁴	1.48 × 10 ²
6.50 × 10 ⁻⁶	4.21 × 10 ⁻⁴	2.99 × 10 ²
6.50 × 10 ⁻⁶	8.42 × 10 ⁻⁴	4.96 × 10 ²

$$k_2 = 5.36 \times 10^5 \text{ L mol}^{-1} \text{ s}^{-1}$$

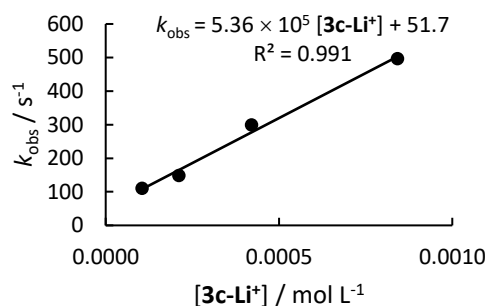
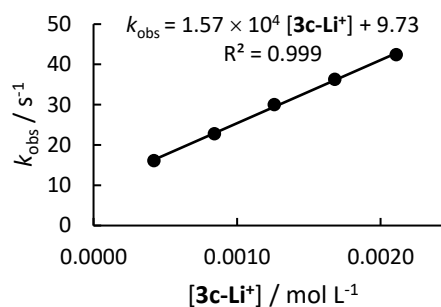


Table 1.8. Kinetics of the reaction of **3c-Li⁺** with **15c** in CH₃CN (20 °C, at 611 nm)

[15c] / mol L ⁻¹	[3c-Li⁺] / mol L ⁻¹	<i>k</i> _{obs} ^[a] / s ⁻¹
7.10 × 10 ⁻⁶	4.21 × 10 ⁻⁴	1.61 × 10 ¹
7.10 × 10 ⁻⁶	8.42 × 10 ⁻⁴	2.28 × 10 ¹
7.10 × 10 ⁻⁶	1.26 × 10 ⁻³	3.00 × 10 ¹
7.10 × 10 ⁻⁶	1.68 × 10 ⁻³	3.63 × 10 ¹
7.10 × 10 ⁻⁶	2.11 × 10 ⁻³	4.24 × 10 ¹

$$k_2 = 1.57 \times 10^4 \text{ L mol}^{-1} \text{ s}^{-1}$$



[a] The decay of the absorbance of the benzhydrylium ion **15c** followed a mono-exponential function until 60% conversion. Only this part of the decay curve was used to calculate k_{obs} .

1.4.5.4 Reactions of **4a-Li⁺**

Table 1.9. Kinetics of the reaction of **4a-Li⁺** with **15b** in CH₃CN (20 °C, at 586 nm)

[15b] / mol L ⁻¹	[4a-Li⁺] / mol L ⁻¹	<i>k</i> _{obs} / s ⁻¹
1.00 × 10 ⁻⁵	5.04 × 10 ⁻⁴	1.07 × 10 ⁻¹
1.00 × 10 ⁻⁵	1.01 × 10 ⁻³	2.06 × 10 ⁻¹
1.00 × 10 ⁻⁵	2.02 × 10 ⁻³	4.74 × 10 ⁻¹
1.00 × 10 ⁻⁵	3.02 × 10 ⁻³	7.27 × 10 ⁻¹
1.00 × 10 ⁻⁵	3.93 × 10 ⁻³	9.06 × 10 ⁻¹

$$k_2 = 2.40 \times 10^2 \text{ L mol}^{-1} \text{ s}^{-1}$$

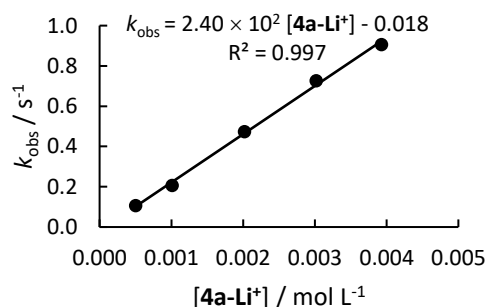
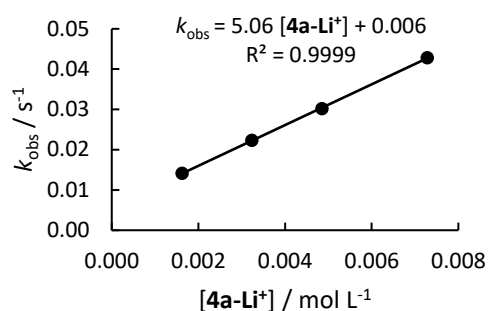


Table 1.10. Kinetics of the reaction of **4a-Li⁺** with **15c** in CH₃CN (20 °C, at 611 nm)

[15c] / mol L ⁻¹	[4a-Li⁺] / mol L ⁻¹	<i>k</i> _{obs} / s ⁻¹
5.90 × 10 ⁻⁶	1.62 × 10 ⁻³	1.41 × 10 ⁻²
5.90 × 10 ⁻⁶	3.23 × 10 ⁻³	2.23 × 10 ⁻²
5.90 × 10 ⁻⁶	4.85 × 10 ⁻³	3.02 × 10 ⁻²
5.90 × 10 ⁻⁶	7.28 × 10 ⁻³	4.28 × 10 ⁻²

$$k_2 = 5.06 \text{ L mol}^{-1} \text{ s}^{-1}$$



1.4.5.5 Reactions of **4c-Li⁺**

Table 1.11. Kinetics of the reaction of **4c-Li⁺** with **15c** in CH₃CN (20 °C, at 611 nm)

[15c] / mol L ⁻¹	[4c-Li⁺] / mol L ⁻¹	<i>k</i> _{obs} / s ⁻¹
6.60 × 10 ⁻⁶	2.93 × 10 ⁻⁴	2.27 × 10 ¹
6.60 × 10 ⁻⁶	5.87 × 10 ⁻⁴	3.74 × 10 ¹
6.60 × 10 ⁻⁶	1.17 × 10 ⁻³	6.20 × 10 ¹
6.60 × 10 ⁻⁶	1.76 × 10 ⁻³	8.19 × 10 ¹
6.60 × 10 ⁻⁶	2.35 × 10 ⁻³	9.98 × 10 ¹

$$k_2 = 3.73 \times 10^4 \text{ L mol}^{-1} \text{ s}^{-1}$$

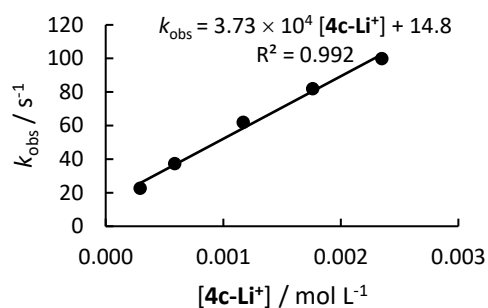
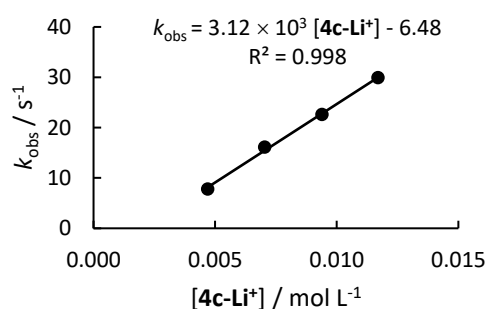


Table 1.12. Kinetics of the reaction of **4c-Li⁺** with **15d** in CH₃CN (20 °C, at 605 nm)

[15d] / mol L ⁻¹	[4c-Li⁺] / mol L ⁻¹	<i>k</i> _{obs} / s ⁻¹
4.80 × 10 ⁻⁶	4.69 × 10 ⁻³	7.78
4.80 × 10 ⁻⁶	7.04 × 10 ⁻³	1.61 × 10 ¹
4.80 × 10 ⁻⁶	9.39 × 10 ⁻³	2.26 × 10 ¹
4.80 × 10 ⁻⁶	1.17 × 10 ⁻²	2.99 × 10 ¹

$$k_2 = 3.12 \times 10^3 \text{ L mol}^{-1} \text{ s}^{-1}$$

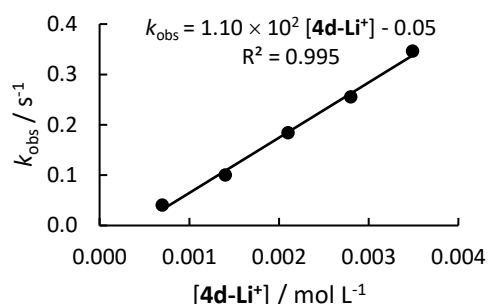


1.4.5.6 Reactions of 4d-Li⁺

Table 1.13. Kinetics of the reaction of 4d-Li⁺ with 15b in CH₃CN (20 °C, at 586 nm)

[15b] / mol L ⁻¹	[4d-Li ⁺] / mol L ⁻¹	<i>k</i> _{obs} ^[a] / s ⁻¹
5.20 × 10 ⁻⁶	6.99 × 10 ⁻⁴	4.05 × 10 ⁻²
5.20 × 10 ⁻⁶	1.40 × 10 ⁻³	1.00 × 10 ⁻¹
5.20 × 10 ⁻⁶	2.10 × 10 ⁻³	1.84 × 10 ⁻¹
5.20 × 10 ⁻⁶	2.80 × 10 ⁻³	2.55 × 10 ⁻¹
5.20 × 10 ⁻⁶	3.49 × 10 ⁻³	3.46 × 10 ⁻¹

$$k_2 = 1.10 \times 10^2 \text{ L mol}^{-1} \text{ s}^{-1}$$

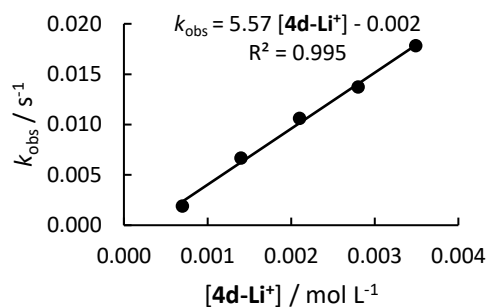


[a] The decay of the absorbance of the benzhydrylium ion 15b followed a mono-exponential function until 60% conversion. Only this part of the decay curve was used to calculate k_{obs} .

Table 1.14. Kinetics of the reaction of 4d-Li⁺ with 15c in CH₃CN (20 °C, at 605 nm)

[4d-Li ⁺] / mol L ⁻¹	[15c] / mol L ⁻¹	<i>k</i> _{obs} ^[a] / s ⁻¹
5.50 × 10 ⁻⁶	6.99 × 10 ⁻⁴	1.90 × 10 ⁻³
5.50 × 10 ⁻⁶	1.40 × 10 ⁻³	6.65 × 10 ⁻³
5.50 × 10 ⁻⁶	2.10 × 10 ⁻³	1.06 × 10 ⁻²
5.50 × 10 ⁻⁶	2.80 × 10 ⁻³	1.37 × 10 ⁻²
5.50 × 10 ⁻⁶	3.49 × 10 ⁻³	1.78 × 10 ⁻²

$$k_2 = 5.57 \text{ L mol}^{-1} \text{ s}^{-1}$$



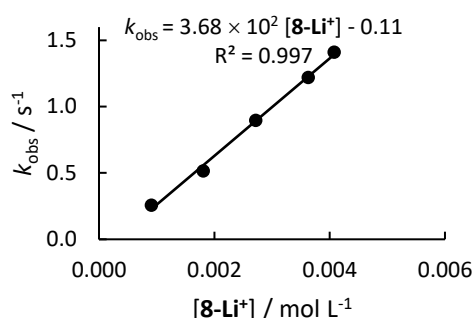
[a] The decay of the absorbance of the benzhydrylium ion 15c followed a mono-exponential function until 60% conversion. Only this part of the decay curve was used to calculate k_{obs} .

1.4.5.7 Reactions of 8-M⁺

Table 1.15. Kinetics of the reaction of 8-Li⁺ with 15b in CH₃CN (20 °C, at 586 nm)

[15b] / mol L ⁻¹	[8-Li ⁺] ^[a] / mol L ⁻¹	<i>k</i> _{obs} / s ⁻¹
9.10 × 10 ⁻⁶	9.07 × 10 ⁻⁴	2.57 × 10 ⁻¹
9.10 × 10 ⁻⁶	1.81 × 10 ⁻³	5.16 × 10 ⁻¹
9.10 × 10 ⁻⁶	2.72 × 10 ⁻³	8.97 × 10 ⁻¹
9.10 × 10 ⁻⁶	3.63 × 10 ⁻³	1.22
9.10 × 10 ⁻⁶	4.08 × 10 ⁻³	1.41

$$k_2 = 3.68 \times 10^2 \text{ L mol}^{-1} \text{ s}^{-1}$$

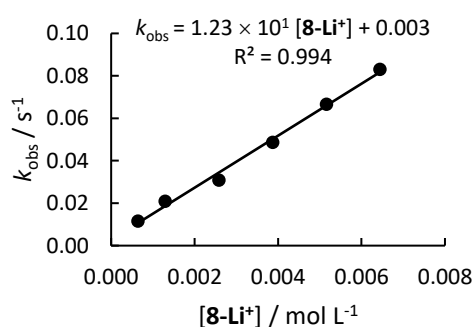


[a] Trace contaminations of 8-Li⁺ with THF (< 5%) have not been considered when calculating [8-Li⁺]

Table 1.16. Kinetics of the reaction of 8-Li⁺ with 15c in CH₃CN (20 °C, at 611 nm)

[15c] / mol L ⁻¹	[8-Li ⁺] / mol L ⁻¹	<i>k</i> _{obs} / s ⁻¹
7.30 × 10 ⁻⁶	6.44 × 10 ⁻⁴	1.15 × 10 ⁻²
7.30 × 10 ⁻⁶	1.29 × 10 ⁻³	2.09 × 10 ⁻²
7.30 × 10 ⁻⁶	2.58 × 10 ⁻³	3.09 × 10 ⁻²
7.30 × 10 ⁻⁶	3.87 × 10 ⁻³	4.87 × 10 ⁻²
7.30 × 10 ⁻⁶	5.16 × 10 ⁻³	6.66 × 10 ⁻²
7.30 × 10 ⁻⁶	6.44 × 10 ⁻³	8.30 × 10 ⁻²

$$k_2 = 1.23 \times 10^1 \text{ L mol}^{-1} \text{ s}^{-1}$$



[a] Trace contaminations of 8-Li⁺ with THF (< 5%) have not been considered when calculating [8-Li⁺]

Table 1.17. Kinetics of the reaction of **8-NEt₄⁺** with **15b** in CH₃CN (20 °C, at 586 nm)

[15b] / mol L ⁻¹	[8-NEt₄⁺] / mol L ⁻¹	<i>k</i> _{obs} / s ⁻¹
8.30 × 10 ⁻⁶	2.69 × 10 ⁻⁴	2.48 × 10 ⁻¹
8.30 × 10 ⁻⁶	5.37 × 10 ⁻⁴	4.65 × 10 ⁻¹
8.30 × 10 ⁻⁶	1.07 × 10 ⁻³	8.61 × 10 ⁻¹
8.30 × 10 ⁻⁶	1.61 × 10 ⁻³	1.18
8.30 × 10 ⁻⁶	2.15 × 10 ⁻³	1.51
8.30 × 10 ⁻⁶	2.69 × 10 ⁻³	1.93

$$k_2 = 6.77 \times 10^2 \text{ L mol}^{-1} \text{ s}^{-1}$$

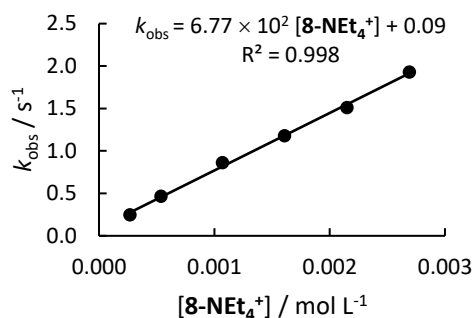
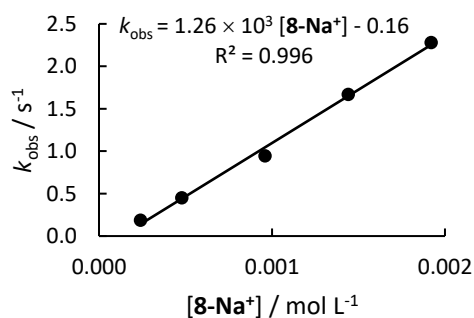


Table 1.18. Kinetics of the reaction of **8-Na⁺** with **15b** in CH₃CN (20 °C, at 586 nm)

[15b] / mol L ⁻¹	[8-Na⁺] / mol L ⁻¹	<i>k</i> _{obs} / s ⁻¹
7.20 × 10 ⁻⁶	2.40 × 10 ⁻⁴	1.85 × 10 ⁻¹
7.20 × 10 ⁻⁶	4.78 × 10 ⁻⁴	4.49 × 10 ⁻¹
7.20 × 10 ⁻⁶	9.59 × 10 ⁻⁴	9.43 × 10 ⁻¹
7.20 × 10 ⁻⁶	1.44 × 10 ⁻³	1.67

$$k_2 = 1.26 \times 10^3 \text{ L mol}^{-1} \text{ s}^{-1}$$



1.4.5.8 Reactions of 9-Li⁺

Table 1.19. Kinetics of the reaction of 9-Li⁺ with 15b in CH₃CN (20 °C, at 586 nm)

[15b] / mol L ⁻¹	[9-Li ⁺] / mol L ⁻¹	<i>k</i> _{obs} / s ⁻¹
8.00 × 10 ⁻⁶	3.33 × 10 ⁻⁴	6.97 × 10 ⁻¹
8.00 × 10 ⁻⁶	6.65 × 10 ⁻⁴	9.49 × 10 ⁻¹
8.00 × 10 ⁻⁶	1.33 × 10 ⁻³	1.66
8.00 × 10 ⁻⁶	2.00 × 10 ⁻³	1.99
8.00 × 10 ⁻⁶	2.66 × 10 ⁻³	2.37
8.00 × 10 ⁻⁶	3.33 × 10 ⁻³	2.75

$$k_2 = 6.82 \times 10^2 \text{ L mol}^{-1} \text{ s}^{-1}$$

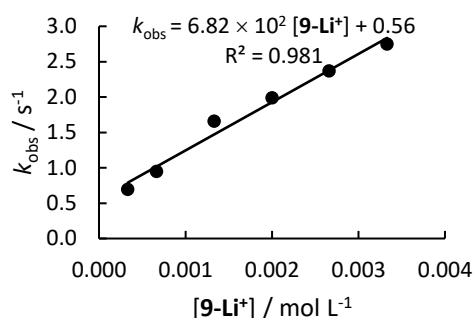
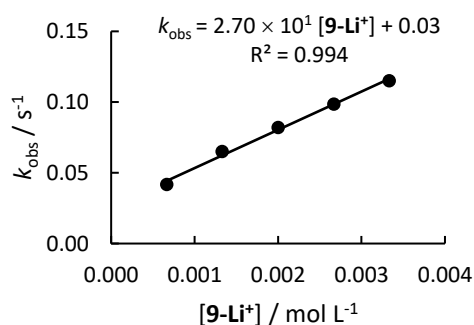


Table 1.20. Kinetics of the reaction of 9-Li⁺ with 15c in CH₃CN (20 °C, at 611 nm)

[15c] / mol L ⁻¹	[9-Li ⁺] / mol L ⁻¹	<i>k</i> _{obs} / s ⁻¹
7.30 × 10 ⁻⁶	6.67 × 10 ⁻⁴	4.16 × 10 ⁻²
7.30 × 10 ⁻⁶	1.33 × 10 ⁻³	6.49 × 10 ⁻²
7.30 × 10 ⁻⁶	2.00 × 10 ⁻³	8.20 × 10 ⁻²
7.30 × 10 ⁻⁶	2.67 × 10 ⁻³	9.84 × 10 ⁻²
7.30 × 10 ⁻⁶	3.33 × 10 ⁻³	1.15 × 10 ⁻¹

$$k_2 = 2.70 \times 10^1 \text{ L mol}^{-1} \text{ s}^{-1}$$



1.4.5.9 Reactions of **10-Li**⁺

Table 1.21. Kinetics of the reaction of **10-Li**⁺ with **15b** in CH₃CN (20 °C, at 586 nm)

[15b] / mol L ⁻¹	[10-Li ⁺] / mol L ⁻¹	<i>k</i> _{obs} / s ⁻¹
6.00 × 10 ⁻⁶	4.59 × 10 ⁻⁴	7.17 × 10 ⁻¹
6.00 × 10 ⁻⁶	9.19 × 10 ⁻⁴	1.25
6.00 × 10 ⁻⁶	1.84 × 10 ⁻³	2.11
6.00 × 10 ⁻⁶	2.76 × 10 ⁻³	2.71
6.00 × 10 ⁻⁶	3.67 × 10 ⁻³	3.32
6.00 × 10 ⁻⁶	4.59 × 10 ⁻³	4.22

$$k_2 = 8.12 \times 10^2 \text{ L mol}^{-1} \text{ s}^{-1}$$

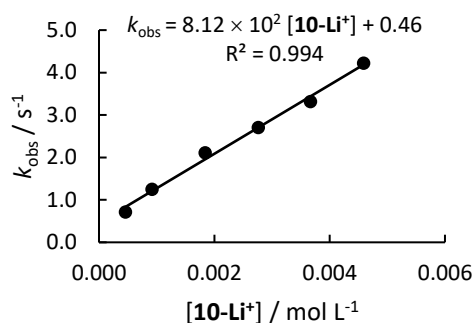
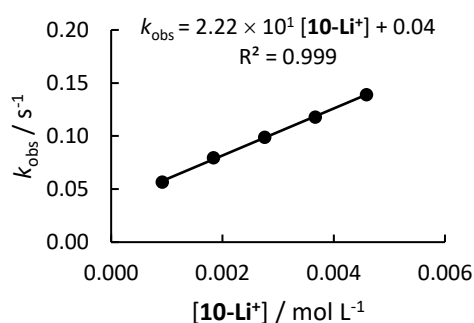


Table 1.22. Kinetics of the reaction of **10-Li**⁺ with **15c** in CH₃CN (20 °C, at 611 nm)

[15c] / mol L ⁻¹	[10-Li ⁺] / mol L ⁻¹	<i>k</i> _{obs} / s ⁻¹
6.00 × 10 ⁻⁶	9.19 × 10 ⁻⁴	5.66 × 10 ⁻²
6.00 × 10 ⁻⁶	1.84 × 10 ⁻³	7.95 × 10 ⁻²
6.00 × 10 ⁻⁶	2.76 × 10 ⁻³	9.89 × 10 ⁻²
6.00 × 10 ⁻⁶	3.67 × 10 ⁻³	1.18 × 10 ⁻¹
6.00 × 10 ⁻⁶	4.59 × 10 ⁻³	1.39 × 10 ⁻¹

$$k_2 = 2.22 \times 10^1 \text{ L mol}^{-1} \text{ s}^{-1}$$



1.4.5.10 Reactions of 11-Li⁺

Table 1.23. Kinetics of the reaction of 11-Li⁺ with 15b in CH₃CN (20 °C, at 586 nm)

[15b] / mol L ⁻¹	[11-Li ⁺] / mol L ⁻¹	<i>k</i> _{obs} / s ⁻¹
8.70 × 10 ⁻⁶	3.51 × 10 ⁻⁴	8.71 × 10 ⁻¹
8.70 × 10 ⁻⁶	7.02 × 10 ⁻⁴	1.50
8.70 × 10 ⁻⁶	1.40 × 10 ⁻³	2.48
8.70 × 10 ⁻⁶	2.11 × 10 ⁻³	3.59
8.70 × 10 ⁻⁶	2.81 × 10 ⁻³	4.56

$$k_2 = 1.49 \times 10^3 \text{ L mol}^{-1} \text{ s}^{-1}$$

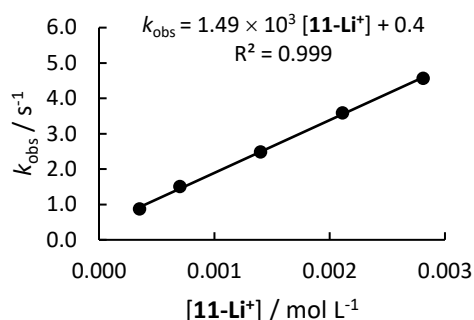
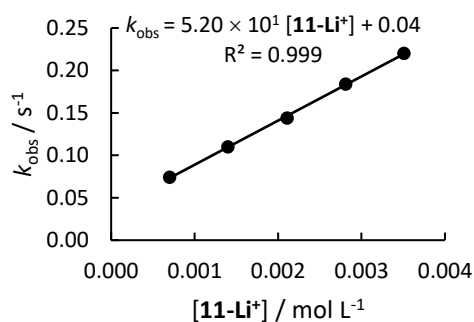


Table 1.24. Kinetics of the reaction of 11-Li⁺ with 15c in CH₃CN (20 °C, at 611 nm)

[15c] / mol L ⁻¹	[11-Li ⁺] / mol L ⁻¹	<i>k</i> _{obs} / s ⁻¹
5.50 × 10 ⁻⁶	7.02 × 10 ⁻⁴	7.42 × 10 ⁻²
5.50 × 10 ⁻⁶	1.40 × 10 ⁻³	1.10 × 10 ⁻¹
5.50 × 10 ⁻⁶	2.11 × 10 ⁻³	1.44 × 10 ⁻¹
5.50 × 10 ⁻⁶	2.81 × 10 ⁻³	1.84 × 10 ⁻¹
5.50 × 10 ⁻⁶	3.51 × 10 ⁻³	2.20 × 10 ⁻¹

$$k_2 = 5.20 \times 10^1 \text{ L mol}^{-1} \text{ s}^{-1}$$



1.4.5.11 Reactions of **12-Li**⁺

Table 1.25. Kinetics of the reaction of **12-Li**⁺ with **15b** in CH₃CN (20 °C, at 586 nm)

[15b] / mol L ⁻¹	[12-Li ⁺] / mol L ⁻¹	<i>k</i> _{obs} / s ⁻¹
6.50 × 10 ⁻⁶	1.97 × 10 ⁻⁴	2.20
6.50 × 10 ⁻⁶	3.94 × 10 ⁻⁴	3.57
6.50 × 10 ⁻⁶	7.87 × 10 ⁻⁴	5.20
6.50 × 10 ⁻⁶	1.18 × 10 ⁻³	7.10
6.50 × 10 ⁻⁶	1.57 × 10 ⁻³	9.19
6.50 × 10 ⁻⁶	1.97 × 10 ⁻³	1.16 × 10 ¹

$$k_2 = 5.14 \times 10^3 \text{ L mol}^{-1} \text{ s}^{-1}$$

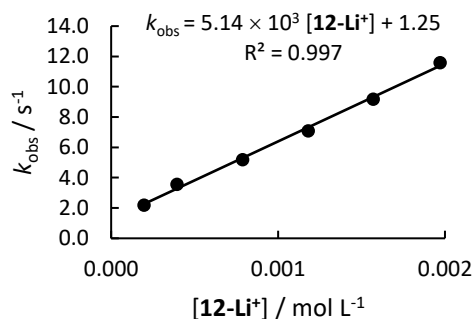
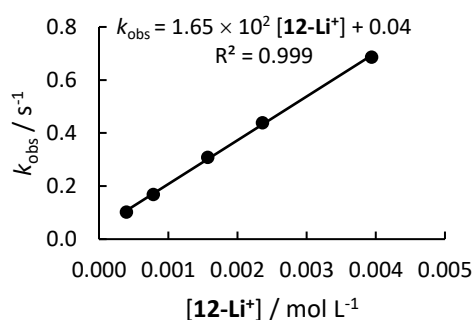


Table 1.26. Kinetics of the reaction of **12-Li**⁺ with **15c** in CH₃CN (20 °C, at 611 nm)

[15c] / mol L ⁻¹	[12-Li ⁺] / mol L ⁻¹	<i>k</i> _{obs} / s ⁻¹
6.20 × 10 ⁻⁶	3.94 × 10 ⁻⁴	1.02 × 10 ⁻¹
6.20 × 10 ⁻⁶	7.87 × 10 ⁻⁴	1.69 × 10 ⁻¹
6.20 × 10 ⁻⁶	1.57 × 10 ⁻³	3.09 × 10 ⁻¹
6.20 × 10 ⁻⁶	2.36 × 10 ⁻³	4.39 × 10 ⁻¹
6.20 × 10 ⁻⁶	3.94 × 10 ⁻³	6.87 × 10 ⁻¹

$$k_2 = 1.65 \times 10^2 \text{ L mol}^{-1} \text{ s}^{-1}$$



1.4.5.12 Reactions of **13**-Li⁺

Table 1.27. Kinetics of the reaction of **13**-Li⁺ with **15b** in CH₃CN (20 °C, at 586 nm)

[15b] / mol L ⁻¹	[13 -Li ⁺] / mol L ⁻¹	<i>k</i> _{obs} / s ⁻¹
5.40 × 10 ⁻⁶	3.09 × 10 ⁻⁴	3.96 × 10 ⁻¹
5.40 × 10 ⁻⁶	6.19 × 10 ⁻⁴	1.09
5.40 × 10 ⁻⁶	1.24 × 10 ⁻³	2.25
5.40 × 10 ⁻⁶	2.47 × 10 ⁻³	4.92

$$k_2 = 2.08 \times 10^3 \text{ L mol}^{-1} \text{ s}^{-1}$$

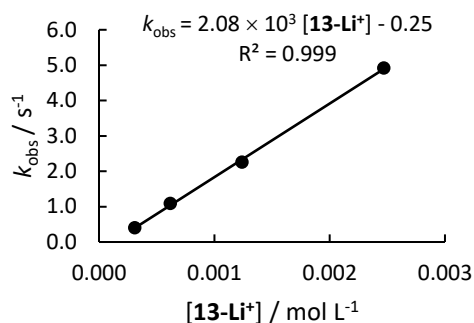
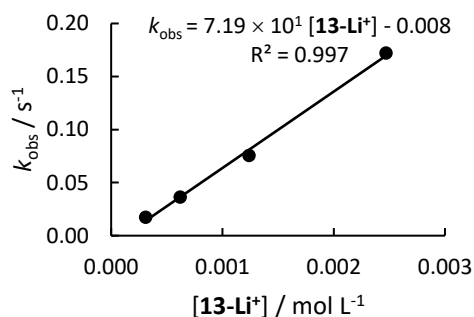


Table 1.28. Kinetics of the reaction of **13**-Li⁺ with **15c** in CH₃CN (20 °C, at 611 nm)

[15c] / mol L ⁻¹	[13 -Li ⁺] / mol L ⁻¹	<i>k</i> _{obs} / s ⁻¹
5.90 × 10 ⁻⁶	3.09 × 10 ⁻⁴	1.72 × 10 ⁻²
5.90 × 10 ⁻⁶	6.19 × 10 ⁻⁴	3.62 × 10 ⁻²
5.90 × 10 ⁻⁶	1.24 × 10 ⁻³	7.56 × 10 ⁻²
5.90 × 10 ⁻⁶	2.47 × 10 ⁻³	1.72 × 10 ⁻¹

$$k_2 = 7.19 \times 10^1 \text{ L mol}^{-1} \text{ s}^{-1}$$



1.4.5.13 Reactions of **14-Li**⁺

Table 1.29. Kinetics of the reaction of **14-Li**⁺ with **15b** in CH₃CN (20 °C, at 586 nm)

[15b] / mol L ⁻¹	[14-Li ⁺] / mol L ⁻¹	<i>k</i> _{obs} / s ⁻¹
7.20 × 10 ⁻⁶	1.98 × 10 ⁻⁴	5.82
7.20 × 10 ⁻⁶	7.91 × 10 ⁻⁴	9.14
7.20 × 10 ⁻⁶	1.58 × 10 ⁻³	1.31 × 10 ¹
7.20 × 10 ⁻⁶	2.37 × 10 ⁻³	1.59 × 10 ¹
7.20 × 10 ⁻⁶	3.17 × 10 ⁻³	1.90 × 10 ¹

$$k_2 = 4.38 \times 10^3 \text{ L mol}^{-1} \text{ s}^{-1}$$

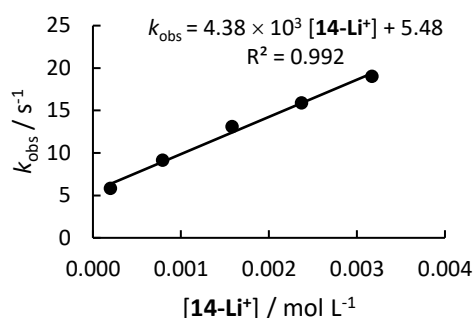
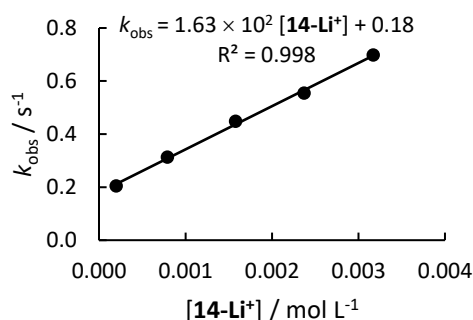


Table 1.30. Kinetics of the reaction of **14-Li**⁺ with **15c** in CH₃CN (20 °C, at 611 nm)

[15c] / mol L ⁻¹	[14-Li ⁺] / mol L ⁻¹	<i>k</i> _{obs} ^[a] / s ⁻¹
7.00 × 10 ⁻⁶	1.98 × 10 ⁻⁴	2.05 × 10 ⁻¹
7.00 × 10 ⁻⁶	7.91 × 10 ⁻⁴	3.13 × 10 ⁻¹
7.00 × 10 ⁻⁶	1.58 × 10 ⁻³	4.48 × 10 ⁻¹
7.00 × 10 ⁻⁶	2.37 × 10 ⁻³	5.54 × 10 ⁻¹
7.00 × 10 ⁻⁶	3.17 × 10 ⁻³	6.98 × 10 ⁻¹

$$k_2 = 1.63 \times 10^2 \text{ L mol}^{-1} \text{ s}^{-1}$$



[a] The decay of the absorbance of the benzhydrylium ion **15c** followed a mono-exponential function until 60% conversion. Only this part of the decay curve was used to calculate *k*_{obs}.

1.5 Crystallographic Data

Single crystals of **3a-Li**⁺ were obtained by crystallization from an acetonitrile solution under an N₂ atmosphere.

Single crystals of **4d-Li**⁺ were obtained by vapor diffusion of *n*-pentane (5 mL) into a solution of **4d-Li**⁺ in THF (50 mg of (**4d-Li**⁺)-OEt₂ in 1 mL of THF) at 0 °C for 1 week in a closed flask under nitrogen.

The X-ray data have been collected by ω-scans by means of an Oxford Diffraction Xcalibur diffractometer. The structures have been solved by direct methods using SIR97 and refined by least-squares methods against *F*² using SHELXL-97. C-bound hydrogen atoms have been calculated in ideal geometry riding on their parent atoms. Crystallographic data have been deposited with the Cambridge Crystallographic Data Centre (CCDC number for the BAC **3a-Li**⁺: 1014813 and for **4d-Li**⁺: 1014814). These supplementary crystallographic data can be

obtained free of charge from The Cambridge Crystallographic Data Centre via www.ccdc.cam.ac.uk/data_request/cif.

1.6 References

- [1] a) H. C. Brown, M. Srebnik, T. E. Cole, *Organometallics* **1986**, *5*, 2300-2303; b) H. C. Brown, N. Vasumathi, N. N. Joshi, *Organometallics* **1993**, *12*, 1058-1067.
- [2] a) G. Zweifel, H. Arzoumanian, C. C. Whitney, *J. Am. Chem. Soc.* **1967**, *89*, 3652-3653; b) G. Zweifel, R. P. Fisher, J. T. Snow, C. C. Whitney, *J. Am. Chem. Soc.* **1972**, *94*, 6560-6561.
- [3] a) A. Bonet, M. Odachowski, D. Leonori, S. Essafi, V. K. Aggarwal, *Nat. Chem.* **2014**, *6*, 584-589; b) D. Leonori, V. K. Aggarwal, *Angew. Chem. Int. Ed. Engl.* **2015**, *54*, 1082-1096.
- [4] a) R. Larouche-Gauthier, T. G. Elford, V. K. Aggarwal, *J. Am. Chem. Soc.* **2011**, *133*, 16794-16797; b) M. Mohiti, C. Rampalakos, K. Feeney, D. Leonori, V. K. Aggarwal, *Chem. Sci.* **2014**, *5*, 602-607.
- [5] C. García-Ruiz, J. L. Y. Chen, C. Sandford, K. Feeney, P. Lorenzo, G. Berionni, H. Mayr, V. K. Aggarwal, *J. Am. Chem. Soc.* **2017**, *139*, 15324-15327.
- [6] L. Zhang, G. J. Lovinger, E. K. Edelstein, A. A. Szymaniak, M. P. Chierchia, J. P. Morken, *Science* **2016**, *351*, 70.
- [7] G. J. Lovinger, M. D. Aparece, J. P. Morken, *J. Am. Chem. Soc.* **2017**, *139*, 3153-3160.
- [8] S. Roscales, A. G. Csaky, *Chem. Soc. Rev.* **2014**, *43*, 8215-8225.
- [9] a) G. Berionni, B. Maji, P. Knochel, H. Mayr, *Chem. Sci.* **2012**, *3*, 878-882; b) G. Berionni, V. Morozova, M. Heininger, P. Mayer, P. Knochel, H. Mayr, *J. Am. Chem. Soc.* **2013**, *135*, 6317-6324.
- [10] H. Mayr, T. Bug, M. F. Gotta, N. Hering, B. Irrgang, B. Janker, B. Kempf, R. Loos, A. R. Ofial, G. Remennikov, H. Schimmel, *J. Am. Chem. Soc.* **2001**, *123*, 9500-9512.
- [11] a) S. Toyota, M. Oki, *Bull. Chem. Soc. Jpn.* **1992**, *65*, 1832-1840; b) H. Höpfl, *J. Organomet. Chem.* **1999**, *581*, 129-149.
- [12] H. Mayr, M. Patz, *Angew. Chem. Int. Ed. Engl.* **1994**, *33*, 938-957.
- [13] T. M. Reetz, S. Hütte, R. Goddard, *J. Prakt. Chem.* **1999**, *341*, 297-301.
- [14] a) F. Kakiuchi, M. Usui, S. Ueno, N. Chatani, S. Murai, *J. Am. Chem. Soc.* **2004**, *126*, 2706-2707; b) M. Takeda, K. Takatsu, R. Shintani, T. Hayashi, *J. Org. Chem.* **2014**, *79*, 2354-2367; c) Y. Zhao, V. Snieckus, *Org. Lett.* **2014**, *16*, 3200-3203.
- [15] A. Adamczyk-Woźniak, M. Jakubczyk, P. Jankowski, A. Sporzyński, P. M. Urbański, *J. Phys. Org. Chem.* **2013**, *26*, 415-419.
- [16] A. Del-Grosso, P. J. Singleton, C. A. Muryn, M. J. Ingleson, *Angew. Chem. Int. Ed.* **2011**, *50*, 2102-2106.
- [17] M. Tobisu, H. Kinuta, Y. Kita, E. Rémond, N. Chatani, *J. Am. Chem. Soc.* **2012**, *134*, 115-118.
- [18] I. I. B. A. Vanchura, S. M. Preshlock, P. C. Roosen, V. A. Kallepalli, R. J. Staples, J. R. E. Maleczka, D. A. Singleton, I. I. I. Smith, R. Milton, *Chem. Comm.* **2010**, *46*, 7724-7726.

- [19] G. A. Molander, O. A. Argintaru, I. Aron, S. D. Dreher, *Org. Lett.* **2010**, 12, 5783-5785.
- [20] C. Schade, W. Bauer, P. Von Ragué Schleyer, *J. Organomet. Chem.* **1985**, 295, 25-28.
- [21] K. Ukai, M. Aoki, J. Takaya, N. Iwasawa, *J. Am. Chem. Soc.* **2006**, 128, 8706-8707.
- [22] S. Claudel, C. Gosmini, J. M. Paris, J. Perichon, *Chem. Comm.* **2007**, 3667-3669.
- [23] M. F. Gotta, H. Mayr, *J. Org. Chem.* **1998**, 63, 9769-9775.

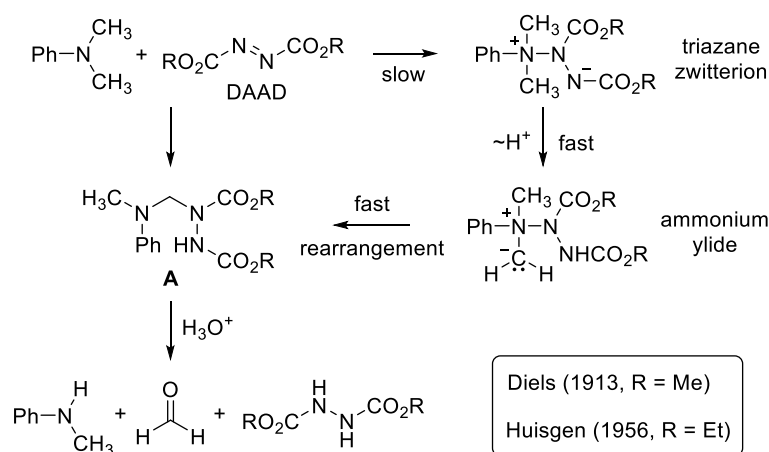
Chapter 2

Transition Metal-Free C-H Activation of Tertiary Amines: Diisopropyl Azodicarboxylate Mediated α -Functionalization

2.1 Introduction

Functionalization of tertiary amines at the sp^3 -hybridized α -carbon has been an emerging field of organic chemistry in recent years.^[1] Using this synthetic method for the introduction of an aryl moiety would furnish benzylic amines, which are a common structural motif of market-relevant pharmaceuticals.^[2] Several methods for the arylation of tertiary amines were developed, which, however, generally rely on the use of stoichiometric or catalytic amounts of metal salts.^[3]

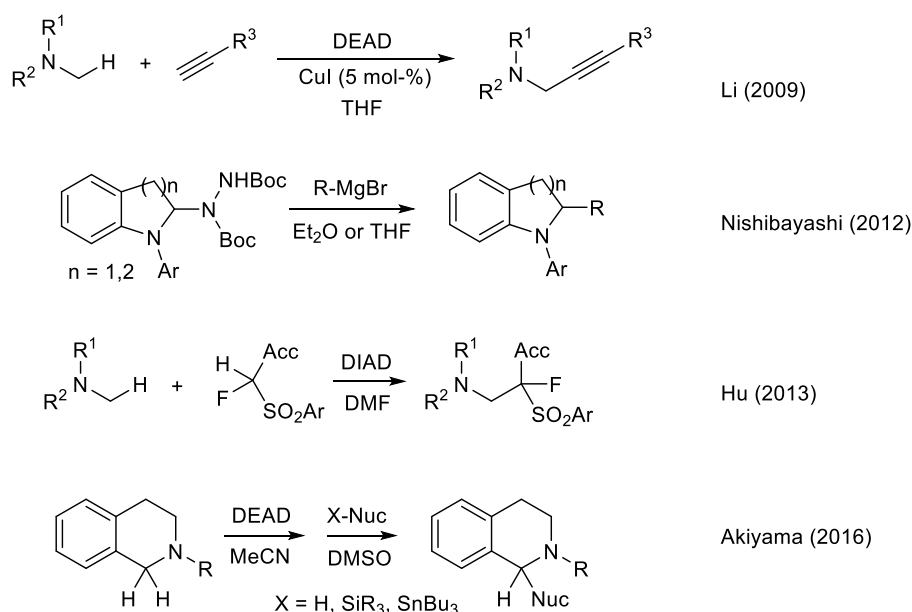
In this context, dialkyl azodicarboxylates (DAADs) appeared attractive reagents since they possess electrophilic as well as oxidative properties.^[4] Combination of these features was first utilized in 1913 by Diels and Paquin,^[5] who achieved demethylation of tertiary amines through hydrolysis of aminal **A** obtained after oxidative addition of dimethyl azodicarboxylate (Scheme 2.1). Slow nucleophilic attack of the amine at the double bond of azodicarboxylate, followed by fast proton transfer and subsequent rearrangement to form aminal **A** were suggested later by Huisgen.^[6]



Scheme 2.1. Demethylation of *N,N*-dimethylaniline through addition of dialkyl azodicarboxylates (DAADs) and subsequent hydrolysis.

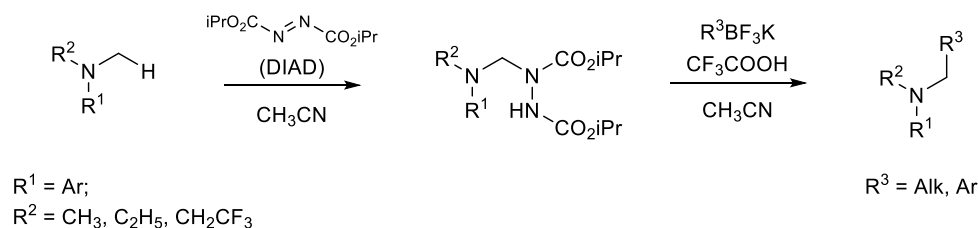
In 2009, first examples of intermolecular CC bond-forming reactions were disclosed by Li and Xu, who successfully applied oxidative C(sp^3)-H bond amination by diethyl azodicarboxylate (DEAD) for CuI-catalyzed alkynylations of aliphatic tertiary methylamines (Scheme 2.2).^[7] Transition metal catalysis was found to be dispensable when acidic pronucleophiles or otherwise activated nucleophiles were used for DAAD-mediated α -functionalizations of tertiary

amines.^[8] Nishibayashi exploited the Lewis acidity of Grignard reagents (2.2 equiv.) in azodicarboxylate-mediated α -arylations of cyclic tertiary amines.^[9] Hu showed that a mixture of diisopropyl azodicarboxylate (DIAD) and CH acidic acceptor-substituted fluoromethylsulfones selectively fluoromethylated NCH_3 groups of tertiary aliphatic amines.^[10] DMSO as a highly polar solvent turned out to be beneficial when Akiyama and co-workers used a set of structurally diverse nucleophiles (silylated enol ethers, CH acids, allylstannanes etc.) in combination with DEAD as the oxidant to functionalize the C-1 position of tetrahydroisoquinolines (THIQs). The authors suggested that the basicity of the dicarboxyhydrazide anion was a further crucial factor for achieving high yielding reactions of the THIQ-DEAD addition products with these (pro)nucleophiles.^[11]



Scheme 2.2. Intermolecular CC bond-forming reactions upon DAAD-mediated oxidation of tertiary amines.

In our work we have synthesised and isolated aminsals, derived from different *N*-alkyl-*N*-methylanilines and diisopropyl azodicarboxylate (DIAD), and investigated their electrophilic properties towards organotrifluoroborates (Scheme 2.3).



Scheme 2.3. α -Amination of selected *N*-methylanilines with DIAD and subsequent α -functionalization by organotrifluoroborates.

2.2 Results and Discussion

In agreement with a recent study,^[11] the amins **2** were obtained after reaction of DIAD (used in slight excess) with corresponding *N*-methylanilines **1** in acetonitrile (Table 2.1).^[12] Even though, the reaction can proceed at ambient temperature, heating the solution to reflux shortened the reaction time significantly. Our study showed exclusive attack of DIAD at α -methyl group in asymmetrical *N*-ethyl-*N*-methylaniline and *N*-methyl-*N*-(2,2,2-trifluoroethyl)aniline. The electrochemical oxidative α -functionalization of the latter is known to proceed at the NCH_2CF_3 group.^[13]

Table 2.1. Synthesis of amins **2a-c**.

Aniline		Product	Time (yield) ^[a]
1a	R, X = Me	2a	4 days (95 %) ^[b]
1b	R = Me, X = OMe	2b	4 hours (81%) ^[b]
1c	R = Me, X = F	2c	2 days (88%) ^[b]
1d	R = Et, X = H	2d	6 days (83%)
1e	R = -CH ₂ CF ₃ , X = H	2e	7 days (39%)

[a] Isolated after column chromatography. [b] From ref. ^[15]

As typically observed for amides or carbamates,^[11, 14] the broad, unresolved signals in the ¹H and ¹³C NMR spectra (CDCl₃, 27 °C) of hydrazine-1,2-dicarboxylates **2** indicated hindered rotations around the N-C bonds in (H)NN-CO and (R)(N)N-CO groups. Significantly improved resolutions and signal-to-noise ratios of the resonances were achieved when the NMR spectra of the hydrazine-1,2-dicarboxylates **2** were acquired in *d*₆-DMSO at 90 °C.

Optimization of reaction conditions showed,^[15] that Lewis (e.g. ZnBr₂ or BF₃·Et₂O) as well as Brønsted acids (e.g. aqueous HCl) facilitate the nucleophilic attack of the aryl trifluoroborates at amins such as **2**. However, best results were achieved by utilizing a stoichiometric amount of trifluoroacetic acid (TFA) in CH₃CN.

Under the conditions above we have tested the scope of potassium organotrifluoroborates that can be used for substituting the hydrazine moiety in amins **2** (Figure 2.1).

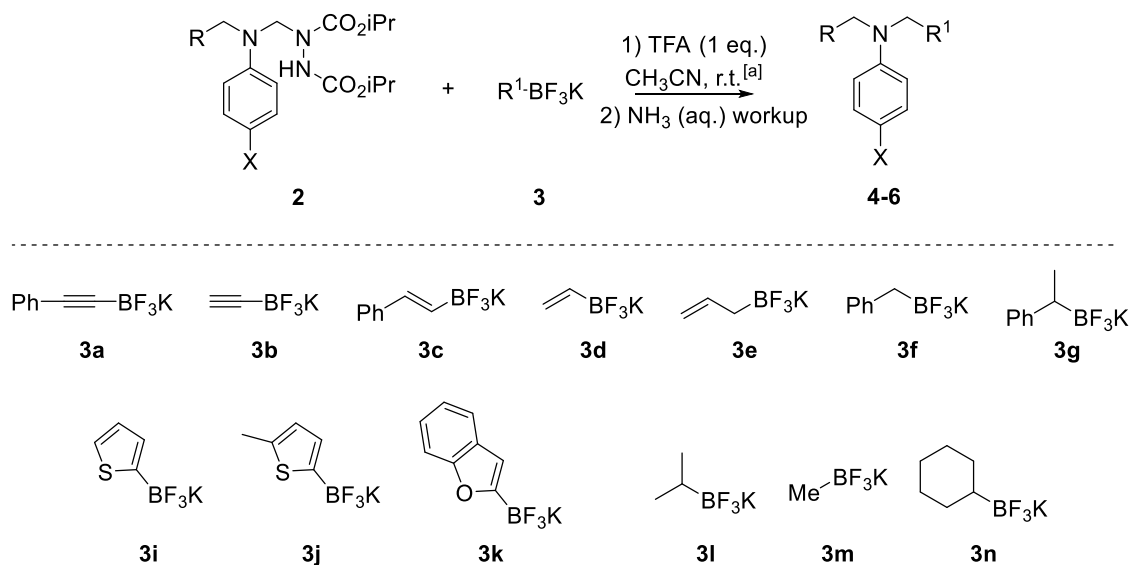


Figure 2.1. General scheme of the reaction between amins **2** and potassium organotrifluoroborates **3** (top); the scope of the studied potassium trifluoroborates **3** (bottom). [a] For the reaction time see Experimental Section.

Substitution in the para position in amins **2a-c** did not have a systematic influence on the overall yield of the reaction. Unsaturated organotrifluoroborates **3a** and **3c** led to formation of substituted anilines **4aa-4ce** (Figure 2.2, top), which were previously obtained only through transition metal catalyzed cross-coupling reactions.^[11] Benzyl- and (α -methyl)benzyltrifluoroborates **3f-g** further widened the scope of this process, giving *N*-methylanilines **4af-4cg** in rather poor, yet significant yield (Figure 2.2, bottom).

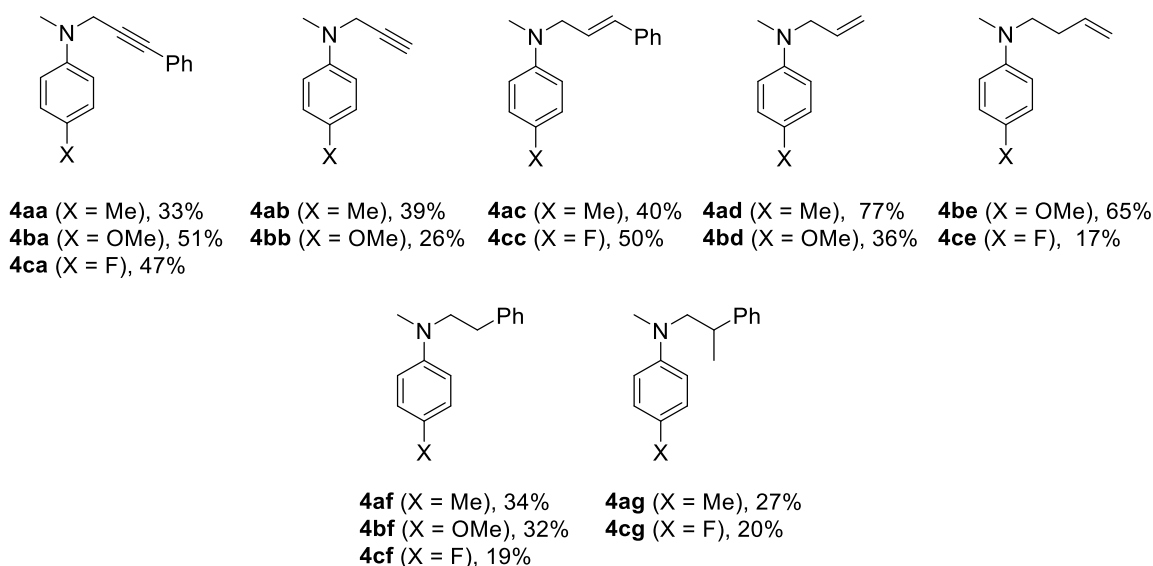


Figure 2.2. Substituted anilines obtained from amins **2a-c** and unsaturated organotrifluoroborates **3a-e** (top) and benzyltrifluoroborates **3f-g** (bottom). Yields refer to isolated products after purification by column chromatography.

In accordance with the selective attack of DIAD at the α -CH₂- group at the substituted *N*-ethyl-*N*-methylanilines **1d-e**, arylated species **4di-4ek** were obtained in moderate yields (Figure 2.3) under standard conditions from corresponding aminals **2d-e** and potassium aryltrifluoroborates **3i-k**.

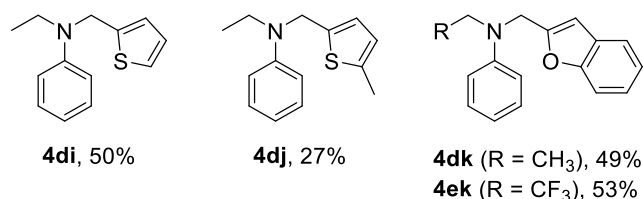


Figure 2.3. *N*-Methyl-*N*-(1-arylated-2,2,2-trifluoroethyl)anilines **4di-4ek** obtained from corresponding aminals **2d-e** and potassium aryltrifluoroborates **3i-k** under standard conditions.

However, reaction between DIAD-activated *N,N*-dimethylaniline **2a** and alkyl-substituted trifluoroborates **3l-m** did not show any conversion of the starting material even after 7 days. Only for potassium cyclohexyltrifluoroborate **3n** the product was detected by GC/MS analysis in trace amount after 7 days of the reaction at the standard conditions.

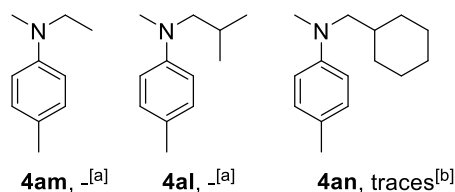
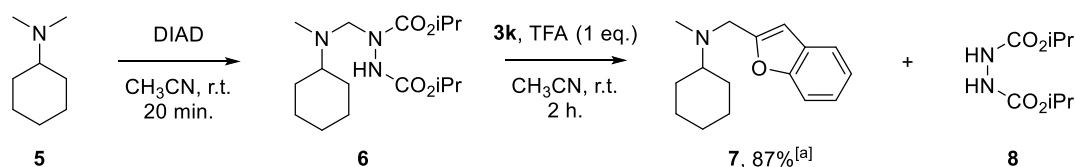


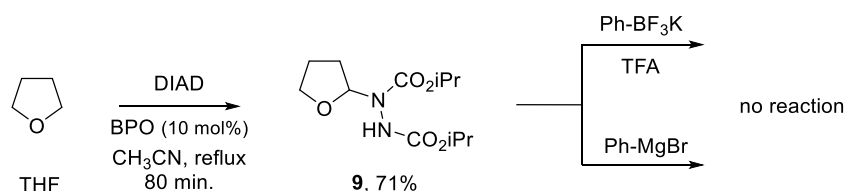
Figure 2.4. Suggested product structures for nucleophilic attack of the aliphatic organotrifluoroborates **3l-k** on the amina **2a**. [a] No conversion after 7 days under standard conditions. [b] Detected by GC/MS.

Attempts to functionalize α -carbon of aliphatic amines using the same DIAD activation method were taken on *N,N*-dimethylcyclohexylamine **5** (Scheme 2.4). The disappearance of the yellow color of DIAD in a reaction with **5** indicated that the reaction was finished within 20 minutes in CH₃CN at ambient temperature. Since the isolation of the intermediate adduct **6** was not possible, a one pot reaction with **3k** and 1 equivalent of TFA (standard conditions) was performed, which furnished a mixture of hydrazine **8** and the 2-substituted benzofuran **7**. However, separation of these two products was not accomplished neither by column chromatography nor by distillation. Best results were achieved by varying the pH value of the aqueous phase at the work-up step: repeated extraction with *n*-pentane gave 1/3 and 1/7 mixtures of **7** and **8** at pH 5 and pH 10 respectively, indicating that this synthetic procedure will need further optimization for each specific mixture of amine, azodicarboxylate and nucleophile.



Scheme 2.4. DIAD-activation of *N,N*-dimethylcyclohexylamine **5**. [a] Calculated from the crude mixture with **8**.

It is known,^[16] that azodicarboxylates can also form adducts with ethers in presence of radical activators. In this way adduct **9** was obtained after reaction of DIAD with THF with 10 mol % of benzoyl peroxide (BPO) at reflux after 80 minutes. However, activated by TFA, hydrazine **9** did not undergo the reaction with potassium phenyltrifluoroborate (Scheme 2.5). Also no conversion was observed in a reaction with phenylmagnesium bromide, which is known to react with DIAD-adducts of anilines.^[9a]



Scheme 2.5. DIAD-activation of tetrahydrofuran.

2.3 Conclusion

Additions of diisopropyl azodicarboxylate (DIAD) to aromatic and aliphatic tertiary amines in acetonitrile generated aminomethylated hydrazine-1,2-dicarboxylates. The insertion of DIAD in the C-H bond of an NCH_3 group thus provided α -functionalization of tertiary amines under mild conditions. The high reactivities of potassium organotrifluoroborates^[17] and their stability under acidic conditions allowed us to transform the DIAD-amine addition products to a series of α -functionalized amines. DIAD demonstrated selective attack on the α - CH_3 group in *N*-alkyl-*N*-methylanilines with subsequent substitution of hydrazine moiety without use of any transition metal catalyst. Furthermore, this method was shown to successfully introduce functional group at the α -methyl position in a series of aliphatic amines, even though, these reactions still require further optimization.

2.4 Experimental Section

2.4.1 General

All reactions were performed in carefully dried Schlenk glassware in an atmosphere of dry nitrogen. The reactions were not optimized for high yields.

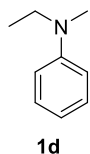
^1H NMR (600, 400, or 300 MHz), ^{13}C NMR (151, 101, or 75.5 MHz), and ^{19}F NMR spectra (376 MHz) were recorded on Varian or Bruker NMR systems in d_6 -DMSO or CDCl_3 . Chemical shifts in ppm refer to the solvent residual signal in d_6 -DMSO (δ_{H} 2.50, δ_{C} 39.52 ppm) or CDCl_3 (δ_{H} 7.26, δ_{C} 77.16 ppm) as internal standard respectively. The following abbreviations are used to describe the multiplicities of ^1H resonances: br s = broad singlet, s = singlet, d = doublet, t = triplet, q = quartet, sept = septet, m = multiplet, app = apparent. NMR signal assignments are based on additional 2D-NMR experiments (COSY, HSQC, and HMBC).

Chemicals. Commercially available acetonitrile (Acros, 99.9%, Extra Dry, AcroSeal) was used as received. Diisopropyl azodicarboxylate (DIAD; 94%, ABCR or Apollo) was purchased and used as received. The following commercially available potassium trifluoroborates were used as received: potassium 2-phenyl-1-ethynyltrifluoroborate **3a**, potassium styryltrifluoroborate **3c**, potassium vinyltrifluoroborate **3d**, potassium 1-phenylethyltrifluoroborate **3g**, potassium methyltrifluoroborate **3m**, potassium isopropyltrifluoroborate **3l**, potassium cyclohexyltrifluoroborate **3n**, potassium thiophene-2-trifluoroborate **3i**. Potassium benzofuran-2-yltrifluoroborate **3k** was recrystallized from acetone/diethyl ether before use.

Potassium 5-methylthiophene-2-trifluoroborate **3i** was synthesized from 5-methylthiophene by subsequent treatment with *n*-BuLi, $\text{B}(\text{OiPr})_3$, and KHF_2 (6 equiv.) in analogy to a procedure described in ref.^[17] Following same methodology, potassium ethynyltrifluoroborate **3b** and potassium benzyltrifluoroborate **3f** were synthesized from their commercially available organomagnesium analogs. The crude material was purified by recrystallization from acetone/diethyl ether.

2.4.2 Synthesis of substituted *N*-methylanilines **1d-e** and amins **2d-e**

N,N-Ethylmethylaniline (**1d**)

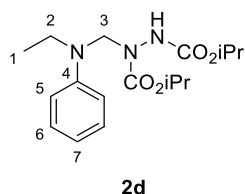


N-Methyl aniline (3.3 ml, 30 mmol, 1 eq.), bromoethane (3.80 ml, 51 mmol, 1.7 eq.) and potassium carbonate (10.4 g, 75 mmol, 2.5 eq.) were mixed together in ethanol (100 ml) and refluxed overnight. Resulting mixture was filtrated, solvent removed by evaporation and crude product was purified by column chromatography (EtOAc/*n*-pentane = 1/30, R_f = 0.36). *N,N*-ethylmethyl aniline (3.1 g, 80%) was obtained as colorless oil.

^1H NMR data is in agreement with the literature.^[18]

Diisopropyl 1-(((phenyl)(ethyl)amino)methyl)hydrazine-1,2-dicarboxylate (**2d**)

N-Ethyl-*N*-methyl aniline (2.00 g, 14.8 mmol, 1.05 eq.) was dissolved in CH_3CN (5 ml), DIAD (2.78 ml, 14.1 mmol, 1 eq.) was added subsequently and the mixture was refluxed for 6 days. After solvent evaporation the crude product was purified by column chromatography ($\text{Et}_2\text{O}/n$ -pentane = 1/10, R_f = 0.19). **2d** was obtained as yellowish viscous oil (4.14 g, 83%).

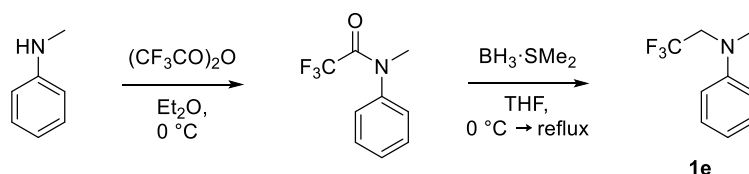


^1H NMR (400 MHz, DMSO, 90 °C) δ = 1.09 – 1.26 (m, 15H, H-1, $2 \times -\text{OCH}(\underline{\text{CH}}_3)_2$), 3.41 (q, 3J = 7.0 Hz, 2H, H-2), 4.74 – 4.91 (m, 2H, $2 \times -\text{OCH}(\underline{\text{CH}}_3)_2$), 4.98 (s, 2H, H-3), 6.67 (t, 3J = 7.2 Hz, 1H, H-7), 6.83 (d, 3J = 8.0 Hz, 2H, H-5), 7.12 – 7.18 (m, 2H, H-6), 8.95 (br s, 1H, NH).

^{13}C NMR (101 MHz, DMSO, 90 °C) δ = 11.8 (C-1), 21.3 ($2 \times -\text{OCH}(\underline{\text{CH}}_3)_2$), 43.1 (C-2), 64.0 (C-3), 67.7 ($-\text{OCH}(\underline{\text{CH}}_3)_2$), 68.8 ($-\text{OCH}(\underline{\text{CH}}_3)_2$), 112.8 (C-5), 116.5 (C-7), 128.3 (C-6), 146.9 (C-4), 154.8 ($-\text{CO}_2^-$), 154.9 ($-\text{CO}_2^-$).

HR-MS (ESI, pos.) m/z calcd. for $\text{C}_{17}\text{H}_{28}\text{N}_3\text{O}_4$ $[\text{M}+\text{H}]^+$ 338.2074, found 338.2076.

N-Methyl-*N*-(2,2,2-trifluoroethyl)aniline (**1e**)



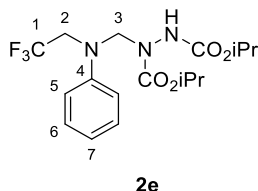
A solution of *N*-methylaniline (3.0 g, 28 mmol, 1 eq.) in Et_2O (6 ml) was added to a solution of trifluoroacetic anhydride (7.8 ml, 56 mmol, 2 eq.) in Et_2O (10 ml) at $0\text{ }^\circ\text{C}$. The reaction mixture was stirred at this temperature for 1 hour before the solvent was evaporated and diluted with ice-water. The obtained solution was extracted CH_2Cl_2 ($3 \times 50\text{ ml}$), the organic phases were combined, washed with brine and dried over MgSO_4 . Crude 2,2,2-trifluoro-*N*-methyl-*N*-phenylacetamide was concentrated in vacuum and used without further purification.

2,2,2-Trifluoro-*N*-methyl-*N*-phenylacetamide (4.2 g, 20.5 mmol, 1 eq.), obtained above, was dissolved in THF (25 ml) and borane dimethyl sulfide complex (technical grade, 95%, 4.1 ml, 41 mmol, 2 eq.) was added dropwise at $0\text{ }^\circ\text{C}$. Subsequently, the mixture was heated to reflux and stirred for another 2h. After cooling down to ambient temperature, the solution was diluted with water (100 ml) and extracted CH_2Cl_2 ($3 \times 50\text{ ml}$). The combined organic layers were washed with brine, dried over MgSO_4 and concentrated in vacuum. The crude material was purified by column chromatography and **1e** was obtained as colorless oil in 62% overall yield.

^1H NMR data is in agreement with the literature.^[13a]

Diisopropyl 1-(((phenyl)(trifluoroethyl)amino)methyl)hydrazine-1,2-dicarboxylate (**2e**)

1c (500 mg, 2.64 mmol, 1 eq.) was dissolved in CH₃CN (5 ml), DIAD (0.52 ml, 2.64 mmol, 1 eq.) was added subsequently and the mixture was refluxed for 7 days. After solvent evaporation crude product was purified by column chromatography (Et₂O/*n*-pentane = 1/10, R_f = 0.19). **2b** was obtained as yellowish viscous oil (406 mg, 39%).



¹H NMR (400 MHz, DMSO, 90 °C) δ = 1.13 (d, 3J = 6.2 Hz, 6H, -OCH(CH₃)₂), 1.22 (d, 3J = 6.2 Hz, 6H, -OCH(CH₃)₂), 4.18 (q, $^3J_{\text{HF}}$ = 9.4 Hz, 2H, H-2), 4.76 (hept, 3J = 6.2 Hz, 1H, -OCH(CH₃)₂), 4.86 (hept, 3J = 6.2 Hz, 1H, -OCH(CH₃)₂), 5.09 (s, 2H, H-3), 6.79 – 6.85 (m, 1H, H-7), 7.02 (d, 3J = 8.1 Hz, 2H, H-5), 7.18 – 7.24 (m, 2H, H-6), 8.97 (s, 1H, NH).

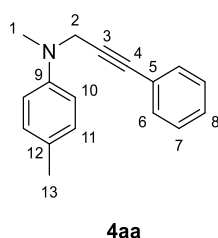
¹³C NMR (101 MHz, DMSO, 90 °C) δ = 21.2 (-OCH(CH₃)₂), 49.30 (q, $^2J_{\text{CF}}$ = 33.1 Hz, C-2), 64.4 (C-3), 67.9 (-OCH(CH₃)₂), 69.2 (-OCH(CH₃)₂), 114.4 (C-5), 118.8 (C-7), 125.39 (q, $^1J_{\text{CF}}$ = 282.9 Hz, C-1) 128.4 (C-6), 146.5 (C-4), 155.0 (-CO₂-).

HR-MS (ESI, neg.) m/z calcd. for C₁₇H₂₃F₃N₃O₄ [M-H]⁻ 390.1646, found 390.1652.

2.4.3 General procedure for reaction of amins 2a-c with potassium organotrifluoroborates

2 (1 eq.) and potassium trifluoroborate (1.05 eq.) were dissolved in dry CH₃CN (5 ml) at room temperature. TFA (1.1 eq.) was added subsequently and the mixture was stirred for 2 hours, unless otherwise stated. Upon completion the reaction mixture was quenched with 2 M NH₃(aq.) until pH~12 and extracted CH₂Cl₂ (3 × 10 ml). The collected organic phases were united, dried over anhydrous MgSO₄ and concentrated under vacuum. The crude product was purified by column chromatography (eluent: Et₂O/*n*-pentane).

N,4-Dimethyl-*N*-(3-phenylprop-2-yn-1-yl)aniline (**4aa**)



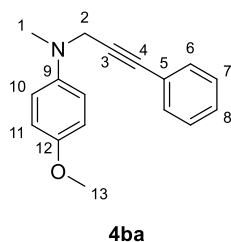
Following general procedure, starting from **2a** (80 mg, 0.24 mmol, 1 eq.) and **3a** (52 mg, 0.25 mmol, 1.04 eq.), **4aa** was obtained as yellow oil in 33% yield (19 mg) after 20 hours.

¹H NMR (300 MHz, CDCl₃): δ = 2.28 (s, 3H, H-13), 3.00 (s, 3H, H-1), 4.23 (s, 2H, H-2), 6.82 – 6.89 (m, 2H, H-10), 7.06 – 7.13 (m, 2H, H-11), 7.23 – 7.29 (m, 3H, H-7, H-8), 7.33 – 7.41 (m, 2H, H-6).

¹³C NMR (75 MHz, CDCl₃): δ = 20.5 (C-13), 39.1 (C-1), 43.9 (C-2), 84.4 (C-4), 85.2 (C-3), 115.1 (C-10), 123.2 (C-5), 127.9 (C-12), 128.2 (C-8), 128.3 (C-7), 129.7 (C-11), 131.9 (C-6), 147.4 (C-9).

HR-MS (EI, pos.) *m/z* calcd. for C₁₇H₁₇N [M]⁺⁺ 235.1356, found 235.1353.

4-Methoxy-N-methyl-N-(3-phenylprop-2-yn-1-yl)aniline (**4ba**)



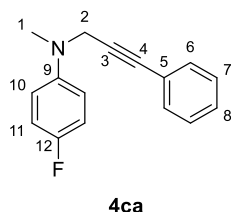
Following general procedure, starting from **2b** (89 mg, 0.24 mmol, 1 eq.) and **3a** (52 mg, 0.25 mmol, 1.04 eq.), **4ba** was obtained as white solid in 51% yield (31 mg).

¹H NMR (400 MHz, CDCl₃) δ = 2.90 (s, 3H, H-1), 3.71 (s, 3H, H-13), 4.11 (s, 2H, H-2), 6.77 – 6.83 (m, 2H, H-10), 6.84 – 6.90 (m, 2H, H-11), 7.18 – 7.22 (m, 3H, H-7, H-8), 7.27 – 7.33 (m, 2H, H-6).

¹³C NMR (101 MHz, CDCl₃) δ = 39.6 (C-1), 44.9 (C-2), 55.6 (C-13), 84.6 (C-3/C-4), 84.9 (C-4/C-3), 114.5 (C-10), 117.2 (C-11), 123.1 (C-5), 128.1 (C-8), 128.2 (C-7), 131.7 (C-6), 143.9 (C-9), 153.2 (C-12).

HR-MS (ESI, pos.) m/z calcd. for C₁₇H₁₈NO [M+H]⁺ 252.1383, found 252.1384.

4-Fluoro-N-methyl-N-(3-phenylprop-2-yn-1-yl)aniline (**4ca**)



Following general procedure, starting from **2c** (85 mg, 0.24 mmol, 1 eq.) and **3a** (52 mg, 0.25 mmol, 1.04 eq.), **4ca** was obtained as yellow oil in 47% yield (27 mg).

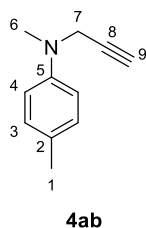
¹H NMR (400 MHz, CDCl₃) δ = 2.92 (s, 3H, H-1), 4.15 (s, 2H, H-2), 6.77 – 6.84 (m, 2H, H-10), 6.88 – 6.96 (m, 2H, H-11), 7.18 – 7.24 (m, 3H, H-7, H-8), 7.28 – 7.33 (m, 2H, H-6).

¹³C NMR (101 MHz, CDCl₃) δ = 39.5 (C-1), 44.4 (C-2), 84.7 (C-3/C-4), 84.7 (C-4/C-3), 115.59 (d, ²J_{CF} = 22.1 Hz, C-11), 116.32 (d, ³J_{CF} = 7.5 Hz, H-10), 123.0 (C-5), 128.3 (C-8), 128.4 (C-7), 131.9 (C-6), 146.1 (C-9), 156.6 (d, ¹J_{CF} = 237.1 Hz, C-12).

¹⁹F NMR (376 MHz, CDCl₃) δ = -126.7 (br s).

HR-MS (ESI, pos.) m/z calcd. for C₁₆H₁₅FN [M+H]⁺ 240.1183, found 240.1183.

N,4-Dimethyl-*N*-(prop-2-yn-1-yl)aniline (**4ab**)



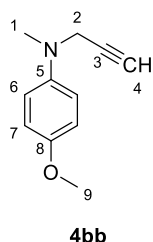
Following general procedure, starting from **2a** (0.7 ml of 0.34 M solution in CH₃CN, 0.24 mmol, 1 eq.) and **3b** (33 mg, 0.25 mmol, 1.04 eq.), **4ab** was obtained as colorless oil in 39% yield (15 mg) after 14 hours.

¹H NMR (400 MHz, CDCl₃): δ = 2.17 (t, 4J = 2.4 Hz, 1H, H-9), 2.28 (s, 3H, H-1), 2.94 (s, 3H, H-6), 4.03 (d, 4J = 2.4 Hz, 2H, H-7), 6.78 – 6.83 (m, 2H, H-4), 7.07 – 7.11 (m, 2H, H-3).

¹³C NMR (100 MHz, CDCl₃): δ = 20.5 (C-1), 39.0 (C-6), 43.1 (C-7), 72.2 (C-9), 79.4 (C-8), 115.0 (C-4), 128.0 (C-2), 129.8 (C-3), 147.1 (C-5).

HR-MS (EI, pos.) m/z calcd. for C₁₁H₁₃N [M]^{•+} 159.1043, found 159.1044.

4-Methoxy-*N*-methyl-*N*-(prop-2-yn-1-yl)aniline (**4bb**)^[19]



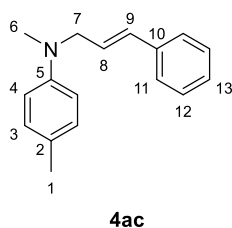
Following general procedure, starting from **2b** (89 mg, 0.24 mmol, 1 eq.) and **3b** (33 mg, 0.25 mmol, 1.04 eq.), **4bb** was obtained as white solid in 26% yield (11 mg).

¹H NMR (400 MHz, CDCl₃) δ = 2.18 (t, 4J = 2.4 Hz, 1H, H-4), 2.90 (s, 3H, H-1), 3.77 (s, 3H, H-9), 3.98 (d, 4J = 2.4 Hz, 2H, H-2), 6.86 (m, 4H, H-6, H-7).

¹³C NMR (101 MHz, CDCl₃) δ = 39.5 (C-1), 44.0 (C-2), 55.8 (C-9), 72.4 (C-4), 79.4 (C-3), 114.7 (C-7/C-6), 117.0 (C-6/C-7), 143.8 (C-5), 153.2 (C-8).

HR-MS (ESI, pos.) m/z calcd. for C₁₁H₁₄NO [M+H]⁺ 176.1070, found 176.1070.

N-Cinnamyl-*N*,4-dimethylaniline (**4ac**)



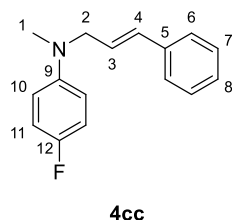
Following general procedure, starting from **2a** (80 mg, 0.24 mmol, 1 eq.) and **3c** (53 mg, 0.25 mmol, 1.04 eq.), **4ac** was obtained as colorless oil in 40% yield (23 mg) after 20 hours.

¹H NMR (400 MHz, CDCl₃): δ = 2.28 (s, 3H, H-1), 2.95 (s, 3H, H-6), 4.06 (dd, ³*J* = 5.6 Hz, ²*J* = 1.5 Hz, 2H, H-7), 6.26 (dt, ³*J* = 15.9 Hz, ³*J* = 5.6 Hz, 1H, H-8), 6.54 (d, ³*J* = 15.9 Hz, 1H, H-9), 6.71 – 6.77 (m, 2H, H-4), 7.04–7.11 (m, 2H, H-3), 7.20 – 7.25 (m, 1H, H-13), 7.27 – 7.34 (m, 2H, H-12), 7.34 – 7.39 (m, 2H, H-11).

¹³C NMR (101 MHz, CDCl₃): δ = 20.4 (C-1), 38.4 (C-6), 55.5 (C-7), 126.1 (C-2), 126.2 (C-8), 126.4 (C-11), 127.5 (C-13), 128.6 (C-12), 129.8 (C-3), 131.4 (C-9), 137.1 (C-10), 147.8 (C-5).

HR-MS (EI, pos.) *m/z* calcd. for C₁₇H₁₉N [M]⁺ 237.1512, found 237.1519.

N-Cinnamyl-4-fluoro-*N*-methylaniline (**4cc**)



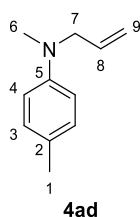
Following general procedure, starting from **2c** (85 mg, 0.24 mmol, 1 eq.) and **3e** (53 mg, 0.25 mmol, 1.04 eq.), **4cc** was obtained as yellowish solid in 50% yield (30 mg).

¹H NMR (400 MHz, CDCl₃) δ = 2.95 (s, 3H, H-1), 4.04 (dd, *J* = 5.6, 1.5 Hz, 2H, H-2), 6.24 (dt, *J* = 15.9, 5.6 Hz, 1H, H-3), 6.53 (d, *J* = 15.9 Hz, 1H, H-4), 6.70 – 6.77 (m, 2H, H-10), 6.93 – 7.00 (m, 2H, H-11), 7.21 – 7.27 (m, 1H, H-8), 7.29 – 7.34 (m, 2H, H-7), 7.35 – 7.39 (m, 2H, H-6).

¹³C NMR (101 MHz, CDCl₃) δ = 38.7 (C-1), 55.9 (C-2), 114.1 (d, ³*J*_{CF} = 7.3 Hz, C-10), 115.6 (d, ²*J*_{CF} = 22.0 Hz, C-11), 125.7 (C-3), 126.4 (C-6), 127.6 (C-8), 128.7 (C-7), 131.7 (C-4), 136.9 (C-5), 146.5 (d, ⁴*J*_{CF} = 1.5 Hz, C-9), 155.7 (d, ¹*J*_{CF} = 235.3 Hz, C-12).

¹⁹F NMR (376 MHz, CDCl₃) δ = -128.9 (tt, *J*_{HF} = 8.5, 4.4 Hz).

N-Allyl-*N*,4-dimethylaniline (**4ad**)



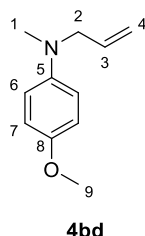
Following general procedure, starting from **2a** (0.7 ml of 0.34 M solution in CH₃CN, 0.24 mmol, 1 eq.) and **3d** (35 mg, 0.25 mmol, 1.04 eq.), **4ad** was obtained as colorless oil in 77% yield (30 mg) after 1 hour.

¹H NMR (300 MHz, CDCl₃): δ = 2.26 (s, 3H, H-1), 2.91 (s, 3H, H-6), 3.89 (d, 3J = 5.2 Hz, 2H, H-7), 5.11-5.23 (m, 2H, H-9), 5.77-5.96 (m, 1H, H-8), 6.68 (d, 3J = 8.4 Hz, 2H, H-4), 7.05 (d, 3J = 8.7 Hz, 2H, H-3).

¹³C NMR (75 MHz, CDCl₃): δ = 20.4 (C-1), 38.3 (C-6), 55.8 (C-7), 113.1 (C-4), 116.3 (C-9), 125.9 (C-2), 129.8 (C-3), 134.2 (C-8), 147.7 (C-5).

HR-MS (EI, pos.) m/z calcd. for C₁₁H₁₅N [M]⁺⁺ 161.1199, found 161.1197.

N-Allyl-4-methoxy-*N*-methylaniline (**4bd**)



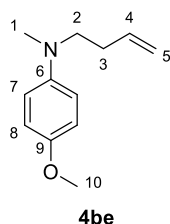
Following general procedure, starting from **2b** (89 mg, 0.24 mmol, 1 eq.) and **3d** (35 mg, 0.25 mmol, 1.04 eq.), **4bd** was obtained as yellowish oil in 36% yield (30 mg).

¹H NMR (400 MHz, CDCl₃) δ = 2.87 (s, 3H, H-1), 3.76 (s, 3H, H-9), 3.84 (dt, J = 5.5, 1.6 Hz, 2H, H-2), 5.13 – 5.22 (m, 2H, H-4), 5.86 (ddt, J = 17.2, 10.3, 5.5 Hz, 1H, H-3), 6.73 – 6.79 (m, 2H, H-6), 6.81 – 6.87 (m, 2H, H-7).

¹³C NMR (101 MHz, CDCl₃) δ = 39.0 (C-1), 55.9 (C-9), 56.9 (C-2), 114.8 (C-7), 115.2 (C-6), 116.9 (C-4), 134.2 (C-3), 144.3 (C-5), 152.2 (C-8).

HR-MS (ESI, pos.) m/z calcd. for C₁₁H₁₆NO [M+H]⁺ 178.1226, found 178.1232.

N-(But-3-en-1-yl)-4-methoxy-*N*-methylaniline (**4be**)



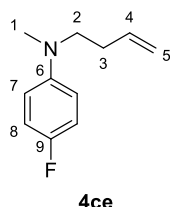
Following general procedure, starting from **2b** (89 mg, 0.24 mmol, 1 eq.) and **3e** (37 mg, 0.25 mmol, 1.04 eq.), **4be** was obtained as white solid in 65% yield (31 mg).

¹H NMR (400 MHz, CDCl₃) δ = 2.26 – 2.35 (m, 2H, H-3), 2.88 (s, 3H, H-1), 3.29 – 3.35 (m, 2H, H-2), 3.77 (s, 3H, H-10), 5.01 – 5.12 (m, 2H, H-5), 5.83 (ddt, J = 17.1, 10.2, 6.9 Hz, 1H, H-4), 6.69 – 6.75 (m, 2H, H-7), 6.82 – 6.88 (m, 2H, H-8).

¹³C NMR (101 MHz, CDCl₃) δ = 31.1 (C-3), 39.1 (C-1), 53.7 (C-2), 55.9 (C-10), 114.7 (C-7/C-8), 114.9 (C-8/C-7), 116.3 (C-5), 136.3 (C-4), 144.3 (C-6), 151.8 (C-9).

HR-MS (ESI, pos.) m/z calcd. for C₁₂H₁₈NO [M+H]⁺ 192.1383, found 192.1386.

N-(But-3-en-1-yl)-4-fluoro-*N*-methylaniline (**4ce**)



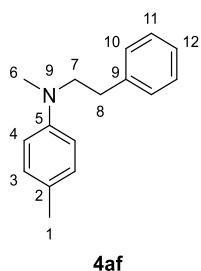
Following general procedure, starting from **2c** (85 mg, 0.24 mmol, 1 eq.) and **3e** (37 mg, 0.25 mmol, 1.04 eq.), **4ce** was obtained as yellowish oil in 17% yield (7 mg).

¹H NMR (400 MHz, CDCl₃) δ = 2.26 – 2.34 (m, 2H, H-3), 2.89 (s, 3H, H-1), 3.31 – 3.38 (m, 2H, H-2), 5.01 – 5.12 (m, 2H, H-5), 5.82 (ddt, J = 17.1, 10.2, 6.9 Hz, 1H, H-4), 6.61 – 6.68 (m, 2H, H-7), 6.90 – 6.97 (m, 2H, H-8).

¹³C NMR (101 MHz, CDCl₃) δ = 31.1 (C-3), 38.9 (C-1), 53.3 (C-2), 113.7 (d, $^3J_{CF}$ = 7.3 Hz, C-7), 115.6 (d, $^2J_{CF}$ = 22.0 Hz, C-8), 116.6 (C-5), 136.0 (C-4), 146.1 (d, $^4J_{CF}$ = 1.6 Hz, C-6), 155.4 (d, $^1J_{CF}$ = 234.8 Hz, C-9).

¹⁹F NMR (376 MHz, CDCl₃) δ = -129.6 (tt, J_{HF} = 8.5, 4.4).

N,4-Dimethyl-*N*-phenethylaniline (**4af**)



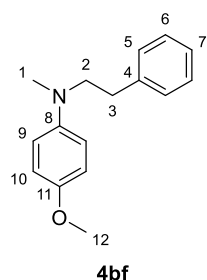
Following general procedure, starting from **2a** (0.7 ml of 0.34 M solution in CH₃CN, 0.24 mmol, 1 eq.) and **3f** (50 mg, 0.25 mmol, 1.04 eq.), **4af** was obtained as colorless oil in 34% yield (18 mg) after 17 hours.

¹H NMR (400 MHz, CDCl₃): δ = 2.29 (s, 3H, H-1), 2.82-2.88 (m, 2H, H-8), 2.89 (s, 3H, H-6), 3.52 – 3.58 (m, 2H, H-7), 6.67 – 6.72 (m, 2H, H-4), 7.06 – 7.11 (m, 2H, H-3), 7.21 – 7.26 (m, 3H, H-10, H-12), 7.29 – 7.35 (m, 2H, H-11).

¹³C NMR (100 MHz, CDCl₃): δ = 20.4 (C-1), 32.9 (C-8), 38.7 (C-6), 55.2 (C-7), 112.7 (C-4), 125.6 (C-2), 126.3 (C-12), 128.6 (C-11), 128.9 (C-10), 129.9 (C-3), 140.1 (C-9), 147.0 (C-5).

HR-MS (EI, pos.) m/z calcd. for C₁₆H₁₉N [M]⁺⁺ 225.1512, found 225.1517.

4-Methoxy-*N*-methyl-*N*-phenethylaniline (**4bf**)



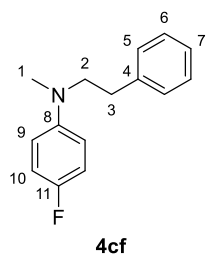
Following general procedure, starting from **2b** (113 mg, 0.34 mmol, 1 eq.) and **3f** (71 mg, 0.36 mmol, 1.06 eq.), **4bf** was obtained as white solid in 32% yield (18 mg).

¹H NMR (400 MHz, CDCl₃) δ = 2.80 – 2.91 (m, 5H, H-3, H-1), 3.46 – 3.53 (m, 2H, H-2), 3.78 (s, 3H, H-12), 6.76 – 6.91 (m, 4H, H-9, H-10), 7.18 – 7.24 (m, 3H, H-5, H-7), 7.27 – 7.33 (m, 2H, H-6).

¹³C NMR (101 MHz, CDCl₃) δ = 32.7 (C-3), 39.2 (C-1, detected by HSQC), 55.8 (C-12), 56.1 (C-2, detected by HSQC), 114.9 (C-10), 126.2 (C-7), 128.5 (C-6), 128.8 (C-5), 140.0 (C-4, detected by HMBC), 152.1 (C-8, detected by HMBC). C-9, C-11 were not detected.

HR-MS (ESI, pos.) m/z calcd. for C₁₆H₂₀NO [M+H]⁺ 242.1539, found 242.1540.

4-Fluoro-*N*-methyl-*N*-phenethylaniline (**4cf**)



Following general procedure, starting from **2c** (85 mg, 0.24 mmol, 1 eq.) and **3f** (50 mg, 0.25 mmol, 1.04 eq.), **4cf** was obtained as yellow oil in 19% yield (9 mg).

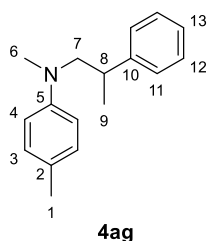
^1H NMR (400 MHz, CDCl_3) δ = 2.80 – 2.88 (m, 5H, H-1, H-3), 3.49 – 3.56 (m, 2H, H-2), 6.61 – 6.71 (m, 2H, H-9), 6.90 – 7.01 (m, 2H, H-10), 7.18 – 7.25 (m, 3H, H-5, H-7), 7.28 – 7.34 (m, 2H, H-6).

^{13}C NMR (101 MHz, CDCl_3) δ = 32.9 (C-3), 39.1 (C-1), 55.6 (C-2), 113.6 (d, $^3J_{\text{CF}}$ = 7.3 Hz, C-9), 115.7 (d, $^2J_{\text{CF}}$ = 22.0 Hz, C-10), 126.4 (C-7), 128.7 (C-6), 128.9 (C-5), 139.9 (C-4), 145.8 (d, $^4J_{\text{CF}}$ = 1.6 Hz, C-8), 155.5 (d, $^1J_{\text{CF}}$ = 234.8 Hz, C-11).

^{19}F NMR (376 MHz, CDCl_3) δ = -129.6 (tt, J_{HF} = 8.5, 4.3 Hz).

HR-MS (ESI, pos.) m/z calcd. for $\text{C}_{15}\text{H}_{17}\text{FN}$ $[\text{M}+\text{H}]^+$ 230.1340, found 230.1340.

N,4-Dimethyl-N-(2-phenylpropyl)aniline (4ag)



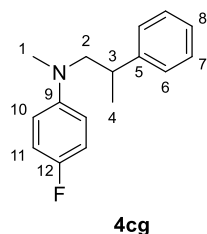
Following general procedure, starting from **2a** (80 mg, 0.24 mmol, 1 eq.) and **3g** (53 mg, 0.25 mmol, 1.04 eq), **4ag** was obtained as yellowish oil in 27% yield (16 mg) after 24 hours.

^1H NMR (300 MHz, CDCl_3): δ = 1.31 (d, 3J = 6.9 Hz, 2H, H-9), 2.28 (s, 3H, H-1), 2.76 (s, 2H, H-6), 3.13-3.27 (m, 1H, H-8), 3.32-3.52 (m, 2H, H-7), 6.61 (d, 3J = 8.6 Hz, 1H, H-4), 7.03 – 7.09 (m, 2H, H-3), 7.19 – 7.25 (m, 3H, H-11, H-13), 7.28 – 7.35 (m, 2H, H-12).

^{13}C NMR (75 MHz, CDCl_3): δ = 19.0 (C-9), 20.3 (C-1), 38.5 (C-8), 39.8 (C-6), 61.4 (C-7), 112.2 (C-4), 125.1 (C-2), 126.4 (C-13), 127.4 (C-11), 128.6 (C-12), 129.8 (C-3), 145.5 (C-10), 147.2 (C-5).

HR-MS (ESI, pos.) m/z calcd. for $\text{C}_{17}\text{H}_{20}\text{N}$ $[\text{M}-\text{H}]^+$ 238.1596, found 238.1589.

4-Fluoro-N-methyl-N-(2-phenylpropyl)aniline (4cg)



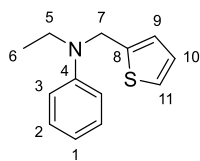
Following general procedure, starting from **2c** (85 mg, 0.24 mmol, 1 eq.) and **3e** (53 mg, 0.25 mmol, 1.04 eq.), **4cg** was obtained as yellowish solid in 20% yield (12 mg).

^1H NMR (400 MHz, CDCl_3) δ = 1.30 (d, 3J = 7.0 Hz, 3H, H-4), 2.72 (s, 3H, H-1), 3.17 (h, 3J = 7.1 Hz, 1H, H-3), 3.31 – 3.49 (m, 2H, H-2), 6.53 – 6.61 (m, 2H, H-), 6.90 – 6.97 (m, 2H), 7.18 – 7.25 (m, 3H, H-6, H-8), 7.28 – 7.34 (m, 2H, H-7).

^{13}C NMR (101 MHz, CDCl_3) δ = 19.0 (C-4), 38.4 (C-3), 40.0 (C-1), 61.8 (C-2), 112.9 (d, $^3J_{\text{CF}}$ = 7.2 Hz, C-10), 115.6 (d, $^2J_{\text{CF}}$ = 21.9 Hz, C-11), 126.6 (C-8), 127.4 (C-6), 128.6 (C-7), 145.2 (C-5), 146.0 (d, $^4J_{\text{CF}}$ = 1.5 Hz, C-9), 155.2 (d, $^1J_{\text{CF}}$ = 234.2 Hz, C-12).

^{19}F NMR (376 MHz, CDCl_3) δ = -130.3 (tt, J_{HF} = 8.5, 4.3 Hz).

N-Ethyl-*N*-(thiophen-2-ylmethyl)aniline (**4di**)



4di

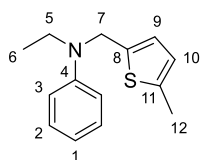
Following general procedure, starting from **2d** (140 mg, 0.42 mmol, 1 eq.) and **3i** (85 mg, 0.44 mmol, 1.05 eq.), **4di** was obtained as white powder in 50% yield (51 mg).

¹H NMR (599 MHz, CDCl₃): δ = 1.23 (t, J = 7.1 Hz, 2 H, H-6), 3.48 (q, J = 7.1 Hz, 2 H, H-5), 4.67 (s, 2 H, H-7), 6.72 – 6.76 (m, 1 H, H-1), 6.80 – 6.84 (m, 2 H, H-3), 6.94 – 6.95 (m, 1H, H-9), 6.97 (dd, J = 5.0, 3.5 Hz, 1 H, H-10), 7.19 (dd, J = 5.0, 1.3 Hz, 1 H, H-11), 7.22 – 7.27 (m, 2 H, H-2).

¹³C NMR (151 MHz, CDCl₃): δ = 12.3 (C-6), 45.0 (C-5), 49.7 (C-7), 113.0 (C-3), 116.9 (C-1), 124.2 (C-11), 124.5 (C-9), 126.9 (C-10), 129.3 (C-2), 143.4 (C-8), 148.2 (C-4).

HR-MS (EI, pos.) m/z calcd. for C₁₃H₁₅NS [M]⁺⁺ 217.0925, found 217.0920.

N-Ethyl-*N*-((5-methylthiophen-2-yl)methyl)aniline (**4dj**)



4dj

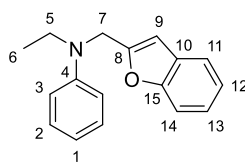
Following general procedure, starting from **2d** (150 mg, 0.44 mmol, 1 eq.) and **3j** (91 mg, 0.44 mmol, 1 eq.), **4dj** was obtained as white powder in 27% (27 mg) yield after 2 hours.

¹H NMR (599 MHz, CDCl₃): δ = 1.19 (t, J = 7.1 Hz, 3 H, H-6), 2.42 (s, 3 H, H-12), 3.44 (q, J = 7.1 Hz, 2 H, H-5), 4.56 (s, 2 H, H-7), 6.56 – 6.58 (m, 1H, H-10), 6.68 – 6.73 (m, 2H, H-1, H-9), 6.79 (d, J = 8.1 Hz, 2 H, H-3), 7.20 – 7.24 (m, 2H, H-2).

¹³C NMR (151 MHz, CDCl₃): δ = 12.4 (C-6), 15.5 (C-12), 44.9 (C-5), 49.8 (C-7), 112.9 (C-3), 116.7 (C-1), 124.5 (C-9), 124.8 (C-10), 129.3 (C-2), 138.8 (C-11), 140.7 (C-8), 148.2 (C-4).

HR-MS (EI, pos.) m/z calcd. for C₁₄H₁₇NS [M]⁺⁺ 231.1082, found 231.1075.

N-(Benzofuran-2-ylmethyl)-*N*-ethylaniline (**4dk**)



4dk

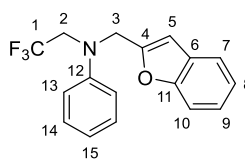
Following general procedure, starting from **2d** (150 mg, 0.44 mmol, 1 eq.) and **3k** (100 mg, 0.44 mmol, 1 eq.), **4dk** was obtained as white powder in 50% yield (54 mg).

¹H NMR (400 MHz, CDCl₃): δ = 1.24 (t, J = 7.1 Hz, 3 H, H-6), 3.53 (q, J = 7.1 Hz, 2 H, H-5), 4.57 – 4.63 (m, 2 H, H-7), 6.50 – 6.54 (m, 1 H, H-9), 6.73 (t, J = 7.2 Hz, 1 H, H-1), 6.82 (d, J = 8.2 Hz, 2 H, H-3), 7.15 – 7.28 (m, 4 H, ArH), 7.40 – 7.51 (m, 2 H, ArH).

¹³C NMR (101 MHz, CDCl₃): δ = 12.5 (C-6), 45.5 (C-5), 48.2 (C-7), 103.9 (C-9), 111.2 (CH), 112.7 (C-3), 116.9 (C-1), 120.8 (CH), 122.8 (CH), 123.8 (CH), 128.6 (C), 129.4 (CH), 148.1 (C-4), 155.1 (C), 155.8 (C-8).

HR-MS (EI, pos.) m/z calcd. for C₁₇H₁₇NO [M]⁺ 251.1310, found 251.1301.

N-(Benzofuran-2-ylmethyl)-*N*-(2,2,2-trifluoroethyl)aniline (**4ek**)



4ek

Following general procedure, starting from **2e** (50 mg, 0.13 mmol, 1 eq.) and **3j** (30 mg, 0.13 mmol, 1 eq.), **4ek** was obtained as white powder in 53% yield (21 mg) after 2 hours.

¹H NMR (400 MHz, CDCl₃) δ = 4.08 (q, $^3J_{\text{HF}}$ = 8.9 Hz, 2H, H-2), 4.78 (s, 2H, h-3), 6.56 (d, 4J = 1.0 Hz, 1H, H-5), 6.88 (t, 3J = 7.3 Hz, 1H, H-15), 6.96 (d, 3J = 8.1 Hz, 2H, H-13), 7.23 (td, J = 7.4, 1.1 Hz, 1H, H-8), 7.26 – 7.33 (m, 3H, H-14, H-9), 7.45 – 7.54 (m, 2H, H-10, H-7).

¹³C NMR (101 MHz, CDCl₃) δ = 48.6 (C-3), 52.67 (q, $^2J_{\text{CF}}$ = 33.1 Hz, C-2), 104.9 (C-5), 111.3 (C-10), 113.7 (C-13), 119.2 (C-15), 121.0 (C-7), 123.0 (C-8), 124.2 (C-9), 125.74 (q, $^1J_{\text{CF}}$ = 282.4 Hz, C-1), 128.3 (C-6), 129.5 (C-14), 147.6 (C-12), 153.8 (C-4), 155.1 (C-11).

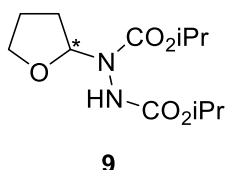
¹⁹F NMR (377 MHz, CDCl₃) δ = -70.06 (t, $^3J_{\text{HF}}$ = 8.9 Hz).

HR-MS (EI, pos.) m/z calcd. for C₁₇H₁₄F₃NO [M]⁺ 305.1022, found 305.1019.

2.5 Appendix

Synthesis of hydrazine 9

Diisopropyl azodicarboxylate (1.0 ml, 5.1 mmol, 1 eq.) was added to a solution of benzoyl peroxide (124 mg, 0.51 mmol, 0.1 eq.) in THF (4 ml). Mixture was heated to reflux and stirred until disappearance of the yellow color. The excess of THF was removed under reduced pressure, and the obtained oil was dissolved in mixture of EtOAc and *n*-pentane (1/4 ratio, 50 ml) and washed through a plug of silica gel. The crude material was distilled at 120 °C at 6×10^{-3} mbar and **9** was obtained as viscous colorless oil in 71% yield.



^1H NMR (300 MHz, CDCl_3) δ = 1.2 – 1.3 (m, 12H, $2 \times -\text{OCH}(\underline{\text{C}}\text{H}_3)_2$), 1.8 – 2.1 (m, 4H, $2 \times -\text{CH}_2-$), 3.7 – 4.0 (m, 2H, $-\text{CH}_2-$), 4.8 – 5.1 (m, 6H, $2 \times -\text{OCH}(\underline{\text{C}}\text{H}_3)_2$), 6.0 (s, 1H, NH), 6.1 – 6.4 (m, 1H, H^*).

^{13}C NMR (75 MHz, CDCl_3) δ = 21.9 ($-\text{OCH}(\underline{\text{C}}\text{H}_3)_2$), 22.0 ($-\text{OCH}(\underline{\text{C}}\text{H}_3)_2$), 25.3 ($-\text{CH}_2-$), 28.2 ($-\text{CH}_2-$), 68.6 ($-\text{CH}_2-$), 69.8 ($-\text{OCH}(\underline{\text{C}}\text{H}_3)_2$), 70.6 ($-\text{OCH}(\underline{\text{C}}\text{H}_3)_2$), 155.0 ($-\text{CO}_2-$), 156.3 ($-\text{CO}_2-$). C^* is not observed.

One-pot reaction of 5, DIAD and 3k

N,N-Dimethylcyclohexylamine **5** (0.08 ml, 0.53 mmol, 1.05 eq.) was dissolved in CH_3CN (1 ml), DIAD (0.1 ml, 0.5 mmol, 1 eq.) was added subsequently at 0 °C, and the mixture was stirred without further cooling. After fading of yellow color of DIAD (20 minutes), a solution of potassium benzofuran-2-yltrifluoroborate **3k** (112 mg, 0.50 mmol, 1 eq.) in CH_3CN (1 ml) was added, followed by TFA (20 μl , 0.5 mmol, 1 eq.). The reaction mixture was stirred at ambient temperature for 2 hours before brine solution (15 ml) was added. Adjusting of pH values with $\text{HCl}(\text{aq.})$ (2 M) or $\text{NH}_3(\text{aq.})$ (2 M) and repeated extraction with *n*-pentane (3×20 ml) gave the following mixtures of products: 1/3 (**7/8**) at pH 5 and 1/7 (**7/8**) at pH 10 (analyzed by GC/MS and ^1H NMR spectroscopy), from which the summarized yield of **7** (87%) was determined.

2.6 References

- [1] a) K. R. Campos, *Chem. Soc. Rev.* **2007**, 36, 1069-1084; b) M. X. Cheng, S. D. Yang, *Synlett* **2017**, 28, 159-174; c) A. Gini, T. Brandhofer, O. G. Mancheno, *Org. Biomol. Chem.* **2017**, 15, 1294-1312; d) K. M. Jones, M. Klussmann, *Synlett* **2012**, 159-162; e) E. A. Mitchell, A. Peschiulli, N. Lefevre, L. Meerpoel, B. U. W. Maes, *Chem. Eur. J.* **2012**, 18, 10092-10142.
- [2] a) N. A. McGrath, M. Brichacek, J. T. Njardarson, *J. Chem. Educ.* **2010**, 87, 1348-1349; b) F. Weber, G. Sedelmeier, *Nachr. Chem.* **2014**, 62, 997.
- [3] a) S. A. Girard, T. Knauber, C. J. Li, *Angew. Chem. Int. Ed.* **2014**, 53, 74-100; b) C. J. Li, *Acc Chem Res* **2009**, 42, 335-344; c) Z. Li, D. S. Bohle, C. J. Li, *Proc. Natl. Acad. Sci. USA* **2006**, 103, 8928-8933; d) X. Zheng, Z. Li in *From C-H to C-C bonds: Cross-Dehydrogenative-Couplings*, Vol. 26 (Ed. C. J. Li), RSC Green Chemistry Series, Royal Society of Chemistry: Cambridge, UK, **2015**, pp. 55-66; e) A. McNally, C. K. Prier, D. W. MacMillan, *Science* **2011**, 334, 1114-1117; f) C. K. Prier, D. W. MacMillan, *Chem. Sci.* **2014**, 5, 4173-4178; g) N. M. Reid, D. A. Proestou, B. W. Clark, W. C. Warren, J. K. Colbourne, J. R. Shaw, S. I. Karchner, M. E. Hahn, D. Nacci, M. F. Oleksiak, D. L. Crawford, A. Whitehead, *Science* **2016**, 354, 1305-1308; h) Q. Li, C. W. Liskey, J. F. Hartwig, *J. Am. Chem. Soc.* **2014**, 136, 8755-8765; i) W. Muramatsu, K. Nakano, C. J. Li, *Org. Biomol. Chem.* **2014**, 12, 2189-2192.
- [4] S. Polanc, J. Košmrlj, M. Kočevár, *Synlett* **2009**, 2009, 2217-2235.
- [5] O. Diels, M. Paquin, *Ber. Dtsch. Chem. Ges.* **1913**, 46, 2000-2013.
- [6] R. Huisgen, F. Jakob, *Liebigs Ann. Chem.* **1954**, 590, 37-54.
- [7] a) X. Xu, X. Li, *Org. Lett.* **2009**, 11, 1027-1029; b) K. Singh, P. Singh, A. Kaur, P. Singh, *Synlett* **2012**, 23, 760-764.
- [8] A. M. Zhironov, A. V. Aksenov, *Russ. Chem. Rev.* **2014**, 83, 502-522.
- [9] a) Y. Miyake, K. Nakajima, Y. Nishibayashi, *Chem. Eur. J.* **2012**, 18, 16473-16477; b) K. Singh, S. Kessar, P. Singh, P. Singh, M. Kaur, A. Batra, *Synthesis* **2014**, 46, 2644-2650.
- [10] W. Huang, C. Ni, Y. Zhao, J. Hu, *New J. Chem.* **2013**, 37, 1684-1687.
- [11] T. Suga, S. Iizuka, T. Akiyama, *Org. Chem. Front.* **2016**, 3, 1259-1264.
- [12] I. Zaltsgendler, Y. Leblanc, M. Bernstein, *Tetrahedron Lett.* **1993**, 34, 2441-2444.
- [13] a) T. Fuchigami, Y. Nakagawa, T. Nonaka, *J. Org. Chem.* **1987**, 52, 5489-5491; b) A. Konno, T. Fuchigami, Y. Fujita, T. Nonaka, *J. Org. Chem.* **1990**, 55, 1952-1954; c) T. Fuchigami, S. Ichikawa, *J. Org. Chem.* **1994**, 59, 607-615.
- [14] a) C. Cox, T. Lectka, *J. Org. Chem.* **1998**, 63, 2426-2427; b) P. R. Rablen, *J. Org. Chem.* **2000**, 65, 7930-7937; c) M. J. Deetz, C. C. Forbes, M. Jonas, J. P. Malerich, B. D. Smith, O. Wiest, *J. Org. Chem.* **2002**, 67, 3949-3952.
- [15] E. N. Wiedemann, A. Gerwien, K. Sommer, A. R. Ofial, *unpublished results*.
- [16] a) R. C. Cookson, I. D. R. Stevens, C. T. Watts, *Chem. Comm.* **1965**, 25, 259-260; b) D. Lee, D. R. Otte, *J. Org. Chem.* **2004**, 69, 3569-3571; c) I. Ryu, A. Tani, T. Fukuyama, D. Ravelli, S. Montanaro, M. Fagnoni, *Org. Lett.* **2013**, 15, 2554-2557.

- [17] G. Berionni, V. Morozova, M. Heininger, P. Mayer, P. Knochel, H. Mayr, *J. Am. Chem. Soc.* **2013**, *135*, 6317-6324.
- [18] A. Wagner, W. Han, P. Mayer, A. R. Ofial, *Adv. Synth. Catal.* **2013**, *355*, 3058-3070.
- [19] B. Rajagopal, C.-H. Chou, C.-C. Chung, P.-C. Lin, *Org. Lett.* **2014**, *16*, 3752-3755

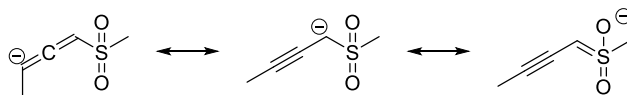
Chapter 3

Reactivity Studies of Alkynyl-Stabilized Carbanions

3.1 Sulfonyl Carbanions Stabilized by the Triple Bond

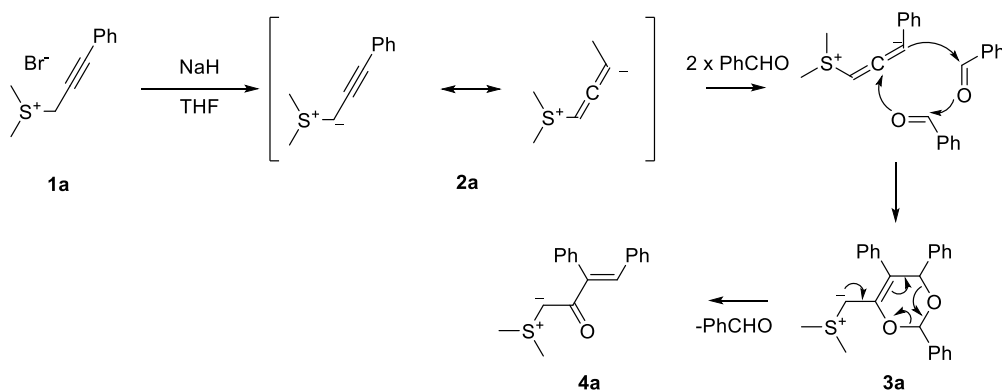
3.1.1 Introduction

Carbanions belong to the most useful nucleophiles in synthetic organic chemistry, which undergo numerous substitutions or additions reactions.^[1] Depending on their structure, stability and reactivity, carbanions vary from intermediates with short life times to nucleophiles that are even stable in aqueous solution.^[2] One of the factors that greatly increase the stability of carbanions is a strong electron-withdrawing group in α -position, especially when the negative charge is stabilized by resonance (Scheme 3.1).



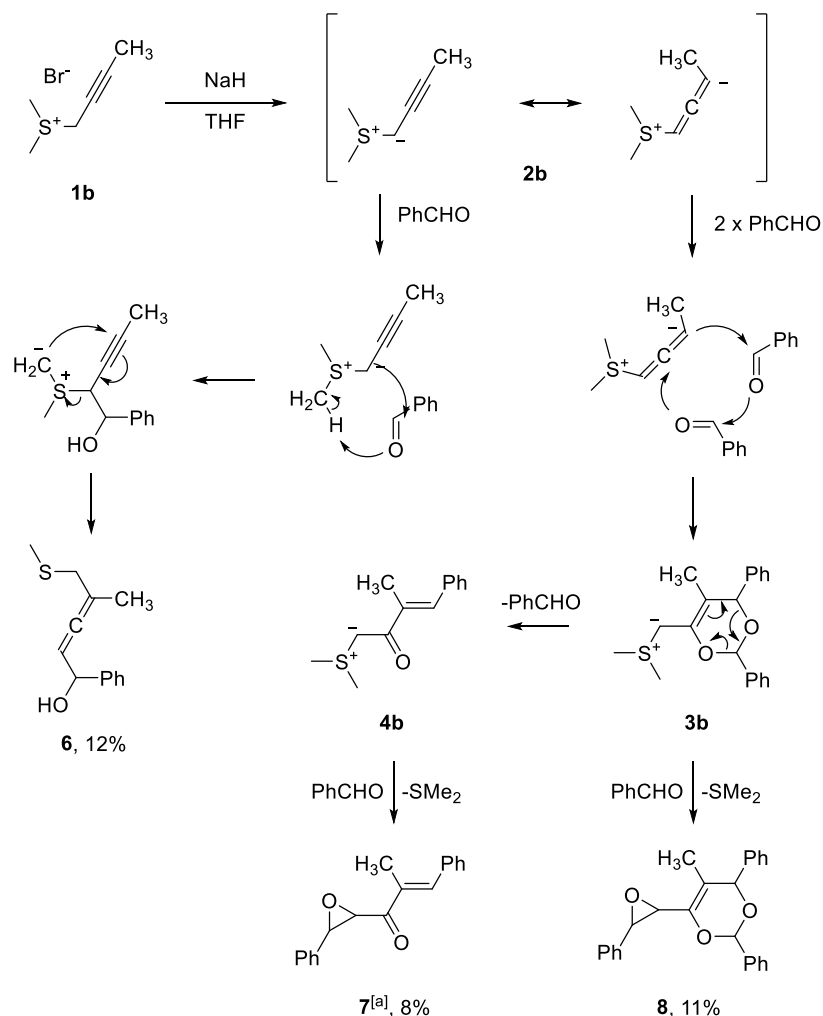
Scheme 3.1. Possible resonance structures of sulfonyl acetylenic carbanion.

In this context carbanions, bearing sulfone and acetylenic fragments are of particular interest for their further functionalization abilities.^[3] During their ylides study,^[4] Kishida et al. has shown that the triple bond next to the carbanionic center enhance the stability of the ylide and modifies its nucleophilic properties. In 1970 they published the detailed mechanism and product analysis of the reaction between dimethyl 3-phenyl-2-propynylsulfonium bromide **1a** and benzaldehyde in presence of sodium hydride as a base (Scheme 3.2).^[5] The intermediate ylide **2a**, formed after base treatment of sulfonium bromide **1a**, was attacked by two molecules of benzaldehyde and formed the six-membered ring intermediate **3a**. After subsequent loss of one benzaldehyde molecule new ylide **4a** was obtained after aqueous work-up in 64% yield (when 2 eq. of benzaldehyde were employed).



Scheme 3.2. Mechanism of the electrophilic addition of benzaldehyde on the dimethyl 3-phenyl-2-propynylsulfonium bromide **1a** in the presence of sodium hydride.

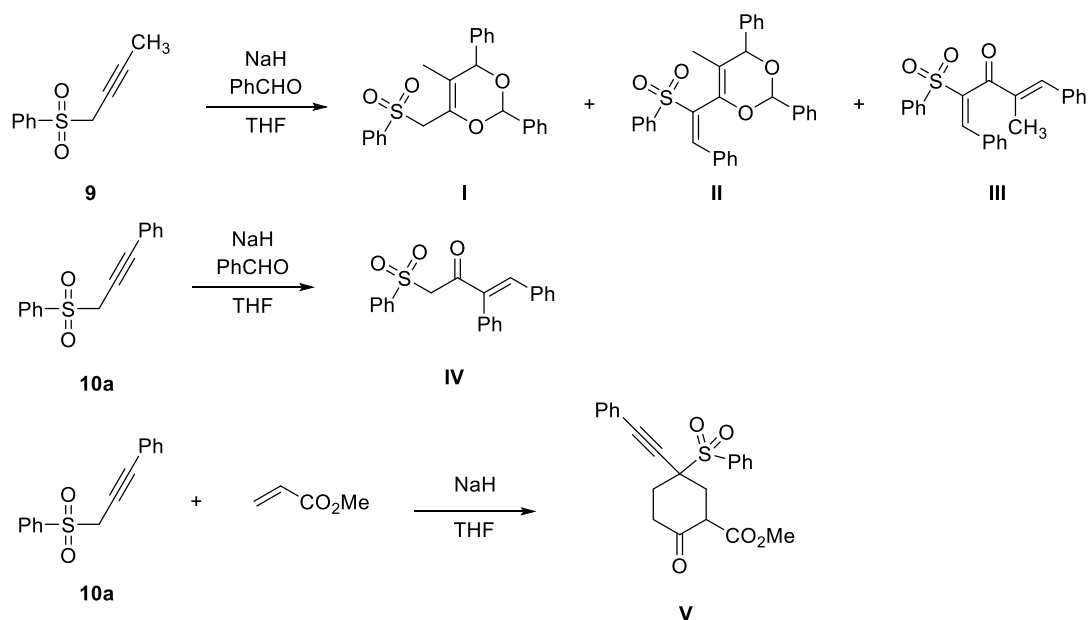
The same mechanism was suggested for a study on the reaction between dimethyl 2-butynylsulfonium bromide **1b** and benzaldehyde in the presence of sodium hydride.^[6] The nucleophilic attack of the *in-situ* formed ylide **2b** on the benzaldehyde molecule followed by intramolecular rearrangement led to the formation of the allenic alcohol **6** (Scheme 3.3). In analogy to **3a** an intermediate dioxene **3b** was transformed to ylide **4b** and furnished an oxirane **7** after reaction with benzaldehyde molecule. The oxirane **8** was obtained after reaction of **3b** with benzaldehyde.



Scheme 3.3. Reaction mechanism of the electrophilic attack of the benzaldehyde on the dimethyl 2-butynylsulfonium bromide **5** in the presence of sodium hydride. [a] Obtained as the mixture of *cis*- and *trans*-isomers.

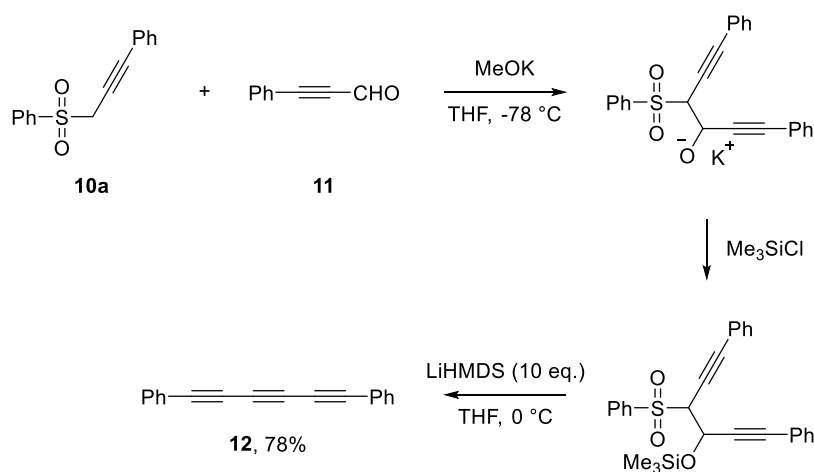
Further investigations brought the authors to the sulfone structures **9** and **10a**, which should possess similar properties as sulfonium salts **1a** and **1b**.^[7] Treating sulfone **9** with sodium hydride with subsequent nucleophilic attack on benzaldehyde led to dioxene **I**, that gave the condensation product **II** with benzaldehyde that rearranged with loss of one benzaldehyde molecule to the acyclic product **III** (Scheme 3.4, top), analogously to transformations showed in Scheme 3.3. Product **IV** that corresponds to a similar structure **4** in Schemes 3.2 and 3.3

was found in the reaction of sulfonyl **10a** with benzaldehyde in the presence of sodium hydride (Scheme 3.4, middle). Sulfonyl **10a** in the presence of the base also showed reactivity towards methyl acrylate yielding the substituted cyclohexanone **V** (Scheme 3.4, bottom). In contrast to ylides **2a-b**, all obtained products retained the sulfone group.



Scheme 3.4. Selected examples of the electrophilic attack on the propargyl sulfones **9** and **10a** in the presence of sodium hydride.^[7]

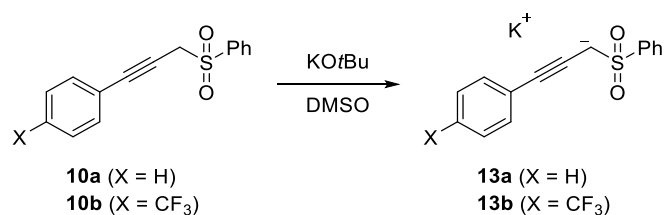
Another application of base-promoted nucleophilic attack of the carbanion, bearing sulfonic and acetylenic groups was published in 1999 by Otera et al.^[8] After coupling **10a** with 3-phenylpropynal **11** using potassium methoxide (**MeOK**) as a base, trapping the resulting alkoxide anion as a silyl ether and treating it with lithium bis(trimethylsilyl)amide (**LiHMDS**) for successive Peterson and sulfone elimination, 1,6-diphenylhexa-1,3,5-triyne **12** was obtained in 78% yield (Scheme 3.5).



Scheme 3.5. Base-promoted coupling of propargyl sulfone **10a** with aldehyde **11**, followed by Peterson and sulfone elimination, yielding triyne **12**.

In order to quantify the effect of the triple bond on the reactivity of sulfonyl carbanions and study the possible reaction pathways, we have studied the reactions of carbanions **13a-b**, derived from sulfones **10a-b**, with reference electrophiles (listed in Table 3.1) in DMSO and calculated the nucleophilicity parameters of these compounds by using the linear free-energy relationship (1).

$$\lg k_2 (20\text{ }^{\circ}\text{C}) = s_N (N + E) \quad (1)$$

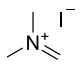
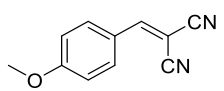


Scheme 3.6. Sulfones **10a-b** and the corresponding anions **13a-b** studied in this work.

Table 3.1. Reference electrophiles **14a-d** and **15a-c** used for the quantification of the reactivities for different sulfonyl stabilized carbanions.

Electrophile		$E^{[a]}$
	14a	-12.76
	14b	-13.56
	14c	-14.68
	14d	-17.18
	15a	-16.11
	15b	-7.02

Table 3.1. Continued.

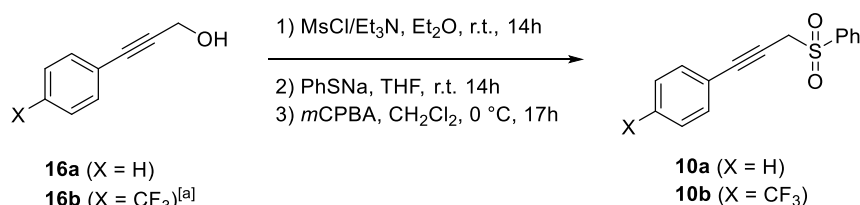
	15c	-6.69
	15d	-10.80

[a] Electrophilicity parameters E were taken from ref. [9]

3.1.2 Results and Discussion

3.1.2.1 Synthesis of the Sulphones 10a-b

Commercially available or synthesized through Sonogashira cross-coupling 3-aryl-2-propyn-1-ols **16a-b** were protected with mesyl chloride followed by substitution with sodium thiophenolate. Obtained sulfides were oxidized with *m*-chloroperoxybenzoic acid (*m*CPBA) yielding the corresponding sulfones (Scheme 3.7).



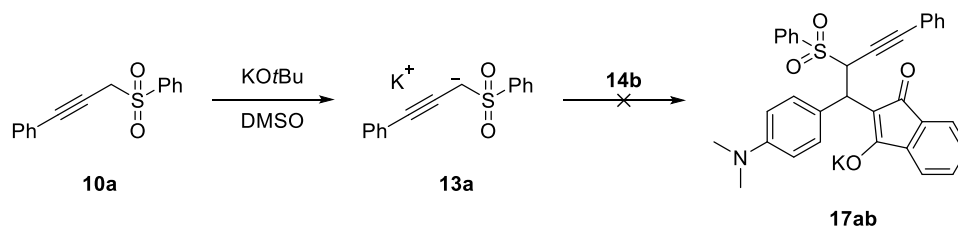
Scheme 3.7. Synthesis of sulfones **10a-b**. [a] Obtained from 4-trifluoromethylbromobenzene and propargyl alcohol as described in ref. [10]

Even though, typical sulfonyl stabilized carbanions may be stable enough for isolation, treating sulfones **10a-b** with different bases (KO^tBu, NaH, *n*-BuLi or KHMDS) in diethyl ether did not lead to any stable product. Therefore, the corresponding nucleophiles were generated by deprotonation with KO^tBu prior to combining them with electrophiles, both in kinetic and product studies.

3.1.2.2 Product Studies

The reaction of the carbanion **13a** with indandione **14b** should lead to an anionic species **17ab**, that can be easily isolated by further acidic work-up as was described previously in ref. [11] However, after treating the sulfone **10a** with 1.05 eq. of KO^tBu and mixing this solution in DMSO with **14b**, no product was obtained after acidic work-up (Scheme 3.8). The experiment

was repeated, varying mixing order and ratio of the reagents but did not lead to any isolated product.



Scheme 3.8. Reaction of the carbanion **13a**, formed in situ from **10a** and KOtBu , and indandione **14b**.

Further attempts to get a stable product in the reaction of carbanion **13a** with different electrophiles are summarized in Table 3.2. Based on previous studies on sulfonyl carbanions^[12] we examined different reaction conditions to get representative products with electrophiles **15a-c**. Changing the base (Entries 1-2 and 9-10), solvent (Entries 1-2 and 5-6), reaction temperature (Entries 6-7) or mixing order (Entries 2-4 and 6-8) did not influence the result. In all shown examples analysis of the reaction mixture after acidic work-up indicated the mixture of undefined substances in the absence of the starting materials. The nature of an electrophile also did not have an effect. An effort to study the reaction course was made (Entry 3), however, the ^1H and ^{13}C NMR spectrum, recorded after addition of electrophile, showed complete consumption of the starting sulfone **10a** and formation of a complicated mixture of products, none of which could be identified.

Table 3.2. Conditions screening for the reaction of sulfone **10a** with reference electrophiles **15a-c**

Entry	Base ^[a]	Electrophile	Conditions ^[b]
1	KOtBu	15a	A ^[c] ; r.t. ^[d] ; DMSO
2	NaH	15a	A; r.t.; THF
3	NaH	15a	A; r.t.; THF- d_8 ^[e]
4	NaH	15a	B; r.t.; THF
5	KOtBu	15b	A; r.t.; DMSO
6	KHMDs ^[f]	15c	A; r.t.; THF
7	KOtBu	15c	A; $-78\text{ }^\circ\text{C}$; THF
8	KOtBu	15c	B; r.t.; THF
9	KOtBu	CH_3I	A; $-78\text{ }^\circ\text{C}$; THF
10	<i>n</i> -BuLi	CH_3I	A; $-78\text{ }^\circ\text{C}$; THF

[a] 1.05 eq. of base was used. [b] Mixing order; temperature; solvent. [c] A – carbanion is generated in situ by mixing base and 10a and electrophile is added subsequently; B – mixture of 10a and electrophile are added to solution of base. [d] r.t. – room temperature, $\sim 23\text{ }^\circ\text{C}$. [e] Reaction performed in the NMR tube. [f] KHMDs – potassium hexamethyldisilazane.

3.1.2.3 Kinetic Investigation

Even though no products were obtained, the nucleophilic species **13** obtained after treating sulfones **10a-b** with KOtBu showed the reaction with reference electrophiles **14** that can be monitored photometrically. Since the nucleophile **13** possess an absorption maximum around 400 nm, all measurements were performed near the absorption maximum of the corresponding electrophiles (500 nm) in DMSO and the remaining absorbance of the excess of the nucleophile was still observed. To simplify the evaluation of the kinetic experiments nucleophile was used in excess, thus the concentration of this component remained constant throughout the reactions. The first-order rate constants k_{obs} were derived by least-squares fitting of the exponential function $A_t = A_0 \exp(-k_{\text{obs}}t) + C$ to the time-dependent absorbances A_t of the electrophile. Second-order rate constants k_2 were obtained as the slopes of plots of k_{obs} versus the concentration of the nucleophile (Figure 3.1).

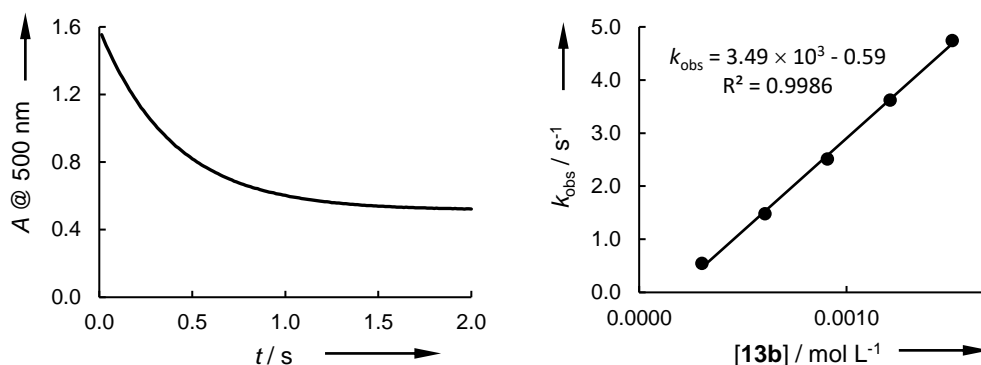
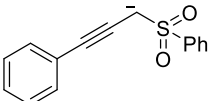
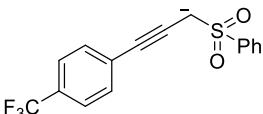


Figure 3.1. Exponential decay of absorbance A (at 500 nm) of the reaction of **13b** ($9.08 \times 10^{-4} \text{ mol L}^{-1}$) with **14c** ($5.73 \times 10^{-5} \text{ mol L}^{-1}$) in DMSO at 20 °C (left). Plot of the first-order rate constants k_{obs} versus the concentration of **13b** (right).

Table 3.3. Second-order rate constants k_2 for the reactions of carbanions **13a-b** with reference electrophiles **14** in DMSO at 20 °C.

Nucleophile	N (s_N)	Electrophile	$k_2 / \text{L mol}^{-1} \text{s}^{-1}$
 13a	23.73 (0.44)	14b	3.83×10^4
			4.04×10^4 [a]
		14c	7.33×10^3
			7.51×10^3 [a]
 13b	21.94 (0.51)	14d	9.07×10^2 [a]
		14a	8.57×10^3 [b]
		14b	1.96×10^4
		14c	3.49×10^3
		14d	2.47×10^2

[a] Kinetic measurements were performed in the presence of 18-crown-6 (1.05 eq. with respect to sulfone **10**). [b] Data not included in the correlation analysis.

For all investigations in DMSO solution, sulfones **10** were deprotonated with 1.05 eq. of KO^tBu, leading to anions with potassium as counter ion. It was found, that the addition of 18-crown-6 ether to coordinate the cation did not influence the obtained k_{obs} values significantly, thus indicating the absence of the counter ion effect on the reactivity of **13**. Thereby the determined rate constants (Table 3.3) reflect the reactivities of the free carbanions.

3.1.2.4 Correlation Analysis

Plots of $\lg k_2$ for the reactions of nucleophiles **13** with reference electrophiles **14b-d** against their electrophilicity parameters E show linear correlations (Figure 3.2). Therefore Equation (1) is applicable and both N and s_N values for the nucleophiles **13a** and **13b** are calculated. The reason for the deviation of the rate of the reaction between **14a** and **13b** is currently unknown and the data is excluded from the linear correlation.

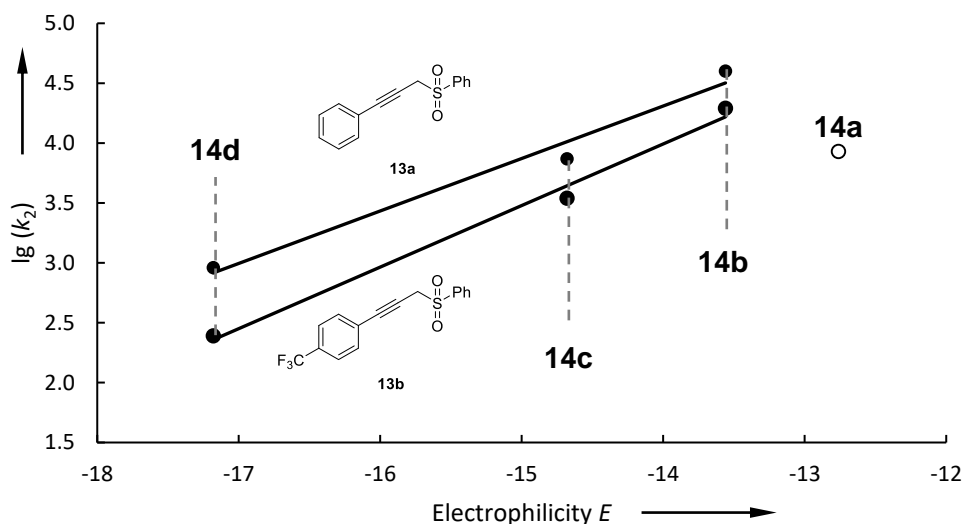


Figure 3.2. Correlation of the logarithms of the rate constants k_2 for the reaction of **13a-b** with electrophiles **14b-d** in DMSO with their electrophilicity parameters E . Reaction between **13b** and **14a** excluded from the correlation due to high deviation (empty circle on the graph).

3.1.2.5 Structure-Reactivity Relationships

The obtained range of the sensitivity parameters (s_N) for nucleophiles **13** reflect the low dependence of relative reactivities on the nature of the attacking electrophile that is typical for carbanions, including sulfonyl stabilized carbanions.^[12]

Figure 3.3 shows the reactivity of **13a** in comparison with previously studied sulfonyl carbanions **18**.^[12a, 13] Due to possible resonance stabilization (Scheme 3.1) the triple bond in the α -position to carbanionic center reduces the reactivity of **18b** towards **14d** by the factor of 71.

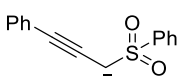
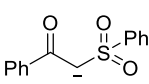
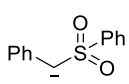
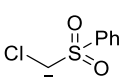
				
	13a	18a	18b	18c
k_2 (14d)	9.07×10^2	$1.01^{[a]}$	6.46×10^4 [a]	4.55×10^4 [a]
k_{rel}	1	0.001	71	50

Figure 3.3. Comparison of absolute (in $\text{L mol}^{-1} \text{s}^{-1}$) and relative rate constants for the reaction of sulfonyl stabilized carbanions **13a** and **18** with quinone methide **14d** in DMSO at 20 °C. [a] Calculated using equation (1).

The effect of the para-substituent in the phenyl ring at the reaction center is generally attenuated by further electron-withdrawing groups attached at the carbanionic center. For trifluoromethylsulfones ($\sigma_p = 0.96$)^[14] **18e-f** CF_3 -group in 4-position in the phenyl ring reduces the reactivity towards **14d** by a factor of 8. The same modification in phenylsulfones ($\sigma_p = 0.68$) **18b-d** changes the reactivity by a factor of 15. However, for the studied nucleophiles **13a-b**, a trifluoromethyl group in the phenyl ring reduces the rate of the addition to quinone methide **14d** by only a factor of 4, since it is not directly attached at the reaction center (Figure 3.4).

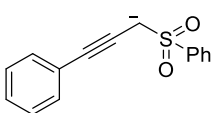
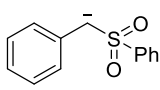
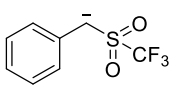
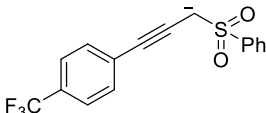
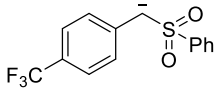
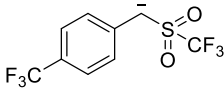
			
	13a	18b	18e
k_2 (14d)	9.07×10^2	6.46×10^4 [a]	1.05×10^1 [a]
k_{rel}	1	71	0.012
			
	13b	18d	18f
k_2 (14d)	2.47×10^2	4.28×10^3 [a]	1.29 [a]
k_{rel}	1	17	0.005

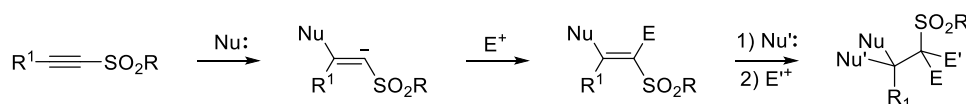
Figure 3.4. Effect of $p\text{-CF}_3$ substitution in the phenyl ring on reactivity of sulfonyl stabilized carbanions **13** and **18b,d-f** towards **14d** in terms of absolute (in $\text{L mol}^{-1} \text{s}^{-1}$) and relative rate constants.

It should be noted, that the nucleophilic species, formed after deprotonation of sulfones **11** was not identified and thus the center of nucleophilic attack at the electrophiles is unknown. It will be shown in the succeeding sections that the triple bond in sulfones **11** is activated enough for a typical Michael addition. Furthermore, in the presence of base propargyl sulfones may isomerize to even more electrophilic allenic and acetylenic compounds. With this in mind one should consider a mixture of nucleophilic oligomers as the reactive intermediates towards reference electrophiles.

3.2 Nucleophilic Attack on the Activated Triple Bond

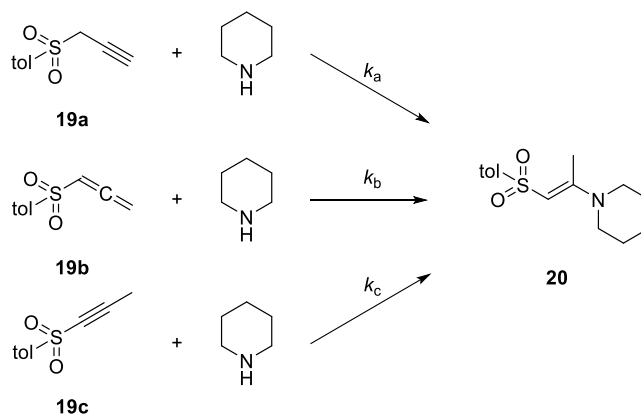
3.2.1 Introduction

A typical nucleophilic attack at the unsaturated electron-deficient C-C bond is among the most often used reactions for building new carbon-carbon and carbon-heteroatom bonds. A strong electron-withdrawing group such as sulfonyl may serve as an activator for an olefin molecule for this transformation. Due to their high reactivity and synthetic versatility, vinyl^[3c, 15] and conjugated dieny^[16] sulfones have received much attention in the past decades. Acetylenic and propargyl sulfones can potentially undergo single or double additions of nucleophiles at the β -position and, subsequently, single or double reactions with electrophiles at the α -position (Scheme 3.9). These abilities and other applications of these sulfones have been reviewed in 2001.^[3a] However, in the context of our study it is necessary to highlight several publications, discussing the nucleophilic attack at the triple bond in a sulfone molecule.



Scheme 3.9. Sequential addition of nucleophile and electrophile on the triple bond activated with the sulfonyl group.

In 1967 Stirling et al. published a kinetic study of amines addition to acetylene-allene isomers **19a-c** in ethanol.^[17] The obtained results showed that formation of the enamine **20** occurred at the same rate either from terminal acetylene **19a** or allene **19b** (Scheme 3.10, Table 3.4). The authors suggested the fast isomerization to **19a** precede the slow addition to allene **19b**. The much slower rate with internal alkyne **19c** is consistent with the direct addition of the amine. This statement is also supported by the very small effect of the *N*-methylpyrrolidine (pK_a in acetonitrile = 18.42),^[18] which should accelerate isomerization of **19c** (Table 3.4), on the rate of enamine formation.



Scheme 3.10. Addition of piperidine to the sulfones **19** in ethanol at 25 °C.

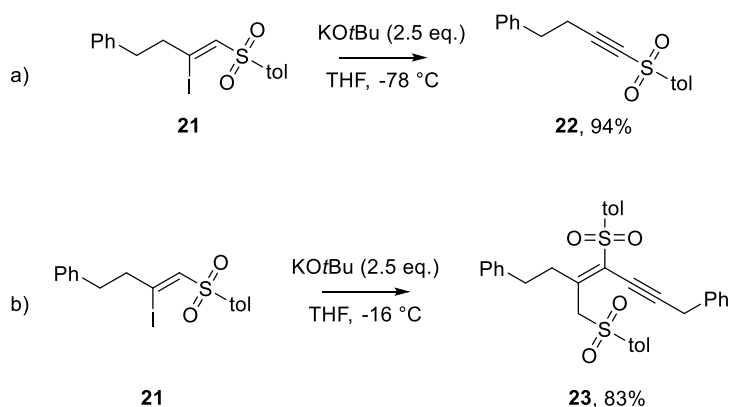
Table 3.4. Rates of addition of piperidine to acetylenic and allenic sulfones **19** in ethanol at 25 °C.

Sulfone	$k_2 / \text{L mol}^{-1} \text{s}^{-1}$
19a	3.87×10^{-1}
19b	3.87×10^{-1}
19c	$3.69 \times 10^{-2}, 3.77 \times 10^{-2}$ [a]

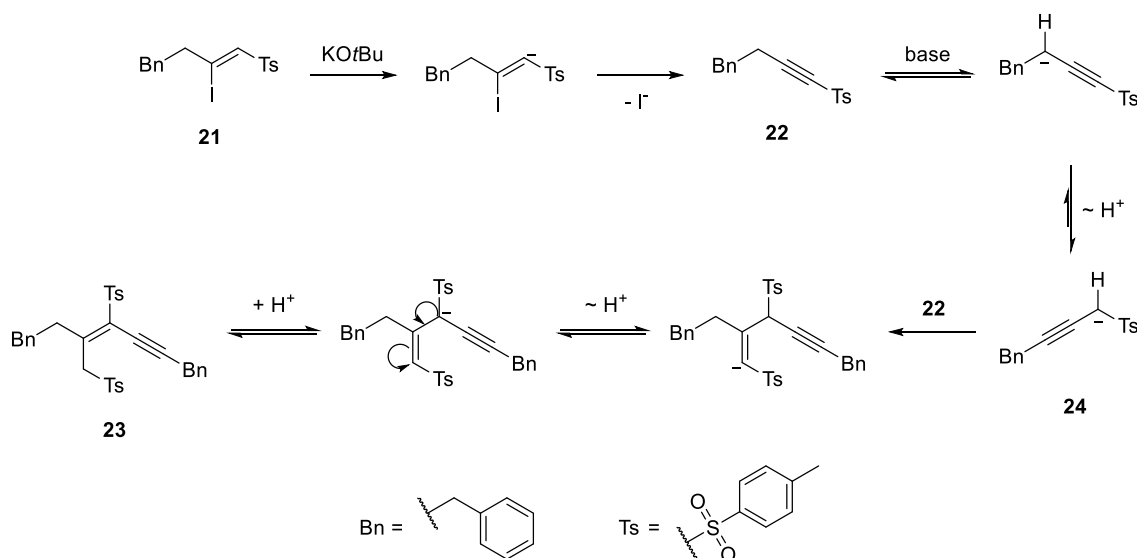
[a] In the presence of 7 moles of *N*-methylpyrrolidine per mole of acetylene

By using the linear free energy relationship (1) and obtained *N*-parameters for piperidine in methanol-acetonitrile mixture,^[19] we can roughly estimate the electrophilicity parameter for propargyl sulfone **19a** to be $E = \log(k_2) / s_N + N = -15$, which makes it more reactive than a typical vinyl sulfone.^[20]

In 1992 Inomata's group reported^[21] on the synthesis of the acetylene **22**, obtained after treating the sulfone **21** with excess of the base at -78 °C (Scheme 3.11a). However, repeating the reaction at higher temperature (-16 °C) led to the formation of enyne **23** in 83% yield (Scheme 3.11b). The suggested reaction mechanism is shown on Scheme 3.12.

**Scheme 3.11.** a) Formation of acetylenic sulfone **22** from sulfone **21** at -78 °C. b) Formation of dimer **23** at -16 °C.

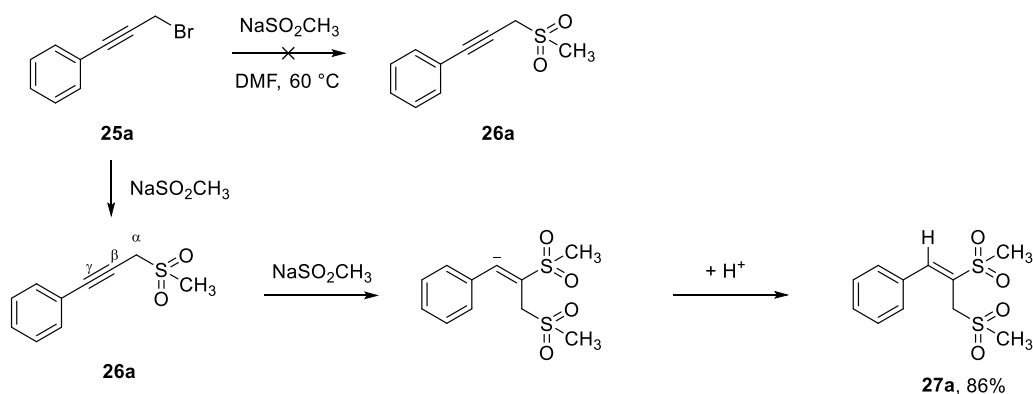
Treating the sulfone **22** with base led to the carbanion **24a** and its isomer **24b**, obtained via protonation equilibrium, well stabilized by the adjacent sulfonyl group. Further nucleophilic attack at the activated triple bond in **22**, subsequent proton migration and final protonation gave the described enyne **23**.



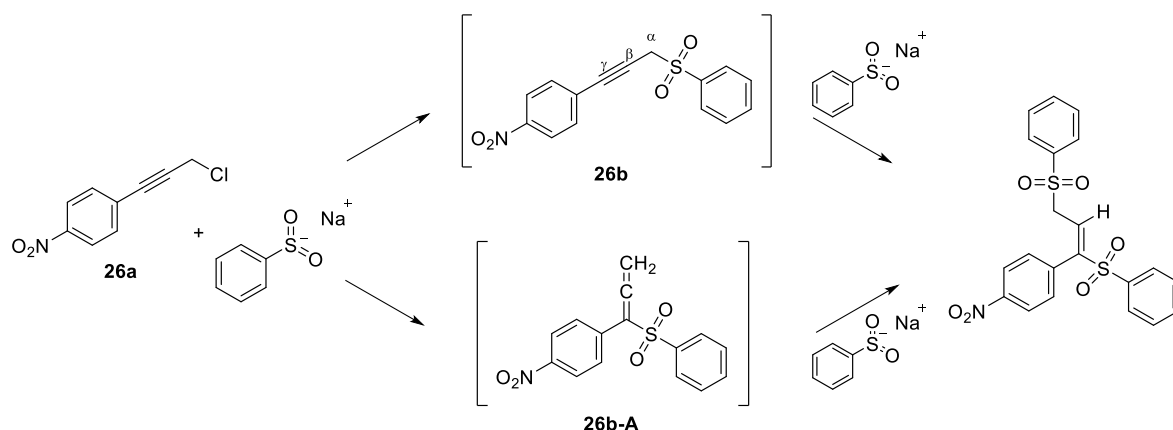
Scheme 3.12. Suggested reaction mechanism of formation of the dimer **23** after treating sulfone **22** with base.

3.2.2 Results and Discussion

For continuation of our study on the nucleophilicity of acetylenic carbanions, we have further functionalized the propargyl skeleton with electron-withdrawing groups. The first attempt was made to introduce the methylsulfonyl group ($-\text{SO}_2\text{CH}_3$) by typical $\text{S}_\text{N}2$ reaction of propargyl bromide **25a** with sodium methanesulfinate in DMF. However, what we have found was the quantitative (with respect to sulfinate) formation of styrene **27** (Scheme 3.13a). The suggested mechanism involved the formation of the desired sulfone **26a**, which was then attacked by the second equivalent of sodium sulfinate, yielding after aqueous work-up the disulfone **27**. It is necessary to emphasize exclusive attack at the β -position in acetylene **26**, which is in contrast to previously reported reactions,^[22] where authors observed γ -attack of sodium phenylsulfinate on an analogous intermediate propargyl sulfonate **26b**, obtained from 1-(3-chloroprop-1-yn-1-yl)-4-nitrobenzene **25b** (Scheme 3.13b). The authors have suggested that the allenic sulfone **26b-A** may be an intermediate structure in this transformation.

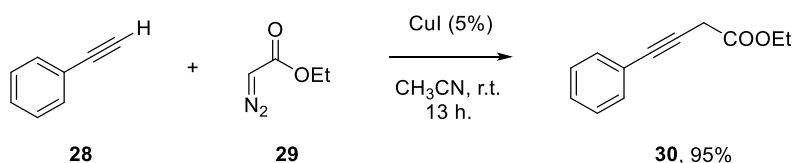


Scheme 3.13a. Formation of the disulfone **27a** after treating the propargyl bromide **25a** with sodium methanesulfinate.



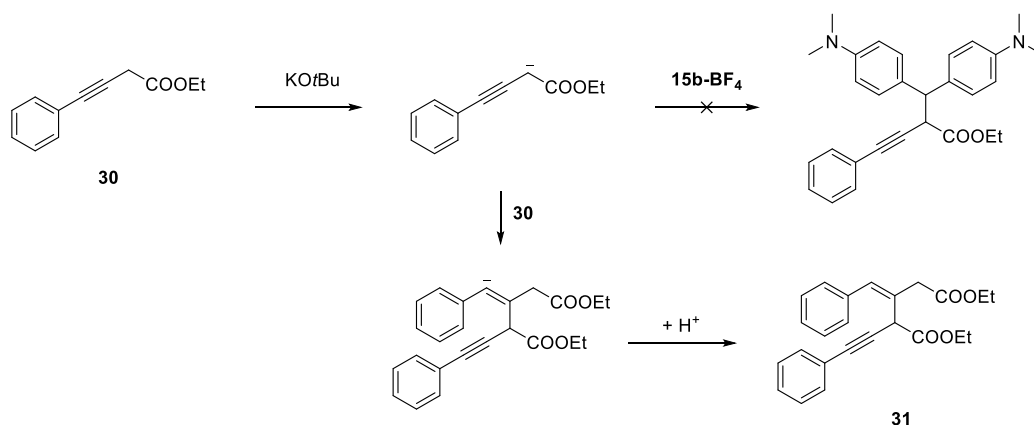
Scheme 3.13b. Suggested mechanism of the attack of the sodium phenylsulfinate at the propargyl chloride **26a**. Adopted from ref. [22]

After unsuccessful results with propargyl sulfones, we switched to propargylic carbanions, stabilized with a weaker electron-withdrawing group, such as an ester group. This replacement should also reduce the reactivity of starting acetylene towards nucleophilic attack. Alkyne **30** was easily prepared from phenylacetylene **28** and ethyl diazoester **29** in presence of catalytic amount of CuI (Scheme 3.14).^[23]



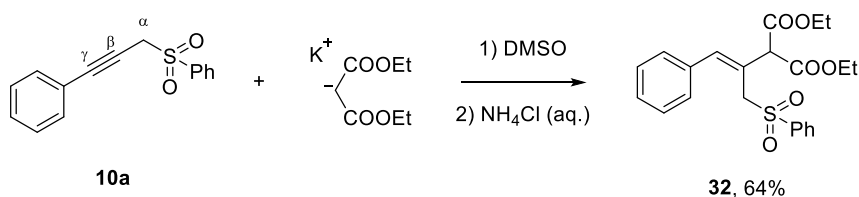
Scheme 3.14. Preparation of the alkyne **30**.

When combined with strong base, such as KO^tBu, alkyne **30** should be deprotonated to furnish a carbanion stabilized by both electron-withdrawing effect of the ester group and resonance effect with the neighboring triple bond. As expected by the nucleophilicity of typical carbanions, reaction with **15b-BF₄** should proceed within milliseconds. However, in the result of this reaction an unidentified mixture of substances was obtained. GC-MS analysis showed a trace amount of dimer **31** (Scheme 3.15), whose formation may be explained by the nucleophilic attack of the obtained carbanion on the activated triple bond of the starting alkyne **30**.



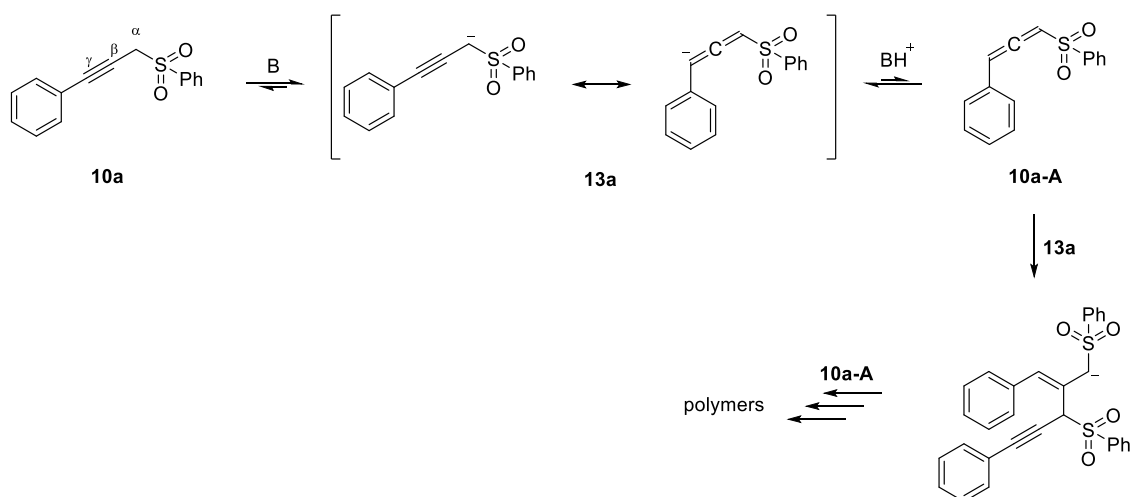
Scheme 3.15. Formation of the dimer **31** in the reaction of **15b-BF₄** and **30**, treated with KOtBu.

To support our suggestion of nucleophilic attack on the triple bond of the sulfone, we have performed the reaction between sulfonyl **10a** and potassium diethyl malonate (prepared *in situ* from diethyl malonate and KOtBu) in DMSO (Scheme 3.16). After acidic work-up and purification by column chromatography, sulfonyl **32** was obtained in 64% yield of the *Z* isomer. It is necessary to point out the same regioselectivity of the nucleophilic attack at the β -position, as was obtained with sodium methanesulfinate.



Scheme 3.16. Nucleophilic attack of the potassium diethyl malonate on the sulfone **10a**.

Thus, we can summarize the possible transformations that occur by mixing sulfone **10a** with base, e.g. KOtBu (Scheme 3.17): initial deprotonation at the α -position leads to an acetylenic carbanion, that can be protonated at γ -position. Even though the equilibrium is highly shifted to carbanion **13a**, low amount of sulfonyl allene **10a-A** is present and are nucleophilically attacked by the previously formed carbanion **13a**. The resulting species still possess an anionic center and can further attack the allene **10a-A**. However, the final composition of the product mixture could not be identified via GC-MS or NMR techniques.

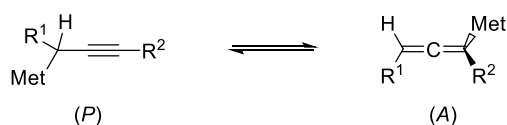


Scheme 3.17. Possible transformations of the propargyl sulfone **10a** induced by Brønsted bases.

3.3 Reactivity of Propargyl and Allenic Organometallic Compounds

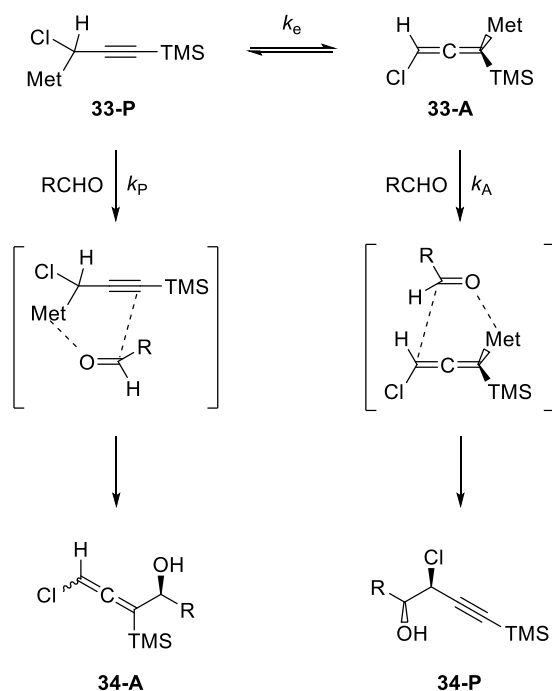
3.3.1 Introduction

Another approach to apply propargyl or allenic motifs in nucleophilic substitution reactions is based on building covalent carbon-metal bonds.^[24] This should reduce the reactivity of such species,^[25] thus preventing oligomerization side-products. The existence of metallotropic equilibrium between propargyl and allenic forms (Scheme 3.18) may also have an impact on the configurational stability of the organometallic species^[26] and influence the regioselectivity of the nucleophilic attack. For example, in reaction with aldehydes (e.g. Scheme 3.18) allenyl stanannes,^[27] indiums^[27] and zincs^[24a, 28] give the products with high selectivity towards propargyl alcohols, while their magnesium,^[29] boron^[30] or titanium^[31] analogues generally react less selective.



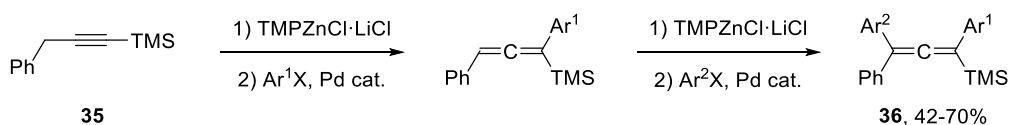
Scheme 3.18. Metallotropic equilibrium between propargyl (*P*) and allenic (*A*) metals.

In 2012 Ferreira et al. published the quantitative study^[32] of metallotropic equilibrium (Scheme 3.20) between 1-chloro-3-(trimethylsilyl)propargyl **33-P** and -allenyl **33-A** metals. They have investigated their reactions with achiral aldehydes and calculated the ratio between allenic and acetylenic products **34**, obtained through cyclic $\text{S}_{\text{E}}2'$ processes^[28a] (Scheme 3.19). The lithium and zinc species were shown to react mainly in their allenic metallotropic forms, whereas the titanium species proved to react in both its forms. General trends for the metallotropic equilibrium are provided in Table 3.5.

**Scheme 3.19.** Addition of metallo-carbenoids **33** to aldehydes.**Table 3.5.** General trends of the metallotropic equilibrium.

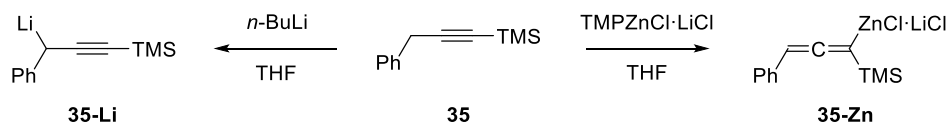
Met =		Conditions
Li	$k_e \gg k_A > k_P$	at -95 °C in Et ₂ O
Ti(OiPr) ₃	$k_e \gg k_A \approx k_P$	at -80 °C and -40 °C in THF/Et ₂ O
ZnBr	$k_e \gg k_A \gg k_P$	at -80 °C in THF

Particularly interesting in the context of further transformations are allenylsilanes and their propargyl subunits. Recently, Knochel has reported^[33] on the preparation of tri- and tetrasubstituted allenes via regioselective metalation of **35** with 2,2,6,6-tetramethylpiperidynyl zinc chloride lithium chloride (TMPZnCl·LiCl) (Scheme 3.20). The procedure includes sequential zincation and Pd-catalyzed coupling with aryl halides and provides allenes **36** with moderate to good yields. This sequence can also be performed in a one-pot procedure.

**Scheme 3.20.** Tetrafunctionalized allenes via successive zincation using TMPZnCl·LiCl and Negishi cross-coupling reactions.

We now aim to quantify the difference in reactivity of lithium **35-Li** and zinc **35-Zn** intermediates, obtained after deprotonation of 1-(trimethylsilyl)-3-phenyl-1-propyne **35**. The exclusive formation of propargyl and allenic species after treating with *n*-BuLi and

TMPZnCl·LiCl respectively (Scheme 3.21) has been determined^[32] from ¹³C NMR spectra of **35-Li** and **35-Zn** in THF-*d*₈.

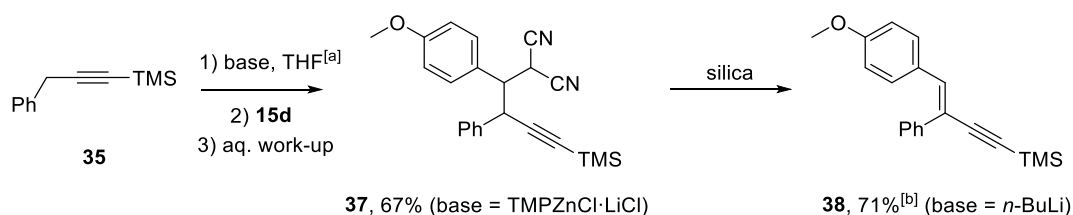


Scheme 3.21. Metallation of **35** with *n*-BuLi or TMPZnCl·LiCl.

3.3.2 Results and Discussion

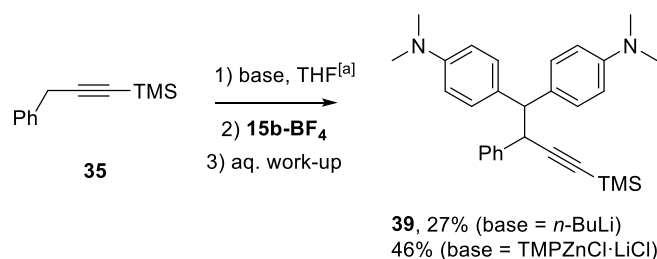
3.3.2.1 Product Analysis

Propyne **35** was metallated either with *n*-BuLi or with TMP-ZnCl·LiCl, leading to **35-Li** and **35-Zn** respectively. The obtained species reacted with **15d** in THF as detected by the disappearance of the yellow color of electrophile. The product **37** was isolated in 67% yield as a 79:21 mixture of two diastereomers without further purification from allenyl zincate **35-Zn**. The same product is expected to form from **35-Li**, however, after purification on silica gel the conjugated enyne **38** was obtained in 71% yield (Scheme 3.22).



Scheme 3.22. Products of the reaction of electrophile **15d** with **35-Li** and **35-Zn**, obtained from **35** after treatment with base. [a] Conditions: r.t., 20 min for TMPZnCl·LiCl; -40 °C, 20 min for *n*-BuLi. [b] Isolated yield after column chromatography purification.

The reaction of metallic species **35-Li** and **35-Zn** with **15b** proceeded to furnish **39** in 27% (from **35** and *n*-BuLi) and 46% (from **35** and TMP-ZnCl·LiCl) yield. It should be noted that despite formation of allenic zincate **35-Zn**, attack at the electrophile leads to a propargyl derivative (Scheme 3.23).



Scheme 3.23. Reaction of **15b-BF₄** with metallic species, obtained after treating **35** with base. [a] Conditions: r.t., 15 min.

3.3.2.2 Kinetic Investigation

The reaction of zincate **35-Zn** and **15b-BF₄** was studied photometrically at 635 nm in THF at 20 °C. Even though the absorbance decay was monoexponential, the k_{obs} values did not correlate linearly with concentration of nucleophiles as demonstrated in Figure 3.5. It should be noted that fast side reactions between the electrophile and TMPH may proceed in the same time range as the desired reaction with **35-Zn** (e.g. half-life time of **15b** is appr. 0.5 sec for **35-Zn** and 0.4 sec for TMP-H with comparable concentrations of the nucleophiles, see Figure 3.6 in the Experimental Section), therefore rate constants couldn't be assigned.

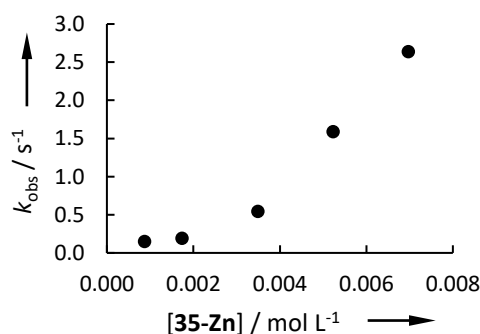


Figure 3.5. Plot of the first-order rate constants k_{obs} versus the concentration of **35-Zn**.

3.4 Conclusion

It has been demonstrated that addition of the base to phenyl-propargyl sulfones **10a-b** form nucleophilic species that show reactivity towards standard electrophiles. These reactions have been investigated photometrically and the obtained rate constants were used to calculate the nucleophilicity parameters. The suggested carbanionic structures **13a-b** showed reactivity similar to previously studied sulfonyl-stabilized carbanions, decreased by 2 orders of magnitude due to resonance stabilization of the anion by the triple bond.

The reaction of propargyl sulfone with potassium diethyl malonate demonstrated high reactivity of such structural motifs towards nucleophiles. Furthermore, compounds with propargyl

skeleton may isomerize in the presence of base to the corresponding allenic forms that are known for their electrophilic activity. Taking the possible oligomerization reactions, i.e. those between carbanions and their protonated allenic forms into account, one could not correctly identify the reactive intermediate in the studied reactions.

To overcome these difficulties propargyl organometallic species **35-Li** and **35-Zn** were used for quantitative kinetic studies. The covalent character of the carbon-metal bonds in these structures should reduce the reactivity towards electrophiles and thus reduce possible side processes. However, the obtained rate constants in the reaction of **35-Zn** with **15b** did not correlate linearly with the nucleophile concentration due to possible self-association of these organometallic species.

3.5 Experimental section

3.5.1 General

All reactions were performed in carefully dried Schlenk glassware in an atmosphere of dry nitrogen. The reactions were not optimized for high yields.

^1H NMR (600, 400, or 300 MHz) and ^{13}C NMR (151, 101, or 75.5 MHz) were recorded on Varian or Bruker NMR systems in d_6 -DMSO, d_8 -THF or CDCl_3 . Chemical shifts in ppm refer to the solvent residual signal in d_6 -DMSO (δ_{H} 2.50, δ_{C} 39.52 ppm), d_8 -THF (δ_{H} 1.72, δ_{C} 67.21 ppm) or CDCl_3 (δ_{H} 7.26, δ_{C} 77.16 ppm) as internal standard respectively. The following abbreviations are used to describe the multiplicities of ^1H resonances: br s = broad singlet, s = singlet, d = doublet, t = triplet, q = quartet, sept = septet, m = multiplet. NMR signal assignments are based on additional 2D-NMR experiments (COSY, HSQC, and HMBC).

Solvents. For the kinetic experiments commercially available DMSO (Sigma-Aldrich, $\geq 99.9\%$, anhydrous, SureSeal) was used as received, THF (Sigma-Aldrich, $\geq 99.9\%$, anhydrous, stabilized with BHT) was distilled over Na/benzophenone. Et_2O (technical grade), DMF (Sigma-Aldrich, 99.8%, anhydrous) and CH_2Cl_2 (technical grade) were used as received.

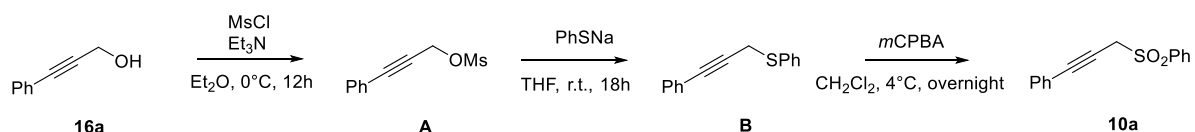
Chemicals. Commercially available chemicals 3-phenyl-2-propyn-1-ol **16a** (99%), methanesulfonyl chloride, sodium thiophenolate (90%, technical grade), 3-Chloroperbenzoic acid (*m*CPBA, $\leq 77\%$), propargyl alcohol (99%), 4-bromobenzotrifluoride (99%), palladium bis(triphenylphosphine) chloride (99%), copper (I) iodide (99%), potassium *tert*-butoxide (99.99%, sublimed grade), sodium methanesulfonate (98%) and diethyl malonate (ReagentPlus, 99%) were purchased from Sigma-Aldrich and used as received. Technical grade triethylamine was dried over KOH and distilled from CaH_2 for Sonogashira cross-

coupling reactions. 3-(4-Trifluoromethylphenyl)-2-propyn-1-ol **16b**,^[34] ethyl 4-phenylbut-3-ynoate **30**,^[23] (3-bromoprop-1-yn-1-yl)benzene **25**,^[35] 1-(trimethylsilyl)-3-phenyl-1-propyne **33**^[33] and $\text{TMPZnCl}\cdot\text{LiCl}$ ^[33] were prepared by the described procedures.

Reference electrophiles were prepared by Nathalie Hampel.

3.5.2 Synthesis of sulfones **10a-b**

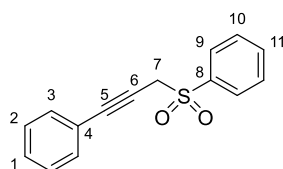
((3-Phenylprop-2-yn-1-yl)sulfonyl)benzene (**10a**) ARLE-10



To a solution of propargyl alcohol **16a** (1.00 g, 7.60 mmol, 1 eq.) and methanesulfonyl chloride (0.88 ml, 11.40 mmol, 1.5 eq.) in Et_2O (20 ml) was added triethylamine (1.59 ml, 11.40 mmol, 1.5 eq.) at 0° C and the mixture was left stirring overnight at r.t. The solid was filtered and the filtrate concentrated in vacuum to give crude **A** (1.6 g, 100 %) which was used subsequently without purification.

To a suspension of sodium thiophenolate (90%, 1.23 g, 8.40 mmol, 1.1 eq.) in THF (25 ml) was added **A** (1.60 g, 7.60 mmol, 1 eq.) and the mixture was stirred for 18 h. Thereafter the reaction mixture was quenched with saturated aqueous NH_4Cl (30 ml) and extracted EtOAc (3 × 30 ml). Organic layers were washed with brine (20 ml), dried over MgSO_4 and concentrated in vacuum to give **B** (1.7 g, 100 %), which was used without further purification.

To a solution of **B** (0.68 g, 3.0 mmol, 1 eq.) in DCM (10 ml) was added dropwise a solution of *m*CPBA (75%, 1.4 g, 6.0 mmol, 2 eq.) in DCM (10 ml) at 0° C and the mixture was kept overnight at 4° C. Thereafter it was diluted with DCM (20 ml) and carefully washed with saturated aqueous Na_2CO_3 (3 × 30 ml). The organic layer was dried over MgSO_4 and concentrated in vacuum. The crude mixture was purified by liquid chromatography on silica gel (*n*-pentane/EtOAc = 4/1, R_f = 0.37) to give 0.62 g (81%) sulfone **16a** as white solid.

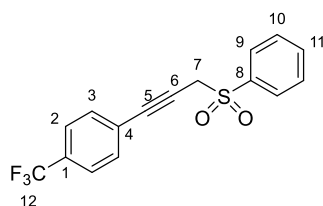
**10a**

^1H NMR (400 MHz, d_6 -DMSO) δ = 4.79 (s, 2H, H-7), 7.28 – 7.36 (m, 2H, H-3), 7.32 – 7.41 (m, 3H, H-2, H-1), 7.68 – 7.73 (m, 2H, H-10), 7.77 – 7.83 (m, 1H, H-11), 7.97 – 8.03 (m, 2H, H-9).

^{13}C NMR (101 MHz, d_6 -DMSO) δ = 47.9 (C-7), 78.8 (C-6), 86.1 (C-5), 121.3 (C-4), 128.4 (C-9), 128.8 (C-2), 129.2 (C-1), 129.3 (C-10), 131.3 (C-3), 134.3 (C-11), 138.0 (C-8).

1-(3-(Phenylsulfonyl)prop-1-yn-1-yl)-4-(trifluoromethyl)benzene (**10b**) ARLE-47

Sulfone **10b** was synthesized analogously to **10a** from 3-(4-(trifluoromethyl)phenyl)prop-2-yn-1-ol **16b** (1.09 g) in overall 81% yield (yellowish solid, 1.42 g).

**10b**

^1H NMR (400 MHz, d_6 -DMSO) δ = 4.87 (s, 2H, H-7), 7.52 – 7.57 (m, 2H, H-3), 7.68 – 7.76 (m, 4H, H-2, H-10), 7.78 – 7.83 (m, 1H, H-11), 7.99 – 8.03 (m, 2H, H-9).

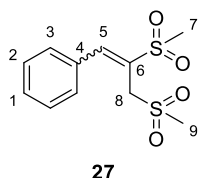
^{13}C NMR (101 MHz, d_6 -DMSO) δ = 47.8 (C-7), 81.8 (C-6), 84.7 (C-5), 123.8 (q, $^1J_{\text{CF}}$ = 272.3 Hz, C-12), 125.7 (q, $^3J_{\text{CF}}$ = 3.8 Hz, C-2), 128.4 (C-9), 129.1 (q, $^2J_{\text{CF}}$ = 32.2 Hz, C-1), 129.4 (C-10), 132.2 (C-3), 134.4 (C-11), 137.9 (C-8).

3.5.3 Product study

Reaction of (3-bromoprop-1-yn-1-yl)benzene **25** with sodium methanesulfinate ALE-99

(3-Bromoprop-1-yn-1-yl)benzene **25** (300 mg, 1.54 mmol, 1 eq.) was added dropwise to a warm (60 °C) suspension of sodium methanesulfinate (189 mg, 1.85 mmol, 1.2 eq.) in DMF (10 ml). Reaction mixture was stirred at this temperature for further 90 minutes, cooled to ambient temperature, poured into water (50 ml) and extracted EtOAc (3 × 30 ml). Combined organic layers were washed with brine (20 ml), dried over MgSO₄ and concentrated in vacuum. Crude material was purified by column chromatography (silica, *n*-pentane/EtOAc = 4/1) and **27** was obtained as white solid (220 mg, 86%).

(2,3-Bis(methylsulfonyl)prop-1-en-1-yl)benzene (**27**)

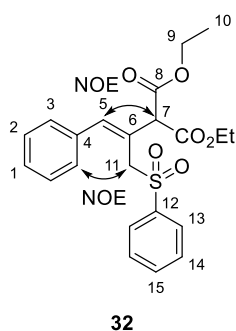


¹H NMR (300 MHz, CDCl₃) δ = 3.05 (s, 3H, H-9), 3.23 (s, 3H, H-7), 4.53 (s, 2H, H-8), 7.45 – 7.50 (m, 3H, H-1, H-2), 7.61 – 7.66 (m, 2H, H-3), 8.09 (s, 1H, H-5).

¹³C NMR (75 MHz, CDCl₃) δ = 43.0 (C-9), 43.9 (C-7), 53.9 (C-8), 129.3 (C-2), 129.5 (C-3), 131.2 (C-1), 131.5 (C-6), 132.2 (C-4), 148.3 (C-5).

Reaction of ((3-phenylprop-2-yn-1-yl)sulfonyl)benzene 10a with potassium diethyl malonate ALE-183

Diethyl malonate (0.15 ml, 1.00 mmol, 1 eq.) was added to a solution of potassium *tert*-butoxide (0.12 g, 1.05 mmol, 1.05 eq.) in THF (10 ml) at ambient temperature. The resulting solution was added to **10a** (0.26 g, 1.00 mmol, 1 eq.), dissolved in THF (10 ml), stirred for 90 minutes, poured into water (50 ml) and extracted EtOAc (3 × 30 ml). The combined organic layers were washed with brine (20 ml), dried over MgSO₄ and concentrated in vacuum. The crude material was purified by column chromatography (silica, *n*-pentane/EtOAc = 5/4) and **32** was obtained as *Z* isomer (white solid, 0.26 g, 64%).

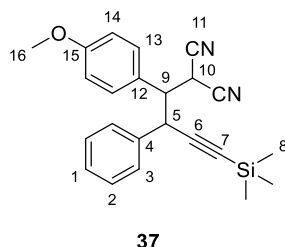
Diethyl (Z)-2-(1-phenyl-3-(phenylsulfonyl)prop-1-en-2-yl)malonate (**32**)


¹H NMR (400 MHz, CDCl₃) δ = 1.32 (t, *J* = 7.1 Hz, 6H, H-10), 4.15 (s, 2H, H-11), 4.28 (q, *J* = 7.1 Hz, 4H, H-9), 4.90 (s, 1H, H-7), 6.71 (d, *J* = 7.2 Hz, 2H, H-3), 6.90 (s, 1H, H-5), 7.10 – 7.17 (m, 3H, H-1, H-2), 7.38 – 7.45 (m, 2H, H-14), 7.57 (t, *J* = 7.4 Hz, 1H, H-15), 7.71 (d, *J* = 8.1 Hz, 2H, H-13).

¹³C NMR (101 MHz, CDCl₃) δ = 14.2 (C-10), 56.2 (C-7), 57.8 (C-11), 62.0 (C-9), 122.4 (C-6), 127.7 (C-1), 127.9 (C-3), 128.4 (C-2), 128.6 (C-13), 129.1 (C-14), 133.9 (C-15), 135.0 (C-4), 138.2 (C-12), 138.7 (C-5), 167.8 (C-8).

Reaction of 35-Zn with 15d ALE-139

To a solution of **35** (87 mg, 0.46 mmol, 1 eq.) in THF (5 ml) was added dropwise a solution of TMP-ZnCl·LiCl (0.81 M in THF, 0.6 ml, 0.49 mmol, 1.07 eq.). After 15 minutes the resulting solution was added to a solution of **15d** (89 mg, 0.48 mmol, 1.05 eq.) in THF (10 ml) and stirred at ambient temperature overnight. Reaction was carefully treated with water (20 ml) and extracted EtOAc (3 × 30 ml). Combined organic layers were washed with brine (20 ml), dried over MgSO₄ and concentrated in vacuum to give **37** as 79:21 mixture of two diastereomers (yellowish solid, 42 mg, 46%).

2-(1-(4-Methoxyphenyl)-2-phenyl-4-(trimethylsilyl)but-3-yn-1-yl)malononitrile (37)

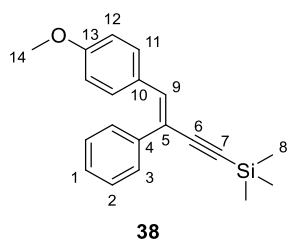
¹H NMR (599 MHz, CDCl₃) δ = 0.13 (s, 9H, H-8, major isomer), 0.23 (s, 9H, H-8, minor isomer), 3.38 (dd, J = 10.3, 5.0 Hz, 1H, H-9, minor isomer), 3.41 (dd, J = 8.7, 7.5 Hz, 1H, H-9, major isomer), 3.77 (s, 3H, H-16, minor isomer), 3.80 (s, 3H, H-16, major isomer), 4.12 (d, J = 8.6 Hz, 1H, H-10, major isomer), 4.21 (d, J = 10.2 Hz, 1H, H-5, minor isomer), 4.37 (d, J = 7.2 Hz, 1H, H-5, major isomer), 4.75 (d, J = 5.0 Hz, 1H, H-10, minor isomer), 6.79 – 6.84 (m, 2H, H-14, both isomers), 7.08 – 7.15 (m, 2H, H-13, both isomers), 7.17 – 7.21 (m, 2H, H-2, major isomer), 7.27 – 7.36 (m, 3H, H-1, H-3, both isomers).

¹³C NMR (151 MHz, CDCl₃) δ = -0.1 (C-8, major isomer), 0.0 (C-8, minor isomer), 27.9 (C-10, major isomer), 28.6 (C-10, minor isomer), 42.2 (C-5, both isomers), 52.1 (C-9, both isomers), 55.3 (C-16, minor isomer), 55.4 (C-16, major isomer), 92.5 (C-7, minor isomer), 92.7 (C-7, major isomer), 102.7 (C-6, major isomer), 104.0 (C-6, minor isomer), 111.7 (CN), 112.3 (CN), 114.0 (C-14, major isomer), 114.4 (C-14, minor isomer), 125.8 (C-12, major isomer), 128.1 (C-2, major isomer), 128.2 (C-1, major isomer), 129.1 (C-3, major isomer), 129.8 (C-13, minor isomer), 130.0 (C-13, major isomer), 136.9 (C-4, major isomer), 160.1 (C-15, minor isomer), 160.2 (C-15, major isomer).

C-1, C-2, C-3, C-4 and C-12 of the minor isomer could not be correctly identified due to superimposition of resonances with those of the major isomer.

Reaction of 35-Li with 15d ALE-136

To a precooled (-40 °C, acetone/liquid N₂) solution of **35** (74 mg, 0.39 mmol, 1 eq.) in THF (2 ml) was added dropwise solution of *n*-BuLi (2.5 M in *n*-hexane, 0.17 ml, 0.41 mmol, 1.05 eq.). The mixture was stirred for 10 minutes at this temperature, warmed up to ambient temperature and stirred for another 10 minutes. After recooling to -40 °C, a solution of **15d** (73 mg, 0.39 mmol, 1 eq.) in THF (4 ml) was added and the mixture was warmed to ambient temperature and stirred for another 20 minutes. Thereafter the mixture was carefully treated with water (20 ml) and extracted EtOAc (3 × 30 ml). The combined organic layers were washed with brine (20 ml), dried over MgSO₄ and concentrated in vacuum. The crude material was purified by column chromatography (silica, *n*-pentane/EtOAc = 10/1) and **38** was obtained as yellow oil (84 mg, 71%).

(E)-(4-(4-Methoxyphenyl)-3-phenylbut-3-en-1-yn-1-yl)trimethylsilane (38)

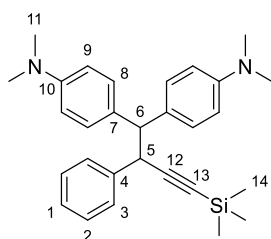
¹H NMR (599 MHz, CDCl₃) δ = 0.31 (s, 9H, H-8), 3.86 (s, 3H, H-14), 6.90 – 6.94 (m, 2H, H-12), 7.13 (s, 1H, H-9), 7.28 – 7.32 (m, 1H, H-1), 7.36 – 7.41 (m, 2H, H-2), 7.69 – 7.73 (m, 2H, H-3), 7.99 – 8.04 (m, 2H, H-11).

¹³C NMR (151 MHz, CDCl₃) δ = 0.0 (C-8), 55.5 (C-14), 103.0 (C-7), 104.5 (C-6), 113.7 (C-12), 119.2 (C-5), 126.4 (C-3), 127.6 (C-1), 128.5 (C-2), 129.5 (C-10), 130.9 (C-11), 135.4 (C-9), 139.6 (C-4), 159.9 (C-13).

HR-MS (EI, pos.) *m/z* calcd. for C₂₀H₂₂OSi⁺⁺ [M]⁺⁺ 306.1434, found 306.1442.

Reaction of 33-Li with 15b-BF₄ ALE-174

To a solution of **35** (36 mg, 0.19 mmol, 1 eq.) in THF (3 ml) was added dropwise a solution of *n*-BuLi (1.85 M in *n*-hexane, 0.11 ml, 0.2 mmol, 1.05 eq.). After 15 minutes the resulting solution was added to a suspension of **15b-BF₄** (64 mg, 0.19 mmol, 1 eq.) in THF (5 ml) and stirred at ambient temperature for 1 hour. Reaction was carefully treated with water (20 ml) and extracted EtOAc (3 × 30 ml). Combined organic layers were washed with brine (20 ml), dried over MgSO₄ and concentrated in vacuum. Crude material was purified by column chromatography (silica, *n*-pentane/EtOAc = 15/1, with 3 vol. % Et₃N) and **39** was obtained as yellowish solid (22 mg, 27%).

4,4'-(2-Phenyl-4-(trimethylsilyl)but-3-yne-1,1-diyl)bis(N,N-dimethylaniline) (39)**39**

¹H NMR (300 MHz, CDCl₃) δ = 0.11 – 0.13 (m, 9H, H-14), 2.89 (s, 6H, H-11'), 2.91 (s, 6H, H-11'), 4.10 (d, *J* = 7.1 Hz, 1H, H-6), 4.40 (d, *J* = 7.1 Hz, 1H, H-5), 6.59 – 6.66 (m, 4H, H-9), 7.04 – 7.11 (m, 2H, H-8), 7.15 – 7.23 (m, 7H, H-1, H-2, H-3, H-7').

¹³C NMR (75 MHz, CDCl₃) δ = 0.1 (C-14), 40.9 (C-11), 41.0 (C-11'), 44.7 (C-5), 57.0 (C-6), 90.0 (C-12), 108.2 (C-13), 112.3 (C-9), 112.6 (C-9'), 126.5 (C-1), 128.0 (C-2), 128.7 (C-3), 129.1 (C-8), 130.1 (C-8'), 130.9 (C-7), 131.9 (C-7'), 141.0 (C-4), 149.1 (C-10), 149.3 (C-10').

HR-MS (EI, pos.) *m/z* calcd. for C₂₉H₃₅N₂Si⁺ [M-H]⁺ 439.2564, found 439.2576.

Reaction of 33-Zn with 15b ALE-113

To a solution of **33** (40 mg, 0.21 mmol, 1 eq.) in THF (3 ml) was added dropwise a solution of TMP-ZnCl·LiCl (1.1 M in THF, 0.21 ml, 0.23 mmol, 1.1 eq.). After 15 minutes the resulting solution was added to suspension of **15b** (71 mg, 0.21 mmol, 1 eq.) in THF (5 ml) and stirred at ambient temperature for 1 hour. Reaction was carefully treated with water (20 ml) and extracted EtOAc (3 × 30 ml). Combined organic layers were washed with brine (20 ml), dried over MgSO₄ and concentrated in vacuum. Crude material was purified by column chromatography (silica, *n*-pentane/EtOAc = 15/1, with 3% Et₃N) and **39** was obtained as white solid (42 mg, 46%).

Analytical data is consistent with that obtained above for **33-Li** and **15b**.

Formation of 31 ALE-180

To a solution of potassium tert-butoxide (60 mg, 0.53 mmol, 1 eq.) in DMSO (5 ml) was added dropwise solution of **30** (0.2 g, 1.1 mmol, 2 eq.) and the mixture was stirred for 30 minutes. Thereafter it was treated with saturated aqueous NH₄Cl (20 ml) solution and extracted EtOAc (3 × 30 ml). Combined organic layers were washed with brine (20 ml), dried over MgSO₄ and concentrated in vacuum. Crude material was subjected to GC-HRMS analysis.

HR-MS (ESI, pos.) *m/z* calcd. for C₂₄H₂₅O₄ [M+H]⁺ 377.1747, found 377.1747.

3.5.4 Kinetic Investigations

3.5.4.1 Reactions of the Sulfone 10a

Table 3.6. Kinetics of the reaction of 13a (generated from 10a by addition of 1.05 equivalents of KOtBu) with 14b in DMSO (stopped-flow, 20 °C, at 500 nm)

[14b] / mol L ⁻¹	[13a] / mol L ⁻¹	[13a] / [14b]	k_{obs} / s ⁻¹
4.33×10^{-5}	3.81×10^{-4}	9	1.20×10^1
4.33×10^{-5}	7.62×10^{-4}	18	2.58×10^1
4.33×10^{-5}	1.14×10^{-3}	26	3.93×10^1
4.33×10^{-5}	1.52×10^{-3}	35	5.54×10^1
4.33×10^{-5}	1.90×10^{-3}	44	6.84×10^1
4.33×10^{-5}	2.28×10^{-3}	53	8.49×10^1

$$k_2 = 3.83 \times 10^4 \text{ L mol}^{-1} \text{ s}^{-1}$$

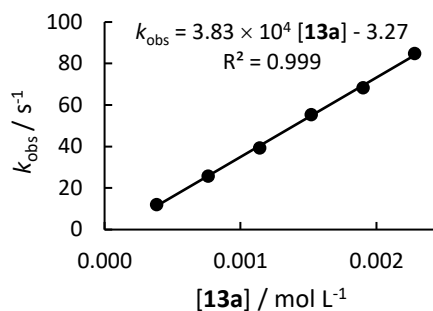


Table 3.7. Kinetics of the reaction of 13a (generated from 10a by addition of 1.05 equivalents of KOtBu) with 14c in DMSO (stopped-flow, 20 °C, at 500 nm)

[14c] / mol L ⁻¹	[13a] / mol L ⁻¹	[13a] / [14c]	k_{obs} / s ⁻¹
5.47×10^{-5}	3.81×10^{-4}	7	1.79
5.47×10^{-5}	7.62×10^{-4}	14	4.62
5.47×10^{-5}	1.14×10^{-3}	21	7.84
5.47×10^{-5}	1.52×10^{-3}	28	1.08×10^1
5.47×10^{-5}	1.90×10^{-3}	35	1.36×10^1
5.47×10^{-5}	2.28×10^{-3}	42	1.53×10^1

$$k_2 = 7.33 \times 10^3 \text{ L mol}^{-1} \text{ s}^{-1}$$

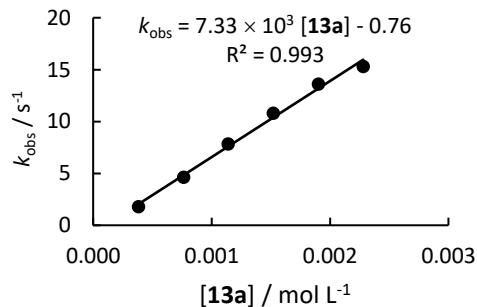


Table 3.8. Kinetics of the reaction of 13a (generated from 10a by addition of 1.05 equivalents of KOtBu) with 14b in DMSO (stopped-flow, 20 °C, at 500 nm) in presence of 18-Crown-6 (1.05 equivalents with respect to 13a)

[14b] / mol L ⁻¹	[13a] / mol L ⁻¹	[13a] / [14b]	<i>k</i> _{obs} / s ⁻¹
5.05 × 10 ⁻⁵	3.49 × 10 ⁻⁴	7	4.94
5.05 × 10 ⁻⁵	6.98 × 10 ⁻⁴	14	2.25 × 10 ¹
5.05 × 10 ⁻⁵	1.05 × 10 ⁻³	21	3.41 × 10 ¹
5.05 × 10 ⁻⁵	1.40 × 10 ⁻³	28	5.14 × 10 ¹
5.05 × 10 ⁻⁵	1.74 × 10 ⁻³	34	6.09 × 10 ¹

$$k_2 = 4.04 \times 10^4 \text{ L mol}^{-1} \text{ s}^{-1}$$

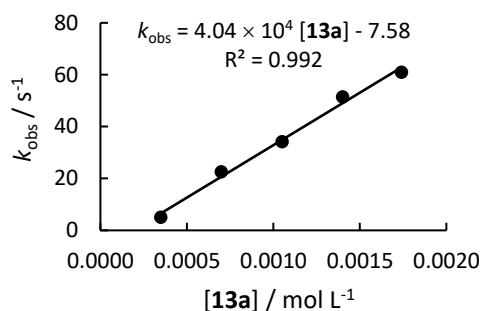


Table 3.9. Kinetics of the reaction of 13a (generated from 10a by addition of 1.05 equivalents of KOtBu) with 14c in DMSO (stopped-flow, 20 °C, at 500 nm) in presence of 18-Crown-6 (1.05 equivalents with respect to 13a)

[14c] / mol L ⁻¹	[13a] / mol L ⁻¹	[13a] / [14c]	<i>k</i> _{obs} / s ⁻¹
5.53 × 10 ⁻⁵	3.49 × 10 ⁻⁴	6	1.62
5.53 × 10 ⁻⁵	6.98 × 10 ⁻⁴	13	4.31
5.53 × 10 ⁻⁵	1.05 × 10 ⁻³	19	6.41
5.53 × 10 ⁻⁵	1.40 × 10 ⁻³	25	1.01 × 10 ¹
5.53 × 10 ⁻⁵	1.74 × 10 ⁻³	31	1.18 × 10 ¹

$$k_2 = 7.51 \times 10^3 \text{ L mol}^{-1} \text{ s}^{-1}$$

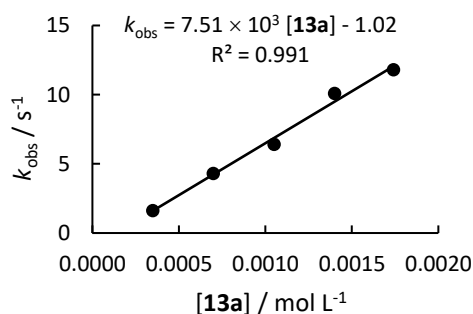
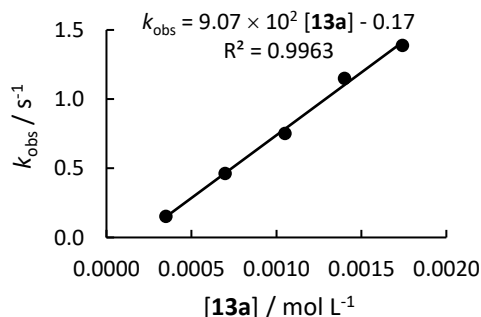


Table 3.10. Kinetics of the reaction of 13a (generated from 10a by addition of 1.05 equivalents of KOtBu) with 14d in DMSO (stopped-flow, 20 °C, at 500 nm) in presence of 18-Crown-6 (1.05 equivalents with respect to 13a)

[14d] / mol L ⁻¹	[13a] / mol L ⁻¹	[13a] / [14d]	<i>k</i> _{obs} / s ⁻¹
5.26 × 10 ⁻⁵	3.49 × 10 ⁻⁴	7	1.53 × 10 ⁻¹
5.26 × 10 ⁻⁵	6.98 × 10 ⁻⁴	13	4.64 × 10 ⁻¹
5.26 × 10 ⁻⁵	1.05 × 10 ⁻³	20	7.53 × 10 ⁻¹
5.26 × 10 ⁻⁵	1.40 × 10 ⁻³	27	1.15
5.26 × 10 ⁻⁵	1.74 × 10 ⁻³	33	1.39

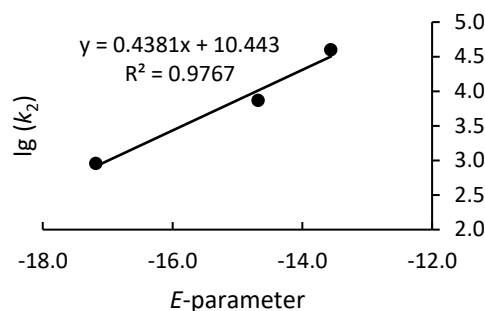
$$k_2 = 9.07 \times 10^2 \text{ L mol}^{-1} \text{ s}^{-1}$$



Determination of the Reactivity Parameters N and s_N for **13a** in DMSOTable 3.11. Rate constants for the reaction of **13a** with different electrophiles (20 °C)

Electrophile	E	$k_2 / \text{L mol}^{-1} \text{s}^{-1}$	$\log k_2$
14b	-13.56	3.94×10^4 [a]	4.60
14c	-14.68	7.42×10^3 [a]	3.87
14d	-17.18	9.07×10^2	2.96

$$N = 23.73, s_N = 0.44$$

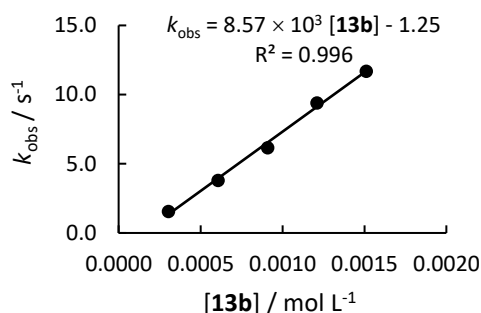


[a] Average of two experiments.

3.5.4.2 Reactions of the Sulfone **10b**Table 3.12. Kinetics of the reaction of **13b** (generated from **10b** by addition of 1.05 equivalents of KOtBu) with **14a** in DMSO (stopped-flow, 20 °C, at 500 nm)

[14a] / mol L ⁻¹	[13b] / mol L ⁻¹	[13b] / [14a]	k_{obs} / s ⁻¹
4.23×10^{-5}	3.03×10^{-4}	7	1.56
4.23×10^{-5}	6.06×10^{-4}	14	3.80
4.23×10^{-5}	9.08×10^{-4}	21	6.17
4.23×10^{-5}	1.21×10^{-3}	29	9.39
4.23×10^{-5}	1.51×10^{-3}	36	1.17×10^1

$$k_2 = 8.57 \times 10^3 \text{ L mol}^{-1} \text{s}^{-1}$$

Table 3.13. Kinetics of the reaction of **13b** (generated from **10b** by addition of 1.05 equivalents of KOtBu) with **14b** in DMSO (stopped-flow, 20 °C, at 500 nm)

[14b] / mol L ⁻¹	[13b] / mol L ⁻¹	[13b] / [14b]	k_{obs} / s ⁻¹
3.02×10^{-5}	3.03×10^{-4}	10	3.25
3.02×10^{-5}	6.06×10^{-4}	20	8.26
3.02×10^{-5}	9.08×10^{-4}	30	1.42×10^1
3.02×10^{-5}	1.21×10^{-3}	40	1.98×10^1
3.02×10^{-5}	1.51×10^{-3}	50	2.71×10^1

$$k_2 = 1.96 \times 10^4 \text{ L mol}^{-1} \text{s}^{-1}$$

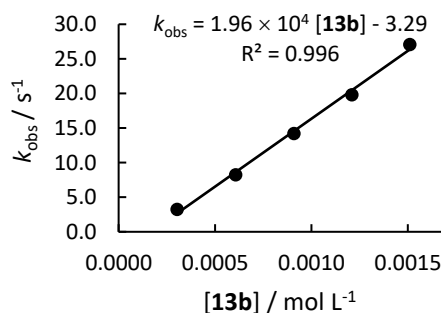


Table 3.14. Kinetics of the reaction of 13b (generated from 10b by addition of 1.05 equivalents of KOtBu) with 14c in DMSO (stopped-flow, 20 °C, at 500 nm)

[14c] / mol L ⁻¹	[13b] / mol L ⁻¹	[13b] / [14c]	<i>k</i> _{obs} / s ⁻¹
5.73 × 10 ⁻⁵	3.03 × 10 ⁻⁴	5	5.41 × 10 ⁻¹
5.73 × 10 ⁻⁵	6.06 × 10 ⁻⁴	11	1.48
5.73 × 10 ⁻⁵	9.08 × 10 ⁻⁴	16	2.51
5.73 × 10 ⁻⁵	1.21 × 10 ⁻³	21	3.62
5.73 × 10 ⁻⁵	1.51 × 10 ⁻³	26	4.74

$$k_2 = 3.49 \times 10^3 \text{ L mol}^{-1} \text{ s}^{-1}$$

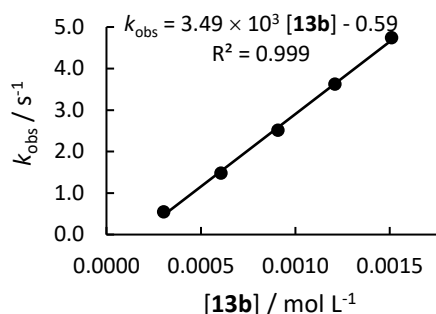
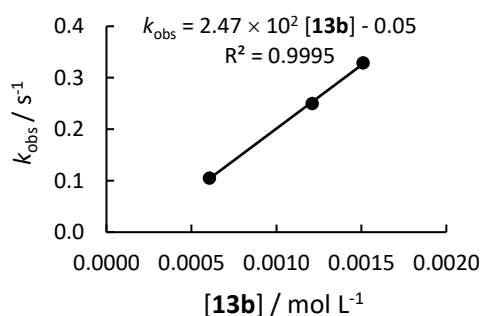


Table 3.15. Kinetics of the reaction of 13b (generated from 10b by addition of 1.05 equivalents of KOtBu) with 14d in DMSO (stopped-flow, 20 °C, at 500 nm)

[14d] / mol L ⁻¹	[13b] / mol L ⁻¹	[13b] / [14d]	<i>k</i> _{obs} / s ⁻¹
3.35 × 10 ⁻⁵	6.06 × 10 ⁻⁴	18	1.05 × 10 ⁻¹
3.35 × 10 ⁻⁵	1.21 × 10 ⁻³	36	2.50 × 10 ⁻¹
3.35 × 10 ⁻⁵	1.51 × 10 ⁻³	45	3.29 × 10 ⁻¹

$$k_2 = 2.47 \times 10^2 \text{ L mol}^{-1} \text{ s}^{-1}$$

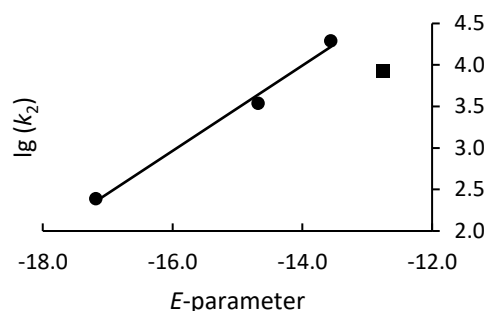


Determination of the Reactivity Parameters *N* and *s_N* for 13b in DMSO

Table 3.16. Rate constants for the reaction of 13b with different electrophiles (20 °C)

Electrophile	<i>E</i>	<i>k</i> ₂ / L mol ⁻¹ s ⁻¹	log <i>k</i> ₂
14a	-12.76	8.57 × 10 ³	3.93 ^[a]
14b	-13.56	1.96 × 10 ⁴	4.29
14c	-14.68	3.49 × 10 ³	3.54
14d	-17.18	2.47 × 10 ²	2.39

$$N = 21.94, s_N = 0.51$$



[a] Not included in the correlation (black square on the graph)

Table 3.17. Kinetics of the reaction of 35-Zn (generated from 35 by addition of 1.05 equivalents of TMPZnCl·LiCl) with 15b in THF (stopped-flow, 20 °C, at 605 nm)

[15b] / mol L ⁻¹	[35-Zn] / mol L ⁻¹	[35-Zn] / [15b]	<i>k</i> _{obs} / s ⁻¹
7.06×10^{-5}	8.72×10^{-4}	12	1.52×10^{-1}
7.06×10^{-5}	1.74×10^{-3}	25	1.95×10^{-1}
7.06×10^{-5}	3.49×10^{-3}	49	5.46×10^{-1}
7.06×10^{-5}	5.23×10^{-3}	74	1.59
7.06×10^{-5}	6.97×10^{-3}	99	2.64

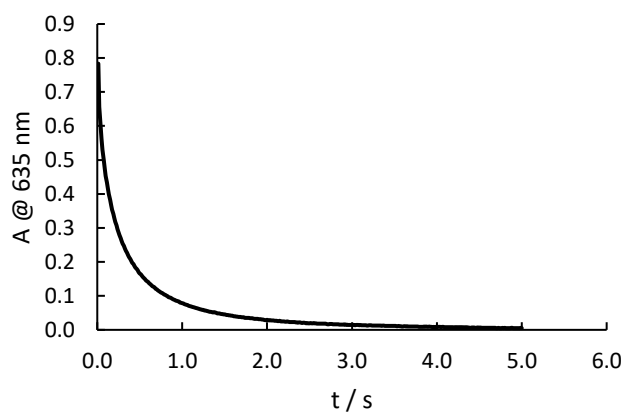
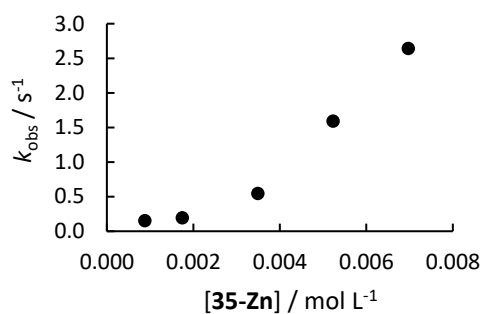


Figure 3.6. Exponential decay of absorbance *A* (at 635 nm) of the reaction of **15b** (7.06×10^{-5} mol L⁻¹) with 2,2,6,6-tetramethylpiperidine (TMPH, 9.16×10^{-4} mol L⁻¹) in THF at 20 °C.

3.6 References

- [1] a) R. B. Bates, C. A. Ogle, *Carbanion Chemistry*, Springer, Berlin, **1983**; b) L. Brandsma, *Preparative Polar Organometallic Chemistry 2*, Springer, Berlin, **1990**; c) V. Snieckus, *Advances in Carbanion Chemistry*, JAI Press, Greenwich, CT, **1992**; d) M. B. Smith in *March's Advanced Organic Chemistry* Wiley, Hoboken, **2013**, pp. 221-234.
- [2] E. Buncl, J. M. Dust, *Carbanion Chemistry*, Oxford, New York, **2003**.
- [3] a) T. G. Back, *Tetrahedron* **2001**, *57*, 5263-5301; b) S. Patai, Z. Rappoport, C. J. M. Stirling, *The Chemistry of Sulphones and Sulphoxides*, Wiley, Chichester, **1988**; c) N. S. Simpkins, *Sulphones in Organic Synthesis*, Pergamon, Oxford, **1993**.
- [4] J. Ide, Y. Kishida, *Chem. Pharm. Bull.* **1968**, *16*, 793-798.
- [5] A. Terada, Y. Kishida, *Chem. Pharm. Bull.* **1970**, *18*, 505-510.
- [6] A. Terada, Y. Kishida, *Chem. Pharm. Bull.* **1970**, *18*, 497-504.
- [7] a) M. Yoshimoto, N. Ishida, Y. Kishida, *Chem. Pharm. Bull.* **1972**, *20*, 2137-2142; b) M. Yoshimoto, Y. Kishida, *Chem. Pharm. Bull.* **1970**, *18*, 2528-2534.
- [8] a) A. Orita, N. Yoshioka, P. Struwe, A. Braier, A. Beckmann, J. Otera, *Chem. Eur. J.* **1999**, *5*, 1355-1363; b) F. G. Ye, A. Orita, A. Doumoto, J. Otera, *Tetrahedron* **2003**, *59*, 5635-5643.
- [9] a) O. Kaumanns, H. Mayr, *J. Org. Chem.* **2008**, *73*, 2738-2745; b) S. T. A. Berger, F. H. Seeliger, F. Hofbauer, H. Mayr, *Org. Biomol. Chem.* **2007**, *5*, 3020-3026; c) D. Richter, N. Hampel, T. Singer, A. R. Ofial, H. Mayr, *Eur. J. Org. Chem.* **2009**, *2009*, 3203-3211; d) R. Lucius, R. Loos, H. Mayr, *Angew. Chem. Int. Ed.* **2002**, *41*, 91-95; e) H. Mayr, T. Bug, M. F. Gotta, N. Hering, B. Irrgang, B. Janker, B. Kempf, R. Loos, A. R. Ofial, G. Remennikov, H. Schimmel, *J. Am. Chem. Soc.* **2001**, *123*, 9500-9512; f) H. Mayr, B. Kempf, A. R. Ofial, *Acc. Chem. Res.* **2003**, *36*, 66-77; g) T. Lemek, H. Mayr, *J. Org. Chem.* **2003**, *68*, 6880-6886.
- [10] J. Panteleev, R. Y. Huang, E. K. Lui, M. Lautens, *Org. Lett.* **2011**, *13*, 5314-5317.
- [11] S. T. Berger, F. H. Seeliger, F. Hofbauer, H. Mayr, *Org. Biomol. Chem.* **2007**, *5*, 3020-3026.
- [12] a) F. Corral-Bautista, R. Appel, J. S. Frickel, H. Mayr, *Chem. Eur. J.* **2015**, *21*, 875-884; b) Z. Zhang, A. Puente, F. Wang, M. Rahm, Y. Mei, H. Mayr, G. K. Prakash, *Angew. Chem. Int. Ed.* **2016**, *55*, 12845-12849.
- [13] Z. Li, Q. Chen, P. Mayer, H. Mayr, *J. Org. Chem.* **2017**, *82*, 2011-2017.
- [14] C. Hansch, A. Leo, R. W. Taft, *Chem. Rev.* **1991**, *91*, 165-195.
- [15] N. S. Simpkins, *Tetrahedron* **1990**, *46*, 6951-6984.
- [16] J. E. Backvall, R. Chinchilla, C. Najera, M. Yus, *Chem. Rev.* **1998**, *98*, 2291-2312.
- [17] S. T. McDowell, C. J. M. Stirling, *J. Chem. Soc. B* **1967**, 351-355.
- [18] K. T. Leffek, P. Pruszyński, K. Thanapaalasingham, *Can. J. Chem.* **1989**, *67*, 590-595.
- [19] B. Phan Thanh, M. Breugst, H. Mayr, *Angew. Chem. Int. Ed.* **2006**, *45*, 3869-3874.
- [20] D. S. Allgäuer, H. Jangra, H. Asahara, Z. Li, Q. Chen, H. Zipse, A. R. Ofial, H. Mayr, *J. Am. Chem. Soc.* **2017**, *139*, 13318-13329.

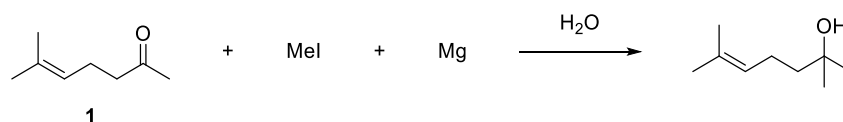
- [21] I. Noriyoshi, M. Tetsuro, K. Toshifumi, A. Takahiro, K. Hideki, I. Katsuhiko, *Bull. Chem. Soc. Jpn.* **1992**, *65*, 1379-1388.
- [22] M. Roche, T. Terme, P. Vanelle, *Tetrahedron Lett.* **2012**, *53*, 4184-4187.
- [23] A. Suarez, G. C. Fu, *Angew. Chem. Int. Ed.* **2004**, *43*, 3580-3582.
- [24] a) J. A. Marshall, *J. Org. Chem.* **2007**, *72*, 8153-8166; b) J. A. Marshall, *Chem. Rev.* **2000**, *100*, 3163-3186; c) C.-H. Ding, X.-L. Hou, *Chem. Rev.* **2011**, *111*, 1914-1937.
- [25] F. Corral-Bautista, L. Klier, P. Knochel, H. Mayr, *Angew. Chem. Int. Ed.* **2015**, *54*, 12497-12500.
- [26] a) R. K. Dress, T. Rölle, R. W. Hoffmann, *Chem. Ber.* **1995**, *128*, 673-677; b) R. W. Hoffmann, R. K. Dress, T. Ruhland, A. Wenzel, *Chem. Ber.* **1995**, *128*, 861-870; c) Y. Tamaru, S. Goto, A. Tanaka, M. Shimizu, M. Kimura, *Angew. Chem. Int. Ed.* **1996**, *35*, 878-880.
- [27] a) J. A. Marshall, *Chem. Rev.* **1996**, *96*, 31-48; b) M. Achmatowicz, L. S. Hegedus, *J. Org. Chem.* **2004**, *69*, 2229-2234.
- [28] a) J. A. Marshall in *Synthesis and Reactions of allenylzinc compounds*, Vol. 1 Eds.: Z. Rappoport, I. Marek, Wiley, New York, **2006**, pp. 421-455; b) T. Harada, T. Katsuhira, A. Osada, K. Iwazaki, K. Maejima, A. Oku, *J. Am. Chem. Soc.* **1996**, *118*, 11377-11390.
- [29] U. Groth, C. Kesenheimer, J. Neidhöfer, *Synlett* **2006**, *2006*, 1859-1862.
- [30] a) E. Favre, M. Gaudemar, *J. Organomet. Chem.* **1975**, *92*, 17-25; b) D. R. Fandrick, K. R. Fandrick, J. T. Reeves, Z. Tan, C. S. Johnson, H. Lee, J. J. Song, N. K. Yee, C. H. Senanayake, *Org. Lett.* **2010**, *12*, 88-91.
- [31] M. Ishiguro, N. Ikeda, H. Yamamoto, *J. Org. Chem.* **1982**, *47*, 2225-2227.
- [32] J. Bejjani, C. Botuha, F. Chemla, F. Ferreira, S. Magnus, A. Pérez-Luna, *Organometallics* **2012**, *31*, 4876-4885.
- [33] P. Quinio, C. François, A. Escribano Cuesta, A. K. Steib, F. Achrainer, H. Zipse, K. Karaghiosoff, P. Knochel, *Org. Lett.* **2015**, *17*, 1010-1013.
- [34] J. Panteleev, R. Y. Huang, E. K. J. Lui, M. Lautens, *Org. Lett.* **2011**, *13*, 5314-5317.
- [35] C. Ritter, N. Nett, C. G. Acevedo-Rocha, R. Lonsdale, K. Kräling, F. Dempwolff, S. Hoebenreich, P. L. Graumann, M. T. Reetz, E. Meggers, *Angew. Chem. Int. Ed.* **2015**, *54*, 13440-13443.

Chapter 4

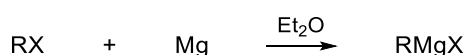
Lewis Acidic and Nucleophilic Properties of Grignard Reagents

4.1 Introduction

In 1900 Victor Grignard was optimizing conditions for reaction between methyl iodide and ketone **1** in the presence of magnesium (now known as Barbier reaction,^[1] Scheme 4.1). He proposed the intermediate in this reaction to be a RMgI species and found a rapid reaction of alkyl halides with magnesium in diethyl ether as the solvent (Scheme 4.2). Addition of these reaction mixtures to ketones or aldehydes and subsequent aqueous work-up afforded the corresponding alcohols in higher yields than in the Barbier procedure.^[2]



Scheme 4.1. Interaction of ketone **1** with methyl iodide in the presence of magnesium in water.^[1]

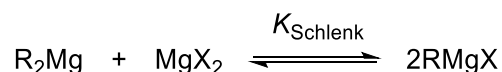


Scheme 4.2. Formation of a reactive species from alkyl halide and magnesium in diethyl ether.

The synthetic potential of the organomagnesium reagents were recognized immediately, resulting in an increasing amount of investigations towards their preparation and application. For his discovery and subsequent development of this finding Grignard was awarded the Nobel Prize in Chemistry in 1912.

4.1.1 Composition and Solvent Effect

For further studies an insight on the nature of Grignard reagents in ethereal solvents is required. The Schlenk equilibrium^[3] (Scheme 4.3) is generally accepted to describe the composition of the Grignard compounds in ethereal solutions.



Scheme 4.3. Schlenk equilibrium.

Since both R₂Mg and RMgX can react with electrophilic substrates, knowledge of this equilibrium is vital for understanding the course of the reaction. As summarized in a review by Ashby in 1974,^[4] Table 4.1 provides equilibrium constants for a number of Grignard reagents

in both diethyl ether and THF solvents. Even with the accuracy limitations, the table displays some rather clear trends: in Et₂O equilibrium constants K_{Schlenk} of magnitude 10²-10³ are obtained, in THF values of 1-10 are most common.

Table 4.1. Values for Schlenk Equilibrium.

Grignard Reagent	Solvent	K_{Schlenk}	Method
CH ₃ MgBr	Et ₂ O	~320	Cal. ^[a]
		~455	Kin. ^[b]
C ₂ H ₅ MgBr	Et ₂ O	480-484	Cal. ^[a]
C ₄ H ₉ MgBr	Et ₂ O	~10 ³	Cal. ^[a]
		~400	Kin. ^[b]
C ₆ H ₅ MgBr	Et ₂ O	55-62	Cal. ^[a]
CH ₃ MgCl	THF	4.5	IR ^[c]
		~1	NMR ^[d]
C ₂ H ₅ MgCl	THF	5.52	Cal. ^[a]
t-C ₄ H ₉ MgCl	THF	1.12	NMR ^[d]
C ₆ H ₅ MgCl	THF	1.66	Cal. ^[a]
CH ₃ MgBr	THF	3.5	IR ^[c]
		~4	NMR ^[d]
C ₂ H ₅ MgBr	THF	5.09	Cal. ^[a]
C ₆ H ₅ MgBr	THF	3.77	Cal. ^[a]
		4.0	NMR ^[d]

[a] Determined by calorimetric experiments from ref. ^[5] [b] Determined by kinetic experiments from ref. ^[6] [c] Determined by infrared experiments from ref. ^[7] [d] Determined by ¹H and ¹³C NMR experiments from ref. ^[8] and ^[9] respectively.

The presence of associated species is another important aspect of solution composition. Early reports describing the degree of aggregation in THF, even for commonly studied compounds (e.g. ethylmagnesium bromide), provided conflicting results.^[10] Diethyl ether solutions, on the other hand, have been examined in more detail. It has been established that alkylmagnesium chlorides are dimeric in a wide range of concentration^[11] while alkyl- and arylmagnesium bromides and iodides exist as monomers at low concentration (<0.1 M),^[11-12] exhibiting increased association with concentration.^[5b, 11, 13]

Results of comprehensive ebullioscopic studies of a series of Grignard and related compounds (Figure 4.1), published by Ashby et al.,^[14] clearly indicate the level of association in ethereal solvents. Figure 1a shows that typical Grignard reagents and their corresponding R₂Mg counterparts are monomeric in THF. In diethyl ether on the other hand alkyl- and

arylmagnesium bromides and iodides are associated in a linear polymeric fashion and difference in association of R_2Mg and MgX_2 indicates that association takes place predominantly through halogen bridge bonds.

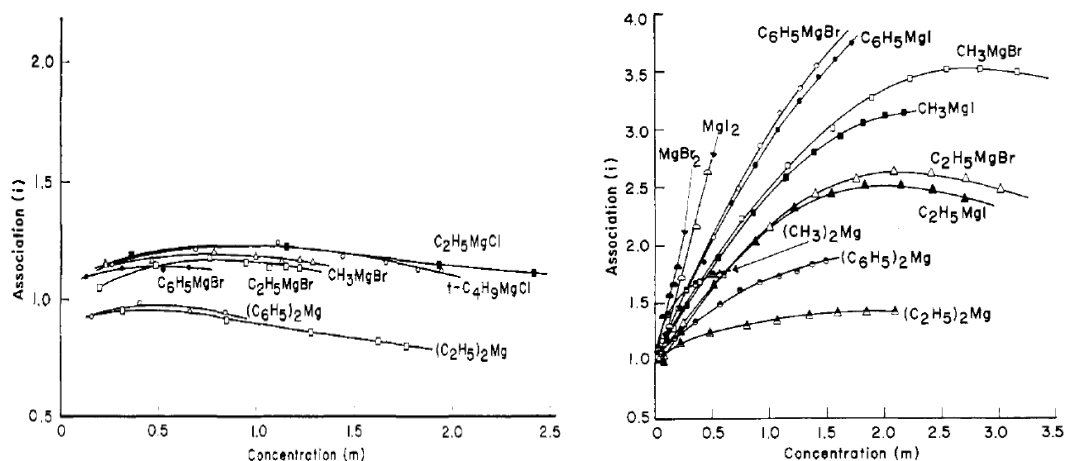


Figure 4.1. Association (expressed as an i value, apparent molecular weight divided by the formula weight) against molar concentration of selected Grignard and related compound solutions in THF (left) and Et_2O (right). Adopted from ref. [14]

From these studies one can conclude the following structure of Grignard reagents in coordinating solvents: in Et_2O (Figure 4.2, left) Grignard reagents (bromides and iodides) are best described by the Schlenk equilibrium highly shifted to $RMgX$, monomeric at concentration below 0.1 M. On the other hand, in THF (Figure 4.2, right) $RMgX$ (for $X = Cl, Br$ and I) are monomeric at all concentrations as well as corresponding R_2Mg and MgX_2 species that exist in THF at appreciable concentrations. Only $RMgF$ and $RMgOR$ form dimers.

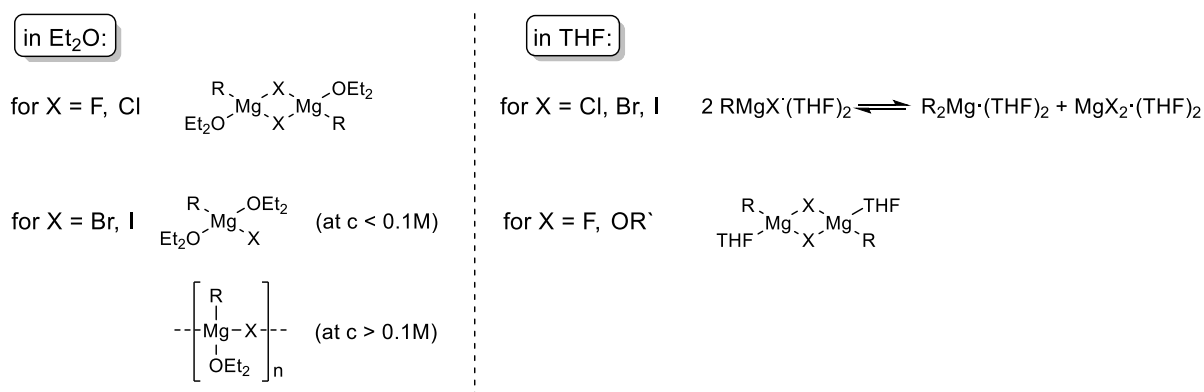
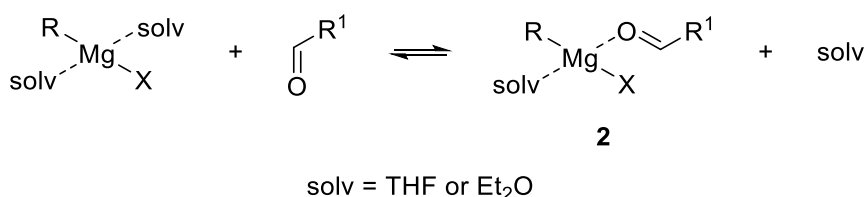


Figure 4.2. Composition of Grignard reagents in Et_2O (left) and THF (right).

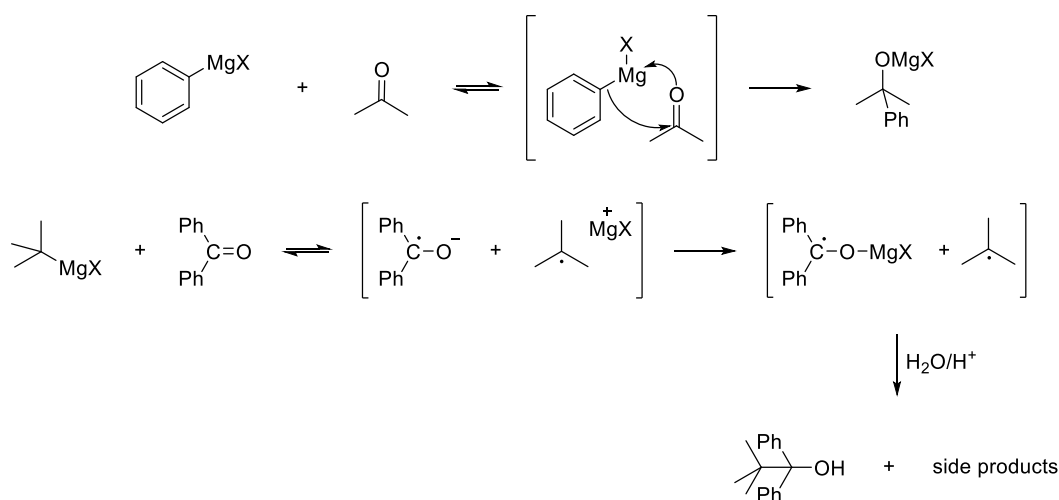
4.1.2 Mechanisms of Grignard Addition

The first step of the attack of the Grignard reagent on the carbonyl compound is substitution of a molecule of coordinating solvent (typically THF or Et₂O) with a molecule of the substrate (Scheme 4.4) to form complex **2** in a very fast equilibrium. Equilibrium constants for this process have been determined by IR and UV spectroscopy. They increase with the Lewis acidity in the series: R₂Mg < RMgCl < RMgBr < RMgI and with Lewis basicity in the series: RCOOR < ArCOAr < ArCOR < RCOR.^[5c] In more coordinating THF the complexation between organometallic species and ketones is quite unfavorable.^[15]



Scheme 4.4. Initial formation of the complex between Grignard reagent and carbonyl compound.

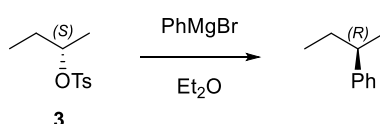
Subsequent attack of the organomagnesium species at the carbonyl carbon may be described by two possible mechanisms.^[6] On the one hand, reactions between Grignard reagents with strong C-Mg bond (e.g. phenylmagnesium bromide) and weak electron acceptors (e.g. acetone) will take place through a polar concerted mechanism (Scheme 4.5, top). On the other hand, reactions between *t*-butylmagnesium bromide (with the weakest C-Mg bond) and benzophenone, which is readily reduced to a stable ketyl radical, occur by a single electron transfer (SET) mechanism (Scheme 4.5, bottom).



Scheme 4.5. Possible mechanisms for nucleophilic attack of Grignard reagents at carbonyl compounds: polar concerted (top) and SET (bottom).

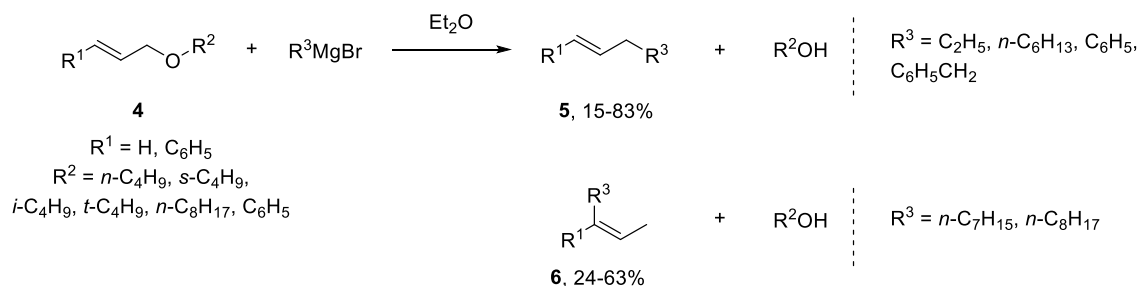
In contrast to nucleophilic additions, the substitution reactions that involve Grignard reagents as the nucleophile are more limited in scope. As for reactions with ketones, a general mechanism that would be used to describe the formation of the new C-C bond in displacing a leaving group does not exist. Instead, depending on the nature of both Grignard reagent and a substrate, at least three mechanisms are possible – an S_N2 mechanism of the direct nucleophilic substitution, an S_N1 mechanism with ionization to a carbocationic intermediate, and a SET mechanism involving radical intermediates.

The SET mechanism is clearly implicated in the reactions of poly-halides due to their low reduction potentials and formation of homo-coupling products. On the other hand, the S_N2 mechanism is suggested by Hill^[16] for sulfonates or phosphates, since the leaving group is relatively reactive without coordination to a metal ion and does not readily accept an electron. Inversion of the configuration was found in the reaction (S)-sec-butyl-*p*-toluenesulfonate **3** with PhMgBr (Scheme 4.6).^[17]



Scheme 4.6. Inversion of configuration in reaction of **3** with PhMgBr in Et₂O.

Substrates that may easily be ionized to stable carbocations should react with Grignard reagents through an S_N1 mechanism. Even though the leaving groups in such substrates (typically ether or ester) are relatively unreactive, coordination to a Lewis acidic organomagnesium species increases their leaving abilities. A representative transformation was demonstrated by Hill^[18] in a range of β,γ -unsaturated ethers **4** with several Grignard reagents (Scheme 4.7) to yield olefins **5** for aryl and alkyl (lower than *n*-heptyl) organometallic species. Formation of 1,4-addition products **6** was found in the reaction of series of unsaturated ethers with *n*-heptyl- and *n*-octylmagnesium bromide.



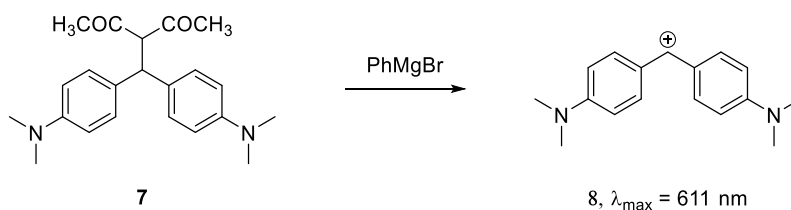
Scheme 4.7. Reaction of unsaturated ethers **4** with Grignard reagents.

Selected examples for the S_N1-type reaction with Grignard reagents are summarized in Table 2. In analogy to a reaction with ketones Hill and co-workers^[18a] suggest that the initial step of the reaction is formation of the complex between the RMgX and substrate ether. Coordination of a Lewis acidic organomagnesium species to the ether molecule leads to increase of electron deficiency at the α-carbon with subsequent nucleophilic attack. In all examples C-O bond is cleaved selectively – either to form the most stable carbocation or, with comparable stability of the carbocation, or to form the more stable anion (Table 4.2, Entry 4-5)

Table 4.2. Selected examples of S_N1-type reactions with Grignard reagents.

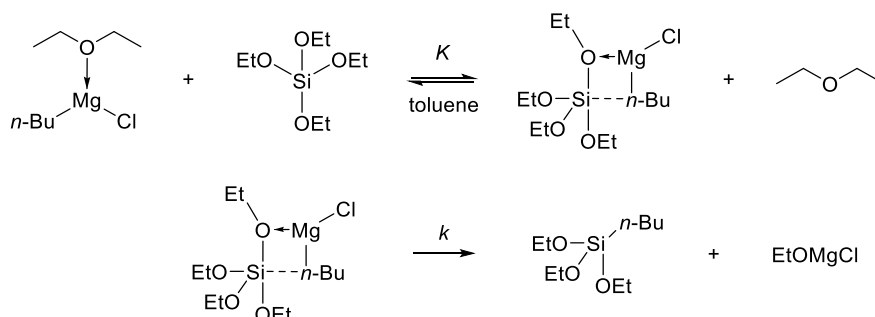
$\text{X}-\text{C}(\text{R})-\text{OR}^1 \xrightleftharpoons[\text{THF}]{\text{R}^3\text{MgX}} \text{X}-\text{C}^+(\text{R}) + [\text{R}^3\text{Mg}(\text{OR}^1)\text{X}]^- \xrightarrow{\text{R}^3\text{MgX}} \text{X}-\text{C}(\text{R})-\text{R}^3$				
Entry	Substrate	Grignard Reagent	Product (yield, %)	Reference
1		Ph-MgBr	(84)	[19]
2		<i>n</i> -C ₃ H ₇ -MgBr	(43)	[20]
3		Ph-MgBr	(89)	[21]
4		<i>n</i> -C ₄ H ₉ -MgBr	(90)	[22]
5		<i>n</i> -C ₄ H ₉ -MgBr	(74)	[23]

Similar interactions involving carbocationic intermediate were found in C-C bond cleavage reactions between the substituted dicarbonyl compound **7** and phenylmagnesium bromide (Scheme 4.8). Authors^[24] reported the formation of a colored species with λ_{max} = 611 nm, which is characteristic for the bis-(*p*-(dimethylamino)phenyl)methylium ion **8**. Unfortunately, detailed information about this experiment is not available.



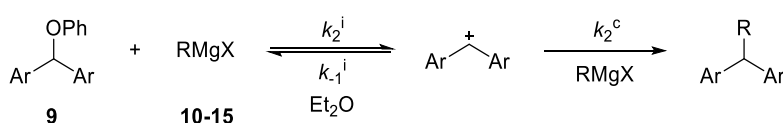
Scheme 4.8. C-C fragmentation of dicarbonyl **7** in reaction with PhMgBr.

Extensive kinetic studies by Tuulmets et al. of the Grignard reaction with silanes in diethyl ether and ether-toluene mixtures provide the insight on the mechanism of such transformations. The authors^[25] have provided the experimental evidence for a two-step reaction: initial replacement of the solvent molecule by the tetraalkoxy silane followed by subsequent rearrangement to products. The use of monosolvated Grignard reagents in toluene solution gave the quantitative data for equilibrium and rate constants (an example is presented on Scheme 4.9). In contrast to tetraalkoxysilanes, the reactions of *n*-BuMgCl with chlorosilanes were faster with increasing solvating power of the ether (THF > diethyl ether > methyl *t*-butyl ether) and were not affected by the replacement of ether by toluene.^[25a] Thus, chlorosilanes are not involved in the initial coordination step.



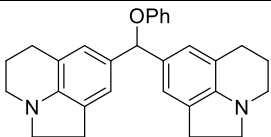
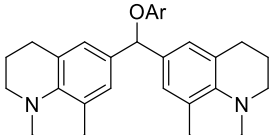
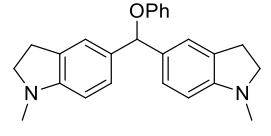
Scheme 4.9. Mechanism of nucleophilic substitution of tetraethoxysilane with monosolvated *n*-butylmagnesium chloride in toluene at 20 °C; $K = 1.03 \text{ L mol}^{-1}$, $k = 0.17 \text{ s}^{-1}$.

In this work we now present the quantitative kinetic analysis of $\text{S}_{\text{N}}1$ -type reactions between benzhydryl phenyl ethers **9** and Grignard reagents **10-15** in diethyl ether. Photometrical observations of the intermediate benzhydrylium ions allowed us to calculate both equilibrium ($K = k_2^{\text{i}} / k_{-1}^{\text{i}}$) and rate constants k_2^{i} for ionization and k_2^{c} consumption reactions shown on Scheme 4.10. The list of employed substrates is shown in Table 4.3 and Scheme 4.11.

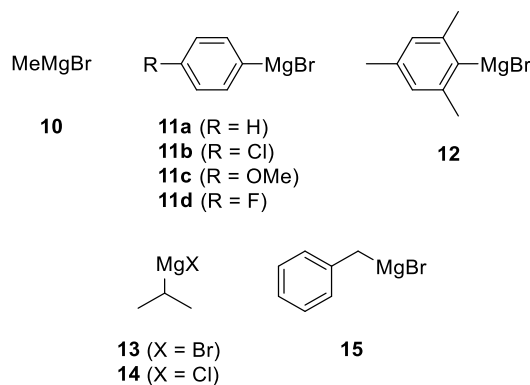


Scheme 4.10. $\text{S}_{\text{N}}1$ -type reaction between benzhydryl phenyl ethers **9** and the Grignard reagents **10-15** in diethyl ether.

Table 4.3. Substrates **9** employed in the study of reactivity of Grignard reagents.

Substrate	$E^{[a]}$	$E_f^{[a]}$	$\lambda_{\max}^{[b]}$ / nm	$\log \varepsilon^{[b]}$
 9a (lil_2CHOPh)	-10.04	5.05	628	5.11
 9b (jul_2CHOPh , Ar = Ph) 9b-CN (Ar = 4-CN-C ₆ H ₄)	-9.45	5.61	632	5.24
 9c (ind_2CHOPh)	-8.76	4.83	616	5.11 ^[c]

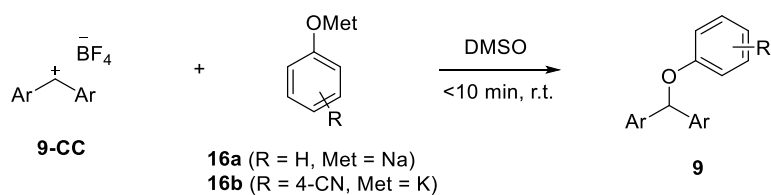
[a] For corresponding carbocation from ref. ^[26] [b] In 10 vol. % CH₂Cl₂ solution in Et₂O. [c] In acetonitrile.

**Scheme 4.11.** Grignard reagents **10-15** used in this study.

4.2 Results and Discussion

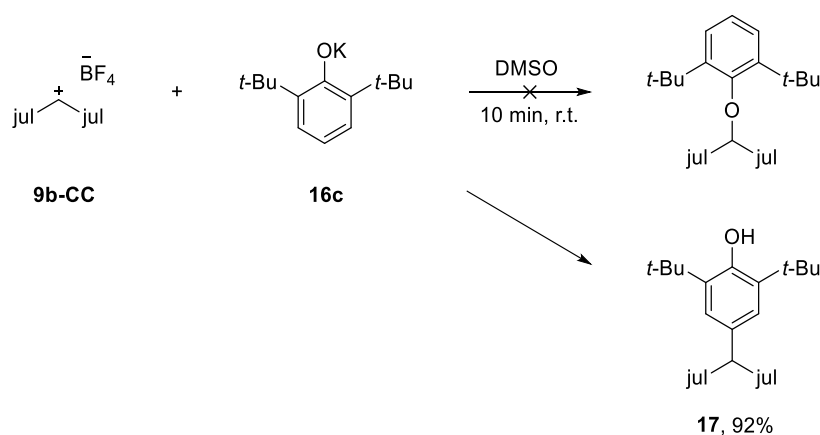
4.2.1 Substrate Synthesis

Benzhydryl phenyl ethers **9** were synthesized from the corresponding carbocations **9-CC** and substituted sodium or potassium phenoxides **16a-b** in DMSO at ambient temperature (Scheme 4.12). After aqueous work-up in presence of 2 M NH₃ (aq.), the crude material was recrystallized from Et₂O/*n*-pentane and used for subsequent studies. The substrate **9b-CN** tends to ionize in the presence of moisture and then forms polymers of unidentified structure. **9b-CN** was, therefore, not suitable for kinetic investigations.



Scheme 4.12. Formation of benzhydryl phenyl ethers **9** from the corresponding benzhydrylium tetrafluoroborates **9-CC**. Structures are shown in Table 4.3.

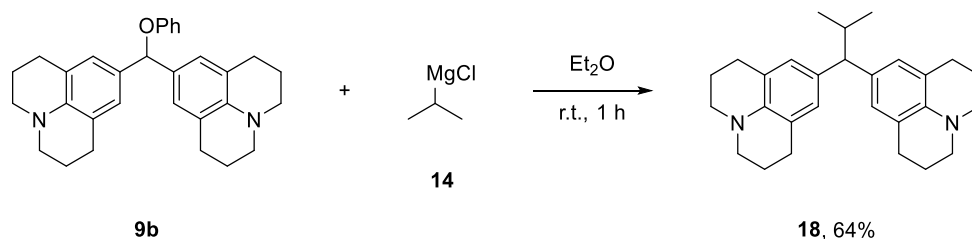
An attempt to prepare a benzhydryl ether with a bulkier leaving group for the succeeding ionization failed since benzhydrylium ion **9b-CC** exclusively attack at the 4-C position of potassium 2,6-di-*tert*-butylphenoxide **16c** (Scheme 4.13).



Scheme 4.13. Formation of **17** in the reaction of benzhydrylium tetrafluoroborate **9b-CC** and **16c** in DMSO.

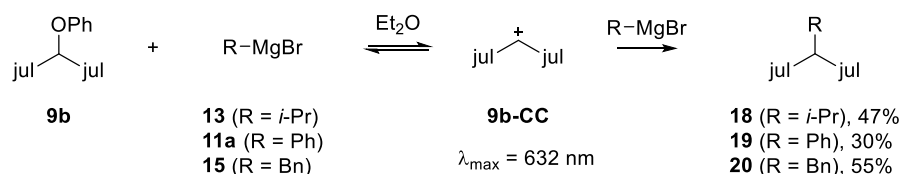
4.2.2 Product Studies

The reaction of benzhydryl phenyl ether **9b** and isopropylmagnesium chloride **14** was performed in Et_2O at ambient temperature (Scheme 4.14). Formation of the intermediate carbocation (as generalized on Scheme 4.10) was not observed visually, however the product of carbon-carbon bond formation **18** was obtained after subsequent work-up and purification using column chromatography in 64% yield.



Scheme 4.14. Reaction of benzhydryl phenyl ether **9b** with isopropylmagnesium chloride **14** in diethyl ether.

The more Lewis acidic Grignard reagents **11a**, **13** and **15** (3-3.5 equiv.) in a reaction with the same substrate **9b** led to the corresponding carbocation that was observed visually ($\lambda_{\text{max}} = 632$ nm) during the reaction course (Scheme 4.15). However, for product **18** 3.5 equivalents of **11a** were not sufficient to speed up the second step of the reaction and approx. 20% of the starting substrate **9b** was still present in the solution after 3 hours.



Scheme 4.15. Reaction of substrate **9b** with Grignard reagents **11a**, **13** and **15** proceeded through the intermediate carbocation **9b-CC** in diethyl ether.

4.2.3 Kinetic Investigations

The reactions of Grignard reagents **10-15** with benzhydryl phenyl ethers **9** were performed in either Et₂O or THF at 20 °C and monitored by UV-Vis spectroscopy at the absorption maxima of the corresponding benzhydrylium cation (listed in Table 4.4). To simplify the reaction mechanism and suppress the effect of the side reactions on the kinetic experiment Grignard reagents were used in very high excess (at least 200 equiv.), thus its concentration remained constant throughout the reactions. The first-order rate constant k_1^i and k_1^c were derived by separate least-squares fitting of the exponential function to the increase and the decrease of the experimental curve of absorbance of the carbocation, respectively (as exemplified in Figure 4.3 for the reaction of **9a** with MeMgBr **10**).

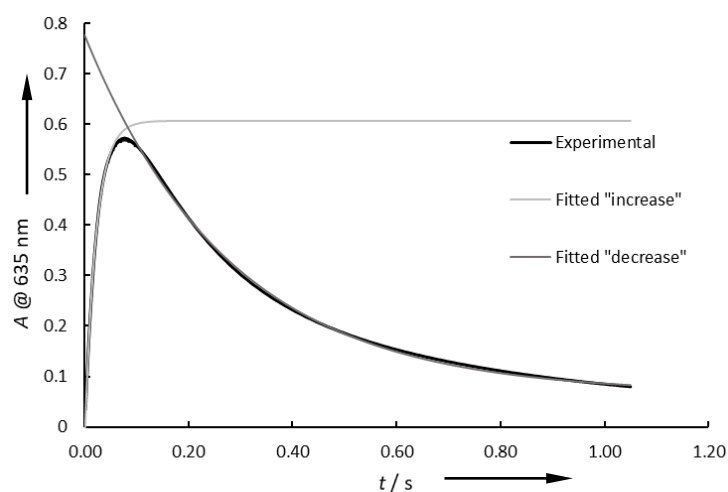


Figure 4.3. Experimental plot of absorbance A (at 635 nm) of the corresponding carbocation **9a-CC** (black) in the reaction of **9a** ($2.18 \times 10^{-5} \text{ mol L}^{-1}$) with **10** ($1.96 \times 10^{-2} \text{ mol L}^{-1}$) in Et₂O at 20 °C; calculated exponential increase (light grey) and decrease (dark grey) for the corresponding parts of experimental curve versus time.

To analyze the Lewis acidic properties of Grignard reagents towards phenoxide groups, the reversibility in the first step of the reaction should be taken into account. Since the mathematical interpretation of the reversible consecutive reaction (Scheme 4.16) is complicated,^[27] quantitative analysis of the kinetic data was performed using the COPASI software (an example for the reaction of **9a** with MeMgBr **10** is shown in Figure 4.4).^[28] For this purpose, the experimentally measured time-dependent absorption curves were converted to concentration vs time curves using the molar absorption coefficients ϵ of the carbocationic intermediates listed in Table 4.4.



Scheme 4.16. Reversible consecutive reaction model used for calculation of the rate constants for reactions of substrates **9** with Grignard reagents (see Scheme 4.10).

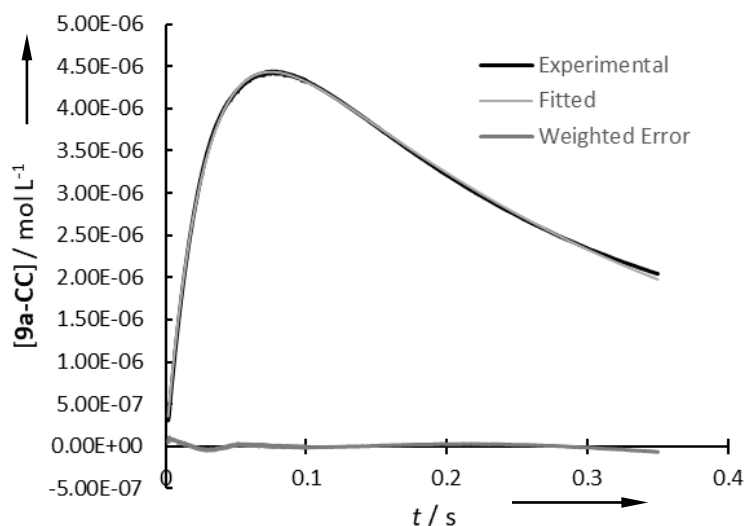


Figure 4.4. Experimental plot of concentration of the corresponding carbocation (black) in the reaction of **9a** ($2.18 \times 10^{-5} \text{ mol L}^{-1}$) with MeMgBr ($1.96 \times 10^{-2} \text{ mol L}^{-1}$) in Et₂O at 20 °C; calculated plot of the concentration (light grey) and weighted error (dark grey) found with COPASI software for a standard consecutive reaction (Scheme 4.16).

Second-order rate constants for both ionization k_2^i and consumption k_2^c steps (Scheme 4.10) are obtained as slopes of linear correlations of k_1 against the concentration of corresponding Grignard reagents. A representative example is shown in Figures 4.5 and 4.6 for separate single-exponential and COPASI analysis respectively for the reaction of **9a** with methylmagnesium bromide (**10**).

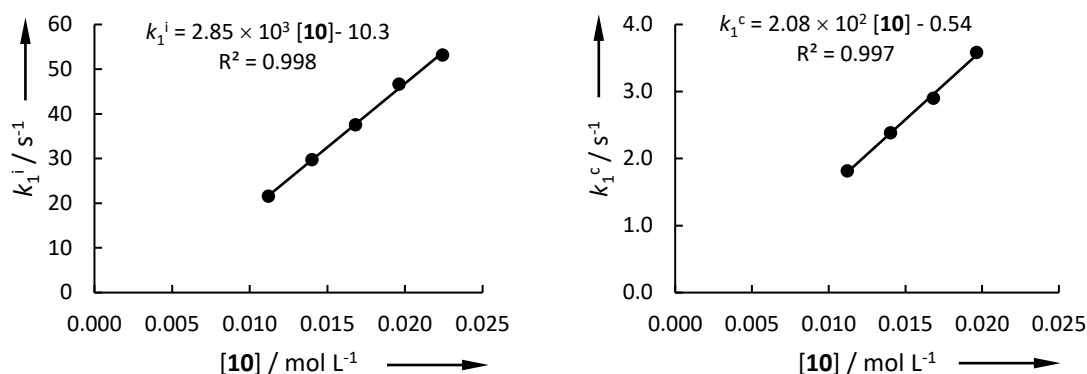


Figure 4.5. Plot of the first-order rate constants k_1^i (for ionisation reaction, left) and k_1^c (for consumption reaction, right), obtained with separate single-exponential analysis, versus the concentration of **10** in reaction with **9a** ($2.18 \times 10^{-5} \text{ mol L}^{-1}$).

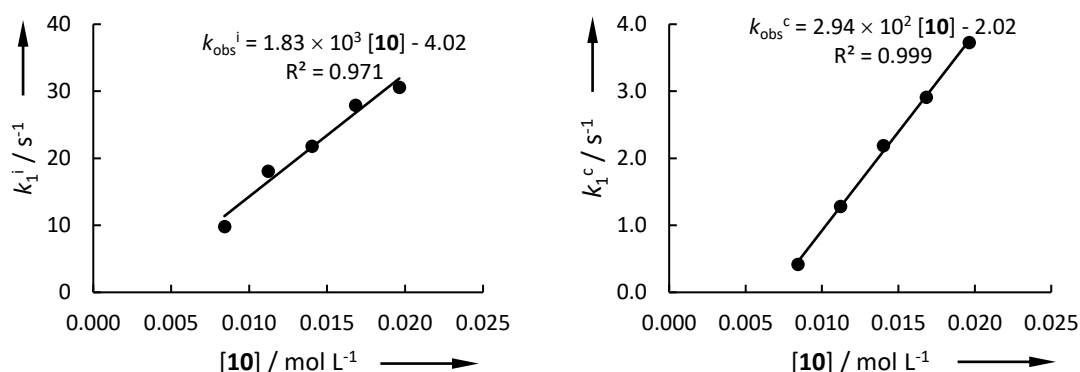


Figure 4.6. Plot of the first-order rate constants k_1^i (for ionisation reaction, left) and k_1^c (for consumption reaction, right), obtained with COPASI software, versus the concentration of **10** in reaction with **9a** ($2.18 \times 10^{-5} \text{ mol L}^{-1}$).

The obtained second-order rate constants k_2^i and k_2^c and equilibrium constant K , calculated as k_2^i/k_1^i (for experiments with low standard deviation) are summarized in Table 4.4. Different values found for separate single-equilibrium analysis and reversible consecutive reaction model analysis with COPASI indicate the impact of the equilibrium of the first step of the transformation (Scheme 4.10).

Table 4.4. Second-order rate constants k_2^i and k_2^c for the reaction of benzhydryl phenyl ethers **9** with Grignard reagents **10-11**, **13** and **15** in Et_2O at 20°C .

Grignard	Substrate	$K / \text{L mol}^{-1}$	$k_2^i / \text{L mol}^{-1} \text{s}^{-1}$ [a] ($k_2^i / \text{L mol}^{-1} \text{s}^{-1}$) [b]	$k_2^c / \text{L mol}^{-1} \text{s}^{-1}$ [a] ($k_2^c / \text{L mol}^{-1} \text{s}^{-1}$) [b]
11a	9c	1.03×10^7	7.13×10^3 (6.47×10^3)	5.34×10^2 (7.63×10^2)
	9b	7.37×10^7	1.40×10^4 (1.40×10^4)	6.74×10^2 (9.39×10^2)

Table 4.4. Continued.

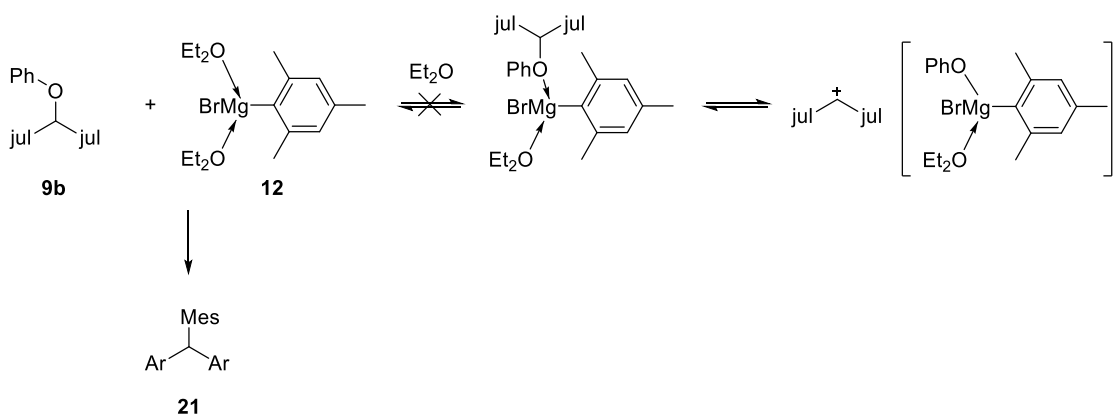
Grignard	Substrate	$K / \text{L mol}^{-1}$	$k_2^i / \text{L mol}^{-1} \text{s}^{-1}$ [a] ($k_2^i / \text{L mol}^{-1} \text{s}^{-1}$) [b]	$k_2^c / \text{L mol}^{-1} \text{s}^{-1}$ [a] ($k_2^c / \text{L mol}^{-1} \text{s}^{-1}$) [b]
11a	9a	1.06×10^6	1.04×10^4 (8.05×10^3)	3.79×10^2 (8.25×10^2)
11b	9b	3.25×10^5	1.04×10^4 (1.10×10^4)	4.36×10^2 (6.41×10^2)
	9a	-	4.77×10^3 (3.37×10^3)	1.97×10^2 (2.53×10^2)
11c	9b	-	—[c]	6.35×10^2
	9a	-	2.27×10^3 (2.12×10^3)	3.29×10^2 (4.99×10^2)
11d	9a	1.21×10^8	4.49×10^3 (5.14×10^3)	1.28×10^2 (1.52×10^2)
10	9c	-	2.71×10^3 (2.92×10^3)	4.88×10^2 (5.89×10^2)
	9b	-	4.17×10^3 (5.48×10^3)	1.09×10^2 (8.83×10^2)
	9a		1.83×10^3 (2.85×10^3)	2.94×10^2 (2.08×10^2)
13	9b	3.77×10^5	7.46×10^2	—[d]
15	9a	4.76×10^4	2.05×10^2	—[d]

[a] Determined using COPASI software. [b] Determined using separate mono-exponential fitting.

[c] Higher reaction order observed. [d] Second step was not observed.

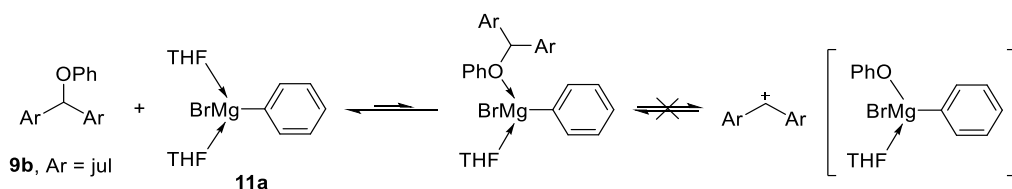
The influence of the MgBr_2 on the rate of the transformation was studied in the reaction of substrate **9b** and Grignard reagent **11a** (Table 4.8, Experimental Section). A linear correlation was found between the observed rate constant of the ionization step and the concentration of the magnesium bromide. The increase of the MgBr_2 concentration (from 0 to 0.15 mol L⁻¹) also leads to increase of the concentration of the nucleophilic species PhMgBr and PhMg_2 due to Schlenk equilibrium (Scheme 4.3) and therefore increase the rate of the consumption step.

The reaction between substrate **9b** and mesitylmagnesium bromide **12** in diethyl ether could not be studied kinetically since the intermediate carbocation was not observed. We suggest that bulky arylmagnesium species prevent the initial coordination step and the formation of a carbocation (Scheme 4.17). Thus, the reaction proceeds directly to the substitution product, presumably through an $\text{S}_{\text{N}}2$ mechanism. In contrast, in the reaction between substrate **9b-CN** and phenylmagnesium bromide **11a**, the intermediate carbocation was observed, albeit at a concentration too low for quantitative analysis, indicating that the rate of consumption of the intermediate is higher than the rate of its formation.



Scheme 4.17. Suggested mechanism for the reaction between substrate **9b** and mesitylmagnesium bromide **12** in diethyl ether.

The corresponding benzhydrylium ion was also not observed when the reaction between the substrate **9b** and Grignard reagent **11a** was performed in THF. Due to the Schlenk equilibrium (Scheme 4.3, Table 4.1) a high concentration of the more Lewis acidic MgBr_2 was present in the solution. Therefore, we expected the acceleration of the ionization step that would lead to increased concentration of the intermediate carbocation. However, the high solvation power of the THF shifted the coordination equilibrium far to the starting material and prevented the formation of the carbocation (Scheme 4.18). This is also supported by the low rate of ionization of the substrate **9b** by MgBr_2 : $\tau_{1/2} > 1000$ s in THF and $\tau_{1/2} < 3$ s for the same reaction in Et_2O (Figures 4.13 and 4.14 in the experimental section respectively).



Scheme 4.18. Suggested mechanism for initial steps of reaction of substrate **9b** with phenylmagnesium bromide **11a** in THF.

As it was observed during the product study, the reaction between substrate **9b** and isopropylmagnesium chloride **14** in diethyl ether did not proceed through an intermediate carbocation and thus could not be studied kinetically. Low Lewis acidity of organomagnesium chlorides corresponds to the shift in the coordination equilibria (in analogy to Scheme 4.18).

4.2.4 Correlation analysis

$$\lg k_2 (20\text{ }^{\circ}\text{C}) = s_N (N + E) \quad (1)$$

Plots of $\lg k_2^{\circ}$ for the reaction of substrates **9** with Grignard reagents against the electrophilicity parameters of the corresponding benzhydrylium ions (Figure 4.7) did not correlate linearly and therefore Equation (1) is not applicable to calculate the nucleophile specific parameters N and s_N for studied Grignard reagents. Several factors may be responsible for these deviations: experimental errors in titration and kinetic investigations, influence of the Schlenk equilibrium that will produce more Lewis acidic MgBr_2 and more nucleophilic R_2Mg , and the contribution of the SET mechanism for the reaction between formed carbocation and organomagnesium species.

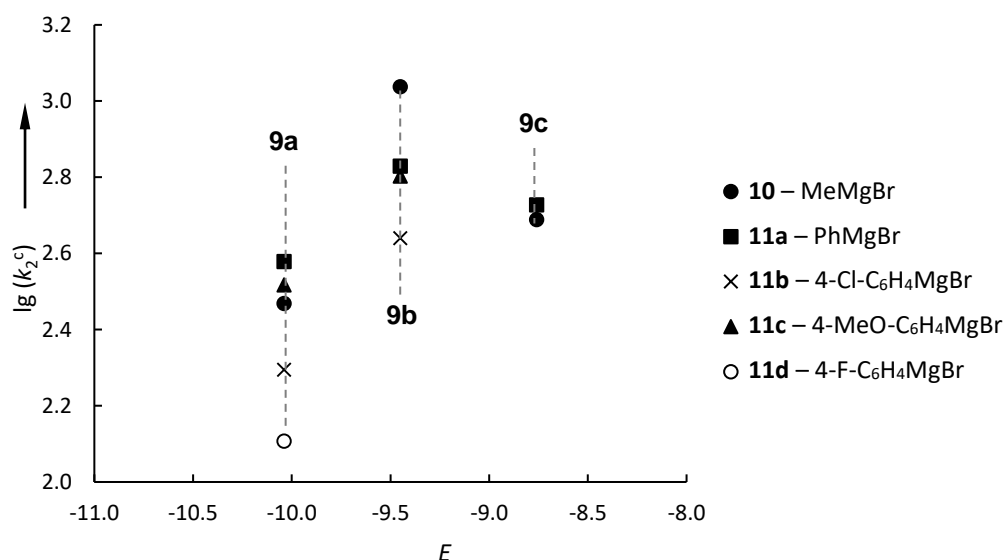


Figure 4.7. Correlation of the logarithms of the second-order rate constants k_2° for the consumption reaction of Grignard reagents **10-11** with the substrates **9** in Et_2O with the electrophilicity parameters E of the corresponding benzhydrylium ions.

Significant deviations were also found during parameter optimization for pseudo-first order reaction conditions (Figure 4.8) when the COPASI software was used. Due to these deviations, for some experiments fitting was performed to match the maximum of the concentration of the intermediate carbocation to estimate the values of the rate constants. The simple consecutive reaction mechanism with reversibility of the first step does not hold with reliable standard deviation for the reaction of **11c** with substrates **9a-b**. Attempts to include the organometallic species present in the solution due to Schlenk equilibrium into the reaction mechanism (Scheme 4.19) increases the number of kinetic parameters and makes the quantitative analysis impossible (standard deviation >10%).

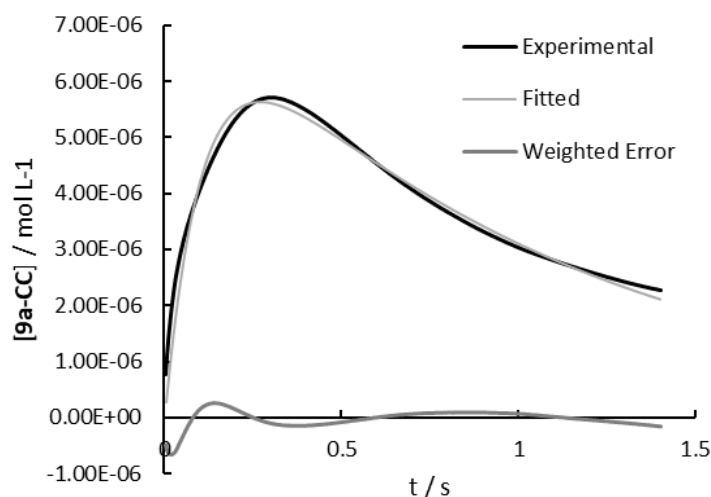
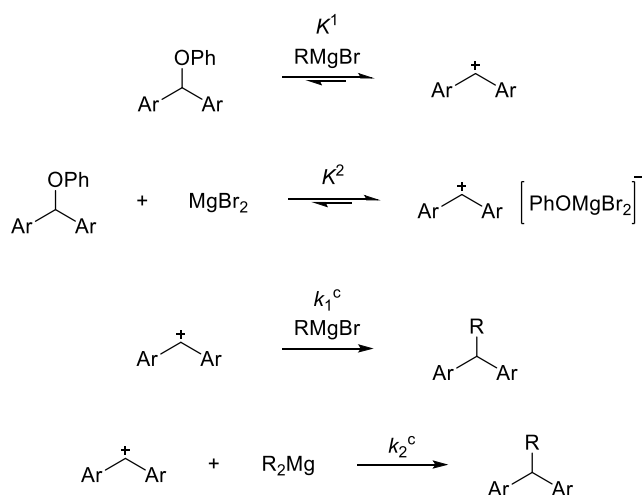


Figure 4.8. Experimental plot of concentration of the corresponding carbocation (black) in the reaction of **9a** ($2.32 \times 10^{-5} \text{ mol L}^{-1}$) with **11c** ($7.86 \times 10^{-3} \text{ mol L}^{-1}$) in Et₂O at 20 °C; calculated plot of the concentration (light grey) and weighted error (dark grey) found with COPASI software for a standard consecutive reaction.



Scheme 4.19. Extended mechanism of the reaction of substrate **9** with Grignard reagents, including organometallic species from Schlenk equilibrium.

At the same time, plots of logarithms of k_2^i for the ionization reaction of substrates **9** with Grignard reagents against the electrofugality parameters of the corresponding benzhydrylium carbocations (Figure 4.9) did not show linear correlations, too. Therefore, the quantitative analysis of activation of the phenoxide as a leaving group by Grignard reagent is not possible.

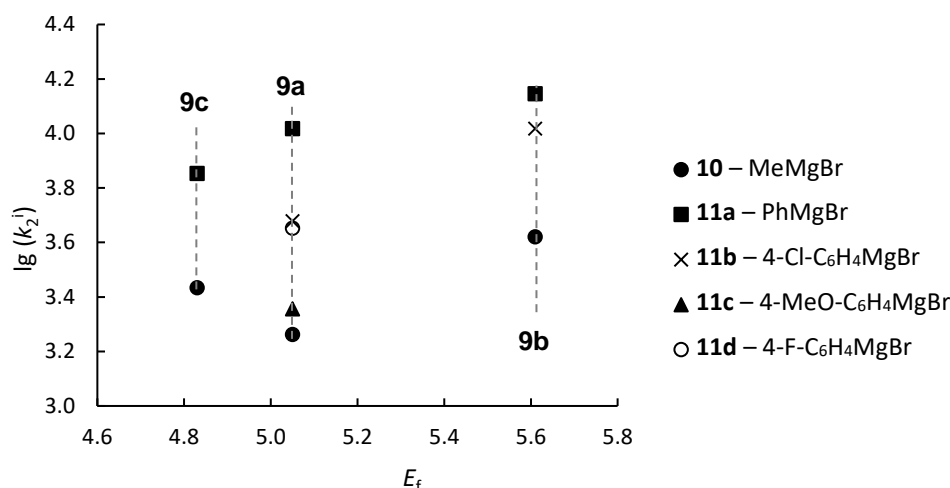


Figure 4.9. Correlation of the logarithms of the rate constants k_2^i for the ionization reaction of the substrates **9** with Grignard reagents **10–11** in Et₂O with the electrofugality parameters E_f of the corresponding benzhydrylium ions.

Even though nucleophile specific parameters for Grignard reagents could not be obtained, it is still possible to compare their reactivities with those of other species. Figure 4.10 shows the comparison of ionization rates of benzhydryl phenyl ether **9a** in presence of >1000 eq. of PhMgBr **11a** ($c = 1.45 \times 10^{-2}$ mol L⁻¹) with those of solvolysis of substrates **22** in various solvents. As demonstrated, coordination of the phenoxy group to PhMgBr makes the rates of ionization of the substrate **9a** in diethyl ether 27 and 7 times faster than solvolysis of the benzhydryl phenylsulfinate **22a** and acetate **22b** in 60% acetonitrile 40% water mixture.

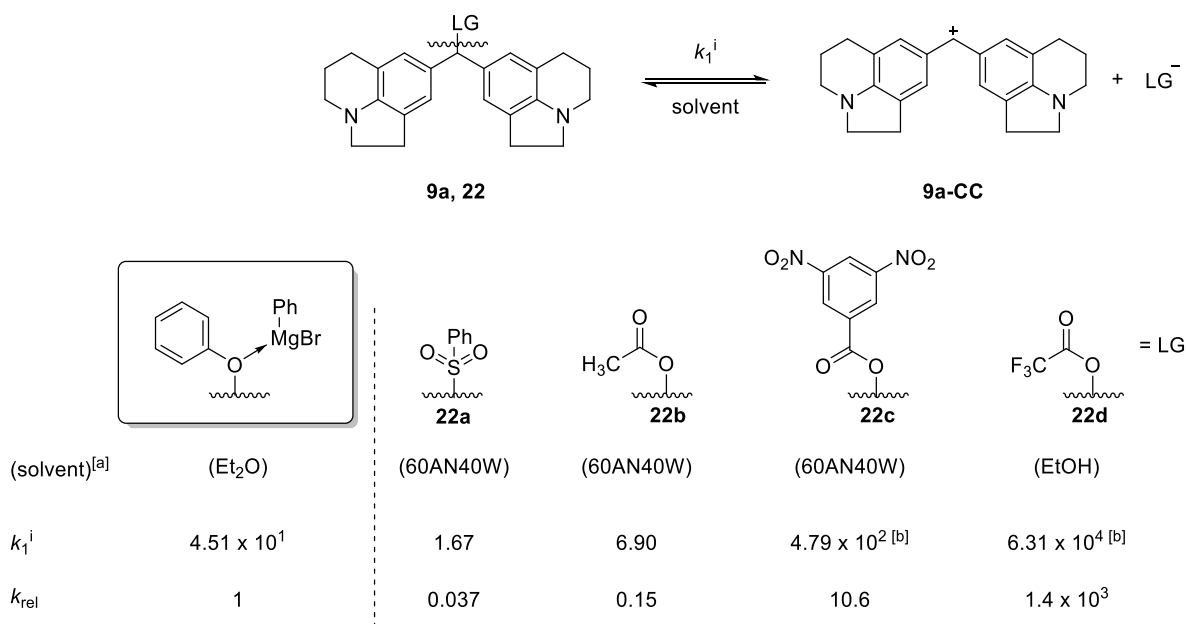


Figure 4.10. General scheme of ionization of substrates **9a** and **22** (top). Comparison of absolute (in s⁻¹) and relative rate constants for the ionization of the benzhydryl phenyl ether **9a** with PhMgBr (1.45×10^{-2} mol L⁻¹) in diethyl ether at 20 °C with those for ionization of substrates **22** in a specific solvent at 20 °C from ref. ^[26b] [a] Mixture of solvents are given as (v/v); AN = acetonitrile, W = water. [b] Calculated using E_f , N_f and s_f parameters from ref. ^[26b]

As one would expect from electron-donating/-withdrawing properties, the ionization power of 4-substituted arylmagnesiumbromides increases in the range: 4-F < 4-Cl < 4-H with an exception of 4-MeO due to its possible intermolecular dimerization that leads to reduced reaction rates (Figure 4.11). The Grignard reagent with a relatively strong C-Mg bond, such as MeMgBr **10**, differs by less than one order of magnitude from PhMgBr **11a** with respect to ionization of **9a**.

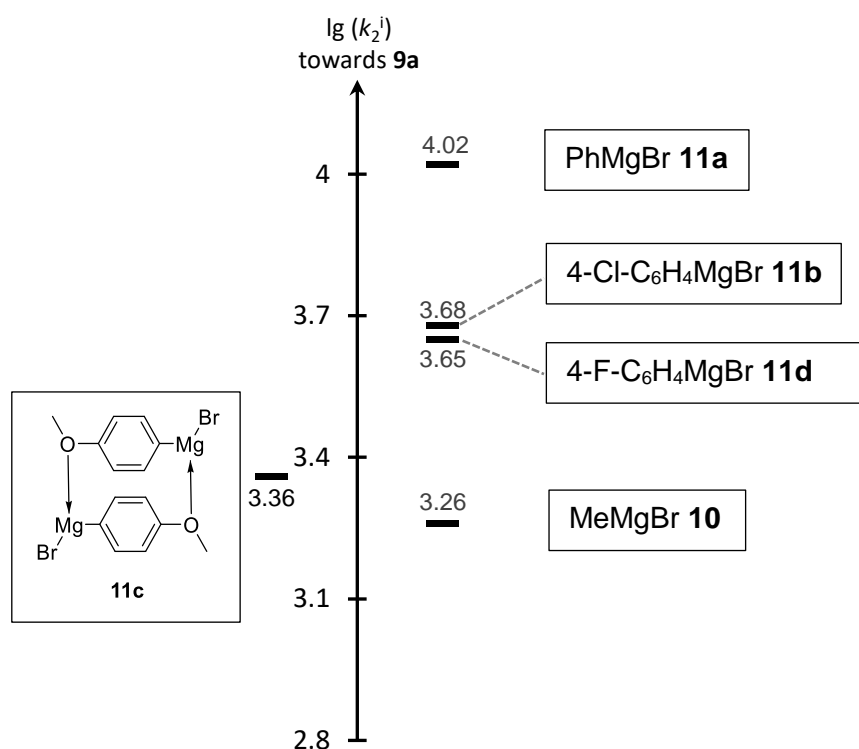


Figure 4.11. Reactivity comparison of studied Grignard reagents **10-11** in terms of logarithms of the second-order constants of the ionization of **9a** in diethyl ether at 20 °C.

Figure 4.12 demonstrates the comparison of rates of reaction between **9a**-derived carbocation (**9a-CC**) with Grignard reagents **10-11** and reference nucleophiles **23-25**. The very narrow range of reactivities of 4-substituted arylmagnesiumbromides **11** shows the same trend that was observed before for ionization reactions (Figure 4.11). However, in terms of nucleophilic reactivity MeMgBr (**10**) differs from the PhMgBr (**11a**) only by a factor of 1.3. This small difference indicates, from one side, the influence of the Schlenk equilibrium and presence of more nucleophilic R₂Mg species for phenylmagnesium bromide that leads to increased values for reactivity of this Grignard reagent. From the other side, the strong C_{sp3}-Mg bond and solvation effects for MeMgBr (**10**) put its reactivity towards carbocations in the S_N1 reaction in the same range as enamines, highly reactive silyl enol ethers and highly stabilized carbanions.

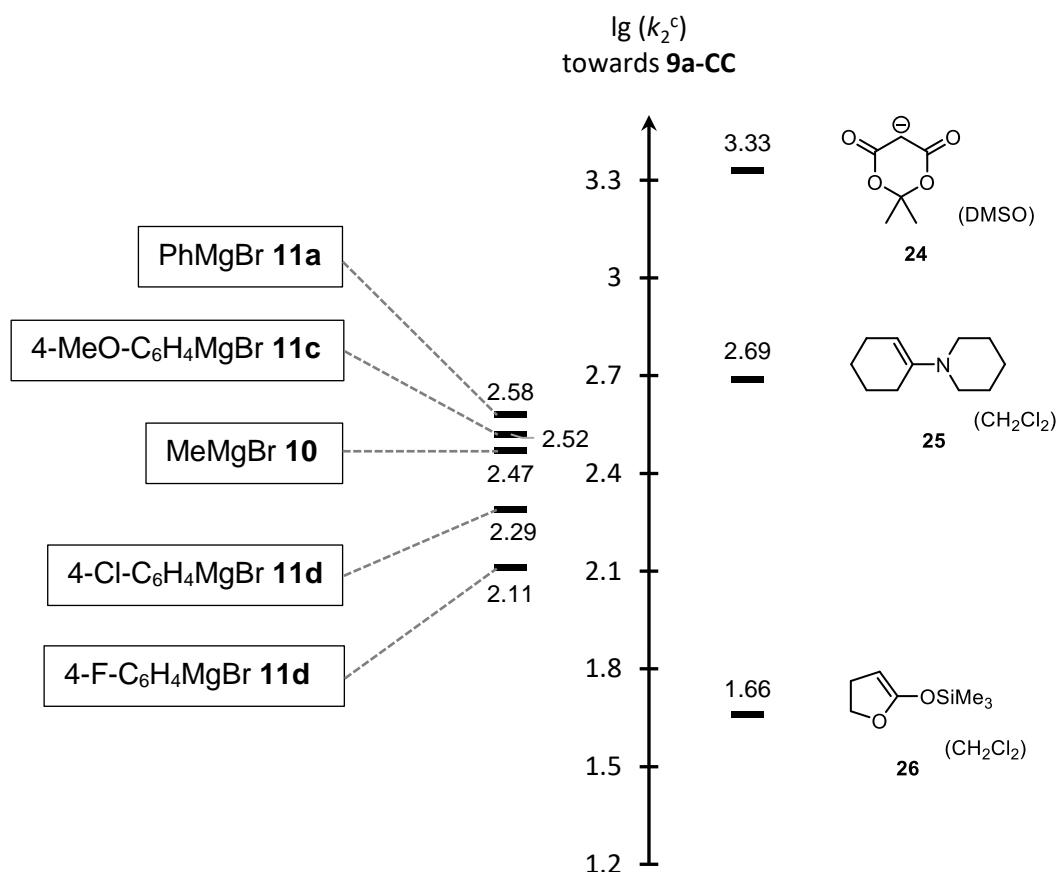


Figure 4.12. Reactivity comparison between studied Grignard reagents and several reference nucleophiles (from ref. [26a, 29]) towards **9a-CC** in diethyl ether and indicated solvent at 20 °C respectively.

4.3 Conclusion

Our study has demonstrated the formation of benzydrylium ions from the corresponding benzydryl phenyl ethers in the presence of the Grignard reagents with successive nucleophilic attack as it is described by the S_N1 mechanism. In addition, we have performed quantitative analysis of the obtained kinetic plots and calculated the rates of the involved reactions. Even with the mechanistic limitations and possible side reactions with different organomagnesium species present in the solution the obtained values provide the estimation of the reactivity of the Grignard reagents both as a Lewis acid and as a nucleophile.

Organomagnesium bromides in diethyl ether have shown the ability to shift the coordination equilibrium and substitute the solvent molecules with the substrate (benzydryl phenyl ether) with following formation of the benzydrylium carbocation. The preliminary experiments showed significant increase of the reaction rates with addition of the $MgBr_2$. In contrast, with the stronger solvating THF or weaker Lewis acidic organomagnesium chlorides the intermediate carbocation is not observed, which may indicate a different mechanism for the nucleophilic displacement of a phenoxy group.

The influence of the Schlenk equilibrium as well as solvent coordination on the course of reaction is still an open question. Significant deviations from the simple consecutive reversible reaction model were found in many reactions indicating the necessity to include these factors into the study.

4.4 Experimental Section

4.4.1 General

All reactions were performed in carefully dried Schlenk glassware in an atmosphere of dry argon. The reactions were not optimized for high yields.

NMR spectra were recorded on Varian NMR instruments (300, 400 and 600 MHz). Chemical shifts are expressed in ppm and refer to CDCl₃ (δ_{H} : 7.26, δ_{C} : 77.16). MS and HRMS were performed on a Finnigan MAT 95 instrument (EI).

Solvents. For the kinetic experiments, *p.a.* grade diethyl ether was dried for 24h with CaCl₂ and distilled over Na/benzophenone in atmosphere of dry N₂ before use. CH₃CN (Sigma-Aldrich, 99.8%, extra dry). CH₂Cl₂ (technical grade) and DMSO (Sigma-Aldrich, 99.8%, anhydrous) were used as received.

Chemicals. Sodium phenoxide **16a** (ABCR, 95%, anhydrous) was used as received. Potassium 1,3-di-*tert*-butylphenolate **16c**, potassium 4-cyanophenolate **16b** and benzhydrylium tetrafluoroborates were prepared by Nathalie Hampel. MgBr₂ was prepared from Mg (Alfa, 99.98%) and freshly distilled 1,2-dibromoethane.

Grignard Reagents. Commercially available phenylmagnesium bromide **11a** (3 M in Et₂O), methylmagnesium bromide **10** (3 M in Et₂O), 4-fluorophenylmagnesium bromide **11d** (2 M in Et₂O), isopropylmagnesium chloride **14** (2 M in Et₂O), 2-mesitylmagnesium bromide **12** (1 M in Et₂O) were purchased from Sigma-Aldrich and used as received. Isopropylmagnesium bromide **13**,^[30] benzylmagnesium bromide **15**,^[31] 4-methoxyphenylmagnesium bromide **11c**^[32] and a control sample of the phenylmagnesium bromide **11a**^[33] were prepared from corresponding freshly distilled bromides and Mg (Alfa, 99.98%) in diethyl ether by the described procedures. 4-Chlorophenyl magnesium bromide **11c** was generously gifted by Dr. Ilya Makarov.

All used Grignard reagents were titrated to iodine or salicylaldehyde phenylhydrazone^[34] in THF at 20 °C. The final concentrations were calculated as an average result of at least three

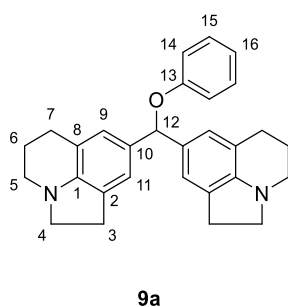
titration experiments. All kinetic investigations were performed within 1-2 days after the final concentration of the Grignard reagent was established.

Kinetic evaluation. All kinetic data was analyzed by a fit to two separate single-exponential functions (see Figure 3). In addition, the “evolutionary programming” optimization method implemented in the COPASI software was used to calculate the rate constants k_1^i , k_{-1}^i and k_1^c (Scheme 10). For this procedure the experimentally measured time-dependent absorption curves were converted to concentration vs time curves using the ε parameters listed in Table 4. A set of equations that describes a simple S_N1 reaction (Scheme 16) was used as input for the COPASI software. The “evolutionary programming” method then searches for a global minimum of the sum of squares of residuals ssq of the adjustable variables (rate constants k_1^i , k_{-1}^i and k_1^c), the experimental kinetic curves, and the initial concentrations of the involved species. The smaller ssq , the better the fit. Due to complications in the reaction mechanism and deviations from the consecutive system, for some experiments fitting was performed to match the maximum of the concentration of the intermediate carbocation to estimate the values of the rate constants.

4.4.2 General procedure for the synthesis of substrates 9

The solution of the corresponding benzhydrylium tetrafluoroborate (1 eq.) in DMSO (5 ml) was added dropwise to the suspension of sodium phenoxide in DMSO (5 ml) at ambient temperature. Upon fading of the color of the cation (typically <10 min.) the reaction mixture was poured into ice-cold water (100 ml) with 2 M aqueous solution NH_3 (20 ml). The resulting precipitate was filtered, dried under high vacuum for 12 h and stored in the glovebox.

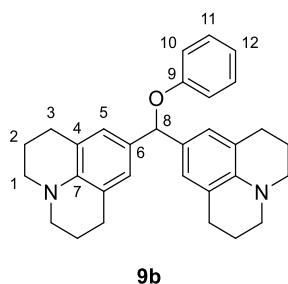
8,8'-(Phenoxymethylene)bis(1,2,5,6-tetrahydro-4H-pyrrolo[3,2,1-ij]quinoline) (9a)



Following the general procedure, starting from $(\text{Iil})_2\text{CH}^+\text{BF}_4^-$ (400 mg, 0.96 mmol, 1 eq.) and sodium phenoxide **16a** (176 mg, 1.44 mmol, 1.5 eq.), **9a** was obtained in 38% (155 mg) yield as light grey powder after recrystallization from Et_2O -pentane mixture.

^1H NMR (599 MHz, CDCl_3): δ = 2.06 (qd, J = 6.5 Hz, 4.4 Hz, 4H, H-6), 2.65 (td, J = 6.6 Hz, 3.5 Hz, 4H, H-7), 2.87 (td, J = 7.6 Hz, 2.6 Hz, 4H, H-3), 2.93 – 2.98 (m, 4H, H-5), 3.23 (t, J = 7.9 Hz, 4H, H-4), 5.97 (s, 1H, H-12), 6.82 – 6.84 (m, 2H, H-9), 6.85 – 6.88 (m, 1H, H-16), 6.94 – 6.97 (m, 4H, H-11, H-14), 7.19 (dd, J = 8.8, 7.3, 1H, H-15).

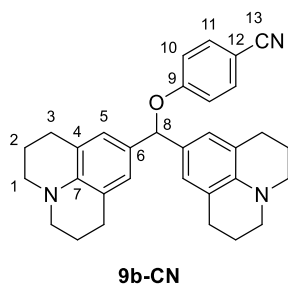
^{13}C NMR (151 MHz, CDCl_3): δ = 23.4 (C-6), 24.1 (C-7), 28.9 (C-3), 47.5 (C-5), 55.4 (C-4), 82.9 (C-12), 116.3 (C-14), 119.2 (C-8), 120.4 (C-16), 121.0 (C-11), 125.4 (C-9), 129.0 (C-2), 129.3 (C-15), 132.5 (C-10), 149.6 (C-1), 159.0 (C-13).

9,9'-(Phenoxymethylene)bis(2,3,6,7-tetrahydro-1H,5H-pyrido[3,2,1-ij]quinoline) (**9b**)

Following the general procedure, starting from $(\text{jul})_2\text{CH}^+\text{BF}_4^-$ (302 mg, 0.68 mmol, 1 eq.) and sodium phenoxide **16a** (118 mg, 1.02 mmol, 1.5 eq.), **9b** was obtained in 39% (120 mg) yield as light blue powder after recrystallization from Et_2O -pentane mixture.

^1H NMR (599 MHz, CDCl_3) δ = 1.91 – 1.98 (m, 4H, H-2), 2.72 (td, J = 6.3 Hz, 3.6 Hz, 4H, H-3), 3.09 – 3.12 (m, 4H, H-1), 5.87 (s, 1H, H-8), 6.78 (s, 4H, H-5), 6.86 (t, J = 7.3 Hz, 1H, H-12), 6.96 (dd, J = 8.8 Hz, 1.0 Hz, 2H, H-10), 7.20 (dd, J = 8.7 Hz, 7.3 Hz, 2H, H-11).

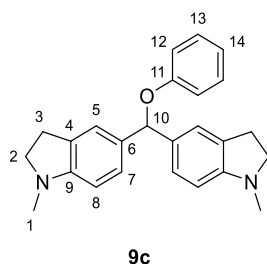
^{13}C NMR (151 MHz, CDCl_3) δ = 22.3 (C-2), 27.9 (C-3), 50.2 (C-1), 82.3 (C-8), 116.3 (C-10), 120.2 (C-12), 121.5 (C-4), 125.8 (C-5), 129.1 (C-6), 129.2 (C-11), 142.4 (C-7), 159.1 (C-9).

4-(Bis(2,3,6,7-tetrahydro-1H,5H-pyrido[3,2,1-ij]quinolin-9-yl)methoxy)benzonitrile (**9b-CN**)

Following the general procedure, starting from $(\text{jul})_2\text{CH}^+\text{BF}_4^-$ (151 mg, 0.34 mmol, 1 eq.) and potassium 4-cyanophenolate **16b** (59 mg, 0.37 mmol, 1.1 eq.), **9b-CN** was obtained in 51% (83 mg) yield as dark blue powder after recrystallization from Et_2O .

^1H NMR (599 MHz, CDCl_3) δ = 1.90 – 1.99 (m, 4H, H-2), 2.67 – 2.75 (m, 4H, H-3), 3.08 – 3.15 (m, 4H, H-1), 5.89 (s, 1H, H-8), 6.73 (s, 4H, H-5), 6.98 (d, J = 8.7 Hz, 2H, H-10), 7.48 (d, J = 8.6 Hz, 2H, H-11).

^{13}C NMR (151 MHz, CDCl_3) δ = 22.1 (C-2), 27.9 (C-3), 50.1 (C-1), 83.0 (C-8), 103.2 (C-12), 116.9 (C-10), 119.7 (C-13), 121.5 (C-4), 125.7 (C-5), 127.4 (C-6), 133.9 (C-11), 142.7 (C-7), 162.4 (C-9).

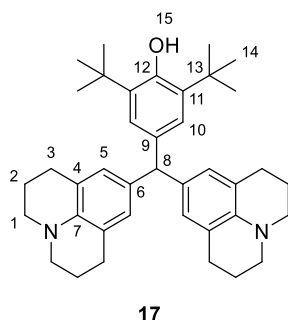
5,5'-(Phenoxymethylene)bis(1-methylindoline) (**9c**)

Following the general procedure, starting from $(\text{ind})_2\text{CH}^+\text{BF}_4^-$ (251 mg, 0.69 mmol, 1 eq.) and sodium phenoxide **16a** (92 mg, 0.76 mmol, 1.1 eq.), **9c** was obtained in 42% (107 mg) yield as light blue powder after recrystallization from Et_2O . Contaminated with <20% of C-attack product.

^1H NMR (599 MHz, CDCl_3) δ = 2.73 (s, 6H, H-1) 2.88 – 2.93 (m, 4H, H-3), 3.24 – 3.31 (m, 4H, H-2), 6.04 (s, 1H, H-10), 6.39 – 6.44 (m, 2H, H-8), 6.86 (tt, J = 7.5 Hz, 1.1 Hz, 1H, H-14), 6.93 – 6.97 (m, 2H, H-12), 7.06 – 7.10 (m, 4H, H-5, H-7), 7.16 – 7.23 (m, 2H, H-13).

^{13}C NMR (151 MHz, CDCl_3) δ = 28.7 (C-3), 36.2 (C-1), 56.2 (C-2), 82.1 (C-10), 106.6 (C-8), 116.1 (C-12), 120.3 (C-14), 123.2 (C-5), 126.4 (C-7), 129.1 (C-13), 130.6 (C-4), 131.2 (C-6), 152.8 (C-9), 158.7 (C-11).

9,9'-((3,5-Di-*tert*-butylphenoxy)methylene)bis(2,3,6,7-tetrahydro-1H,5H-pyrido[3,2,1-*ij*]quinoline) (17)



Following the general procedure, starting from $(\text{jul})_2\text{CH}^+\text{BF}_4^-$ (151 mg, 0.34 mmol, 1 eq.) and potassium 1,3-di-*tert*-butylphenolate **16c** (91 mg, 0.37 mmol, 1.1 eq.), **17** was obtained in 92% (176 mg) yield as light pink powder after recrystallization from Et_2O .

^1H NMR (599 MHz, CDCl_3) δ = 1.38 (s, 18H, H-14), 1.95 (p, J = 6.4 Hz, 8H, H-2), 2.68 (t, J = 6.5 Hz, 8H, H-3), 3.05 – 3.11 (m, 8H, H-1), 4.96-5.00 (m, 2H, H-8, H-15), 6.55 (s, 4H, H-5), 6.98 (s, 2H, H-10).

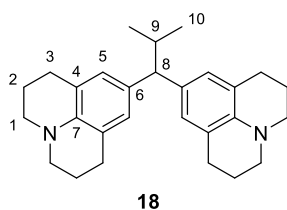
^{13}C NMR (151 MHz, CDCl_3) δ = 22.5 (C-2), 27.8 (C-3), 30.6 (C-14), 34.5 (C-13), 50.4 (C-1), 55.8 (C-8), 121.3 (C-4), 126.1 (C-10), 127.9 (C-5), 133.5 (C-6), 135.1 (C-11), 135.7 (C-9), 141.0 (C-7), 151.8 (C-12).

4.4.3 Product studies

Reaction of substrate **9b** with isopropylmagnesium chloride **14**

A suspension of **9b** (50 mg, 0.11 mmol, 1 eq.) in Et₂O (5 ml) was treated with a solution of isopropylmagnesium chloride **13** (1.95 M in Et₂O, 0.2 ml, 0.39 mmol, 3.5 eq.) at ambient temperature. The resulting mixture was stirred for 1 hour, treated with water (50 ml) and extracted with CH₂Cl₂ (3 × 20 ml). The combined organic phase was washed with brine (20 ml) and dried over MgSO₄. The crude material was purified with column chromatography (silica gel, 1/10 mixture of Et₂O/pentane) to get 28 mg (64%) of **18** as white solid.

9,9'-(2-Methylpropane-1,1-diyl)bis(2,3,6,7-tetrahydro-1H,5H-pyrido[3,2,1-ij]quinoline) (**18**)



¹H NMR (599 MHz, CDCl₃) δ = 0.84 (d, J = 6.5 Hz, 6H, H-10), 1.90 – 1.98 (m, 8H, H-2), 2.27 (ddt, J = 13.0 Hz, 10.8 Hz, 6.5 Hz, 1H, H-9), 2.71 (t, J = 6.6 Hz, 8H, H-3), 2.95 (d, J = 10.6 Hz, 1H, H-8), 3.01 – 3.07 (m, 8H, H-1), 6.63 (s, 4H, H-5).

¹³C NMR (151 MHz, CDCl₃) δ = 22.4 (C-10), 22.5 (C-2), 27.8 (C-3), 32.0 (C-9), 50.3 (C-3), 59.4 (C-8), 121.5 (C-4), 126.4 (C-5), 133.8 (C-6), 141.0 (C-7).

HR-MS (EI, pos.) m/z calcd. for C₂₈H₃₆N₂ [M]⁺⁺ 400.2873, found 400.2881.

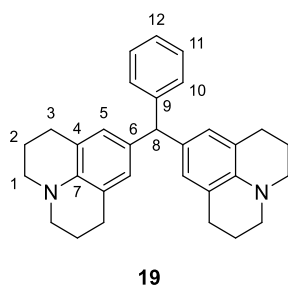
Reaction of substrate **9b** with isopropylmagnesium bromide **13**

Reaction was performed in analogy to **18** from **9b** (50 mg, 0.11 mmol, 1 eq.) and solution of *i*PrMgBr **13** (1.02 M in Et₂O, 0.33ml, 0.33 mmol, 3 eq.). **19** was obtained as white solid in 47% (21 mg) yield.

Analytical data is in agreement with that from **18**.

Reaction of substrate 9b with phenylmagnesium bromide 11a

The reaction was performed in analogy to **18** from **9b** (52 mg, 0.12 mmol, 1 eq.) and a solution of PhMgBr **11a** (2.87 M in Et₂O, 0.14 ml, 0.40 mmol, 3.5 eq.). **19** was obtained after 3 hours as white solid in 30% (16 mg) yield.

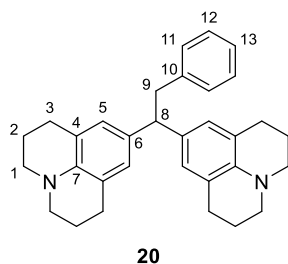
9,9'-(Phenylmethylene)bis(2,3,6,7-tetrahydro-1H,5H-pyrido[3,2,1-ij]quinoline) (19)

¹H NMR (599 MHz, CDCl₃) δ = 1.95 (dt, J = 12.1 Hz, 6.5 Hz, 8H, H-2), 2.68 (t, J = 6.6 Hz, 8H, H-3), 3.07 – 3.12 (m, 8H, H-1), 5.15 (s, 1H, H-8), 6.54 (s, 4H, H-5), 7.15 – 7.18 (m, 3H, H-10, H-12), 7.24 – 7.27 (m, 2H, H-11).

¹³C NMR (151 MHz, CDCl₃) δ = 22.4 (C-2), 27.8 (C-3), 50.3 (C-1), 55.6 (C-8), 121.5 (C-4), 125.7 (C-12), 128.0 (C-5), 128.1 (C-11), 129.6 (C-10), 132.4 (C-6), 141.2 (C-7), 145.9 (C-9).

Reaction of substrate 9b with benzylmagnesium bromide 15

Reaction was performed in analogy to **18** from **9b** (50 mg, 0.11 mmol, 1 eq.) and solution of BnMgBr (1.31 M in Et₂O, 0.25 ml, 0.33 mmol, 3 eq.). **20** was obtained as white solid in 55% (27 mg) yield.

9,9'-(2-Phenylethane-1,1-diyl)bis(2,3,6,7-tetrahydro-1H,5H-pyrido[3,2,1-ij]quinoline) (20)

¹H NMR (599 MHz, CDCl₃) δ = 1.93 – 1.98 (m, 8H, H-2), 2.70 (t, J = 6.6 Hz, 8H, H-3), 3.05 – 3.09 (m, 8H, H-1), 3.22 (d, J = 7.6 Hz, 2H, H-9), 3.83 (t, J = 7.6 Hz, 1H, H-8), 6.62 (s, 4H, H-5), 7.02 – 7.06 (m, 2H, H-11), 7.11 (t, J = 7.3 Hz, 1H, H-13), 7.15 – 7.21 (m, 2H, H-12).

¹³C NMR (151 MHz, CDCl₃) δ = 22.4 (C-2), 27.8 (C-3), 42.8 (C-9), 50.3 (C-1), 51.6 (C-8), 121.6 (C-4), 125.5 (C-13), 126.5 (C-5), 127.9 (C-12), 129.3 (C-11), 133.3 (C-6), 141.2 (C-7), 141.7 (C-10).

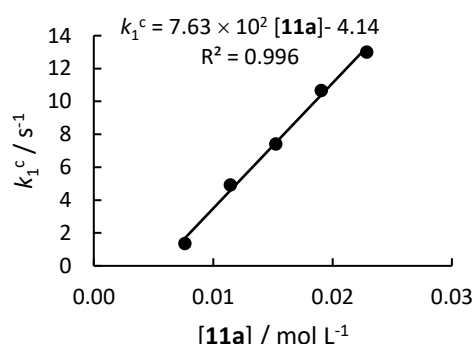
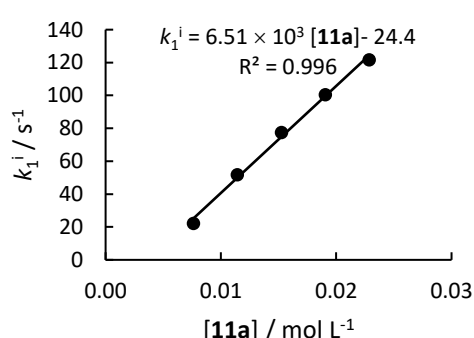
HR-MS (EI, pos.) m/z calcd. for C₃₂H₃₆N₂ [M]⁺⁺ 448.2873, found 448.2866.

4.4.4 Kinetic investigations

Reactions of phenylmagnesium bromide 11a

Table 4.4. Kinetics of the reaction of 9c with 11a in Et₂O (stopped flow, 20 °C at 620 nm) derived from separate single-exponential analysis.

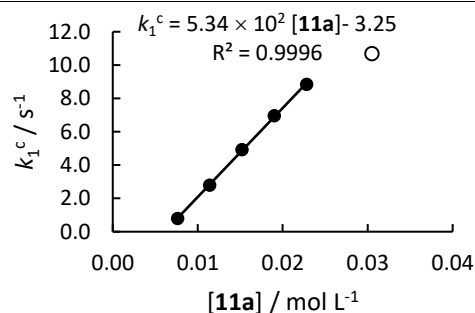
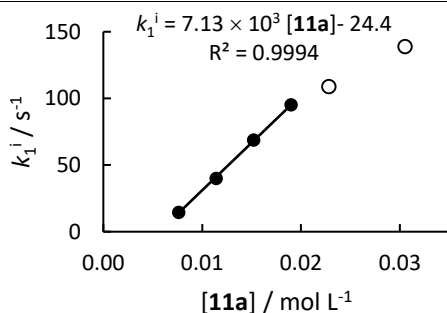
Entry	[11a] / mol L ⁻¹	[9c] / mol L ⁻¹	[11a] / [9c]	k_1^i / s ⁻¹	k_1^c / s ⁻¹
1	7.62×10^{-3}	2.83×10^{-5}	269	2.22×10^1	1.36
2	1.14×10^{-2}	2.83×10^{-5}	403	5.17×10^1	4.92
3	1.52×10^{-2}	2.83×10^{-5}	537	7.75×10^1	7.42
4	1.90×10^{-2}	2.83×10^{-5}	672	1.01×10^2	1.07×10^1
5	2.28×10^{-2}	2.83×10^{-5}	806	1.22×10^2	1.30×10^1



$$k_2^i = 6.51 \times 10^3 \text{ L mol}^{-1} \text{ s}^{-1}; k_2^c = 7.63 \times 10^2 \text{ L mol}^{-1} \text{ s}^{-1}$$

Table 4.5. Kinetics of the reaction of 9c with 11a in Et₂O (stopped flow, 20 °C at 620 nm) derived from COPASI analysis.

Entry	[11a] / mol L ⁻¹	[9c] / mol L ⁻¹	[9c] / [11a]	k_1^i / s ⁻¹	k_{-1}^i / s ⁻¹	k_1^c / s ⁻¹	ssq
1	7.62×10^{-3}	2.83×10^{-5}	269	1.46×10^1	-[b]	7.96×10^{-1}	1.03×10^{-7}
2	1.14×10^{-2}	2.83×10^{-5}	403	3.99×10^1	-[b]	2.79	1.89×10^{-7}
3	1.52×10^{-2}	2.83×10^{-5}	537	6.88×10^1	6.67×10^{-4}	4.92	7.59×10^{-8}
4	1.90×10^{-2}	2.83×10^{-5}	672	9.51×10^1	6.39×10^{-4}	6.97	1.03×10^{-7}
5	2.28×10^{-2}	2.83×10^{-5}	806	1.09×10^2 [a]	7.57×10^{-4}	8.84	7.05×10^{-8}
6	3.05×10^{-2}	2.83×10^{-5}	1075	1.39×10^2 [a]	-[b]	1.07×10^1 [a]	1.67×10^{-7}

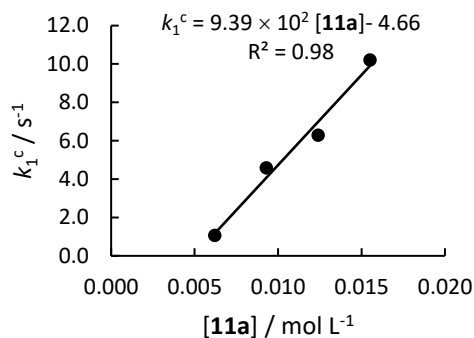
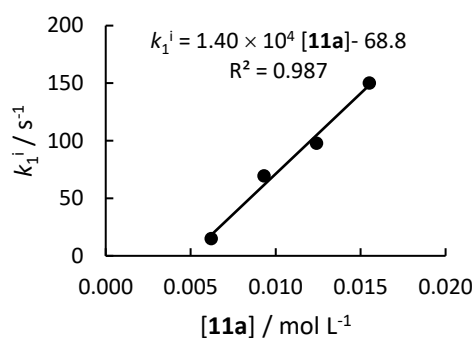


$$k_2^i = 7.13 \times 10^3 \text{ L mol}^{-1} \text{ s}^{-1}; k_2^c = 5.34 \times 10^2 \text{ L mol}^{-1} \text{ s}^{-1}; k_{-1}^i = 6.89 \times 10^{-4} \text{ s}^{-1}$$

[a] high deviations due to oligomers formation, not included in the correlation, empty circles on the graph; [b] standard deviations exceed 10%

Table 4.6. Kinetics of the reaction of 9b with 11a in Et₂O (stopped flow, 20 °C at 635 nm) derived from separate single-exponential analysis.

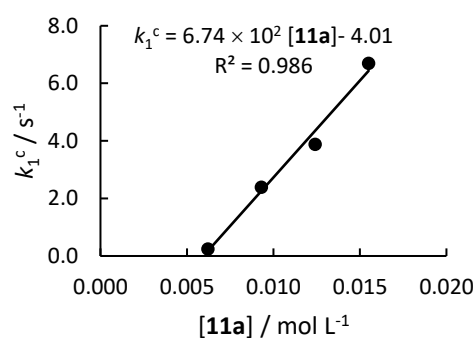
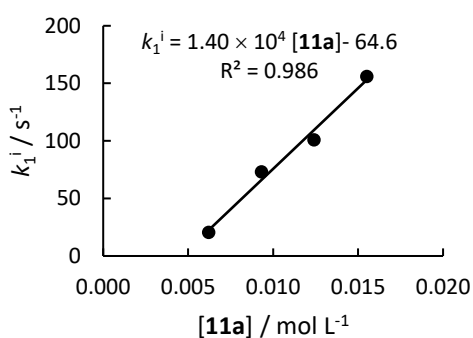
Entry	[11a] / mol L ⁻¹	[9b] / mol L ⁻¹	[11a] / [9b]	k_1^i / s ⁻¹	k_1^c / s ⁻¹
1	6.20×10^{-3}	1.40×10^{-5}	442	1.49×10^1	1.06
2	9.30×10^{-3}	1.40×10^{-5}	663	6.94×10^1	4.58
3	1.24×10^{-2}	1.40×10^{-5}	883	9.79×10^1	6.28
4	1.55×10^{-2}	1.40×10^{-5}	1104	1.50×10^2	1.02×10^1



$$k_2^i = 1.40 \times 10^4 \text{ L mol}^{-1} \text{ s}^{-1}; k_2^c = 9.39 \times 10^2 \text{ L mol}^{-1} \text{ s}^{-1}$$

Table 4.7. Kinetics of the reaction of 9b with 11a in Et₂O (stopped flow, 20 °C at 635 nm) derived from COPASI analysis.

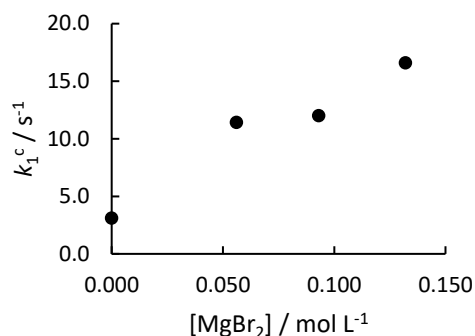
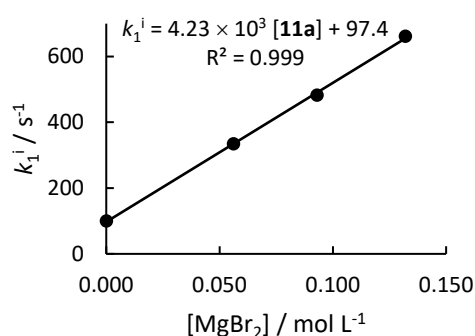
Entry	[11a] / mol L ⁻¹	[9b] / mol L ⁻¹	[11a] / [9b]	k_1^i / s ⁻¹	k_{-1}^i / s ⁻¹	k_1^c / s ⁻¹	ssq
1	6.20×10^{-3}	1.40×10^{-5}	442	2.04×10^1	8.50×10^{-5}	2.37×10^{-1}	4.53×10^{-7}
2	9.30×10^{-3}	1.40×10^{-5}	663	7.30×10^1	1.86×10^{-4}	2.39	1.03×10^{-7}
3	1.24×10^{-2}	1.40×10^{-5}	883	1.01×10^2	1.98×10^{-4}	3.88	8.47×10^{-8}
4	1.55×10^{-2}	1.40×10^{-5}	1104	1.56×10^2	2.90×10^{-4}	6.70	1.54×10^{-7}



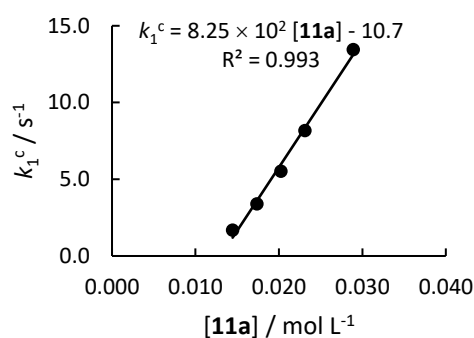
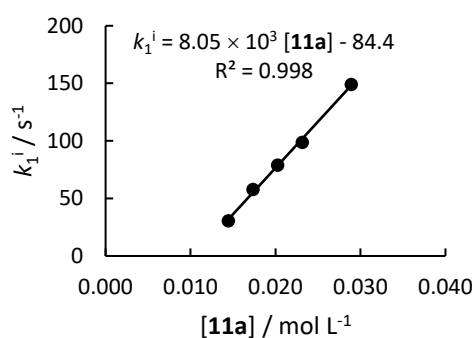
$$k_2^i = 1.40 \times 10^4 \text{ L mol}^{-1} \text{ s}^{-1}; k_2^c = 6.74 \times 10^2 \text{ L mol}^{-1} \text{ s}^{-1}; k_{-1}^i = 1.90 \times 10^{-4} \text{ s}^{-1}$$

Table 4.8. Kinetics of the reaction of 9b ($1.40 \times 10^{-5} \text{ mol L}^{-1}$) with 11a ($1.55 \times 10^{-2} \text{ mol L}^{-1}$) in Et₂O (stopped flow, 20 °C at 635 nm) in presence of MgBr₂ derived from COPASI analysis.

Entry	[MgBr ₂] / mol L ⁻¹	[MgBr ₂] / [11a]	k_1^i / s ⁻¹	k_1^i / s ⁻¹	k_1^c / s ⁻¹	ssq
1	0	0	1.00×10^2	3.46×10^{-4}	3.10	4.53×10^{-7}
2	5.61×10^{-2}	4	3.34×10^2	3.59×10^{-3}	1.14×10^1	1.03×10^{-7}
3	9.30×10^{-2}	6	4.82×10^2	3.28×10^{-3}	1.20×10^1	8.47×10^{-8}
4	1.32×10^{-2}	9	6.61×10^2	-[a]	1.66×10^1	1.54×10^{-7}

Table 4.9. Kinetics of the reaction of 9a with 11a in Et₂O (stopped flow, 20 °C at 630 nm) derived from separate single-exponential analysis.

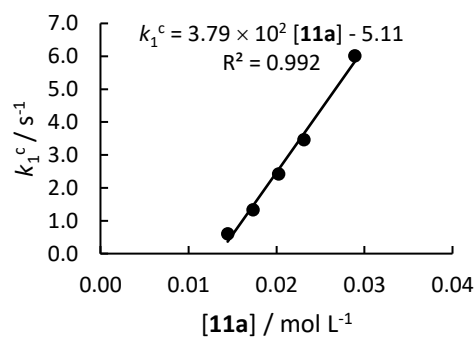
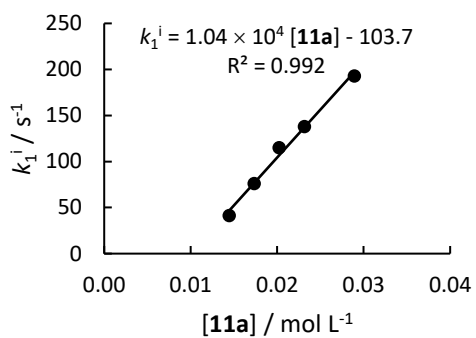
Entry	[11a] / mol L ⁻¹	[9a] / mol L ⁻¹	[11a] / [9a]	k_1^i / s ⁻¹	k_1^c / s ⁻¹
1	1.45×10^{-2}	1.19×10^{-5}	1212	3.05×10^1	1.69
2	1.73×10^{-2}	1.19×10^{-5}	1454	5.78×10^1	3.40
3	2.02×10^{-2}	1.19×10^{-5}	1696	7.89×10^1	5.51
4	2.31×10^{-2}	1.19×10^{-5}	1938	9.86×10^1	8.17
5	2.89×10^{-2}	1.19×10^{-5}	2423	1.49×10^2	1.34×10^1



$$k_2^i = 8.05 \times 10^3 \text{ L mol}^{-1} \text{ s}^{-1}; k_2^c = 8.25 \times 10^2 \text{ L mol}^{-1} \text{ s}^{-1}$$

Table 4.10. Kinetics of the reaction of 9a with 11a in Et₂O (stopped flow, 20 °C at 630 nm) derived from COPASI analysis.

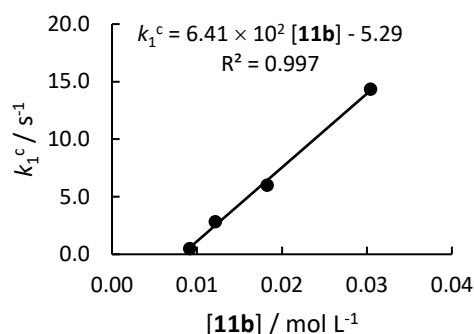
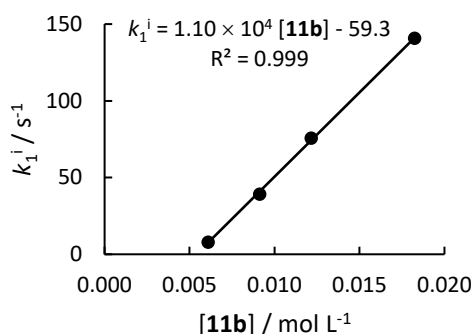
Entry	[11a] / mol L ⁻¹	[9a] / mol L ⁻¹	[11a] / [9a]	k_1^i / s ⁻¹	k_{-1}^i / s ⁻¹	k_1^c / s ⁻¹	ssq
1	1.45×10^{-2}	1.19×10^{-5}	1212	4.15×10^1	6.86×10^{-3}	6.06×10^{-1}	2.43×10^{-7}
2	1.73×10^{-2}	1.19×10^{-5}	1454	7.63×10^1	1.67×10^{-2}	1.34	1.89×10^{-7}
3	2.02×10^{-2}	1.19×10^{-5}	1696	1.15×10^2	9.44×10^{-3}	2.43	1.40×10^{-7}
4	2.31×10^{-2}	1.19×10^{-5}	1938	1.38×10^2	6.16×10^{-3}	3.47	9.92×10^{-8}
5	2.89×10^{-2}	1.19×10^{-5}	2423	1.93×10^2	1.01×10^{-2}	6.02	6.75×10^{-8}



$$k_2^i = 1.04 \times 10^4 \text{ L mol}^{-1} \text{ s}^{-1}; k_2^c = 3.79 \times 10^2 \text{ L mol}^{-1} \text{ s}^{-1}; k_{-1}^i = 9.85 \times 10^{-3} \text{ s}^{-1}$$

Reactions of 4-chlorophenylmagnesium bromide **11b**Table 4.11. Kinetics of the reaction of **9b** with **11b** in Et₂O (stopped flow, 20 °C at 635 nm) derived from separate single-exponential analysis.

Entry	[11b] / mol L ⁻¹	[9b] / mol L ⁻¹	[9b] / [11b]	k_1^i / s ⁻¹	k_1^c / s ⁻¹
1	6.08×10^{-3}	3.11×10^{-5}	196	8.01	— ^[a]
2	9.12×10^{-3}	3.11×10^{-5}	293	3.92×10^1	5.12×10^{-1}
3	1.22×10^{-2}	3.11×10^{-5}	391	7.58×10^1	2.84
4	1.82×10^{-2}	3.11×10^{-5}	587	1.41×10^2	6.01
5	3.04×10^{-2}	3.11×10^{-5}	978	— ^[b]	1.43×10^1

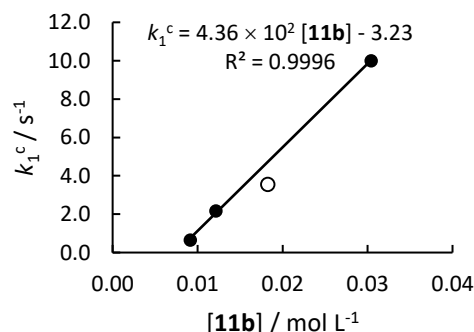
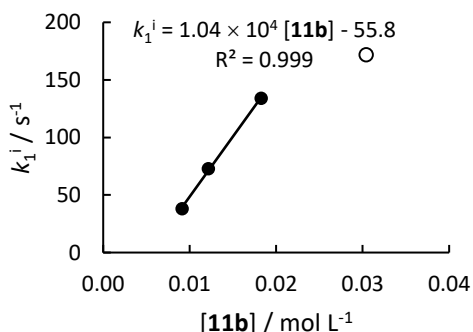


$$k_2^i = 1.10 \times 10^4 \text{ L mol}^{-1} \text{ s}^{-1}; k_2^c = 6.41 \times 10^2 \text{ L mol}^{-1} \text{ s}^{-1}$$

[a] rate constant too slow for analysis; [b] rate constant too big for analysis

Table 4.12. Kinetics of the reaction of **9b** with **11b** in Et₂O (stopped flow, 20 °C at 635 nm) derived from COPASI analysis.

Entry	[11b] / mol L ⁻¹	[9b] / mol L ⁻¹	[11b] / [9b]	k_1^i / s ⁻¹	k_{-1}^i / s ⁻¹	k_1^c / s ⁻¹	ssq
1	9.12×10^{-3}	3.11×10^{-5}	293	3.82×10^1	2.10×10^{-2}	6.55×10^{-1}	1.43×10^{-7}
2	1.22×10^{-2}	3.11×10^{-5}	391	7.29×10^1	3.84×10^{-2}	2.17	2.24×10^{-7}
3	1.82×10^{-2}	3.11×10^{-5}	587	1.34×10^2	6.83×10^{-3} ^[a]	3.56 ^[a]	4.40×10^{-8}
4	3.04×10^{-2}	3.11×10^{-5}	978	1.72×10^2 ^[a]	3.66×10^{-2}	1.00×10^1	3.08×10^{-7}

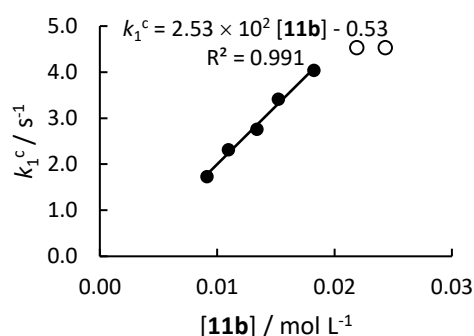
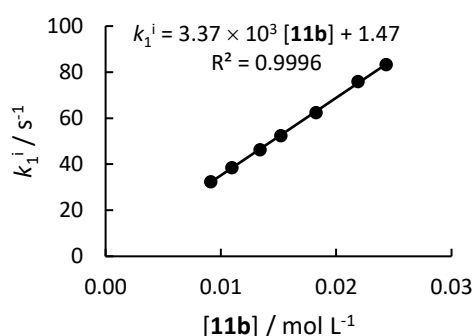


$$k_2^i = 1.04 \times 10^4 \text{ L mol}^{-1} \text{ s}^{-1}; k_2^c = 4.36 \times 10^2 \text{ L mol}^{-1} \text{ s}^{-1}; k_{-1}^i = 3.20 \times 10^{-2} \text{ s}^{-1}$$

[a] not used in the correlation, empty circle on the graph

Table 4.13. Kinetics of the reaction of 9a with 11b in Et₂O (stopped flow, 20 °C at 630 nm) derived from separate single-exponential analysis.

Entry	[11b] / mol L ⁻¹	[9a] / mol L ⁻¹	[11b] / [9a]	k_1^i / s ⁻¹	k_1^c / s ⁻¹
1	9.12×10^{-3}	2.78×10^{-5}	328	3.24×10^1	1.73
2	1.09×10^{-2}	2.78×10^{-5}	393	3.85×10^1	2.32
3	1.34×10^{-2}	2.78×10^{-5}	481	4.63×10^1	2.76
4	1.52×10^{-2}	2.78×10^{-5}	546	5.25×10^1	3.41
5	1.82×10^{-2}	2.78×10^{-5}	655	6.25×10^1	4.04
6	2.19×10^{-2}	2.78×10^{-5}	786	7.59×10^1	4.53 ^[a]
7	2.43×10^{-2}	2.78×10^{-5}	874	8.33×10^1	4.54 ^[a]

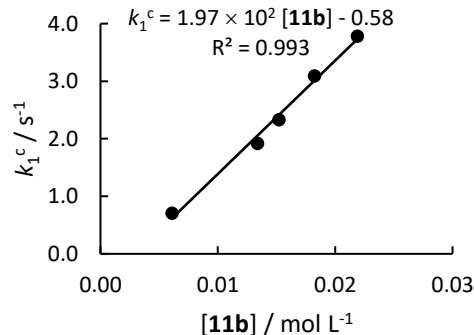
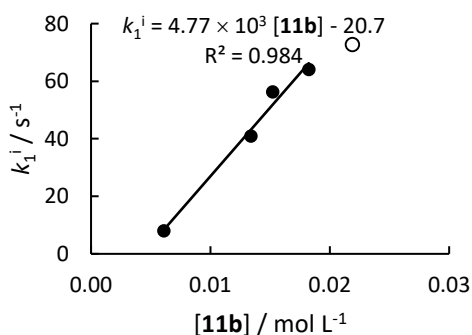


$$k_2^i = 3.37 \times 10^3 \text{ L mol}^{-1} \text{ s}^{-1}; k_2^c = 2.53 \times 10^2 \text{ L mol}^{-1} \text{ s}^{-1}$$

[a] high deviations due to oligomers formation, not included in the correlation, empty circles on the graph

Table 4.14. Kinetics of the reaction of 9a with 11b in Et₂O (stopped flow, 20 °C at 630 nm) derived from COPASI analysis.

Entry	[11b] / mol L ⁻¹	[9a] / mol L ⁻¹	[11b] / [9a]	k_1^i / s ⁻¹	k_{-1}^i / s ⁻¹	k_1^c / s ⁻¹	ssq
1	6.08×10^{-3}	2.78×10^{-5}	218	7.98	6.53	7.04×10^{-1}	1.92×10^{-7}
2	1.34×10^{-2}	2.78×10^{-5}	481	4.09×10^1	5.02	1.92	2.40×10^{-7}
3	1.52×10^{-2}	2.78×10^{-5}	546	5.63×10^1	1.24×10^{-1}	2.33	2.26×10^{-7}
4	1.82×10^{-2}	2.78×10^{-5}	655	6.41×10^1	4.92×10^{-2}	3.09	1.55×10^{-7}
5	2.19×10^{-2}	2.78×10^{-5}	786	7.27×10^1 ^[a]	1.31×10^{-1}	3.78	1.40×10^{-7}



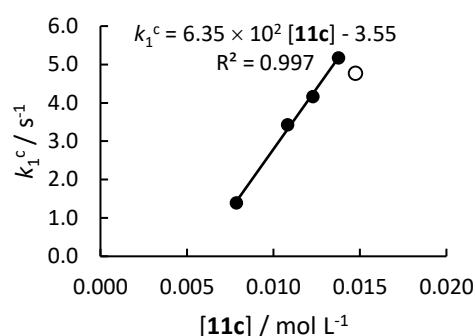
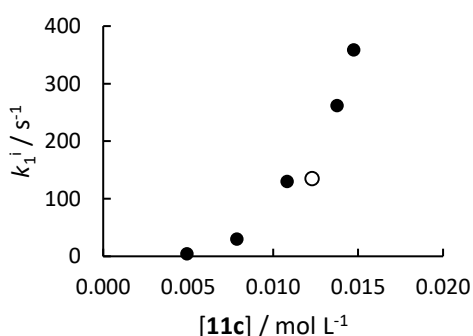
$$k_2^i = 4.77 \times 10^3 \text{ L mol}^{-1} \text{ s}^{-1}; k_2^c = 1.97 \times 10^2 \text{ L mol}^{-1} \text{ s}^{-1}; k_{-1}^i \text{ could not be identified due to high deviation values}$$

[a] not used in the correlation, empty circle on the graph

Reactions of 4-methoxyphenylmagnesium bromide

Table 4.15. Kinetics of the reaction of 9b with 11c in Et₂O (stopped flow, 20 °C at 635 nm) derived from COPASI analysis.

Entry	[11c] / mol L ⁻¹	[9b] / mol L ⁻¹	[11c] / [9b]	k_1^i / s ⁻¹	k_1^c / s ⁻¹	k_1^c / s ⁻¹	ssq
1	4.91×10^{-3}	2.35×10^{-5}	209	4.27	5.65×10^{-3}	–[b]	1.96×10^{-7}
2	7.86×10^{-3}	2.35×10^{-5}	334	3.01×10^1	5.59×10^{-2}	1.39	1.41×10^{-7}
3	1.08×10^{-2}	2.35×10^{-5}	459	1.30×10^2	2.55×10^{-1}	3.43	9.82×10^{-8}
4	1.23×10^{-2}	2.35×10^{-5}	522	$1.35 \times 10^{2[a]}$	4.36	4.16	9.66×10^{-8}
5	1.38×10^{-2}	2.35×10^{-5}	584	2.62×10^2	1.13×10^1	5.17	6.10×10^{-8}
6	1.47×10^{-2}	2.35×10^{-5}	626	3.59×10^2	2.02	$4.77^{[a]}$	1.03×10^{-7}

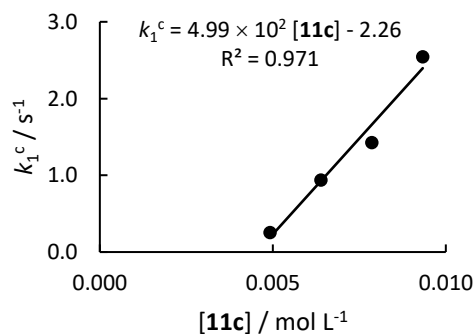
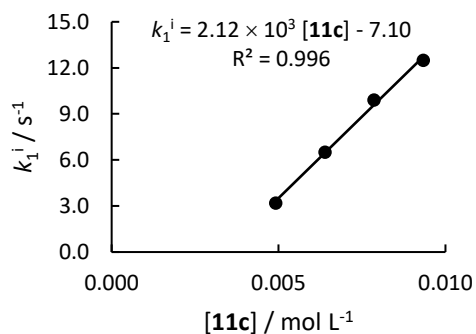


k_2^i = not identified; k_2^c = 6.35×10^2 L mol⁻¹ s⁻¹; k_1^i could not be identified due to high deviation values

[a] not used in the correlation, empty circle on the graph; [b] rate constant too low for analysis

Table 16. Kinetics of the reaction of 9a with 11c in Et₂O (stopped flow, 20 °C at 630 nm) derived from separate single-exponential analysis.

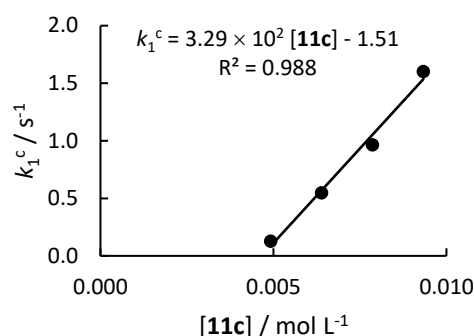
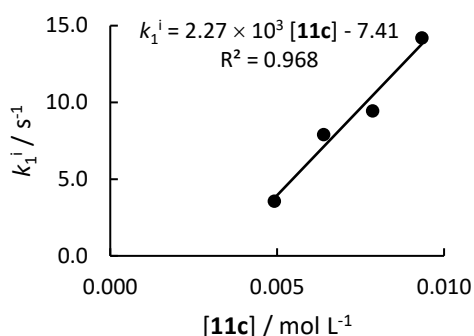
Entry	[11c] / mol L ⁻¹	[9a] / mol L ⁻¹	[11c] / [9a]	k_1^i / s ⁻¹	k_1^c / s ⁻¹
1	4.91×10^{-3}	2.32×10^{-5}	212	3.19	2.56×10^{-1}
2	6.39×10^{-3}	2.32×10^{-5}	275	6.50	9.38×10^{-1}
3	7.86×10^{-3}	2.32×10^{-5}	339	9.91	1.43
4	9.33×10^{-3}	2.32×10^{-5}	402	1.25×10^1	2.55



k_2^i = 2.12×10^3 L mol⁻¹ s⁻¹; k_2^c = 4.99×10^2 L mol⁻¹ s⁻¹

Table 4.17. Kinetics of the reaction of 9a with 11c in Et₂O (stopped flow, 20 °C at 630 nm) derived from COPASI analysis.

Entry	[11c] / mol L ⁻¹	[9a] / mol L ⁻¹	[11c] / [9a]	k_1^i / s ⁻¹	k_{-1}^i / s ⁻¹	k_1^c / s ⁻¹	ssq
1	4.91×10^{-3}	2.32×10^{-5}	212	3.55	2.45×10^{-3}	1.25×10^{-1}	2.40×10^{-7}
2	6.39×10^{-3}	2.32×10^{-5}	275	7.90	9.77×10^{-6}	5.47×10^{-1}	1.71×10^{-7}
3	7.86×10^{-3}	2.32×10^{-5}	339	9.44	2.15×10^{-5}	9.64×10^{-1}	1.50×10^{-7}
4	9.33×10^{-3}	2.32×10^{-5}	402	1.42×10^1	1.00×10^{-6}	1.60	1.57×10^{-7}

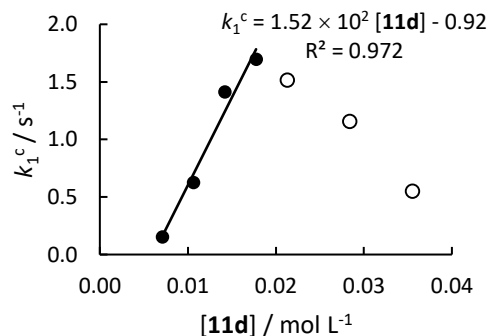
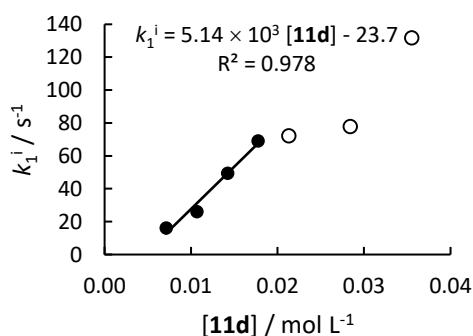


$k_2^i = 2.27 \times 10^3 \text{ L mol}^{-1} \text{ s}^{-1}$; $k_2^c = 3.29 \times 10^2 \text{ L mol}^{-1} \text{ s}^{-1}$; k_{-1}^i could not be identified due to high deviation values

Reactions of 4-fluorophenylmagnesium bromide

Table 4.18. Kinetics of the reaction of 9a with 11d in Et₂O (stopped flow, 20 °C at 630 nm) derived from separate single-exponential analysis.

Entry	[11d] / mol L ⁻¹	[9a] / mol L ⁻¹	[11d] / [9a]	k_1^i / s ⁻¹	k_1^c / s ⁻¹
1	7.10×10^{-3}	3.76×10^{-5}	189	1.61×10^1	1.54×10^{-1}
2	1.07×10^{-2}	3.76×10^{-5}	283	2.61×10^1	6.25×10^{-1}
3	1.42×10^{-2}	3.76×10^{-5}	377	4.95×10^1	1.41
4	1.78×10^{-2}	3.76×10^{-5}	472	6.91×10^1	1.70
5	2.13×10^{-2}	3.76×10^{-5}	566	7.22×10^1 [a]	1.52[a]
6	2.84×10^{-2}	3.76×10^{-5}	755	7.79×10^1 [a]	1.16[a]
7	3.55×10^{-2}	3.76×10^{-5}	943	1.32×10^2 [a]	5.49×10^{-1} [a]

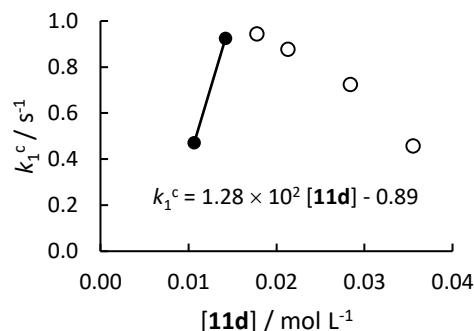
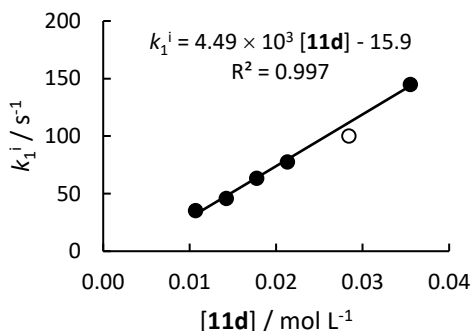


$k_2^i = 5.14 \times 10^3 \text{ L mol}^{-1} \text{ s}^{-1}$; $k_2^c = 1.52 \times 10^2 \text{ L mol}^{-1} \text{ s}^{-1}$

[a] high deviations due to oligomers formation, not included in the correlation, empty circles on the graph

Table 4.19. Kinetics of the reaction of 9a with 11d in Et₂O (stopped flow, 20 °C at 630 nm) derived from COPASI analysis.

Entry	[11d] / mol L ⁻¹	[9a] / mol L ⁻¹	[11d] / [9a]	k_1^i / s ⁻¹	k_{-1}^i / s ⁻¹	k_1^c / s ⁻¹	ssq
1	1.07×10^{-2}	3.76×10^{-5}	283	3.52×10^1	1.55×10^{-5}	4.71×10^{-1}	3.86×10^{-7}
2	1.42×10^{-2}	3.76×10^{-5}	377	4.59×10^1	4.01×10^{-5}	9.24×10^{-1}	6.05×10^{-7}
3	1.78×10^{-2}	3.76×10^{-5}	472	6.35×10^1	5.75×10^{-5}	1.04[a]	6.12×10^{-7}
4	2.13×10^{-2}	3.76×10^{-5}	566	7.75×10^1	2.47×10^{-5}	9.73×10^{-1} [a]	4.64×10^{-7}
5	2.84×10^{-2}	3.76×10^{-5}	755	1.00×10^2 [a]	5.89×10^{-5}	7.84×10^{-1} [a]	4.43×10^{-7}
6	3.55×10^{-2}	3.76×10^{-5}	943	1.45×10^2	1.32×10^{-4}	4.57×10^{-1} [a]	3.19×10^{-7}



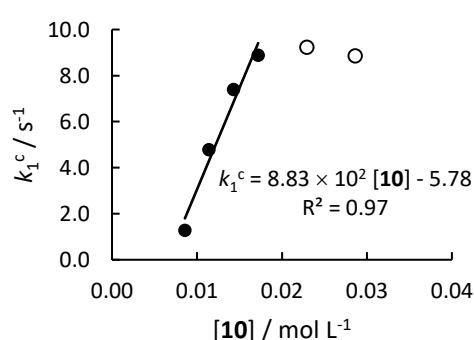
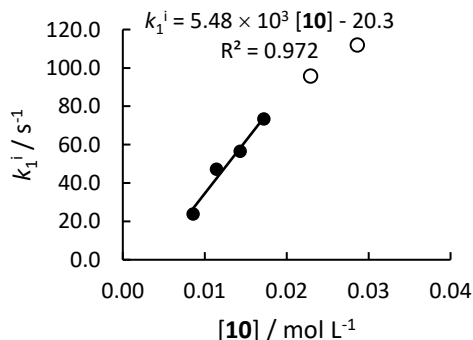
$$k_2^i = 4.49 \times 10^3 \text{ L mol}^{-1} \text{ s}^{-1}; k_2^c = 1.28 \times 10^2 \text{ L mol}^{-1} \text{ s}^{-1}; k_{-1}^i = 3.71 \times 10^{-5} \text{ s}^{-1}$$

[a] high deviations due to oligomers formation, not included in the correlation, empty circles on the graph

Reactions of methylmagnesium bromide

Table 4.20. Kinetics of the reaction of 9b with 10 in Et₂O (stopped flow, 20 °C at 635 nm) derived from separate single-exponential analysis.

Entry	[10] / mol L ⁻¹	[9b] / mol L ⁻¹	[10] / [9b]	k_1^i / s ⁻¹	k_1^c / s ⁻¹
1	8.58×10^{-3}	1.34×10^{-5}	640	2.39×10^1	1.28
2	1.14×10^{-2}	1.34×10^{-5}	851	4.72×10^1	4.78
3	1.43×10^{-2}	1.34×10^{-5}	1067	5.65×10^1	7.40
4	1.72×10^{-2}	1.34×10^{-5}	1284	7.34×10^1	8.88
5	2.29×10^{-2}	1.34×10^{-5}	1709	9.58×10^1 [a]	9.23[a]
6	2.86×10^{-2}	1.34×10^{-5}	2134	1.12×10^2 [a]	8.85[a]

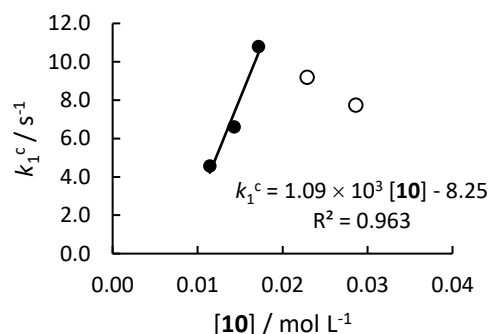
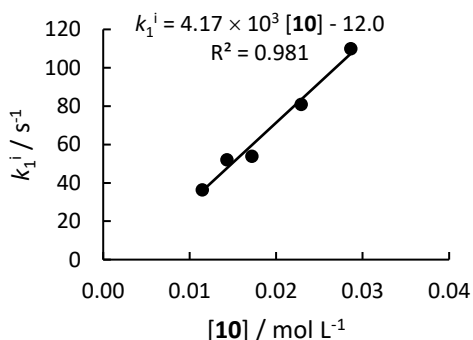


$$k_2^i = 5.48 \times 10^3 \text{ L mol}^{-1} \text{ s}^{-1}; k_2^c = 8.83 \times 10^2 \text{ L mol}^{-1} \text{ s}^{-1}$$

[a] high deviations due to oligomers formation, not included in the correlation, empty circles on the graph

Table 4.21. Kinetics of the reaction of 9b with 10 in Et₂O (stopped flow, 20 °C at 635 nm) derived from COPASI analysis.

Entry	[10] / mol L ⁻¹	[9b] / mol L ⁻¹	[10] / [9b]	k_1^i / s ⁻¹	k_{-1}^i / s ⁻¹	k_1^c / s ⁻¹	ssq
1	1.14×10^{-2}	1.15×10^{-5}	991	3.65×10^1	9.90	4.57	2.10×10^{-8}
2	1.43×10^{-2}	1.15×10^{-5}	1238	5.21×10^1	4.51	6.62	1.71×10^{-8}
3	1.72×10^{-2}	1.15×10^{-5}	1486	5.40×10^1	9.80	1.08×10^1	2.38×10^{-8}
4	2.29×10^{-2}	1.15×10^{-5}	1981	8.09×10^1	1.32	9.20 ^[b]	3.31×10^{-8}
5	2.86×10^{-2}	1.15×10^{-5}	2476	1.10×10^2	-[a]	7.74 ^[b]	5.00×10^{-8}

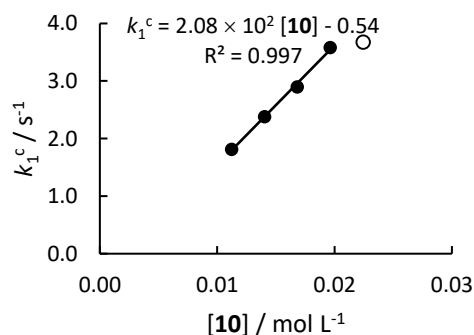
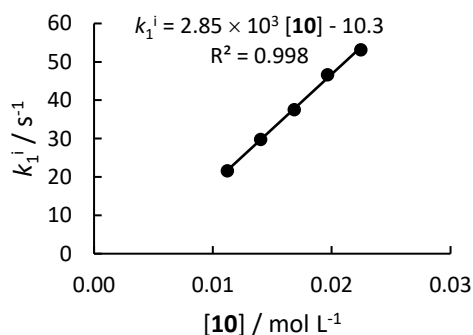


$k_2^i = 4.17 \times 10^3 \text{ L mol}^{-1} \text{ s}^{-1}$; $k_2^c = 1.09 \times 10^3 \text{ L mol}^{-1} \text{ s}^{-1}$; k_{-1}^i = could not be identified due to high deviation values

[a] standard deviations exceed 10%; [b] high deviations due to oligomers formation, not included in the correlation, empty circles on the graph

Table 4.22. Kinetics of the reaction of 9a with 10 in Et₂O (stopped flow, 20 °C at 630 nm) derived from separate single-exponential analysis.

Entry	[10] / mol L ⁻¹	[9a] / mol L ⁻¹	[10] / [9a]	k_1^i / s ⁻¹	k_1^c / s ⁻¹
1	1.12×10^{-2}	2.18×10^{-5}	515	2.16×10^1	1.81
2	1.40×10^{-2}	2.18×10^{-5}	644	2.97×10^1	2.38
3	1.68×10^{-2}	2.18×10^{-5}	773	3.75×10^1	2.90
4	1.96×10^{-2}	2.18×10^{-5}	902	4.66×10^1	3.58
5	2.24×10^{-2}	2.18×10^{-5}	1030	5.31×10^1	3.67 ^[a]

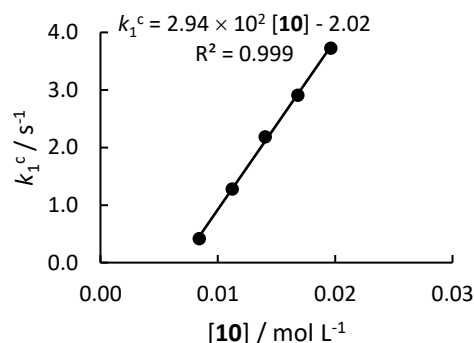
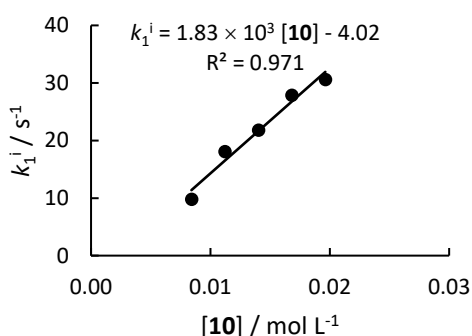


$k_2^i = 2.85 \times 10^3 \text{ L mol}^{-1} \text{ s}^{-1}$; $k_2^c = 2.08 \times 10^2 \text{ L mol}^{-1} \text{ s}^{-1}$

[a] high deviations due to oligomers formation, not included in the correlation, empty circle on the graph

Table 4.23. Kinetics of the reaction of 9a with 10 in Et₂O (stopped flow, 20 °C at 630 nm) derived from COPASI analysis.

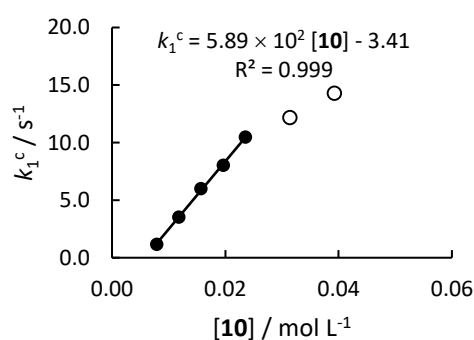
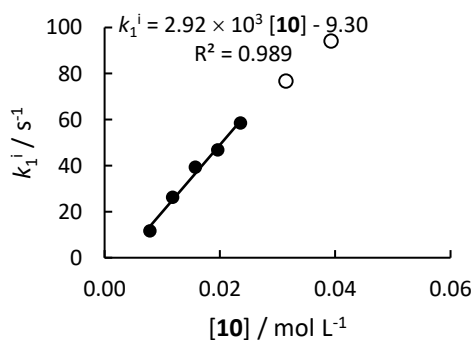
Entry	[10] / mol L ⁻¹	[9a] / mol L ⁻¹	[10] / [9a]	k_1^i / s ⁻¹	k_{-1}^i / s ⁻¹	k_1^c / s ⁻¹	ssq
1	8.41×10^{-3}	2.18×10^{-5}	386	9.83	1.58×10^{-2}	4.17×10^{-1}	3.64×10^{-8}
2	1.12×10^{-2}	2.18×10^{-5}	515	1.81×10^1	3.16×10^{-2}	1.28	4.34×10^{-8}
3	1.40×10^{-2}	2.18×10^{-5}	644	2.18×10^1	1.19	2.19	2.03×10^{-8}
4	1.68×10^{-2}	2.18×10^{-5}	773	2.79×10^1	8.76×10^{-1}	2.91	2.94×10^{-8}
5	1.96×10^{-2}	2.18×10^{-5}	902	3.06×10^1	3.50	3.73	2.82×10^{-8}



$k_2^i = 1.83 \times 10^3 \text{ L mol}^{-1} \text{ s}^{-1}$; $k_2^c = 2.94 \times 10^2 \text{ L mol}^{-1} \text{ s}^{-1}$; k_{-1}^i = could not be identified due to high deviation values

Table 4.24. Kinetics of the reaction of 9c with 10 in Et₂O (stopped flow, 20 °C at 620 nm) derived from separate single-exponential analysis.

Entry	[10] / mol L ⁻¹	[9c] / mol L ⁻¹	[10] / [9c]	k_1^i / s ⁻¹	k_1^c / s ⁻¹
1	7.85×10^{-3}	5.31×10^{-5}	296	1.16×10^1	1.17
2	1.18×10^{-2}	5.31×10^{-5}	443	2.62×10^1	3.52
3	1.57×10^{-2}	5.31×10^{-5}	591	3.93×10^1	6.00
4	1.96×10^{-2}	5.31×10^{-5}	739	4.68×10^1	8.04
5	2.36×10^{-2}	5.31×10^{-5}	887	5.85×10^1	1.05×10^1
6	3.14×10^{-2}	5.31×10^{-5}	1182	7.67×10^1 [a]	1.22×10^1 [a]
7	3.93×10^{-2}	5.31×10^{-5}	1478	9.41×10^1 [a]	1.43×10^1 [a]

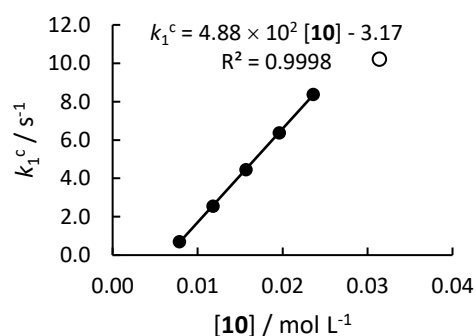
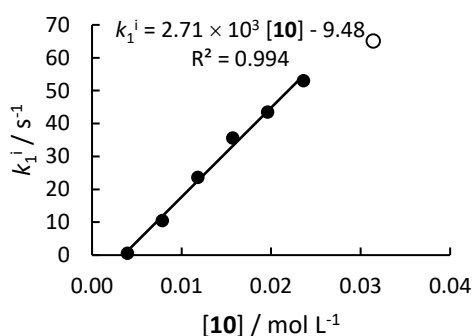


$k_2^i = 2.92 \times 10^3 \text{ L mol}^{-1} \text{ s}^{-1}$; $k_2^c = 5.89 \times 10^2 \text{ L mol}^{-1} \text{ s}^{-1}$

[a] high deviations due to oligomers formation, not included in the correlation, empty circles on the graph

Table 4.25. Kinetics of the reaction of 9c with 10 in Et₂O (stopped flow, 20 °C at 620 nm) derived from COPASI analysis.

Entry	[10] / mol L ⁻¹	[9c] / mol L ⁻¹	[10] / [9c]	k_1^i / s ⁻¹	k_{-1}^i / s ⁻¹	k_1^c / s ⁻¹	ssq
1	3.93×10^{-3}	2.66×10^{-5}	148	6.18×10^{-1}	9.01×10^{-3}	-[a]	4.61×10^{-8}
2	7.85×10^{-3}	2.66×10^{-5}	296	1.05×10^1	2.41×10^{-3}	7.02×10^{-1}	1.20×10^{-7}
3	1.18×10^{-2}	2.66×10^{-5}	443	2.37×10^1	3.56×10^{-6}	2.55	5.01×10^{-8}
4	1.57×10^{-2}	2.66×10^{-5}	591	3.56×10^1	1.39×10^{-5}	4.46	5.36×10^{-8}
5	1.96×10^{-2}	2.66×10^{-5}	739	4.35×10^1	4.34×10^{-5}	6.37	3.73×10^{-8}
6	2.36×10^{-2}	2.66×10^{-5}	887	5.31×10^1	2.16×10^{-3}	8.38	4.28×10^{-8}
7	3.14×10^{-2}	2.66×10^{-5}	1182	6.51×10^1 [b]	2.88×10^{-4}	1.02×10^1 [b]	4.62×10^{-8}



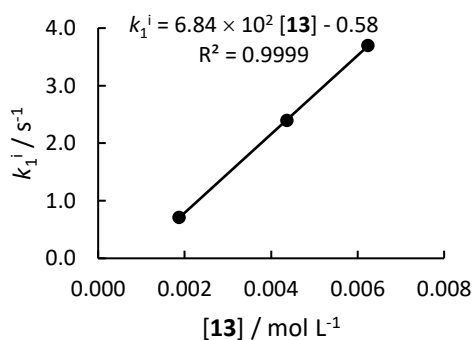
$k_2^i = 2.71 \times 10^3 \text{ L mol}^{-1} \text{ s}^{-1}$; $k_2^c = 4.88 \times 10^2 \text{ L mol}^{-1} \text{ s}^{-1}$; k_{-1}^i = could not be identified due to high deviation values

[a] rate constant too low for analysis [b] high deviations due to oligomers formation, not included in the correlation, empty circles on the graph

Reaction of isopropylmagnesium bromide

Table 4.26. Kinetics of the reaction of 9b with 13 in Et₂O (stopped flow, 20 °C at 635 nm) derived from single-exponential analysis.

Entry	[13] / mol L ⁻¹	[9b] / mol L ⁻¹	[13] / [9b]	k_1^i / s ⁻¹	$k_1^{c[a]}$ / s ⁻¹
1	1.87×10^{-3}	2.59×10^{-5}	72	7.09×10^{-1}	-
2	4.37×10^{-3}	2.59×10^{-5}	168	2.39	-
3	6.24×10^{-3}	2.59×10^{-5}	240	3.70	-



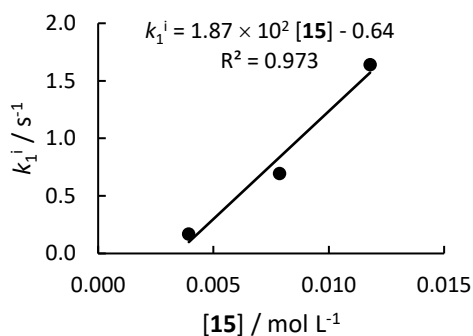
$$k_2^i = 6.84 \times 10^2 \text{ L mol}^{-1} \text{ s}^{-1}$$

[a] second step was not observed

Reaction of benzylmagnesium bromide

Table 27. Kinetics of the reaction of 9b with 15 in Et₂O (stopped flow, 20 °C at 635 nm) derived from single-exponential analysis.

Entry	[15] / mol L ⁻¹	[9b] / mol L ⁻¹	[15] / [9b]	k_1^i / s ⁻¹	$k_1^{c[a]}$ / s ⁻¹
1	3.93×10^{-3}	2.75×10^{-5}	143	1.70×10^{-1}	-
2	7.86×10^{-3}	2.75×10^{-5}	285	6.94×10^{-1}	-
3	1.18×10^{-2}	2.75×10^{-5}	428	1.64	-



$$k_2^i = 1.87 \times 10^2 \text{ L mol}^{-1} \text{ s}^{-1}$$

[a] second step was not observed

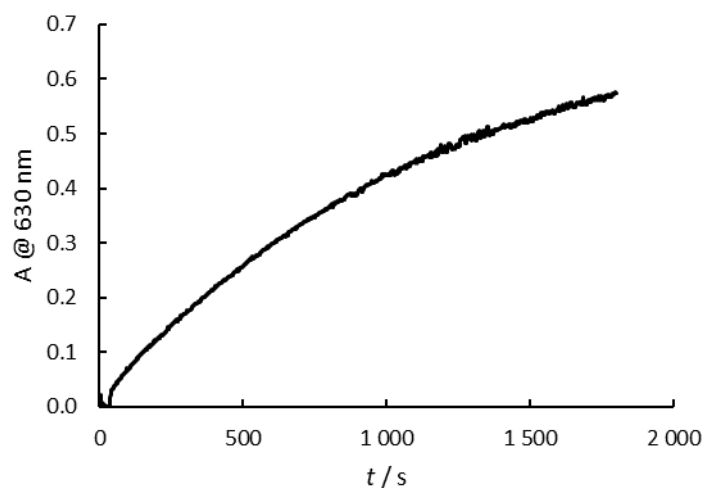


Figure 11. Curve of absorbance of the corresponding carbocation **9b-CC** (at 630 nm) formed in the reaction of substrate **9b** ($5.84 \times 10^{-6} \text{ mol L}^{-1}$) and MgBr_2 ($5.35 \times 10^{-5} \text{ mol L}^{-1}$) in THF at 20 °C versus time.

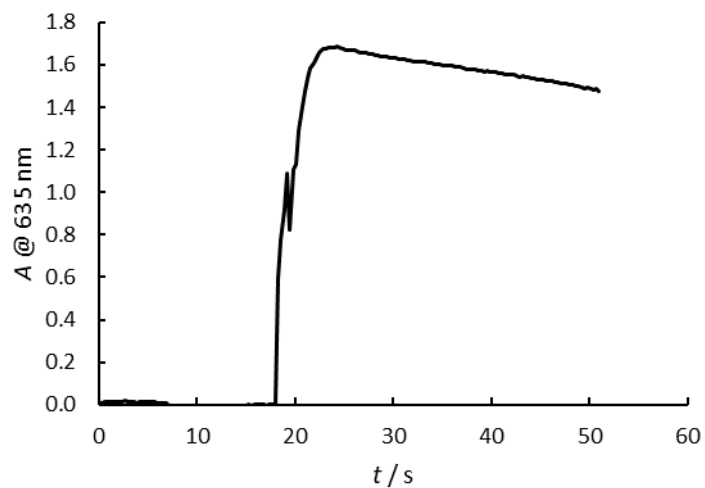


Figure 12. Curve of absorbance of the corresponding carbocation **9b-CC** (at 635 nm) formed in the reaction of substrate **9b** ($5.84 \times 10^{-6} \text{ mol L}^{-1}$) and MgBr_2 ($5.35 \times 10^{-5} \text{ mol L}^{-1}$) in Et₂O at 20 °C versus time.

4.5 References

- [1] P. Barbier, *Compt. Rend. Acad. Sci.* **1899**, 128, 110-111.
- [2] V. Grignard, *Compt. Rend. Acad. Sci.* **1900**, 130, 1322-1324.
- [3] W. Schlenk, W. Schlenk, Jr., *Ber. Dtsch. Chem. Ges.* **1929**, 62, 920-924.
- [4] E. C. Ashby, J. Laemmle, H. M. Neumann, *Acc. Chem. Res.* **1974**, 7, 272-280.
- [5] a) T. Holm, *Acta Chem. Scand.* **1969**, 23, 579-586; b) M. B. Smith, W. E. Becker, *Tetrahedron* **1966**, 22, 3027-3036; c) T. Holm, *Acta Chem. Scand.* **1966**, 20, 2821-2828; d) M. B. Smith, W. E. Becker, *Tetrahedron* **1967**, 23, 4215-4227.
- [6] a) E. C. Ashby, J. Laemmle, H. M. Neumann, *J. Am. Chem. Soc.* **1971**, 93, 4601-4602; b) E. C. Ashby, J. Laemmle, H. M. Neumann, *J. Am. Chem. Soc.* **1972**, 94, 5421-5434; c) J. Laemmle, E. C. Ashby, H. M. Neumann, *J. Am. Chem. Soc.* **1971**, 93, 5120-5127; d) T. Holm, *Acta Chem. Scand.* **1967**, 21, 2753-2758.
- [7] R. M. Salinger, H. S. Mosher, *J. Am. Chem. Soc.* **1964**, 86, 1782-1786.
- [8] D. F. Evans, G. V. Fazakerley, *J. Chem. Soc. A* **1971**, 184-189.
- [9] E. C. Ashby, G. E. Parris, *J. Am. Chem. Soc.* **1971**, 93, 1206-1213.
- [10] a) E. C. Ashby, W. E. Becker, *J. Am. Chem. Soc.* **1963**, 85, 118-119; b) H. Hashimoto, T. Nakano, H. Okada, *J. Org. Chem.* **1965**, 30, 1234-1239.
- [11] E. C. Ashby, M. B. Smith, *J. Am. Chem. Soc.* **1964**, 86, 4363-4370.
- [12] A. D. Vreugdenhil, C. Blomberg, *Recl. Trav. Chim. Pays-Bas* **1963**, 82, 461-463.
- [13] W. Slough, A. R. Ubbelohde, *J. Chem. Soc. (Resumed)* **1955**, 108-114.
- [14] F. W. Walker, E. C. Ashby, *J. Am. Chem. Soc.* **1969**, 91, 3845-3850.
- [15] a) N. M. Bikales, E. I. Becker, *Chem. Ind. (London)* **1961**, 11, 1831-1832; b) N. M. Bikales, E. I. Becker, *Can. J. Chem.* **1963**, 41, 1329-1343.
- [16] E. A. Hill in *Grignard Reagents New Developments*, (Ed. H. G. Richey, Jr), Wiley, Chichester, **2000**, pp. 27-59.
- [17] J. Kenyon, H. Phillips, V. P. Pittman, *J. Chem. Soc. (Resumed)* **1935**, 1072-1084.
- [18] a) C. M. Hill, L. Haynes, D. E. Simmons, M. E. Hill, *J. Am. Chem. Soc.* **1953**, 75, 5408-5409; b) C. M. Hill, R. M. Prigmore, G. J. Moore, *J. Am. Chem. Soc.* **1955**, 77, 352-354; c) C. M. Hill, D. E. Simmons, M. E. Hill, *J. Am. Chem. Soc.* **1955**, 77, 3889-3892.
- [19] F. G. Mann, F. H. C. Stewart, *J. Chem. Soc. (Resumed)* **1954**, 4127-4134.
- [20] J. P. Mason, M. Zief, *J. Am. Chem. Soc.* **1940**, 62, 1450-1452.
- [21] H. Walther, L. Haase, H. Gross, B. Costisella, I. Keitel, *J. Prakt. Chem.* **1980**, 322, 902-908.
- [22] H. Stetter, E. Reske, *Chem. Ber.* **1970**, 103, 643-644.
- [23] L. Poncini, *N. Z. J. Sci.* **1983**, 103, 31-31.
- [24] Ю. Н. Поливин, *Конференция молодых ученых УДН им. П. Лумумбы* **1988**.

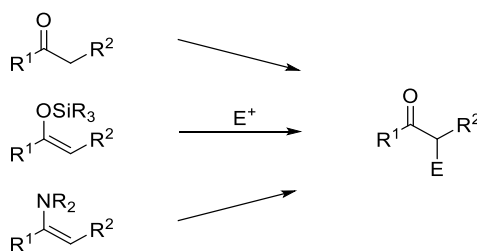
- [25] a) A. Tuulmets, B. T. Nguyen, D. Panov, M. Sassian, J. Järv, *J. Org. Chem.* **2003**, *68*, 9933-9937; b) A. Ploom, D. Panov, J. Järv, A. Tuulmets, *J. Organomet. Chem.* **2008**, *693*, 2351-2354.
- [26] a) H. Mayr, T. Bug, M. F. Gotta, N. Hering, B. Irrgang, B. Janker, B. Kempf, R. Loos, A. R. Ofial, G. Remennikov, H. Schimmel, *J. Am. Chem. Soc.* **2001**, *123*, 9500-9512; b) N. Streidl, B. Denegri, O. Kronja, H. Mayr, *Acc. Chem. Res.* **2010**, *43*, 1537-1549.
- [27] T. J. Park, *Bull. Korean Chem. Soc.* **2013**, *34*, 243-245.
- [28] S. Hoops, S. Sahle, R. Gauges, C. Lee, J. Pahle, N. Simus, M. Singhal, L. Xu, P. Mendes, U. Kummer, *Bioinformatics* **2006**, *22*, 3067-3074.
- [29] R. Lucius, R. Loos, H. Mayr, *Angew. Chem. Int. Ed.* **2002**, *41*, 91-95.
- [30] W. Muramatsu, K. Nakano, *Tetrahedron Lett.* **2015**, *56*, 437-440.
- [31] T. Korenaga, K. Nitatori, H. Muraoka, S. Ogawa, K. Shimada, *Org. Lett.* **2015**, *17*, 5500-5503.
- [32] S. Handa, Y. L. N. Mathota Arachchige, L. M. Slaughter, *J. Org. Chem.* **2013**, *78*, 5694-5699.
- [33] S. Yoshida, Y. Nakamura, K. Uchida, Y. Hazama, T. Hosoya, *Org. Lett.* **2016**, *18*, 6212-6215.
- [34] B. E. Love, E. G. Jones, *J. Org. Chem.* **1999**, *64*, 3755-3756.

Chapter 5

Reactivity Comparison of Structurally Related Enamines and Silyl Enol Ethers

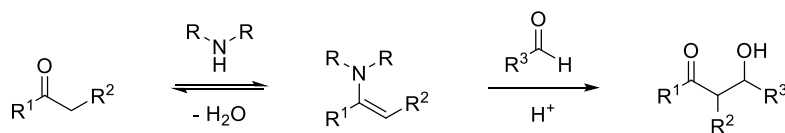
5.1 Introduction

Enamines^[1] and silylated enol ethers^[2] represent important classes of carbon nucleophiles widely used in organic synthesis. Their utilization in electrophilic functionalizations towards α -substituted carbonyl compounds includes numerous examples of fluorinations,^[3] trifluoromethylthiolations^[4] and trifluoromethylations^[5] (Scheme 5.1). Even though, many of these transformations are known to proceed directly from the carbonyl substrates, such reactions often lead to increased number of side-products, lower yields and loss of stereoselectivity.



Scheme 5.1. General scheme of electrophilic α -functionalization of carbonyl compounds.

Mukaiyama in 1973 reported^[6] on the successful application of silicon enolates in directed aldol reactions, that has become a valuable method for constructing new carbon-carbon bonds and found its application in natural product synthesis.^[7] On the other hand, the development of amine-catalyzed aldol reactions has proven to be a powerful tool for constructing complex carbon skeleton with defined stereochemistry.^[8] Extensive studies by Cordova,^[9] Tsogoeva,^[10] Jacobsen^[11] and others have provided evidence for *in situ* formation of catalytically active enamines (Scheme 5.2).



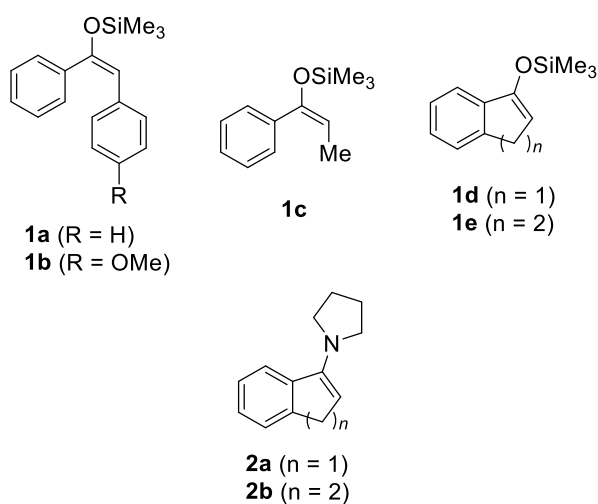
Scheme 5.2. General scheme of amine-catalyzed aldol reaction.

In this context the reactivity of enamines and silyl enol ethers are of particular interest. During the last decades, Mayr and co-workers have developed a comprehensive nucleophilicity scale,^[12] which also include these types of compounds.^[12a, c, 13] The second-order rate

constants of reactions of various nucleophiles with benzhydrylium ions, quinone methides, diethyl benzylidenemalonates and benzylidenemalononitriles have been described by Equation 1, where E is an electrophile-specific parameter, and N and s_N are nucleophile-specific parameters.^[14]

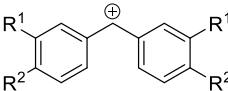
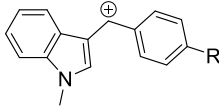
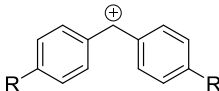
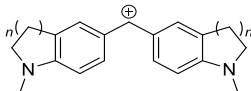
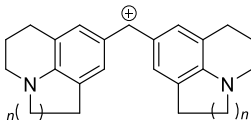
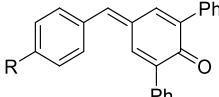
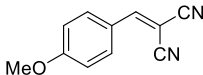
$$\lg k_2 (20\text{ }^\circ\text{C}) = s_N (N + E) \quad (1)$$

To quantify the difference in reactivity between these C-centered nucleophiles, we have studied the kinetics of the reactions of silyl enol ethers **1a-e** and enamines **2a-b** (Scheme 5.3) with reference electrophiles (listed in Table 5.1) in CH₃CN and calculated the nucleophilicity parameters of these compounds by using the linear free-energy relationship (1).



Scheme 5.3. Silyl enol ethers **1a-e** and enamines **2a-b** used for the quantification of reactivities for different C-nucleophiles.

Table 5.1. Indolylmethyl cations **3c-e**, benzhydrylium ions **3a-b** and **3f-o** and quinone methides **3p-q** employed as reference electrophiles in this study.

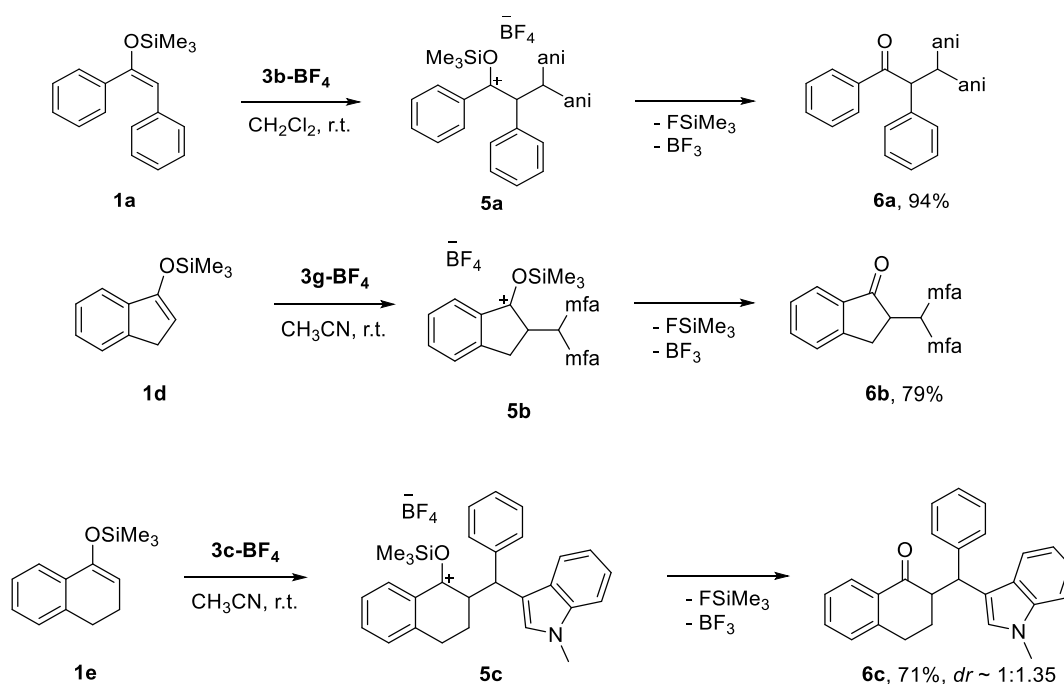
Electrophile			$E^{[a]}$	$\lambda_{\max}^{[b]}$
	$R^1 = H; R^2 = OCH_3$	3a	0.00	513 ^[c]
	$R^2, R^1 = -O(CH_2)_2-$	3b	-1.36	535 ^[c]
	$R = H$	3c	-1.80	413
	$R = CH_3$	3d	-2.19	434
	$R = OCH_3$	3e	-3.02	471
	$R = N(Ph)CH_2CF_3$	3f	-3.14	601 ^[d]
	$R = N(CH_3)CH_2CF_3$	3g	-3.85	586
	$R = N(Ph)_2$	3h	-4.72	622 ^[d]
	$R = N(CH_2CH_2)_2O$	3i	-5.53	612
	$R = N(CH_3)_2$	3j	-7.02	605
	$R = N(CH_2)_4$	3k	-7.69	612
	$n = 2$	3l	-8.22	620
	$n = 1$	3m	-8.76	616
	$n = 2$	3n	-9.45	635
	$n = 1$	3o	-10.04	632
	$R = H$	3p	-11.87	384
	$R = OCH_3$	3q	-12.18	414
		3r	-10.80	354

[a] Electrophilicity parameters E were taken from ref. ^[12a, b, e, 15] [b] In nm in CH_3CN solution. [c] In CH_2Cl_2 .

5.2 Results and Discussion

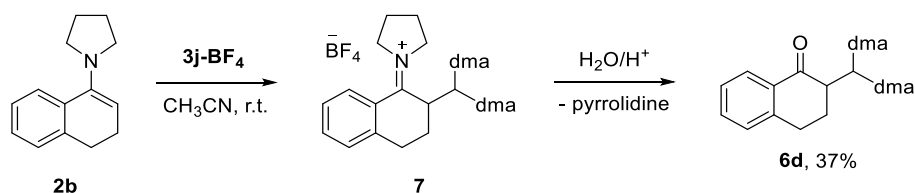
5.2.1 Product Studies

The reactions of silyl enol ethers **1a**, **1d** and **1e** with reference electrophiles, either benzhydrylium or indolylmethyl cation tetrafluoroborates, proceeded through intermediate siloxy substituted carbenium ions **5**. Due to fast subsequent desilylation, ketones **6a-c** were obtained in high yields (Scheme 5.4) after purification by column chromatography and characterized by NMR spectroscopy and mass spectrometry. Electrophilic attack of asymmetrical carbocation **3c** led to the mixture (approx. 1:1.35, determined by NMR spectroscopy) of two diastereomers for product **6c**.



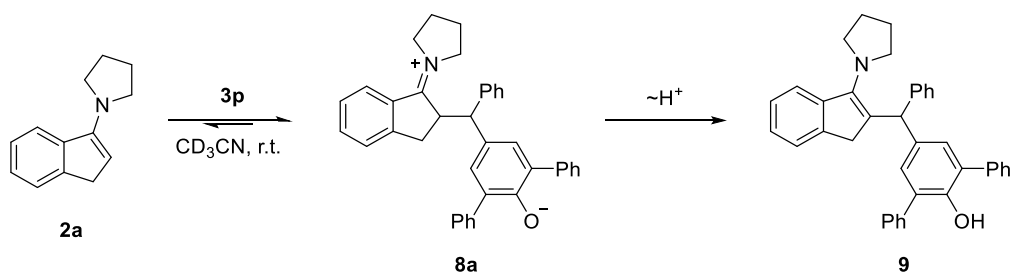
Scheme 5.4. Reactions of silyl enol ethers **1a**, **1e-d** with reference electrophiles (ani = 4-methoxyphenyl; mfa = 4-(methyl(trifluoroethyl)amino)phenyl). Yields refer to isolated products.

Nucleophilic attack of enamine **2b** at benzhydrylium ion **3j** led to quantitative formation of the iminium salt **7**. Though it was not isolated, the ^1H and ^{13}C NMR spectra clearly indicated the formation of **7**, when the reaction was performed in CD_3CN . Upon the hydrolysis of the iminium ion **7**, the ketone **6d** was obtained in rather poor yet significant yield (Scheme 5.5).



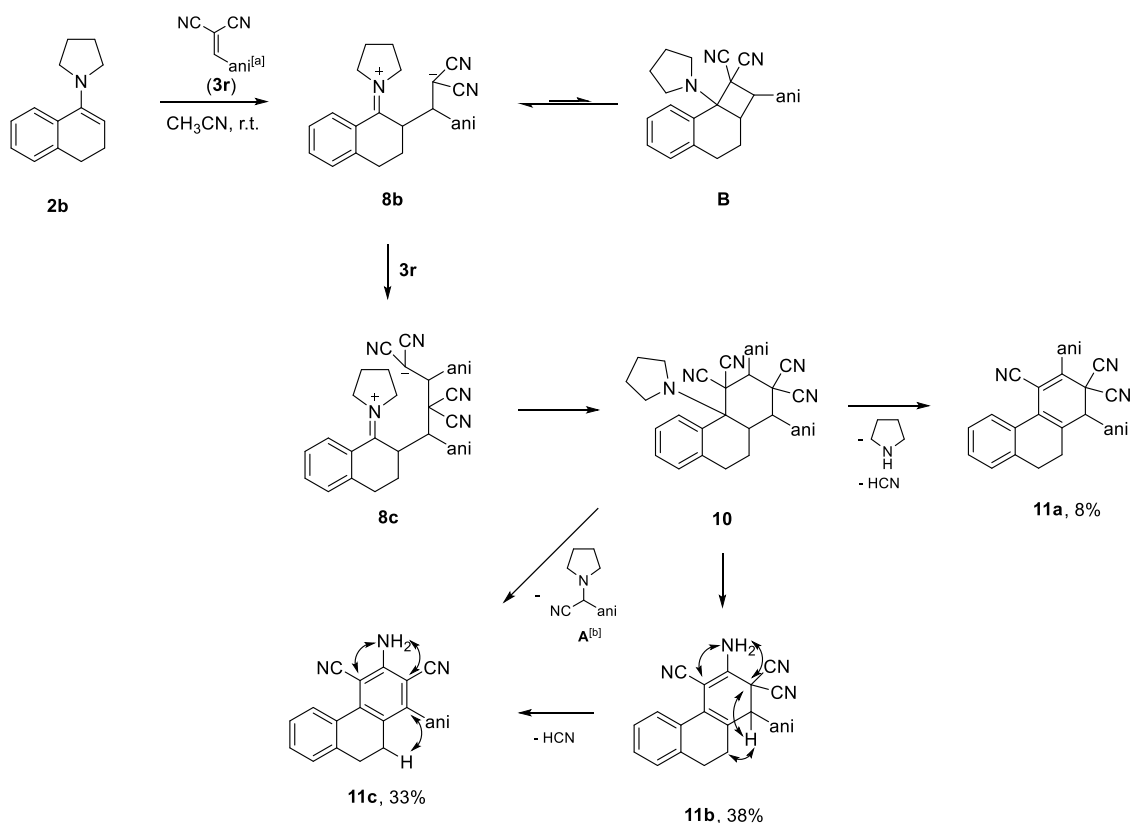
Scheme 5.5. Reaction of the enamine **2b** with reference electrophile **3j-BF₄**. dma = 4-(dimethylamino)phenyl.

The reaction between two neutral compounds, enamine **2a** and quinone methide **3p**, should be highly reversible and give the zwitter-ionic structure **8a**. However, the subsequent proton shift is much faster than the backward reaction, and therefore the product **9** was obtained quantitatively already after 30 minutes as determined by NMR spectroscopy (Scheme 5.6). The enamine structure was confirmed by 2D NMR spectroscopy.



Scheme 5.6. Reaction between enamine **2a** and quinone methide **3p**.

Following the previous scenario, the attack of the enamine **2b** at the benzylidenemalonitrile **3r** led to the zwitter-ionic species **8b** (presumably in equilibrium with cyclobutane **B**),^[16] which is nucleophilic enough to attack a second molecule of the electrophile to give another zwitterion **8c**, which cyclized by intramolecular attack of the malononitrile anion moiety at the iminium carbon^[16c] to give the tricyclic product **10** (Scheme 5.7). Upon aqueous work-up, the crude reaction mixture was purified by column chromatography and each of the obtained compounds was characterized by NMR spectroscopy and mass spectrometry. Formation of the compound **11a** can be explained by direct elimination of the amine in **10** and subsequent loss of one HCN molecule. When the same reaction was performed in CD_3CN , the ^1H NMR acquired after 1 hour indicated quantitative formation of **11c** and an equimolar amount of an α -aminonitrile **A** without identification of intermediate structures. However, detailed mechanism of the intramolecular transformations towards **11b-c** still remains to be elucidated.



Scheme 5.7. Products of the reaction of the enamine **2b** with benzylidenemalononitrile **3n** in CH_3CN at room temperature and HMBC correlations (double-headed arrows in formulas **11b-c**). Yields refer to isolated products after column chromatography. [a] ani = *p*-Methoxyphenyl. [b] Observed via ^1H and ^{13}C NMR spectroscopy in CD_3CN .^[17]

5.2.2 Kinetic Investigations

The reactions of silyl enol ethers **1a-e** and enamines **2a-b** with reference electrophiles **3c-q** were performed in either CH_3CN or CH_2Cl_2 at 20°C and monitored by UV-Vis spectroscopy at the absorption maxima of the electrophile (listed in Table 5.2). To simplify the evaluation of the kinetic experiments, the nucleophile was used in large excess (at least 9 equiv.), thus the concentration of this component remained constant throughout the reactions. The first-order rate constants k_{obs} were derived by least-squares fitting of the exponential function $A_t = A_0 \exp(-k_{\text{obs}}t) + C$ to the time-dependent absorbances A_t of the electrophile. Second-order rate constants k_2 were obtained as the slopes of plots of k_{obs} versus the concentration of the nucleophile as exemplified in the Figure 5.1 for the reaction of the silyl enol ether **1b** with reference electrophile **3c**.

The second-order rate constants for all investigated reactions are collected in Table 5.2.

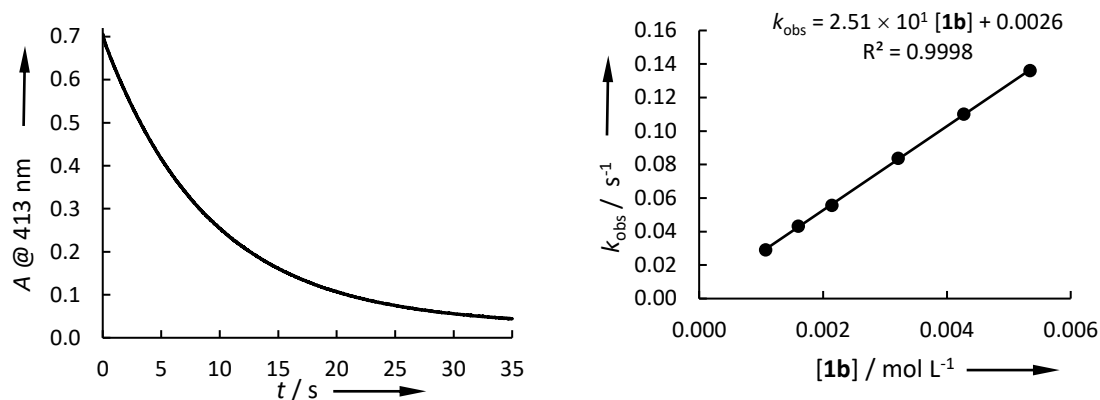


Figure 5.1. Exponential decay of absorbance A (at 413 nm) of the reaction of **1b** ($6.10 \times 10^{-3} \text{ mol L}^{-1}$) with **3c** ($7.16 \times 10^{-5} \text{ mol L}^{-1}$) in CH_3CN at 20°C (left). Plot of the first-order rate constants k_{obs} versus the concentration of **1b** (right).

Table 5.2. Second-order rate constants k_2 for the reactions of the silyl enol ethers **1a-e** and enamines **2a-b** with reference electrophiles **3** in CH_3CN at 20°C .

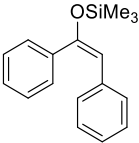
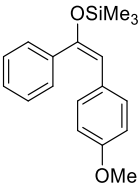
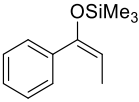
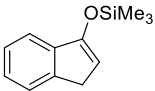
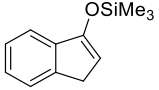
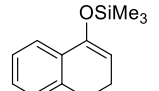
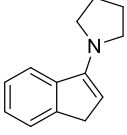
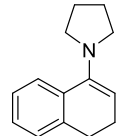
Nucleophile	N (S_N) ^[a]	Electrophile	λ / nm ^[b]	k_2 / $\text{L mol}^{-1} \text{ s}^{-1}$
 1a	3.00 (0.82) 3.13 (0.82) ^[c]	3c	413	9.54
			425 ^[c]	1.24×10^1 ^[c]
		3d	434	4.77
		3e	471 492 ^[c]	9.67×10^{-1} 1.23 ^[c]
 1b	3.51 (0.80)	3c	413	2.51×10^1
		3d	434	1.00×10^1
		3e	471	2.53
 1c	5.16 (0.94)	3c	413	1.32×10^3
		3d	434	7.26×10^2
		3e	471	1.00×10^2
 1d	7.34 (0.82)	3c	413	2.60×10^4
		3d	434	1.39×10^4
		3e	471	4.94×10^3

Table 5.2. continued.

Nucleophile	N (S_N) ^[a]	Electrophile	λ / nm ^[b]	k_2 / L mol ⁻¹ s ⁻¹
 1d	7.34 (0.82)	3g	586	8.94×10^2
		3i	612	3.34×10^1
		3j	605	1.36
 1e	5.04 (0.91)	3c	413	8.41×10^2
		3d	434	3.53×10^2
		3e	471	9.29×10^1
		3i	612	3.48×10^{-1}
 2a	15.27 (0.92)	3n	635	2.23×10^5
		3o	632	7.73×10^4
		3p	384	1.57×10^3
		3q	414	7.00×10^2
 2b	14.11 (0.66)	3j	605	4.34×10^4
		3k	612	1.74×10^4
		3l	620	8.87×10^3
		3m	616	3.03×10^3
		3n	635	1.14×10^3
		3r	354	1.53×10^2 ^[d]

[a] Determination see Section 5.2.3. [b] Monitored wavelength. [c] Measured in CH₂Cl₂. [d] Calculated, using eq. 1.

Even though the reactions between enamine **2a** and quinone methides **3p-q** should be reversible, subsequent proton transfer is significantly faster than backward reaction, thereby the equilibrium were not observed during the kinetic investigations. However, the less reactive enamine **2b** slows down the proton transfer reaction as well as initial C-C bond formation, and interaction with quinone methide **3p** did not follow second-order kinetics.

Attempts to measure the kinetics of the reactions of enamines **2a-b** and benzylidenemalononitrile **3r** were unsuccessful due to high absorbance overlap of the enamines and reaction products with **3r**.

5.2.3 Correlation Analysis

Plots of $\lg k_2$ for the reactions of the silyl enol ethers **1** and enamines **2** with indolylmethyl cations **3d-e**, benzhydrylium ions **3g-o** and quinone methides **3p-q** against their electrophilicity parameters E showed linear correlations for all studied nucleophiles (Figure 5.2). Therefore

Equation (1) is applicable and the N and s_N parameters for the nucleophiles **1** and **2** were calculated (Table 5.2).

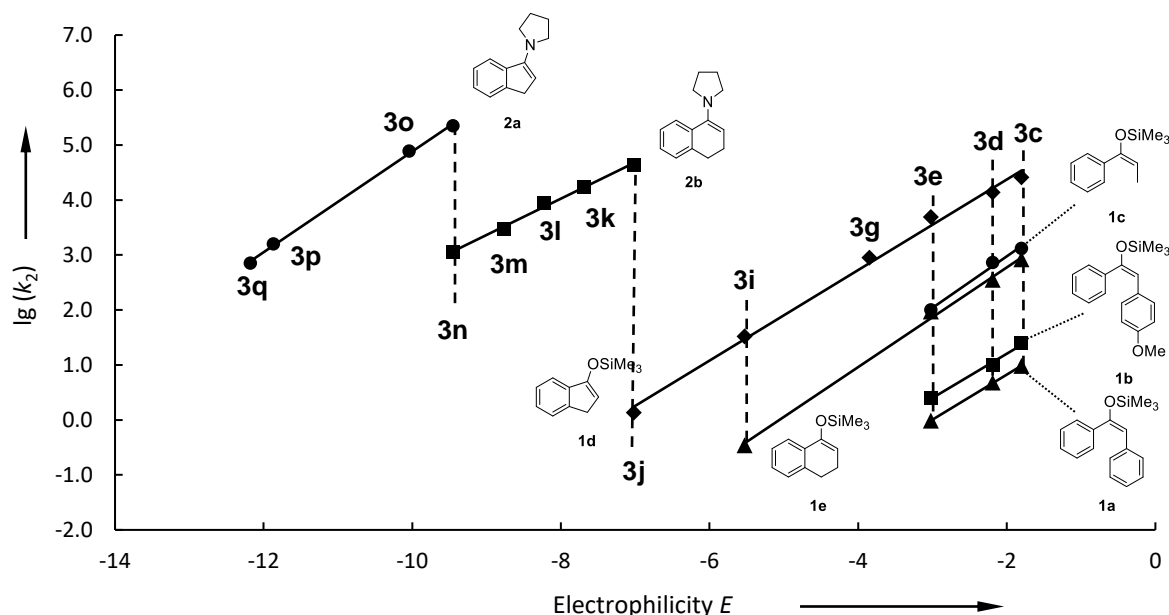


Figure 5.2. Correlations of the second-order rate constants $\lg(k_2)$ for the reactions of C-nucleophiles **1** and **2** with the electrophiles **3** in CH_3CN at 20°C with the electrophilicity parameters E of **3**.

These correlations do not only confirm the consistency of the rate constants determined in this work, but also allow to extrapolate rate constants for reactions that cannot be directly measured.

5.2.4 Structure-Reactivity Relationships

The obtained narrow range of nucleophile-specific susceptibilities ($0.80 < s_N < 0.94$) for silyl enol ethers **1** indicates a low dependence of relative reactivities of these π -systems on the nature of the attacking electrophile. Therefore, the reactivities towards carbenium ions, both indolylmethylium **3c-e** and benzhydrylium **3g-o**, reflect general structure-reactivity trends.

Figure 5.3 demonstrates the reactivities of silyl enol ethers **1a** and **1c** compared to those of **12a-b**, studied before.^[12a] Introduction of a methyl group at the β -position in enol ether **12a** stabilizes the intermediate carbenium cation in the reaction of **1c** with cationic electrophiles (e.g. Scheme 5.4) only slightly. However, this effect is not enough to overcome the steric hindrance at the reaction center and the reactivity is reduced by 1 order of magnitude (**12a** \rightarrow **1c**). Substitution of a methyl group by a phenyl not only further reduces the reactivity by a factor of 1000, but also makes the nucleophile less sensitive towards changes in the reactivities of the electrophiles: $s_N(\mathbf{1c}) = 0.94$; $s_N(\mathbf{1a}) = 0.82$.

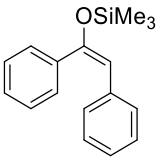
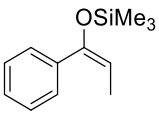
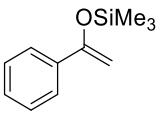
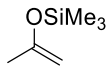
				
	1a	1c	12a	12b
k_2 (3d)	4.77	7.26×10^2	7.39×10^3 [a]	8.52×10^3 [a]
k_{rel}	0.007	1	10	12

Figure 5.3. Comparison of absolute (in $\text{L mol}^{-1} \text{s}^{-1}$) and relative rate constants for the reaction of silyl enol ethers **1a** and **1c** with indolymethylum ion **3d** in CH_3CN at 20°C with those for the reaction of **12a-b** with **3d** in CH_2Cl_2 at 20°C . [a] Calculated using equation (1).

Annulation of an aromatic system to the cyclic enol ethers **12c** and **12d** reduces their sensitivity towards the nature of the electrophile: s_N is reduced by the value of 0.1 for both **1d** and **1e**. In case of the five-member ring, the reactivity towards **3i** is increased by a factor of 3.6 (**12c** \rightarrow **1d**). At the same time for 1-(trimethylsiloxy)cyclohexene (**12d**) addition of a planar moiety does not have a significant effect on the reactivity (**12d** \rightarrow **1e**).

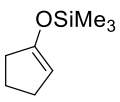
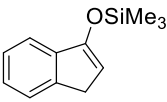
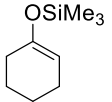
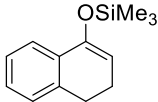
				
	12c	1d	12d	1e
k_2 (3i)	$9.27^{[a]}$	3.34×10^1	4.79×10^{-1} [a]	3.48×10^{-1}
k_{rel}	1	3.6	1	0.73

Figure 5.4. Comparison of absolute (in $\text{L mol}^{-1} \text{s}^{-1}$) and relative rate constants for the reaction of silyl enol ethers **1d** and **1e** with benzhydrylium ion **3i** in CH_3CN at 20°C with those for the reaction of **12c-d** with **3i** in CH_2Cl_2 at 20°C . [a] Calculated using equation (1).

It has been shown before, that reactivity of enamines is increased in more polar solvents, e.g. from dichloromethane to acetonitrile (see ref. ^[13c] and ^[13d]), however, this reactivity difference is neglected for the comparison below. Annulation of an aromatic system to 1-(*N*-pyrrolidino)cyclohexene (**13c**) reduces the reactivity by a factor of 40 towards the benzhydrylium ion **3n** (Figure 5.5). However, this structural change has a dramatic effect on the sensitivity parameter s_N (0.86 and 0.66 for **13c** and **2b** respectively) making the reactivity order highly dependent on the nature of the electrophile. Though, the nucleophilicity of **13d** was not studied in CH_3CN , one can expect, that addition of an aromatic moiety does not have a great influence on reactivity of such enamines (see **13d** and **2a**).

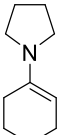
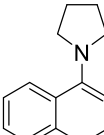
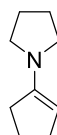
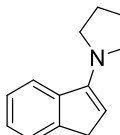
				
	13c	2b	13d	2a
k_2 (3n)	4.96×10^4 [a]	1.14×10^3	3.59×10^5 [a]	2.23×10^5
k_{rel}	1	0.023	1	0.62

Figure 5.5. Comparison of absolute (in $\text{L mol}^{-1} \text{s}^{-1}$) and relative rate constants for the reaction of enamines **2a** and **2b** with benzhydrylium ion **3n** in CH_3CN at 20°C with those for the reaction of **13c-d** with **3n** in CH_2Cl_2 at 20°C . [a] Calculated using equation (1).

The effect of *para*-substitution at the phenyl ring at the reaction center is nearly the same for silyl enol ethers **1a-b** than for enamines **13a-b** (Figure 5.6).^[13e] Due to increased electron density at the reaction center and stabilization of the intermediate carbenium and iminium ion, the electron-donating methoxy group increases the reactivity of enols and enamines by 3 and 2 times respectively (with negligible difference in s_N parameters). A greater difference is observed in compounds with formal negative charge (carbanions **14a** and **14b**), e.g. methoxy group increases the N parameter by 4 orders of magnitude.^[18] This substitution also significantly changes the s_N parameter for these carbanions, making the comparison of their reactivity highly dependent on the nature of the electrophile.

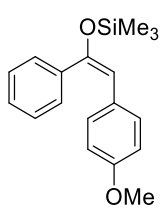
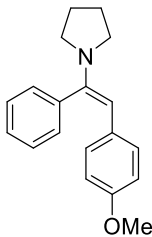
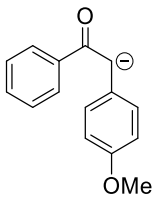
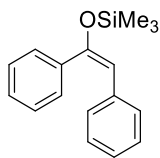
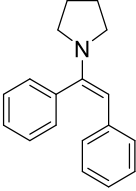
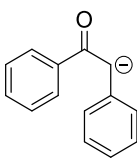
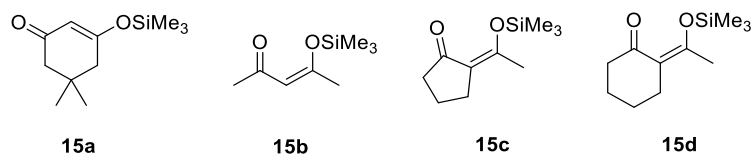
		
1b	13b	14b
3.51 (0.80)	11.99 (0.84)	27.46 (0.41) ^[a]
		
1a	13a	14a
3.00 (0.82)	11.66 (0.82)	23.15 (0.60) ^[a]

Figure 5.6. Effect of *para*-substitution at the phenyl ring at the reaction center for the series of deoxybenzoin-derived C-nucleophiles **1a-b**, **13a-b** and **14a-b** in CH_3CN . [a] In DMSO.

5.3 Silyl Enol Ethers, Derived from 1,3-Dicarbonyl Compounds

5.3.1 Introduction

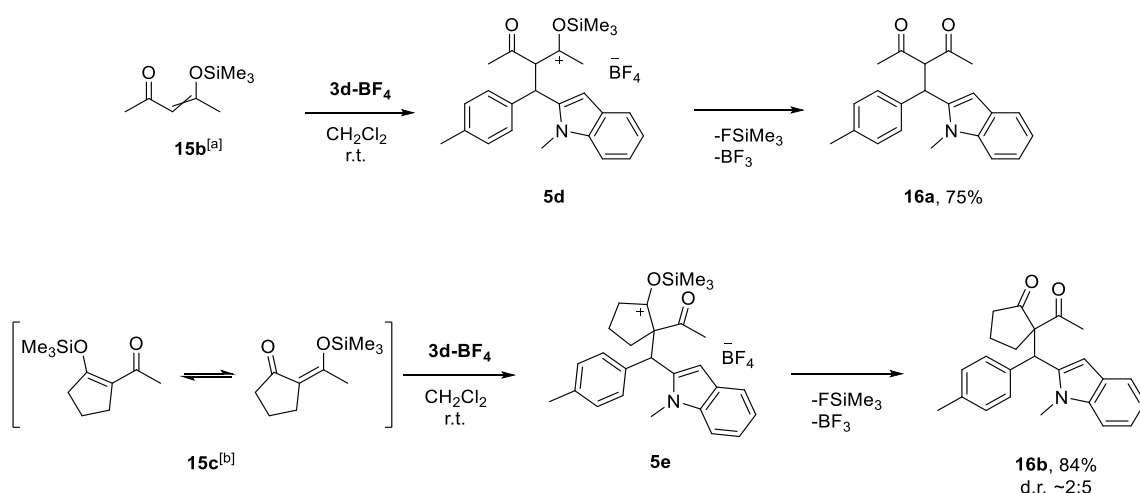
Silyl enol ethers, derived from 1,3-dicarbonyl compounds are versatile nucleophiles, which may be easily functionalized at β -carbon atom and utilized as substrates for [3+3]-cycloadditions.^[19] One of the crucial steps in such transformations is an electrophilic attack at silyl enol ether. To quantify the effect of an acetyl group on the reactivity of these compounds we have investigated the reactions between nucleophiles **15** (Scheme 5.8) and selected reference electrophiles.



Scheme 5.8. Silyl enol ethers **15a-d**, derived from 1,3-dicarbonyl compounds, used in this study.

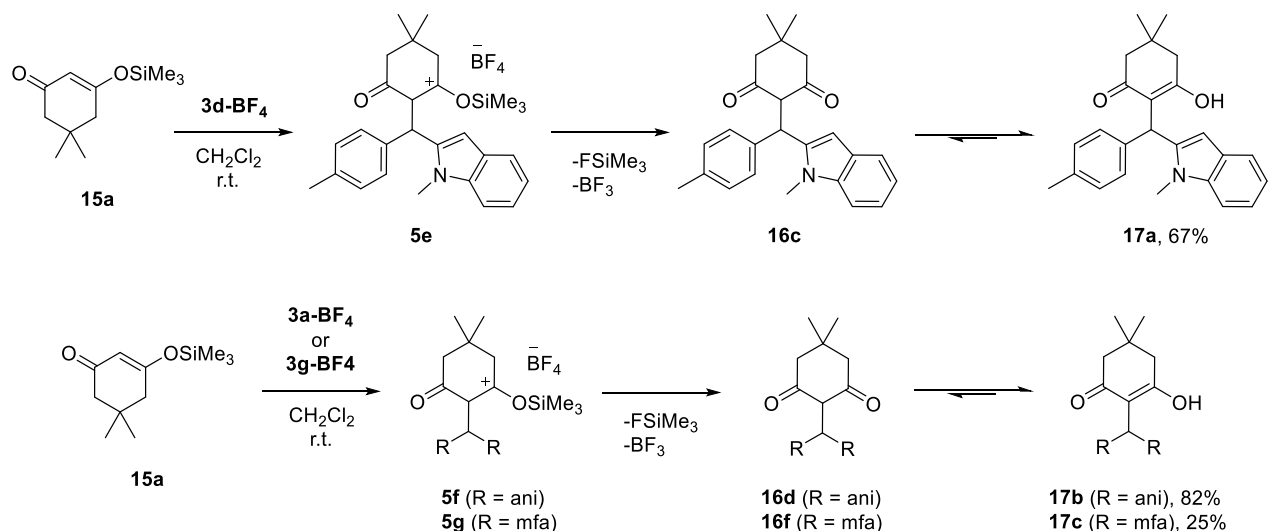
5.3.2 Product Analysis

Electrophilic attack of the indolylmethylm tetrafluoroborate (**3b**) at the enol ethers **15b-c** proceeded through intermediate cations **5d-e** and after fast desilylation yielded the diketones **16a** and **16b**, respectively. After purification by column chromatography products were obtained in a good yield (Scheme 5.9). It has been reported^[20] that unsymmetrical β -keto-silyl enol ethers (e.g. **15c**) may undergo 1,5-sigmatropic rearrangement and may exist in a solution as a mixture of two regioisomers.



Scheme 5.9. Reaction between silyl enol ethers **15b-c** and indolylmethylm cation **3d-BF₄**. [a] As 3/1 mixture of *E/Z* isomers respectively. [b] As 55/45 mixture of two regioisomers.

The same mechanism could be applied for the reaction between silyl enol ether **15a** and several studied carbocations, e.g. indolylmethyl cation **3d**, benzhydrylium **3a** and **3g** tetrafluoroborates. The obtained ketones **16c-f** were isolated in their enol forms **17a-c** (Scheme 5.10).



Scheme 5.10. Reaction between silyl enol ether **15a** and reference electrophiles **3a**, **3d** and **3g**. (ani) = 4-Methoxyphenyl; (mfa) = 4-(methyl(trifluoroethyl)amino)phenyl.

5.3.3 Kinetic Investigation

The reactions of silyl enol ether **15a** with electrophiles **3a-c** were performed in CH_2Cl_2 or CH_3CN at 20 °C and monitored by UV-Vis spectroscopy at the absorption maxima of the electrophile (listed in Table 5.2). To simplify the evaluation of the kinetic experiments nucleophiles were used in large excess (at least 9 equiv.), thus the concentration of this component remained constant throughout the reactions. The first-order rate constants k_{obs} were derived by least-squares fitting of the exponential function $A_t = A_0 \exp(-k_{\text{obs}}t) + C$ to the time-dependent absorbances A_t of the electrophile. Second-order rate constants were obtained as the slopes of plots of k_{obs} versus the concentration of the nucleophile (Figure 5.8).

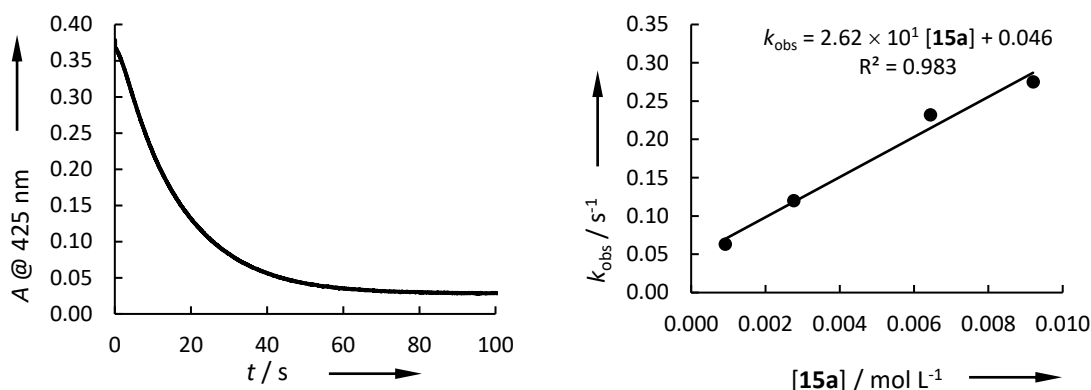
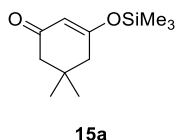


Figure 5.8. Exponential decay of absorbance A (at 425 nm) in the reaction of **15a** ($9.20 \times 10^{-4} \text{ mol L}^{-1}$) with **3c** ($4.38 \times 10^{-5} \text{ mol L}^{-1}$) in CH_2Cl_2 at 20°C (left). Plot of the first-order rate constants k_{obs} versus the concentration of **15a** (right).

Table 5.3. Second-order rate constants k_2 for the reactions of the silyl enol ether **15a** with reference electrophiles in CH_2Cl_2 at 20°C .

Nucleophile (N , S_N) ^[a]	Electrophile ^[b] (E)	k_2 / $\text{L mol}^{-1} \text{ s}^{-1}$
	3b-GaCl₄ (-1.36)	— ^[c]
	3c-BF₄ (-1.80)	2.62×10^1
	3d-BF₄ (-2.19)	1.15×10^1
	3f-BF₄ (-3.14)	4.26
		7.17×10^1 ^[d]
	3g-BF₄ (-3.85)	— ^[c]
	3h-BF₄ (-4.72)	— ^[c]

[a] For determination see Section 5.2.3. [b] From ref. ^[12a] [c] Rate constants could not be obtained, see text. [d] Measured in CH_3CN .

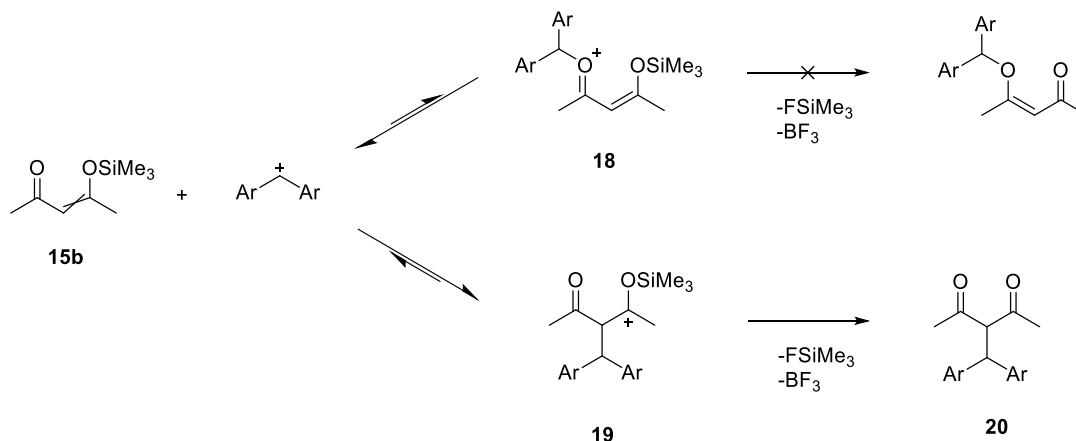


As shown in Table 5.3, the reactivity of **15a** is increased by a factor of 17 when moving from dichloromethane to more polar acetonitrile, indicating the impact of stability of intermediate cation on the nucleophilicity of the enol ether. Kinetic investigations of the reactions between **3b-GaCl₄** and enol ether **15a** showed significant deviations from first-order behavior, when the reaction was performed in CH_2Cl_2 with $[\text{3b}] = 2.26 \times 10^{-5} \text{ mol L}^{-1}$ and $[\text{15a}] = 3.01 \times 10^{-4} \div 1.51 \times 10^{-3} \text{ mol L}^{-1}$ (i.e. $[\text{15a}]/[\text{3b}]$ from 13 to 67 equivalents), therefore determination of second-order rate constant was not possible. Similar deviations were found for reactions between **15a** and cations **3d-BF₄** and **3h-BF₄** in CH_2Cl_2 (see Figures 5.10-12 in the Appendix). Experiments

between **3g** and **15a** in CH_2Cl_2 showed that obtained k_{obs} values did not correlate linearly with the concentration of the nucleophile (see Table 5.46 in the Experimental Section), thus one can expect a more comprehensive mechanism for the formation of the product **17c**. The results of the kinetic investigations of the reactions between **15c-d** and **3d** demonstrate the first order of these reactions with respect to the nucleophile (Tables 5.47-5.48 in the Experimental Section).

It was found, that reactions between ethers **15b-c** and carbocations **3c** and **3g** did not follow expected mechanism (e.g. Scheme 5.9). The obtained decays of the absorbance for certain electrophiles in reactions with high excess of **15b-c** (up to 200 equiv.) showed extreme deviations from the first-order kinetics (see Figures 5.13-14 in the Appendix). Addition of $\text{Bu}_4\text{N}^+\text{BCl}_4^-$ to exclude the counter-ion influence on the rate of desilylation did not improve the situation.

To explain such a behavior, one can suggest an equilibrium, leading to the fast formation of an unstable oxygen-adduct **18**, which does not transform further. At the same time reversible attack at the C-center of the nucleophile is slower but leads to an irreversible desilylation of the carbenium ion **19** to yield a desired diketone **20** (Scheme 5.11). In addition, as different stereo- and regioisomers (e.g. for **15c**, Scheme 5.9) present in a solution may have different nucleophilic reactivities, significant deviations from mono-exponential behavior were observed in the kinetic investigations of β -keto-silyl enol ethers **15**.



Scheme 5.11. Proposed mechanism for reaction between silyl enol ethers, derived from 1,3-dicarbonyl compounds (e.g. **15b**) and carbocations (e.g. benzhydrylium ion).

5.4 Conclusion

The rate constants for the reaction of C-nucleophiles, such as silyl enol ethers and enamines, with reference electrophiles, either indolylmethylium or benzhydrylium cations, in CH_2Cl_2 and CH_3CN followed the linear free-energy relationship (Equation 1), that allowed us to determine

nucleophilicity parameters and compare those with other nucleophiles. Variation of the substituent in the aromatic ring in the deoxybenzoin silyl enol ethers from $X = H$ to $X = OCH_3$ increases the reactivity by a factor of 7. Substitution at the beta position to siloxy group has greater influence, reducing the nucleophilicity by 1 (for $R = Me$) and 3 (for $R = Ph$) orders of magnitude. Addition of the planar aromatic moiety to the skeleton of the nucleophile has almost no effect on the N -parameter, though reduces the sensitivity towards electrophile strength.

With the obtained data it is possible to compare deoxybenzoin derived enolates, enamines and silyl enol ethers (Figure 5.9). In terms of nucleophilicity the reactivity of the anionic species is increased by 9 and 20 orders of magnitude from their neutral analogous enamines and silyl enol ethers, respectively. For the synthetic use of these species, the change in the reactivity should be considered: the high reaction rates with the electrophiles will increase the number of side-product and lead to loss of stereoselectivity.

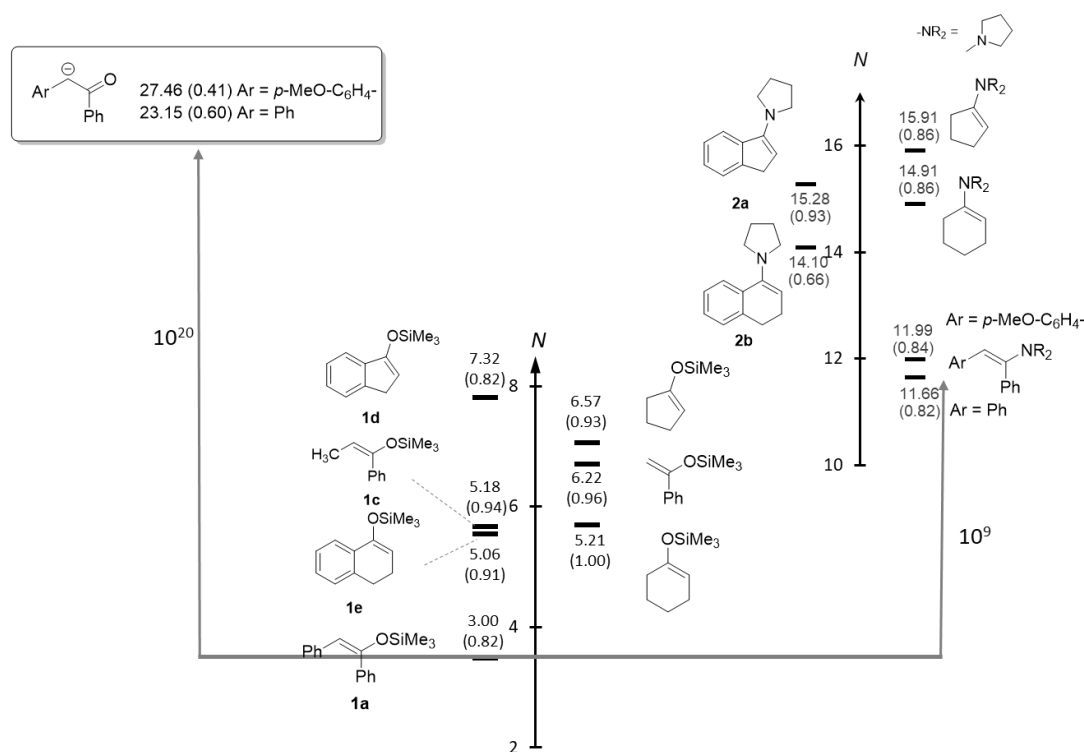


Figure 5.9. Comparison of the nucleophilicities of silyl enol ethers, enamines and enolates.

The addition of a planar aromatic moiety to cyclopentanone- and cyclohexanone-derived enamines and silyl enol ethers, while influencing the nucleophilicity only slightly, has shown a significant effect on the sensitivity parameter making these substrates less sensitive towards changes in the nature of the electrophile (except for **2a**). While the nucleophilicities of the enamines are increased in more polar solvent, it has almost no effect on the reactivity of the silyl enol ethers.

The kinetic parameters for the reactions between enamine **2a** and neutral electrophiles **3l-m** are in line with those obtained from reactions with benzhydrylium cations **3j-k**, thus allowing us to include these data in the correlation analysis. Therefore, the Equation (1) is applicable for characterization of reactions between neutral species as was shown before for the reactions of enamines with β -nitrostyrenes.^[21]

The reactions of β -keto-silyl enol ethers **15** with various reference electrophiles did not follow the second-order behavior and thus their reactivities cannot be described in terms of nucleophile-specific parameters using the Equation 1. Different reactivities of stereo- and regioisomers, produced by 1,5-sigmatropic rearrangements in unsymmetrical ethers cause significant deviations in the kinetic measurements.

5.5 Experimental Section

5.5.1 General

All reactions were performed in carefully dried Schlenk glassware in an atmosphere of dry nitrogen. The reactions were not optimized for high yields.

¹H NMR (400 MHz), ¹³C NMR (100 MHz), and ¹⁹F NMR spectra (376 MHz) were recorded on Varian NMR spectrometers in CD₃CN or CDCl₃. Chemical shifts in ppm refer to the solvent residual signal in CD₃CN (δ_{H} 1.94, δ_{C} 118.7 ppm) or CDCl₃ (δ_{H} 7.24, δ_{C} 77.2 ppm) as internal standard or to external CFC₃ (δ_{F} 0.0 ppm), respectively. The following abbreviations were used to describe the multiplicities of resonances: br s = broad singlet, s = singlet, d = doublet, t = triplet, q = quartet, sept = septet, m = multiplet. NMR signal assignments are based on additional 2D-NMR experiments (COSY, HSQC, HMBC, and NOESY). HRMS was performed on a Finnigan MAT 95 (EI) or a Thermo Finnigan LTQ FT (ESI) mass spectrometer.

Solvents. For the kinetic experiments commercially available acetonitrile (Acros, 99.9%, Extra Dry, AcroSeal) was used as received. Dichloromethane (Merck, *p.a.* grade) was successively treated with concentrated sulfuric acid, water, 10% NaHCO₃ solution, and water. After drying with CaCl₂, it was freshly distilled over CaH₂ under exclusion of moisture (N₂ atmosphere).

Chemicals. Phenylacetone, α -tetralone, indan-1-one, dimedone, acetylacetone, 2-acetylcyclopentanone, 2-acetylcyclohexanone, 2-(4-methoxyphenyl)acetyl chloride and pyrrolidine were purchased from Aldrich and used as received. Triethylamine was dried over KOH, distilled and stored in an atmosphere of dry nitrogen. Chlorotrimethylsilane was purchased from Aldrich and distilled before use.

Nucleophiles. Trimethylsilyl enol ethers **1a**,^[22] **1b**,^[23] **1c**,^[24] **1e**^[24] and **1d**^[25] were prepared by the general procedure from ref. ^[22] and distilled before use. 1-(3,4-dihydro-1-naphthyl)pyrrolidine **2b**^[26] and 1-(3H-inden-1-yl)pyrrolidine **2a**^[27] were prepared by the described procedures and distilled before use.

Reference Electrophiles. Benzhydrylium tetrafluoroborates **3f-o** and quinone methides **3p-q** were obtained from Nathalie Hampel. Indolylmethylum tetrafluoroborates **3c-e**^[15b] were synthesized according to literature procedures.

5.5.2 Synthesis of enol ethers 15a-d

5,5-Dimethyl-3-((trimethylsilyl)oxy)cyclohex-2-en-1-one (15a)

Dimedone (1.00 g, 7.13 mmol, 1 eq.) was dissolved in CH₂Cl₂ (20 ml) under nitrogen atmosphere and hexamethyldisilazane (2.00 ml, 9.54 mmol, 1.3 eq.) was added subsequently. Reaction was stirred for 1.5 h at room temperature and after removing volatiles under reduced pressure crude material was purified by distillation at 1.4 mbar / 123 °C.

¹H NMR data is in agreement with the literature.^[28]

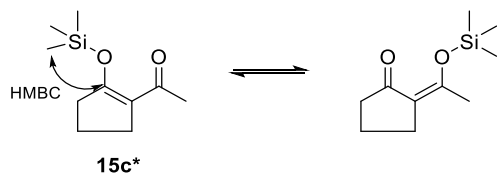
4-((Trimethylsilyl)oxy)pent-3-en-2-one (15b)

Acetylacetone (1.00 mL, 9.79 mmol, 1 eq.) was dissolved in Et₂O (20 ml), Et₃N (2.05 mL, 14.7 mmol, 1.5 eq.) and TMSCl (1.86 mL, 14.7 mmol, 1.5 eq.) were added simultaneously at 0 °C. Precipitate was formed and reaction was left stirring overnight at room temperature. Upon completion, suspension was filtered through the plug of celite and washed with Et₂O (3 × 25 mL). All volatiles were removed under reduced pressure and crude material was dried at 10 mbar at ambient temperature, followed by distillation at 10 mbar / 70 °C to give **15b** as 3:1 mixture of E and Z isomers respectively.

¹H NMR data is in agreement with the literature.^[29]

1-(2-((Trimethylsilyl)oxy)cyclopent-1-en-1-yl)ethan-1-one (**15c**)

Synthesized following the procedure for **15b** from 2-acetylcyclopentanone (1.00 mL, 8.27 mmol, 1 eq.), Et₃N (1.26 mL, 9.92 mmol, 1.2 eq.) and TMSCl (1.38 mL, 9.92 mmol, 1.2 eq.) and used without further purification. Obtained as 55:45 mixture of two isomers.



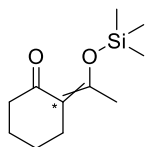
¹H NMR (599 MHz, CDCl₃) δ = 0.24 (s, 9H, -Si-CH₃, major isomer), 0.29 (s, 9H, -Si-CH₃, minor isomer), 1.75 – 1.84 (m, 4H, 2 × -CH₂-), 2.28-2.31 (m, 5H, -C(O)-CH₃, major isomer, -CH₂-), 2.32 (s, 3H, -C(O)-CH₃, minor isomer), 2.47 – 2.54 (m, 4H, 2 × -CH₂-), 2.54 – 2.60 (m, 2H, -CH₂-).

¹³C NMR (151 MHz, CDCl₃) δ = 0.9 (-Si-CH₃, major isomer), 1.1 (-Si-CH₃, minor isomer), 19.2 (-CH₂-), 19.5 (-CH₂-, -C(O)-CH₃, major isomer), 27.8 (-CH₂-), 28.3 (-CH₂-), 29.8 (-C(O)-CH₃, minor isomer), 36.2 (-CH₂-), 41.0 (-CH₂-), 118.2 (C-2), 119.3 (C-2'), 160.7 (C-1), 165.7 (C-1'), 195.8 (C-3, minor isomer), 207.8 (C-3, major isomer).

²⁹Si NMR (79 MHz, CDCl₃) δ = 19.8, 22.0.

1-(2-((Trimethylsilyl)oxy)cyclohex-1-en-1-yl)ethan-1-one (**15d**)

Synthesized following the procedure for **15b** from 2-acetylcyclohexanone (1.00 mL, 7.69 mmol, 1 eq.), Et₃N (1.07 mL, 8.46 mmol, 1.1 eq.) and TMSCl (1.29 mL, 9.23 mmol, 1.2 eq.) and distilled at 1 mbar / 96 °C.

**15d**

¹H NMR (400 MHz, CDCl₃) δ = 0.28 (m, 9H, -Si-CH₃),^[a] 1.49 – 1.58 (m, 2H, -CH₂-), 1.62 – 1.71 (m, 2H, -CH₂-), 2.18 – 2.29 (m, 4H, 2 × -CH₂-), 2.36 (m, 3H, -CH₃).^[a]

¹³C NMR (101 MHz, CDCl₃) δ = 1.4 (-Si-CH₃), 22.3 (-CH₂-), 23.1 (-CH₂-), 24.3 (-CH₂-), 32.4 (C-CH₂-), 32.7 (-CH₃), 118.6 (C*), 161.4 (-C-O-Si(CH₃)₃), 199.4 (-C=O).

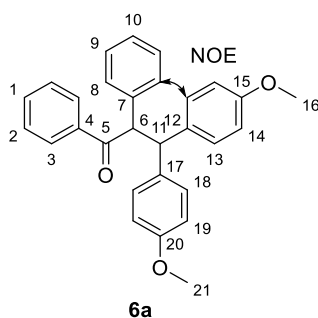
²⁹Si NMR (79 MHz, CDCl₃) δ = 18.7.

[a] Splitting of the resonance signal is splitting into two singlets may correspond to the mixture of two stereoisomers.

5.5.3 Products analysis

3,3-Bis(4-methoxyphenyl)-1,2-diphenylpropan-1-one (6a)

A solution of silyl enol ether **1a** (171 mg, 0.64 mmol, 2 eq.) in CH₂Cl₂ (5 mL) was added to solution of **3a** (100 mg, 0.32 mmol, 1 eq.) in CH₂Cl₂ (5 mL) and reaction mixture was stirred until disappearance of red color. After the removal of volatiles under reduced pressure, the crude material was purified by flash column chromatography on silica gel, using Et₂O/*n*-pentane (1/4) mixture as eluent (*R*_f = 0.57). **6a** obtained as white solid (128 mg, 94%)



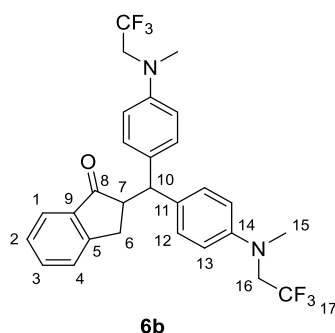
¹H NMR (400 MHz, CDCl₃) δ = 3.67 (s, 3H, H-16), 3.70 (s, 3H, H-21), 4.85 (d, ³*J* = 11.6 Hz, 1H, H-11), 5.37 (d, ³*J* = 11.6 Hz, 1H, H-6), 6.58 – 6.63 (m, 2H, H-14), 6.71 – 6.76 (m, 2H, H-19), 6.87 – 6.92 (m, 2H, H-13), 7.05 – 7.11 (m, 1H, H-10), 7.11 – 7.17 (m, 2H, H-9), 7.18 – 7.25 (m, 4H, H-18, H-8), 7.34 – 7.40 (m, 2H, H-2), 7.44 – 7.50 (m, 1H, H-1), 7.89 – 7.95 (m, 2H, H-3) ppm.

¹³C NMR (101 MHz, CDCl₃) δ = 53.5 (C-11), 55.2 (C-16/C-21), 55.3 (C-21/C-16), 58.8 (C-6), 113.6 (C-14), 114.1 (C-19), 127.1 (C-10), 128.6-128.7 (C-2, C-3, C-8, C-9), 129.2 (C-18), 129.5 (C-13), 133.0 (C-1), 135.2 (C-12), 136.1 (C-17), 137.4 (C-4/C-7), 137.5 (C-7/C-4), 157.8 (C-15), 157.9 (C-20), 199.1 (C-5) ppm.

HR-MS (EI, pos.) *m/z* calcd. for C₂₉H₂₆O₃ [M]⁺ 422.1876, found 422.1884.

2-(Bis(4-(methyl(2,2,2-trifluoroethyl)amino)phenyl)methyl)-2,3-dihydro-1H-inden-1-one (6b)

Silyl enol ether **1d** (100 mg, 0.49 mmol, 2 eq.) was dissolved in CH₃CN (5 mL) and added dropwise to a solution of indolyl cation **3g** (116 mg, 0.25 mmol, 1 eq.) in CH₃CN (5 mL) and stirred for 2 hours. After fading of yellow color reaction mixture was treated with aqueous ammonia (20 mL) and extracted with CH₂Cl₂ (3 × 25 mL). The combined organic layers were dried over MgSO₄ and the solvent was evaporated under reduced pressure. The crude product was purified by column chromatography using Et₂O/n-pentane (gradient from 1/9 to 1/4) mixture as eluent. **6b** was obtained as white solid (100 mg, 79% yield).



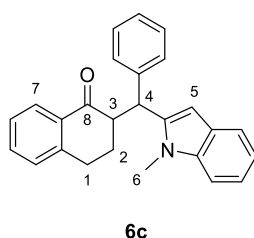
¹H NMR (400 MHz, CDCl₃) δ = 2.94 (s, 3H, H-15/H-15'), 3.05 (s, 3H, H-15'/H-15), 3.09 (dd, ¹J = 16.9 Hz, ³J = 3.9 Hz, 1H, H-6a), 3.32 – 3.47 (m, 2H, H-6b, H-7), 3.74 (q, ³J_{H-F} = 9.0 Hz, 2H, H-16/H-16'), 3.85 (q, ³J_{H-F} = 9.0 Hz, 2H, H-16'/H-16), 4.73 (d, ³J = 5.1 Hz, 1H, H-10), 6.60 (d, ³J = 8.8 Hz, 2H, H-13/H-13'), 6.79 (d, ³J = 8.8 Hz, 2H, H-13'/H-13), 6.97 (d, ³J = 8.7 Hz, 2H, H-12/H-12'), 7.22 (d, ³J = 8.7 Hz, 2H, H-12'/H-12), 7.30 – 7.40 (m, 2H, H-2, H-4), 7.50 – 7.56 (m, 1H, H-3), 7.74 (d, ³J = 7.6 Hz, 1H, H-1).

¹³C NMR (101 MHz, CDCl₃) δ = 30.9 (C-6), 39.1 (C-15/C-15'), 39.2 (C-15'/C-15), 49.2 (C-10), 52.0 (C-7), 54.5 (q, ²J_{C-F} = 32.6 Hz, C-16/C-16'), 54.6 (q, ²J_{C-F} = 32.5 Hz, C-16'/C-16), 112.6 (C-13/C-13'), 112.8 (C-13'/C-13), 123.9 (C-1), 125.6 (q, ¹J_{C-F} = 282.7 Hz, C-17/C-17'), 125.7 (q, ¹J_{C-F} = 282.7 Hz, C-17'/C-17), 126.5 (C-4), 127.3 (C-2), 129.2 (C-12/C-12'), 129.6 (C-12'/C-12), 132.0 (C-11/C-11'), 133.6 (C-11'/C-11), 134.6 (C-3), 137.0 (C-9), 147.1 (C-14/C-14'), 147.2 (C-14'/C-14), 153.7 (C-5), 207.2 (C-8).

HR-MS (EI, pos.) *m/z* calcd. for C₂₈H₂₆F₆N₂O [M]⁺⁺ 520.1944, found 520.1935

2-((1-Methyl-1H-indol-2-yl)(phenyl)methyl)-3,4-dihydronaphthalen-1(2H)-one (**6c**)

The reaction was performed following the above procedure for **6b** from **1e** (100 mg, 0.64 mmol, 2 eq.) and **3c** (70 mg, 0.23 mmol, 1 eq.). After column chromatography (silica gel, Et₂O/n-pentane, 1/9, *R_f* = 0.52) **6c** was obtained as 43/57 mixture of two diastereoisomers, pale-yellow solid (60 mg, 71%).



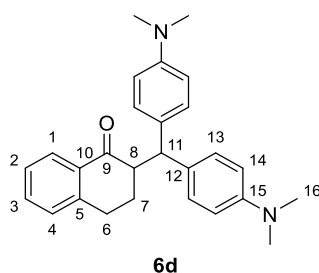
¹H NMR (400 MHz, CDCl₃, both isomers) δ = 1.83 – 1.96 (m, 1H, H-2a, minor isomer), 2.10 – 2.23 (m, 1H, H-2b, minor isomer), 2.26 – 2.42 (m, 2H, H-2, major isomer), 2.91 – 3.17 (m, 4H, H-1), 3.42 – 3.51 (m, 2H, H-3), 3.75 (s, 3H, H-6, major isomer), 3.81 (s, 3H, H-6, minor isomer), 5.16 (d, ³*J* = 7.0 Hz, 1H, H-4 major isomer), 5.27 (d, ³*J* = 6.2 Hz, 1H, H-4, minor isomer), 6.95 (s, 1H, H-5, major isomer), 6.97 – 7.09 (m, 2H, Ar-H), 7.14 (s, 1H, H-4, minor isomer), 7.16 – 7.52 (m, 28H, Ar-H), 7.99 – 8.05 (m, 2H, H-7).

¹³C NMR (101 MHz, CDCl₃, both isomers) δ = 26.5 (C-2, minor isomer), 26.6 (C-2, major isomer), 28.3 (C-1, minor isomer), 28.4 (C-1, major isomer), 32.8 (C-6, major isomer), 32.8 (C-6, minor isomer), 40.8 (C-4, minor isomer), 41.4 (C-4, major isomer), 52.5 (C-3), 52.9 (C-3*), 109.1, 109.1, 115.3, 116.6, 118.7, 118.9, 119.7, 120.1, 121.5, 121.6, 126.1, 126.2, 126.4, 126.6, 126.6, 127.6, 127.7, 127.8, 127.9, 128.2, 128.3, 128.6, 128.7, 129.2, 133.0, 133.1, 133.1, 137.0, 137.1, 142.5, 143.5, 143.6, 143.8, 198.9 (C-8, minor isomer), 199.1 (C-8, major isomer).

HR-MS (EI, pos.) *m/z* calcd. for C₂₆H₂₃NO [M]⁺ 365.1774, found 365.1775

2-(Bis(4-(dimethylamino)phenyl)methyl)-3,4-dihydronaphthalen-1(2H)-one (**6d**)

A solution of **2d** (50 mg, 0.25 mmol, 1.2 eq.) in CH₃CN (5 mL) was added dropwise to a solution of **3j** (70 mg, 0.21 mmol, 1 eq.) in CH₃CN (5 mL). After fading of the blue color, the reaction was treated with 2 M aqueous HCl (20 mL) and stirred for another 20 min following by extraction with CH₂Cl₂ (3 × 20 mL). The combined organic layers were dried over MgSO₄, and the solvent was evaporated under reduced pressure. The crude product was purified by column chromatography using Et₂O/n-pentane (1/4) mixture as eluent (*R*_f = 0.41). **6d** was obtained as a white solid (31 mg, 37% yield).



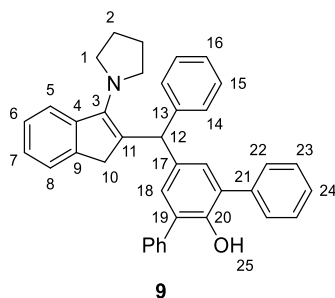
¹H NMR (599 MHz, CDCl₃) δ = 1.89 – 1.96 (m, 1H, H-7a), 2.17 – 2.23 (m, 1H, H-7b), 2.88 – 2.91 (m, 12H, H-16/H-16'), 2.91 – 2.95 (m, 1H, H-6a), 3.03 – 3.10 (m, 1H, H-6b), 3.38 (td, ³*J* = 8.6 Hz, ³*J* = 4.0 Hz, 1H, H-8), 4.52 (d, ³*J* = 8.6 Hz, 1H, H-11), 6.63 – 6.68 (m, 4H, H-14/H-14'), 7.09 – 7.15 (m, 4H, H-13/H-13'), 7.22 (d, ³*J* = 7.6 Hz, 1H, H-4), 7.25 – 7.30 (m, 1H, H-2), 7.45 (td, ³*J* = 7.5 Hz, ⁴*J* = 1.4 Hz, 1H, H-3), 7.93 (dd, ³*J* = 7.8 Hz, ⁴*J* = 1.0 Hz, 1H, H-1).

¹³C NMR (151 MHz, CDCl₃) δ = 26.5 (C-7), 27.4 (C-6), 40.7 (C-16/C-16'), 40.7 (C-16'/C-16), 47.8 (C-11), 51.8 (C-8), 112.7 (C-14/C14'), 112.7 (C-14'/C-14), 126.5 (C-2), 127.7 (C-1), 128.5 (C-13/C-13'), 128.6 (C-4), 129.3 (C-13'/C-13), 131.3 (C-12/C-12'), 132.0 (C-12'/C-12), 132.9 (C-3), 133.1 (C-10), 143.4 (C-5), 148.9 (C-15/C-15'), 149.0 (C-15'/C-15), 199.7 (C-9).

HR-MS (EI, pos.) *m/z* calcd. for C₂₇H₃₀N₂O [M]⁺⁺ 398.2353, found 398.2353

5'-(Phenyl(3-(pyrrolidin-1-yl)-1H-inden-2-yl)methyl)-[1,1':3',1''-terphenyl]-2'-ol (**9**)

The reaction was performed directly in the NMR tube by mixing **2a** (12 mg, 0.06 mmol, 1 eq.) and **3p** (20 mg, 0.06 mmol, 1 eq.) in CD₃CN (0.6 mL). The ¹H NMR spectrum was acquired 30 minutes after mixing and showed quantitative formation of **9**.



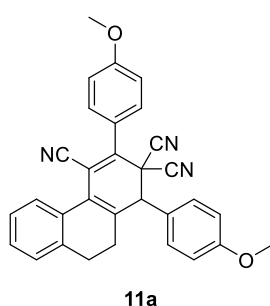
¹H NMR (400 MHz, CD₃CN) δ = 1.80 – 1.88 (m, 4H, H-2), 3.10 – 3.25 (m AB-system, 2H, H-10), 3.25 – 3.34 (m, 4H, H-1), 5.84 (s, 1H, H-12), 6.09 (bs, 1H, H-25), 7.01 (s, 2H, H-18), 7.07 (t, ³*J* = 7.4 Hz, 1H, H-ind), 7.15-7.21 (m, 2H, H-16), 7.22 – 7.35 (m, 7H, H-14), 7.36 – 7.44 (m, 5H, H-23, H-ind), 7.44 – 7.49 (m, 4H).

¹³C NMR (101 MHz, CD₃CN) δ = 26.3 (C-2), 38.5 (C-10), 49.6 (C-12), 51.5 (C-1), 121.1 (ind), 124.9, 125.1 (ind), 126.7 (C-16), 127.1, 128.3, 129.3, 129.5 (C-23), 129.9 (C-14), 130.4, 131.4, 134.1 (C-3), 137.7 (C-2), 139.3 (C-21), 143.7 (ind), 143.9, 145.7, 145.8, 149.2 (C-20).

HR-MS (EI, pos.) *m/z* calcd. for C₃₈H₃₃NO [M]⁺ 519.2557, found 519.2559

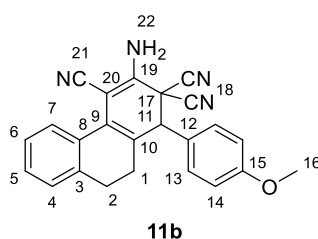
Reaction of enamine 2b with 3r

A solution of **2b** (50 mg, 0.25 mmol, 1.2 eq.) in CH₃CN (5 mL) was added dropwise to a solution of **3r** (40 mg, 0.21 mmol, 1 eq.) in CH₃CN (5 mL). After 5 min, the reaction mixture was treated with water and extracted with CH₂Cl₂ (3 × 20 mL). The combined organic layers were dried over MgSO₄ and the solvent was evaporated under reduced pressure. The crude product was purified by column chromatography using Et₂O/*n*-pentane (gradient from 1/10 to 1/1) mixture as eluent.

1,3-Bis(4-methoxyphenyl)-9,10-dihydrophenanthrene-2,2,4(1H)-tricarbonitrile (11a)

11a obtained as mixture with **11b** 3 to 7 respectively (4 mg, 8%)

HR-MS (EI, pos.) *m/z* calcd. for C₃₁H₂₃N₃O₂ [M]⁺⁺ 469,1785 found 469.1800

3-Amino-1-(4-methoxyphenyl)-9,10-dihydrophenanthrene-2,2,4(1H)-tricarbonitrile (11b)

11b was obtained as pale-yellow solid (15 mg, 38% yield)

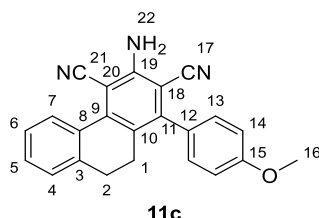
¹H NMR (599 MHz, CDCl₃) δ = 2.08 – 2.16 (m, 1H, H-1a), 2.41 – 2.51 (m, 1H, H-1b), 2.67 – 2.73 (m, 2H, H-2), 3.83 (s, 3H, H-16), 3.99 (s, 1H, H-11), 5.28 (s, 2H, H-22), 6.91 – 6.94 (m, 2H, H-14), 7.19 (d, ³*J* = 7.3 Hz, 1H, H-4), 7.27 (t, ³*J* = 7.0 Hz, 1H, H-5), 7.28 – 7.32 (m, 2H, H-13), 7.33 (t, ³*J* = 7.5 Hz, 1H, H-6), 7.64 (d, ³*J* = 7.7 Hz, 1H, H-7).

¹³C NMR (151 MHz, CDCl₃) δ = 26.9 (C-1), 28.7 (C-2), 42.3 (C-17), 52.2 (C-11), 55.3 (C-16), 80.1 (C-20), 111.2 (C-18), 112.5 (C-18), 114.7 (C-14), 116.5 (C-21), 122.6 (C-12), 124.6 (C-

7), 126.1 (C-9), 126.9 (C-6), 127.8 (C-4), 127.9 (C-10), 128.3 (C-5), 130.5 (C-8), 130.8 (C-13), 136.0 (C-3), 143.4 (C-19), 160.9 (C-15).

HR-MS (EI, pos.) m/z calcd. for $C_{24}H_{18}N_4O$ $[M]^{++}$ 378.1475, found 378.1456

3-Amino-1-(4-methoxyphenyl)-9,10-dihydrophenanthrene-2,4-dicarbonitrile (**11c**)



11c was obtained as yellow oil (12 mg, 33% yield).

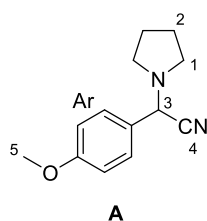
1H NMR (599 MHz, $CDCl_3$) δ = 2.46 – 2.50 (m, 2H, H-1), 2.62 – 2.66 (m, 2H, H-2), 3.88 (s, 3H, H-16), 5.23 (s, 2H, H-22), 7.00 – 7.04 (m, 2H, H-14), 7.23 – 7.26 (m, 2H, H-13), 7.27 – 7.29 (m, 1H, H-4), 7.37 – 7.44 (m, 2H, H-5, H-6), 8.24 – 8.28 (m, 1H, H-7).

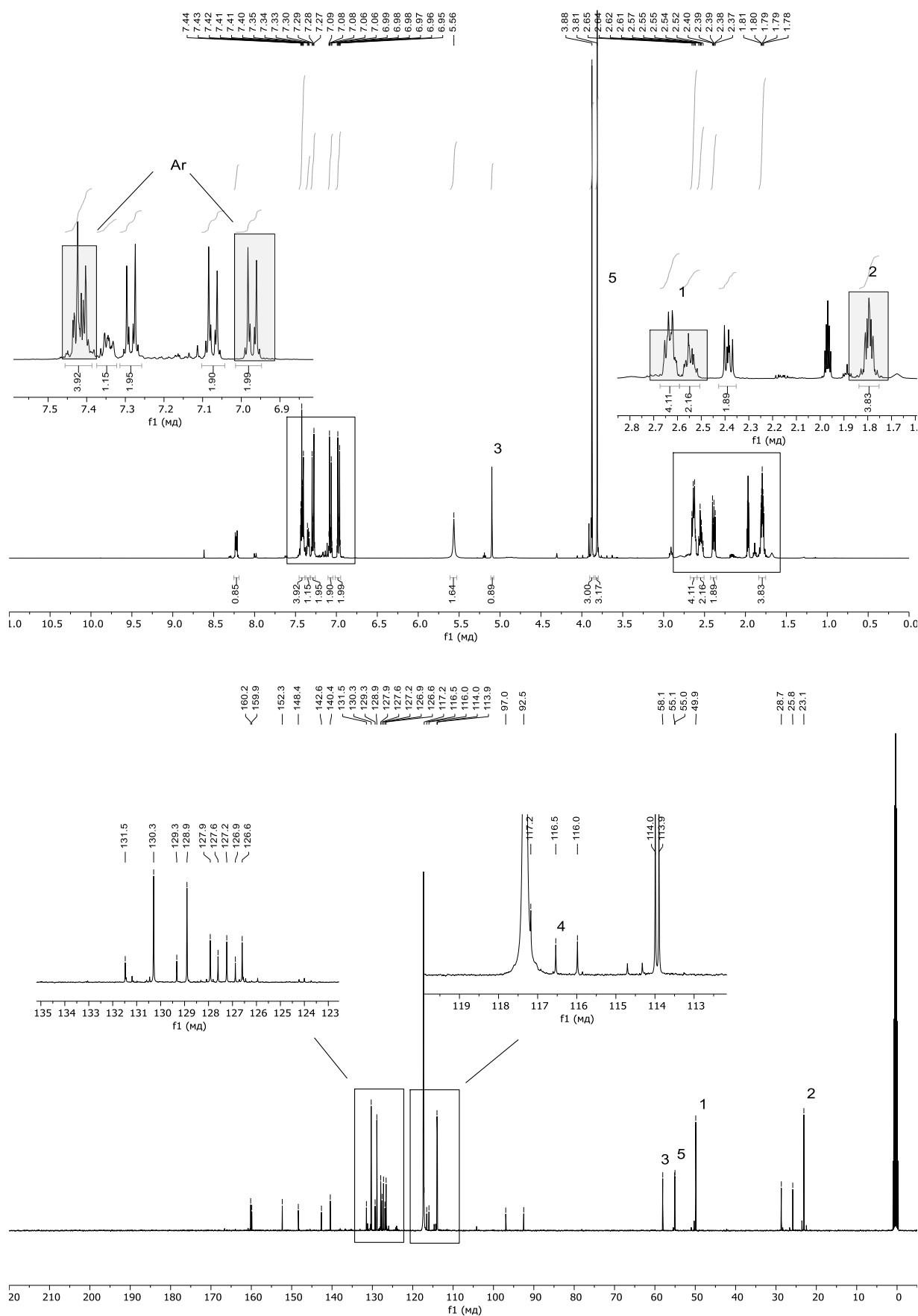
^{13}C NMR (151 MHz, $CDCl_3$) δ = 26.3 (C-1), 29.3 (C-2), 55.5 (C-16), 92.6 (C-20/C-18), 97.1 (C-18/C-20), 114.3 (C-14), 116.3 (C-21/C-17), 117.5 (C-17/C-21), 127.2 (C-6), 127.4 (C-7), 127.9 (C-10), 128.0 (C-4), 129.1 (C-12), 130.3 (C-13), 130.5 (C-5), 131.6 (C-8), 140.0 (C-3), 143.0 (C-9), 148.4 (C-11), 151.8 (C-19), 160.3 (C-15).

HR-MS (EI, pos.) m/z calcd. for $C_{23}H_{17}N_3O$ $[M]^{++}$ 351.1366, found 351.1375

In addition, the reaction was performed directly in the NMR tube by mixing **2b** (20 mg, 0.10 mmol, 1 eq.) and **3r** (18 mg, 0.10 mmol, 1 eq.) in CD_3CN (0.6 mL). The 1H NMR spectrum was acquired 1 hour after mixing and showed quantitative formation of **11c** and α -aminonitrile **A**.^[28]

2-(4-methoxyphenyl)-2-(pyrrolidin-1-yl)acetonitrile (**A**)^[17]



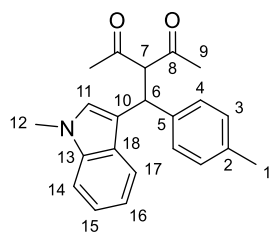


General procedure for product studies of silyl enol ethers 15a-d

A solution of the silyl enol ether (3 eq.) in CH_2Cl_2 (5 mL) was added dropwise to the solution of carbocation (1 eq.) in CH_2Cl_2 (5 mL). Reaction mixture was stirred at ambient temperature for 3 h or until fading the color of the cation. Upon completion, the solution was passed through a plug of Al_2O_3 (neutral) and concentrated under reduced pressure to give the crude product, which was further purified using column chromatography on SiO_2 .

3-((1-methyl-1H-indol-3-yl)(p-tolyl)methyl)pentane-2,4-dione (16a)

Following GP from **15b** (170 mg, 1 mmol) and **3d** (100 mg, 0.33 mmol) **16a** was obtained as pale-yellow solid in 75% (82 mg) yield.

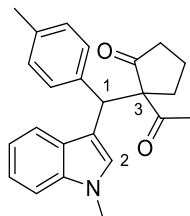
**16a**

^1H NMR (400 MHz, CDCl_3) δ = 1.95 (s, 3H, H-9/H-9'), 2.05 (s, 3H, H-9'/H-9), 2.24 (s, 3H, H-1), 3.73 (s, 3H, H-12), 4.63 (d, 3J = 12.3 Hz, 1H, H-7), 5.05 (d, 3J = 12.3 Hz, 1H, H-6), 6.95 (s, 1H, H-11), 7.01 – 7.06 (m, 3H, H-3, H-16), 7.14 – 7.25 (m, 4H, H-4, H-14, H-15), 7.53 (d, 3J = 8.0 Hz, 1H, H-17).

^{13}C NMR (101 MHz, CDCl_3) δ = 21.1 (C-1), 27.9 (C-9/C-9'), 31.4 (C-9'/C-9), 33.0 (C-12), 42.9 (C-6), 75.6 (C-7), 109.3 (C-14), 115.3 (C-14), 119.3 (C-10), 122.2 (C-17, C-16), 125.9 (C-15), 126.9 (C-11), 128.0 (C-18), 129.5 (C-4), 136.4 (C-3), 137.2 (C-13), 138.7 (C-5), 203.8 (C-8/C-8'), 204.4 (C-8'/C-8).

2-Acetyl-2-((1-methyl-1H-indol-3-yl)(p-tolyl)methyl)cyclopentan-1-one (**16b**)

Following GP from **15c** (200 mg, 1 mmol) and **3d** (100 mg, 0.33 mmol) **16b** was obtained as 5:2 mixture of two diastereoisomers as pale yellow solid in 84% (100 mg) yield.

**16b**

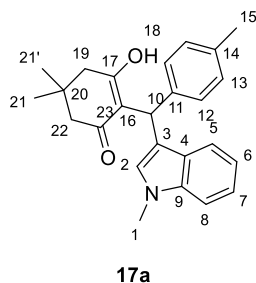
¹H NMR (400 MHz, CDCl₃, major isomer) δ = 1.64 – 1.85 (m, 2H, -CH₂-), 2.17-2.23 (s, 5H, -C(O)-CH₃, -CH₂-), 2.29 (s, 3H, Ar-CH₃), 3.04 – 3.18 (m, 2H, -CH₂-), 3.78 (s, 3H, N-CH₃), 5.56 (s, 1H, H-1), 6.90 (s, 1H, H-2), 6.96 – 7.12 (m, 4H, Ar-H), 7.16 – 7.31 (m, 4H, Ar-H).

¹H NMR (400 MHz, CDCl₃, minor isomer) δ = 1.36 – 1.45 (m, 2H, -CH₂-), 1.64 – 1.86 (m, 2H, -CH₂-), 2.16 (s, 3H, -C(O)-CH₃), 2.32 (s, 3H, Ar-CH₃), 3.72 (s, 3H, N-CH₃), 5.44 (s, 1H, H-1), 6.83 (s, 1H, H-2), 6.96 – 7.12 (m, 4H, Ar-H), 7.16 – 7.31 (m, 3H, Ar-H), 7.40 (d, ³J = 8.1 Hz, 1H, Ar-H).

¹³C NMR (101 MHz, CDCl₃, both isomers) δ = 19.8 (-CH₂-), 19.8 (-CH₂-), 21.1 (Ar-CH₃, major isomer), 21.1 (Ar-CH₃, minor isomer), 25.9 (-C(O)-CH₃, major isomer), 26.3 (-C(O)-CH₃, minor isomer), 26.5 (-CH₂-), 32.9 (N-CH₃, minor isomer), 33.0 (N-CH₃, major isomer), 39.3 (-CH₂-), 39.4 (-CH₂-), 46.5 (C-1, major isomer), 47.7 (C-1, minor isomer), 74.4 (C-3, minor isomer), 74.5 (C-3, major isomer), 109.1 (-CH-, Ar), 113.4 (-C-, Ar), 114.6 (-C-, Ar), 119.2 (Ar), 119.4 (Ar), 119.5 (Ar), 120.3 (Ar), 121.6 (Ar), 122.1 (Ar), 127.1 (Ar), 127.3 (Ar), 127.5 (Ar), 128.7 (Ar), 129.0 (Ar), 129.4 (Ar), 129.7 (Ar), 129.8 (Ar), 136.2 (Ar), 136.5 (Ar), 136.9 (Ar), 137.0 (Ar), 137.0 (Ar), 138.4 (Ar), 204.0 (-C(O)-CH₃, major isomer), 204.0 (-C(O)-CH₃, minor isomer), 215.3 (-C(O)-, major isomer), 215.9 (-C(O)-, minor isomer).

3-Hydroxy-5,5-dimethyl-2-((1-methyl-1H-indol-3-yl)(p-tolyl)methyl)cyclohex-2-en-1-one (17a)

Following GP from **15a** (231 mg, 1.09 mmol, 5 eq.) and **3d** (70 mg, 0.22 mmol, 1 eq.) **17a** was obtained as pale-yellow solid in 67% (55 mg) yield.



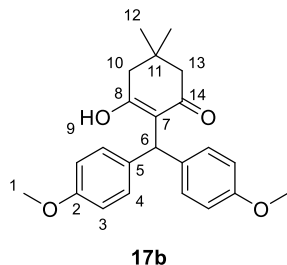
¹H NMR (599 MHz, CDCl₃) δ = 1.08 (s, 3H, H-21/H-21'), 1.12 (s, 3H, H-21'/H-21), 2.24 – 2.40 (m, 7H, H-15, H-19, H-22), 3.68 (s, 3H, H-1), 5.88 (s, 1H, H-10), 6.44 (d, J = 1.0, 1H, H-2), 6.98 (s, 1H, H-18), 7.08 – 7.12 (m, 1H, H-6), 7.15 (d, 3J = 8.0 Hz, 2H, H-13), 7.23 (d, 3J = 8.0 Hz, 2H, H-14), 7.25 – 7.32 (m, 2H, H-7, H-8), 7.45 (d, 3J = 8.0 Hz, 1H, H-5).

¹³C NMR (151 MHz, CDCl₃) δ = 21.2 (C-15), 28.4 (C-21/C-21'), 28.7 (C-21'/C-21), 31.9 (C-20), 32.9 (C-1), 36.5 (C-10), 43.1 (C-19), 50.8 (C-22), 109.6 (C-8), 115.8 (C-16), 116.7 (C-3), 119.8 (C-6), 119.9 (C-5), 123.0 (C-7), 127.2 (C-4), 128.0 (C-2), 128.3 (C-12), 129.5 (C-13), 136.3 (C-14), 138.2 (C-9), 138.8 (C-11), 171.4 (C-17), 197.1 (C-23).

HR-MS (EI, pos.) m/z calc. for C₂₅H₂₇NO₂ [M]⁺ 373.2036, found 373.2042

2-(Bis(4-methoxyphenyl)methyl)-3-hydroxy-5,5-dimethylcyclohex-2-en-1-one (17b)

Following GP from **15a** (203 mg, 0.96 mmol) and **3a-BF₄** (100 mg, 0.32 mmol) **17b** was obtained as pale-yellow solid in 82% (96 mg) yield.



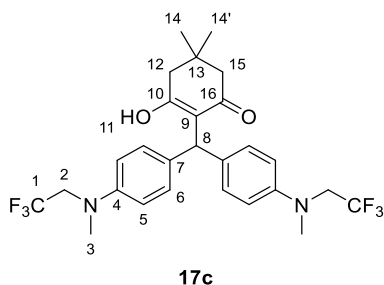
¹H NMR (599 MHz, CDCl₃) δ = 1.08 (s, 6H, H-12), 2.29 (s, 2H, H-13), 2.33 (s, 2H, H-10), 3.79 (s, 6H, H-1), 5.70 (s, 1H, H-6), 6.04 (s, 1H, H-9), 6.84 – 6.87 (m, 4H, H-3), 7.06 – 7.09 (m, 4H, H-4).

¹³C NMR (151 MHz, CDCl₃) δ = 28.5 (C-12), 31.9 (C-11), 43.0 (C-6), 43.3 (C-10), 50.6 (C-13), 55.4 (C-1), 114.6 (C-3), 117.7 (C-7), 129.8 (C-4), 133.8 (C-5), 158.7 (C-2), 170.4 (C-8), 197.3 (C-14).

HR-MS (EI, pos.) m/z calc. for C₂₃H₂₆O₄ [M]⁺⁺ 366.1826, found 366.1834

2-(Bis(4-(methyl(2,2,2-trifluoroethyl)amino)phenyl)methyl)-3-hydroxy-5,5-dimethylcyclohex-2-en-1-one (17c)

Following GP1 from **15a** (156 mg, 0.75 mmol, 5 eq.) and **3g** (70 mg, 0.15 mmol, 1 eq.) **17c** was obtained as pale yellow solid in 25% yield.



¹H NMR (800 MHz, CDCl₃) δ = 1.08 (s, 6H, H-14/H-14'), 2.28 (s, 2H, H-15), 2.33 (s, 2H, H-12), 3.03 (s, 6H, H-3), 3.83 (q, ³J_{H-F} = 8.9 Hz, 4H, H-2), 5.64 (s, 1H, H-8), 6.12 (s, 1H, H-11), 6.75 (d, ³J = 8.8 Hz, 4H, H-5), 7.05 (d, ³J = 8.5 Hz, 4H, H-6).

¹³C NMR (201 MHz, CDCl₃) δ = 28.5 (C-14/C-14'), 31.9 (C-13), 39.3 (C-3), 42.6 (C-8), 43.3 (C-12), 50.7 (C-15), 54.6 (q, ²J_{C-F} = 32.7 Hz, C-2), 113.4 (C-5), 117.7 (C-9), 125.7 (q, ¹J_{C-F} = 282.8 Hz, C-1), 129.6 (C-6), 131.3 (C-7), 147.8 (C-4), 170.3 (C-10), 197.3 (C-16).

¹⁹F NMR (376 MHz, CDCl₃) δ = -70.51 (t, ³J_{H-F} = 8.9 Hz).

HR-MS (EI, pos.) m/z calc. for C₂₇H₃₀F₆N₂O₂ [M]⁺⁺ 528.2206, found 528.2209

5.5.4 Kinetic experiments

5.5.4.1 Reactions of the Silyl Enol Ether 1a

Table 5.4. Kinetics of the reaction of **1a** with **3c** in CH₃CN (diode array spectrophotometer, 20 °C, at 413 nm)

[3c] / mol L ⁻¹	[1a] / mol L ⁻¹	[1a] / [3c]	<i>k</i> _{obs} / s ⁻¹
9.27 × 10 ⁻⁵	8.82 × 10 ⁻⁴	10	9.60 × 10 ⁻³
8.74 × 10 ⁻⁵	1.66 × 10 ⁻³	19	1.76 × 10 ⁻²
9.16 × 10 ⁻⁵	2.62 × 10 ⁻³	29	2.73 × 10 ⁻²
8.96 × 10 ⁻⁵	3.13 × 10 ⁻³	35	3.07 × 10 ⁻²

$$k_2 = 9.54 \text{ L mol}^{-1} \text{ s}^{-1}$$

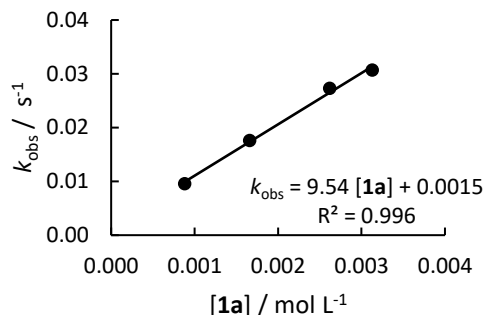


Table 5.5. Kinetics of the reaction of **1a** with **3d** in CH₃CN (diode array spectrophotometer, 20 °C, at 434 nm)

[3d] / mol L ⁻¹	[1a] / mol L ⁻¹	[1a] / [3d]	<i>k</i> _{obs} / s ⁻¹
6.41 × 10 ⁻⁵	5.64 × 10 ⁻⁴	9	5.60 × 10 ⁻³
6.77 × 10 ⁻⁵	1.19 × 10 ⁻³	18	7.90 × 10 ⁻³
6.37 × 10 ⁻⁵	1.68 × 10 ⁻³	26	1.07 × 10 ⁻²
6.80 × 10 ⁻⁵	2.39 × 10 ⁻³	35	1.39 × 10 ⁻²
6.40 × 10 ⁻⁵	2.81 × 10 ⁻³	44	1.62 × 10 ⁻²

$$k_2 = 4.77 \text{ L mol}^{-1} \text{ s}^{-1}$$

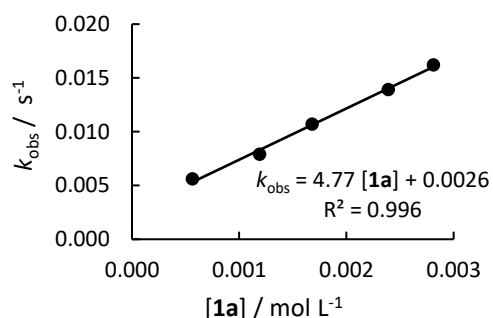
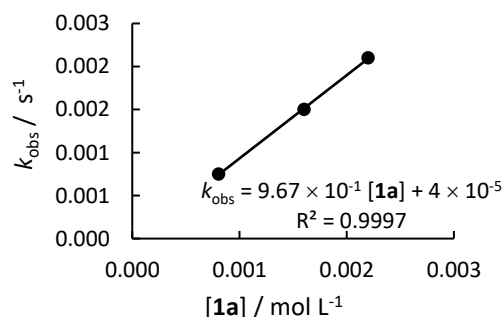


Table 5.6. Kinetics of the reaction of **1a** with **3e** in CH₃CN (diode array spectrophotometer, 20 °C, at 471 nm)

[3e] / mol L ⁻¹	[1a] / mol L ⁻¹	[1a] / [3e]	<i>k</i> _{obs} / s ⁻¹
6.85 × 10 ⁻⁵	8.07 × 10 ⁻⁴	12	7.50 × 10 ⁻⁴
6.80 × 10 ⁻⁵	1.60 × 10 ⁻³	24	1.50 × 10 ⁻³
6.23 × 10 ⁻⁵	2.20 × 10 ⁻³	35	2.10 × 10 ⁻³

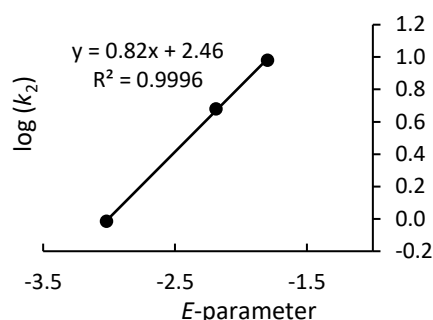
$$k_2 = 9.67 \times 10^{-1} \text{ L mol}^{-1} \text{ s}^{-1}$$



Determination of the Reactivity Parameters N and s_N for the silyl enol ether **1a** in CH_3CN **Table 5.7.** Rate constants for the reaction of **1a** with different electrophiles (20 °C)

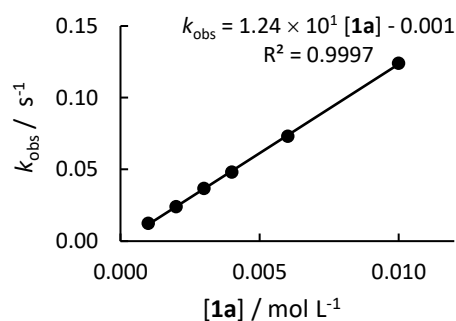
Electrophile	E	$k_2 / \text{L mol}^{-1} \text{s}^{-1}$	$\log k_2$
3c	-1.80	9.54	0.98
3d	-2.19	4.77	0.68
3e	-3.02	9.67×10^{-1}	-0.015

$$N = 3.00, s_N = 0.82$$

**Table 5.8.** Kinetics of the reaction of **1a** with **3c** in CH_2Cl_2 (stopped-flow, 20 °C, at 425 nm)

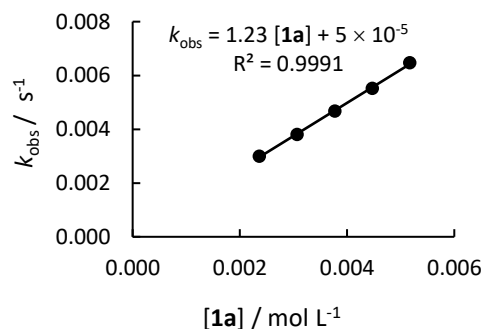
$[\mathbf{3c}] / \text{mol L}^{-1}$	$[\mathbf{1a}] / \text{mol L}^{-1}$	$[\mathbf{1a}] / [\mathbf{3c}]$	$k_{\text{obs}} / \text{s}^{-1}$
5.93×10^{-5}	1.00×10^{-3}	17	1.23×10^{-2}
5.93×10^{-5}	2.00×10^{-3}	34	2.40×10^{-2}
5.93×10^{-5}	3.00×10^{-3}	51	3.68×10^{-2}
5.93×10^{-5}	4.00×10^{-3}	67	4.81×10^{-2}
5.93×10^{-5}	6.01×10^{-3}	101	7.31×10^{-2}
5.93×10^{-5}	1.00×10^{-2}	169	1.24×10^{-1}

$$k_2 = 1.24 \times 10^1 \text{ L mol}^{-1} \text{s}^{-1}$$

**Table 5.9.** Kinetics of the reaction of **1a** with **3e** in CH_2Cl_2 (diode array spectrophotometer, 20 °C, at 492 nm)

$[\mathbf{3e}] / \text{mol L}^{-1}$	$[\mathbf{1a}] / \text{mol L}^{-1}$	$[\mathbf{1a}] / [\mathbf{3e}]$	$k_{\text{obs}} / \text{s}^{-1}$
5.08×10^{-5}	2.36×10^{-3}	46	3.00×10^{-3}
5.08×10^{-5}	3.07×10^{-3}	60	3.81×10^{-3}
5.07×10^{-5}	3.77×10^{-3}	74	4.67×10^{-3}
5.06×10^{-5}	4.47×10^{-3}	88	5.52×10^{-3}
5.06×10^{-5}	5.17×10^{-3}	102	6.47×10^{-3}

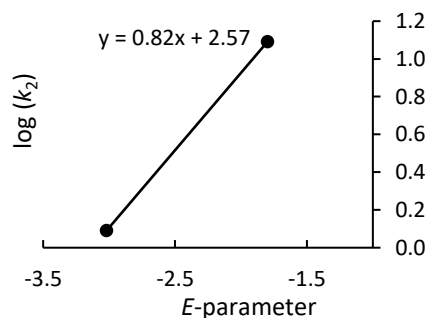
$$k_2 = 1.23 \text{ L mol}^{-1} \text{s}^{-1}$$



Determination of the Reactivity Parameters N and s_N for the silyl enol ether **1a** in CH_2Cl_2 **Table 5.10.** Rate constants for the reaction of **1a** with different electrophiles (20 °C)

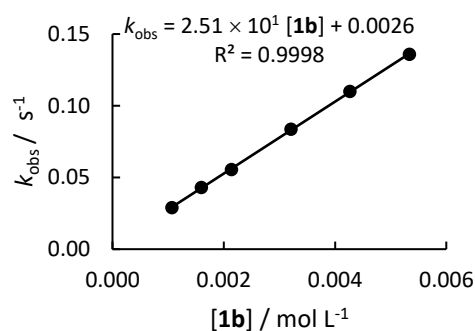
Electrophile	E	$k_2 / \text{L mol}^{-1} \text{s}^{-1}$	$\log k_2$
3c	-1.80	1.24×10^1	1.09
3e	-3.02	1.23	0.09

$$N = 3.13, s_N = 0.82$$

5.5.4.2 Reactions of the Silyl Enol Ether **1b****Table 5.11.** Kinetics of the reaction of **1b** with **3c** in CH_3CN (stopped-flow, 20 °C, at 413 nm)

$[\mathbf{3c}] / \text{mol L}^{-1}$	$[\mathbf{1b}] / \text{mol L}^{-1}$	$[\mathbf{1b}] / [\mathbf{3c}]$	$k_{\text{obs}} / \text{s}^{-1}$
7.16×10^{-5}	1.07×10^{-3}	15	2.91×10^{-2}
7.16×10^{-5}	1.60×10^{-3}	22	4.31×10^{-2}
7.16×10^{-5}	2.14×10^{-3}	30	5.56×10^{-2}
7.16×10^{-5}	3.21×10^{-3}	45	8.36×10^{-2}
7.16×10^{-5}	4.27×10^{-3}	60	1.10×10^{-1}
7.16×10^{-5}	5.34×10^{-3}	75	1.36×10^{-1}

$$k_2 = 2.51 \times 10^1 \text{ L mol}^{-1} \text{s}^{-1}$$

**Table 5.12.** Kinetics of the reaction of **1b** with **3d** in CH_3CN (stopped-flow, 20 °C, at 434 nm)

$[\mathbf{3d}] / \text{mol L}^{-1}$	$[\mathbf{1b}] / \text{mol L}^{-1}$	$[\mathbf{1b}] / [\mathbf{3d}]$	$k_{\text{obs}} / \text{s}^{-1}$
5.61×10^{-5}	2.14×10^{-3}	38	2.39×10^{-2}
5.61×10^{-5}	3.21×10^{-3}	57	3.51×10^{-2}
5.61×10^{-5}	4.27×10^{-3}	76	4.59×10^{-2}
5.61×10^{-5}	5.34×10^{-3}	95	5.59×10^{-2}

$$k_2 = 1.00 \times 10^1 \text{ L mol}^{-1} \text{s}^{-1}$$

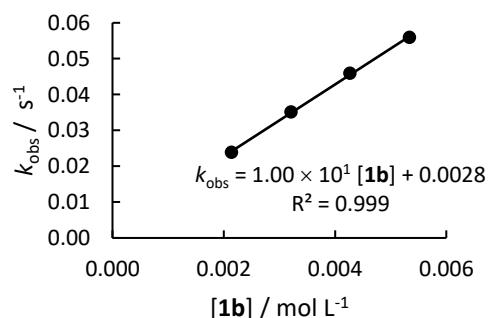
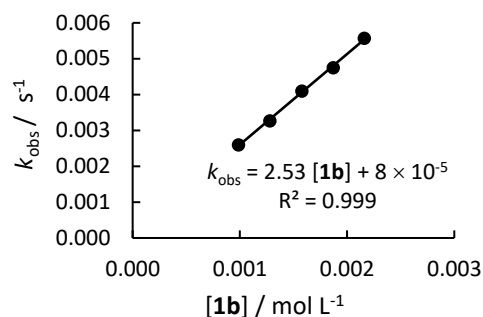


Table 5.13. Kinetics of the reaction of **1b** with **3e** in CH₃CN (stopped-flow, 20 °C, at 471 nm)

[3e] / mol L ⁻¹	[1b] / mol L ⁻¹	[1b] / [3e]	<i>k</i> _{obs} / s ⁻¹
5.33 × 10 ⁻⁵	1.41 × 10 ⁻³	19	2.60 × 10 ⁻³
5.32 × 10 ⁻⁵	1.83 × 10 ⁻³	24	3.27 × 10 ⁻³
5.31 × 10 ⁻⁵	2.25 × 10 ⁻³	30	4.10 × 10 ⁻³
5.31 × 10 ⁻⁵	2.67 × 10 ⁻³	35	4.75 × 10 ⁻³
5.30 × 10 ⁻⁵	3.08 × 10 ⁻³	41	5.57 × 10 ⁻³

$$k_2 = 2.53 \text{ L mol}^{-1} \text{ s}^{-1}$$

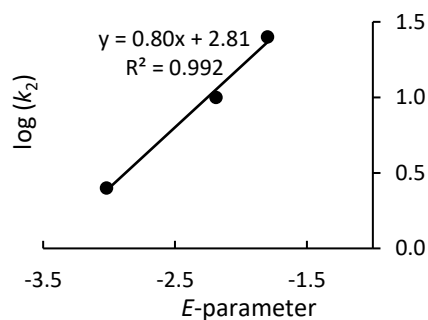


Determination of the Reactivity Parameters *N* and *s_N* for the silyl enol ether **1b** in CH₃CN

Table 5.14. Rate constants for the reaction of **1b** with different electrophiles (20 °C)

Electrophile	<i>E</i>	<i>k</i> ₂ / L mol ⁻¹ s ⁻¹	log <i>k</i> ₂
3c	-1.80	2.51 × 10 ¹	1.40
3d	-2.19	1.00 × 10 ¹	1.00
3e	-3.02	2.53	0.40

$$N = 3.51, s_N = 0.80$$



5.5.4.3 Reactions of the Silyl Enol Ether **1c**

Table 5.15. Kinetics of the reaction of **1c** with **3a** in CH₃CN (stopped-flow, 20 °C, at 413 nm)

[3c] / mol L ⁻¹	[1c] / mol L ⁻¹	[1c] / [3c]	<i>k</i> _{obs} / s ⁻¹
8.80 × 10 ⁻⁵	6.64 × 10 ⁻⁴	8	9.19 × 10 ⁻¹
8.80 × 10 ⁻⁵	1.99 × 10 ⁻³	23	2.77
8.80 × 10 ⁻⁵	2.66 × 10 ⁻³	30	3.61
8.80 × 10 ⁻⁵	3.32 × 10 ⁻³	38	4.46
8.80 × 10 ⁻⁵	3.98 × 10 ⁻³	45	5.33

$$k_2 = 1.32 \times 10^3 \text{ L mol}^{-1} \text{ s}^{-1}$$

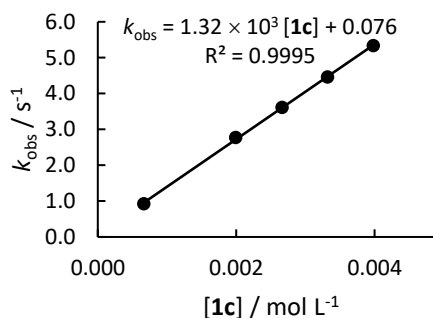
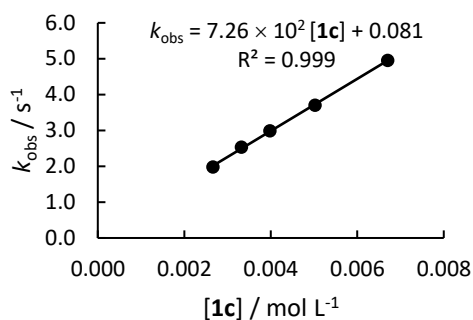


Table 5.16. Kinetics of the reaction of **1c** with **3d** in CH₃CN (stopped-flow, 20 °C, at 434 nm)

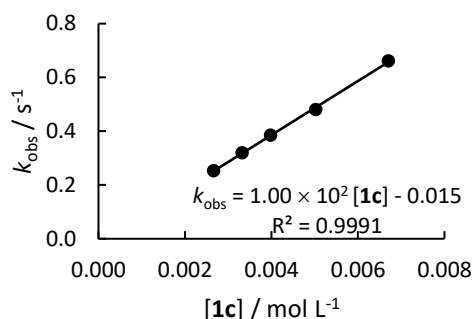
[3d] / mol L ⁻¹	[1c] / mol L ⁻¹	[1c] / [3d]	k _{obs} / s ⁻¹
7.37 × 10 ⁻⁵	2.66 × 10 ⁻³	36	1.98
7.37 × 10 ⁻⁵	3.32 × 10 ⁻³	45	2.53
7.37 × 10 ⁻⁵	3.98 × 10 ⁻³	54	2.99
7.37 × 10 ⁻⁵	5.02 × 10 ⁻³	68	3.70
7.37 × 10 ⁻⁵	6.70 × 10 ⁻³	91	4.95

$$k_2 = 7.26 \times 10^2 \text{ L mol}^{-1} \text{ s}^{-1}$$

**Table 5.17.** Kinetics of the reaction of **1c** with **3e** in CH₃CN (stopped-flow, 20 °C, at 471 nm)

[3e] / mol L ⁻¹	[1c] / mol L ⁻¹	[1c] / [3e]	k _{obs} / s ⁻¹
5.60 × 10 ⁻⁵	2.66 × 10 ⁻³	47	2.53 × 10 ⁻¹
5.60 × 10 ⁻⁵	3.32 × 10 ⁻³	59	3.19 × 10 ⁻¹
5.60 × 10 ⁻⁵	3.98 × 10 ⁻³	71	3.85 × 10 ⁻¹
5.60 × 10 ⁻⁵	5.02 × 10 ⁻³	90	4.80 × 10 ⁻¹
5.60 × 10 ⁻⁵	6.70 × 10 ⁻³	120	6.61 × 10 ⁻¹

$$k_2 = 1.00 \times 10^2 \text{ L mol}^{-1} \text{ s}^{-1}$$

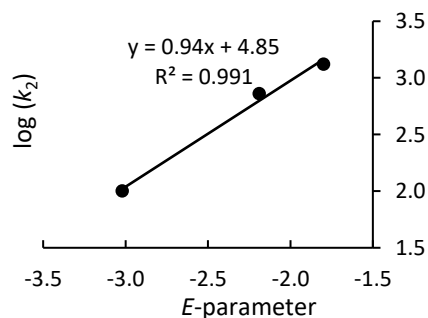


Determination of the Reactivity Parameters N and s_N for the silyl enol ether **1c** in CH₃CN

Table 5.18. Rate constants for the reaction of **1c** with different electrophiles (20 °C)

Electrophile	E	k ₂ / L mol ⁻¹ s ⁻¹	log k ₂
3c	-1.80	1.32 × 10 ³	1.25
3d	-2.19	7.26 × 10 ²	0.85
3e	-3.02	1.00 × 10 ²	0.25

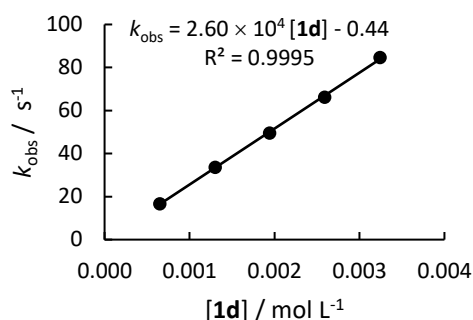
$$N = 5.16, s_N = 0.94$$



5.5.4.4 Reactions of the Silyl Enol Ether **1d****Table 5.19.** Kinetics of the reaction of **1d** with **3c** in CH₃CN (stopped-flow, 20 °C, at 413 nm)

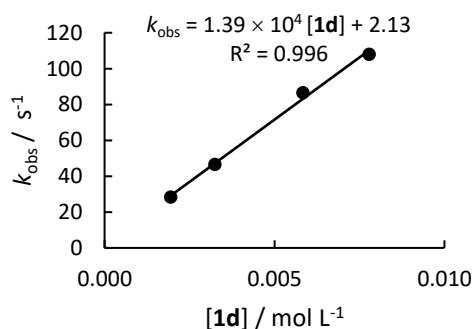
[3c] / mol L ⁻¹	[1d] / mol L ⁻¹	[1d] / [3c]	<i>k</i> _{obs} / s ⁻¹
1.13 × 10 ⁻⁴	6.48 × 10 ⁻⁴	6	1.67 × 10 ¹
1.09 × 10 ⁻⁴	1.30 × 10 ⁻³	12	3.36 × 10 ¹
1.06 × 10 ⁻⁴	1.94 × 10 ⁻³	18	4.95 × 10 ¹
1.04 × 10 ⁻⁴	2.59 × 10 ⁻³	25	6.62 × 10 ¹
9.96 × 10 ⁻⁵	3.24 × 10 ⁻³	33	8.46 × 10 ¹

$$k_2 = 2.60 \times 10^4 \text{ L mol}^{-1} \text{ s}^{-1}$$

**Table 5.20.** Kinetics of the reaction of **1d** with **3d** in CH₃CN (stopped-flow, 20 °C, at 434 nm)

[3d] / mol L ⁻¹	[1d] / mol L ⁻¹	[1d] / [3d]	<i>k</i> _{obs} / s ⁻¹
6.41 × 10 ⁻⁵	1.94 × 10 ⁻³	30	2.84 × 10 ¹
6.41 × 10 ⁻⁵	3.24 × 10 ⁻³	51	4.65 × 10 ¹
6.41 × 10 ⁻⁵	5.83 × 10 ⁻³	91	8.65 × 10 ¹
6.41 × 10 ⁻⁵	7.78 × 10 ⁻³	121	1.08 × 10 ²

$$k_2 = 1.39 \times 10^4 \text{ L mol}^{-1} \text{ s}^{-1}$$

**Table 5.21.** Kinetics of the reaction of **1d** with **3e** in CH₃CN (stopped-flow, 20 °C, at 471 nm)

[3e] / mol L ⁻¹	[1d] / mol L ⁻¹	[1d] / [3e]	<i>k</i> _{obs} / s ⁻¹
8.87 × 10 ⁻⁵	1.31 × 10 ⁻³	15	6.14
8.52 × 10 ⁻⁵	2.62 × 10 ⁻³	31	1.25 × 10 ¹
8.45 × 10 ⁻⁵	3.92 × 10 ⁻³	46	1.87 × 10 ¹
8.17 × 10 ⁻⁵	5.23 × 10 ⁻³	64	2.54 × 10 ¹
7.96 × 10 ⁻⁵	6.54 × 10 ⁻³	82	3.20 × 10 ¹

$$k_2 = 4.94 \times 10^3 \text{ L mol}^{-1} \text{ s}^{-1}$$

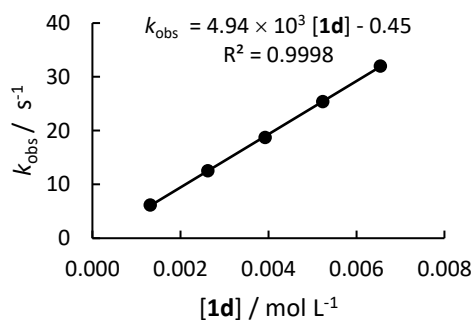
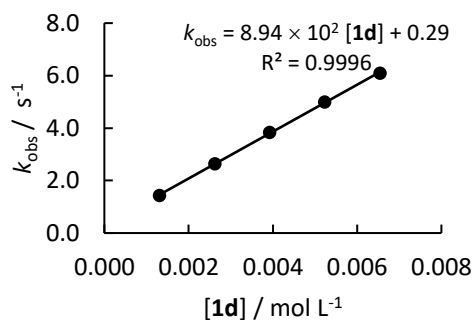


Table 5.22. Kinetics of the reaction of **1d** with **3g** in CH₃CN (stopped-flow, 20 °C, at 586 nm)

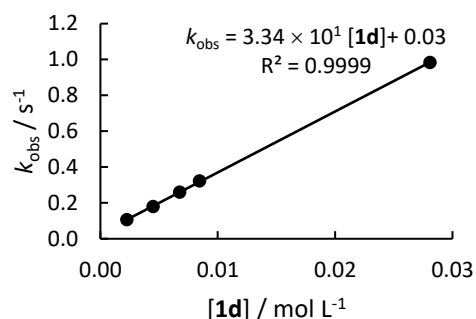
[3g] / mol L ⁻¹	[1d] / mol L ⁻¹	[1d] / [3g]	<i>k</i> _{obs} / s ⁻¹
3.43 × 10 ⁻⁵	1.31 × 10 ⁻³	38	1.43
3.43 × 10 ⁻⁵	2.62 × 10 ⁻³	76	2.64
3.43 × 10 ⁻⁵	3.92 × 10 ⁻³	115	3.83
3.43 × 10 ⁻⁵	5.23 × 10 ⁻³	153	5.00
3.43 × 10 ⁻⁵	6.54 × 10 ⁻³	191	6.09

$$k_2 = 8.94 \times 10^2 \text{ L mol}^{-1} \text{ s}^{-1}$$

**Table 5.23.** Kinetics of the reaction of **1d** with **3i** in CH₃CN (stopped-flow, 20 °C, at 612 nm)

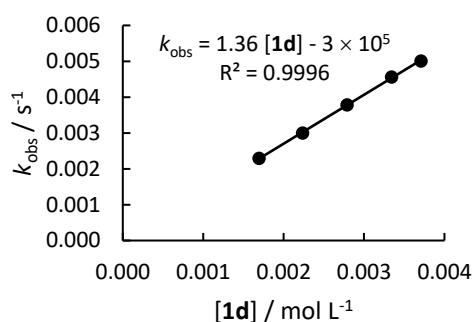
[3i] / mol L ⁻¹	[1d] / mol L ⁻¹	[1d] / [3i]	<i>k</i> _{obs} / s ⁻¹
1.78 × 10 ⁻⁵	2.25 × 10 ⁻³	126	1.05 × 10 ⁻¹
1.78 × 10 ⁻⁵	4.49 × 10 ⁻³	253	1.79 × 10 ⁻¹
1.78 × 10 ⁻⁵	6.74 × 10 ⁻³	379	2.60 × 10 ⁻¹
1.78 × 10 ⁻⁵	8.42 × 10 ⁻³	474	3.22 × 10 ⁻¹
1.78 × 10 ⁻⁵	2.81 × 10 ⁻²	1581	9.83 × 10 ⁻¹

$$k_2 = 3.34 \times 10^1 \text{ L mol}^{-1} \text{ s}^{-1}$$

**Table 5.24.** Kinetics of the reaction of **1d** with **3j** in CH₃CN (stopped-flow, 20 °C, at 605 nm)

[3j] / mol L ⁻¹	[1d] / mol L ⁻¹	[1d] / [3j]	<i>k</i> _{obs} / s ⁻¹
1.72 × 10 ⁻⁵	1.69 × 10 ⁻³	98	2.29 × 10 ⁻³
1.89 × 10 ⁻⁵	2.23 × 10 ⁻³	118	3.00 × 10 ⁻³
1.89 × 10 ⁻⁵	2.79 × 10 ⁻³	148	3.78 × 10 ⁻³
1.88 × 10 ⁻⁵	3.34 × 10 ⁻³	177	4.56 × 10 ⁻³
1.71 × 10 ⁻⁵	3.71 × 10 ⁻³	217	5.01 × 10 ⁻³

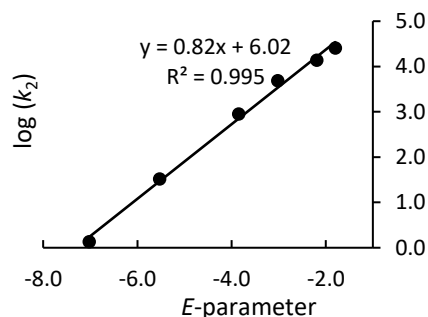
$$k_2 = 1.36 \text{ L mol}^{-1} \text{ s}^{-1}$$



Determination of the Reactivity Parameters N and s_N for the silyl enol ether **1d** in CH_3CN **Table 5.25.** Rate constants for the reaction of **1d** with different electrophiles (20 °C)

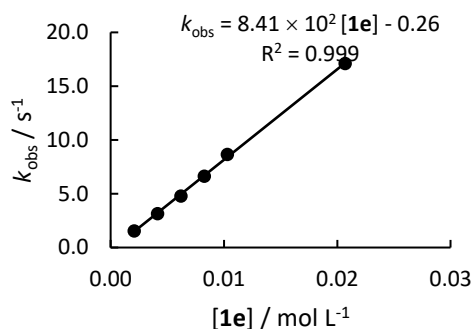
Electrophile	E	$k_2 / \text{L mol}^{-1} \text{s}^{-1}$	$\log k_2$
3c	-1.80	2.60×10^4	4.41
3d	-2.19	1.39×10^4	4.14
3e	-3.02	4.94×10^3	3.69
3g	-3.85	8.94×10^2	2.95
3i	-5.53	3.34×10^1	1.52
3j	-7.02	1.36	0.13

$$N = 7.34, s_N = 0.82$$

5.5.4.5 Reactions of the Silyl Enol Ether **1e****Table 5.26.** Kinetics of the reaction of **1e** with **3c** in CH_3CN (stopped-flow, 20 °C, at 413 nm)

$[\mathbf{3c}] / \text{mol L}^{-1}$	$[\mathbf{1e}] / \text{mol L}^{-1}$	$[\mathbf{1e}] / [\mathbf{3c}]$	$k_{\text{obs}} / \text{s}^{-1}$
2.34×10^{-4}	2.07×10^{-3}	9	1.55
2.34×10^{-4}	4.13×10^{-3}	18	3.15
2.34×10^{-4}	6.20×10^{-3}	26	4.80
2.34×10^{-4}	8.27×10^{-3}	35	6.65
2.34×10^{-4}	1.03×10^{-2}	44	8.67
2.34×10^{-4}	2.07×10^{-2}	88	1.71×10^1

$$k_2 = 8.41 \times 10^2 \text{ L mol}^{-1} \text{s}^{-1}$$

**Table 5.27.** Kinetics of the reaction of **1e** with **3d** in CH_3CN (stopped-flow, 20 °C, at 434 nm)

$[\mathbf{3d}] / \text{mol L}^{-1}$	$[\mathbf{1e}] / \text{mol L}^{-1}$	$[\mathbf{1e}] / [\mathbf{3d}]$	$k_{\text{obs}} / \text{s}^{-1}$
7.69×10^{-5}	2.96×10^{-3}	39	1.11
7.69×10^{-5}	4.44×10^{-3}	58	1.66
7.69×10^{-5}	5.91×10^{-3}	77	2.17
7.69×10^{-5}	7.39×10^{-3}	96	2.72
7.69×10^{-5}	2.46×10^{-2}	320	8.76

$$k_2 = 3.53 \times 10^2 \text{ L mol}^{-1} \text{s}^{-1}$$

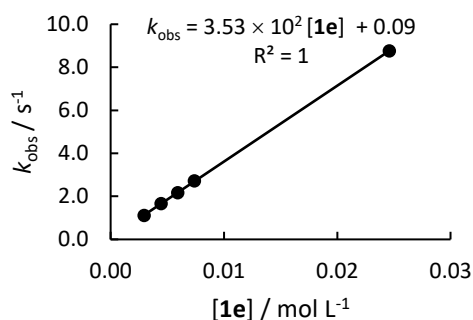
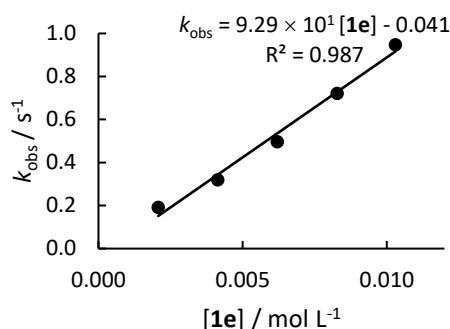


Table 5.28. Kinetics of the reaction of **1e** with **3e** in CH₃CN (stopped-flow, 20 °C, at 471 nm)

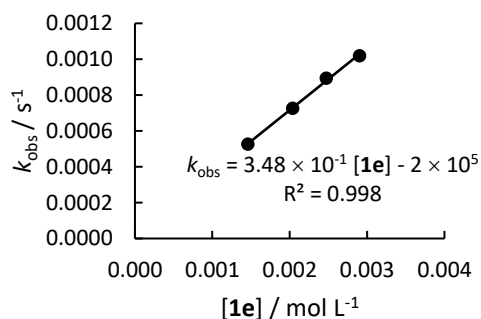
[3e] / mol L ⁻¹	[1e] / mol L ⁻¹	[1e] / [3e]	<i>k</i> _{obs} / s ⁻¹
1.10 × 10 ⁻⁴	2.07 × 10 ⁻³	19	1.91 × 10 ⁻¹
1.10 × 10 ⁻⁴	4.13 × 10 ⁻³	37	3.19 × 10 ⁻¹
1.10 × 10 ⁻⁴	6.20 × 10 ⁻³	56	4.96 × 10 ⁻¹
1.10 × 10 ⁻⁴	8.27 × 10 ⁻³	75	7.21 × 10 ⁻¹
1.10 × 10 ⁻⁴	1.03 × 10 ⁻²	93	9.47 × 10 ⁻¹

$$k_2 = 9.29 \times 10^1 \text{ L mol}^{-1} \text{ s}^{-1}$$

**Table 5.29.** Kinetics of the reaction of **1e** with **3i** in CH₃CN (stopped-flow, 20 °C, at 612 nm)

[3i] / mol L ⁻¹	[1e] / mol L ⁻¹	[1e] / [3i]	<i>k</i> _{obs} / s ⁻¹
2.84 × 10 ⁻⁵	1.46 × 10 ⁻³	51	5.26 × 10 ⁻⁴
2.83 × 10 ⁻⁵	2.04 × 10 ⁻³	72	7.26 × 10 ⁻⁴
2.83 × 10 ⁻⁵	2.47 × 10 ⁻³	87	8.94 × 10 ⁻⁴
2.82 × 10 ⁻⁵	2.90 × 10 ⁻³	103	1.02 × 10 ⁻³

$$k_2 = 3.48 \times 10^{-1} \text{ L mol}^{-1} \text{ s}^{-1}$$

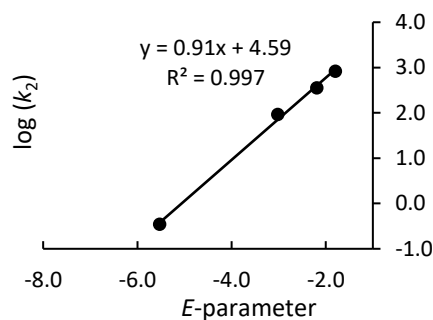


Determination of the Reactivity Parameters *N* and *s_N* for the silyl enol ether **1e** in CH₃CN

Table 5.30. Rate constants for the reaction of **1e** with different electrophiles (20 °C)

Electrophile	<i>E</i>	<i>k</i> ₂ / L mol ⁻¹ s ⁻¹	log <i>k</i> ₂
3c	-1.80	8.41 × 10 ²	2.92
3d	-2.19	3.53 × 10 ²	2.55
3e	-3.02	9.29 × 10 ¹	1.97
3i	-5.53	3.48 × 10 ⁻¹	-0.46

$$N = 5.04, s_N = 0.91$$

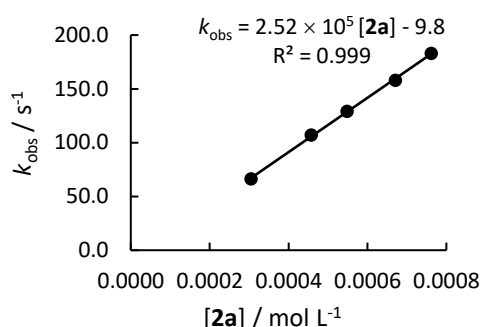


5.5.4.5 Reactions of the Enamine 2a

Table 5.31. Kinetics of the reaction of **2a** with **3l** in CH₃CN (stopped-flow, 20 °C, at 635 nm)

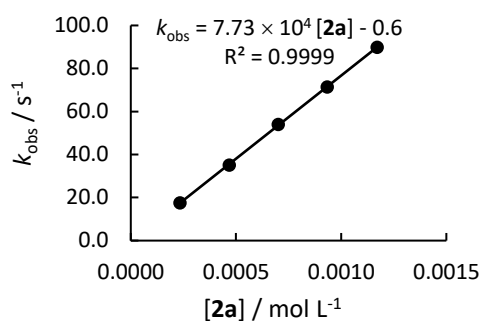
[3l] / mol L ⁻¹	[2a] / mol L ⁻¹	[2a] / [3l]	<i>k</i> _{obs} / s ⁻¹
7.48 × 10 ⁻⁶	3.05 × 10 ⁻⁴	41	6.63 × 10 ¹
7.48 × 10 ⁻⁶	4.57 × 10 ⁻⁴	61	1.07 × 10 ²
7.48 × 10 ⁻⁶	5.48 × 10 ⁻⁴	73	1.29 × 10 ²
7.48 × 10 ⁻⁶	6.70 × 10 ⁻⁴	90	1.58 × 10 ²
7.48 × 10 ⁻⁶	7.62 × 10 ⁻⁴	102	1.83 × 10 ²

$$k_2 = 2.52 \times 10^5 \text{ L mol}^{-1} \text{ s}^{-1}$$

**Table 5.32.** Kinetics of the reaction of **2a** with **3m** in CH₃CN (stopped-flow, 20 °C, at 632 nm)

[3m] / mol L ⁻¹	[2a] / mol L ⁻¹	[2a] / [3m]	<i>k</i> _{obs} / s ⁻¹
7.59 × 10 ⁻⁶	2.33 × 10 ⁻⁴	31	1.75 × 10 ¹
7.59 × 10 ⁻⁶	4.67 × 10 ⁻⁴	62	3.51 × 10 ¹
7.59 × 10 ⁻⁶	7.00 × 10 ⁻⁴	92	5.40 × 10 ¹
7.59 × 10 ⁻⁶	9.33 × 10 ⁻⁴	123	7.14 × 10 ¹
7.59 × 10 ⁻⁶	1.17 × 10 ⁻³	154	8.98 × 10 ¹

$$k_2 = 7.73 \times 10^4 \text{ L mol}^{-1} \text{ s}^{-1}$$

**Table 5.33.** Kinetics of the reaction of **2a** with **3p** in CH₃CN (stopped-flow, 20 °C, at 384 nm)

[3p] / mol L ⁻¹	[2a] / mol L ⁻¹	[2a] / [3p]	<i>k</i> _{obs} / s ⁻¹
2.47 × 10 ⁻⁵	2.33 × 10 ⁻⁴	9	3.93 × 10 ⁻¹
2.47 × 10 ⁻⁵	4.67 × 10 ⁻⁴	19	8.07 × 10 ⁻¹
2.47 × 10 ⁻⁵	7.00 × 10 ⁻⁴	28	1.18
2.47 × 10 ⁻⁵	9.33 × 10 ⁻⁴	38	1.54
2.47 × 10 ⁻⁵	1.17 × 10 ⁻³	47	1.86

$$k_2 = 1.57 \times 10^3 \text{ L mol}^{-1} \text{ s}^{-1}$$

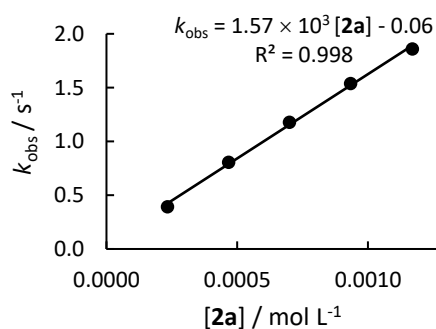
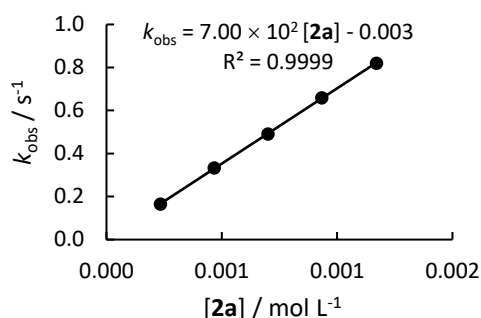


Table 5.34. Kinetics of the reaction of **2a** with **3q** in CH₃CN (stopped-flow, 20 °C, at 414 nm)

[3q] / mol L ⁻¹	[2a] / mol L ⁻¹	[2a] / [3q]	<i>k</i> _{obs} / s ⁻¹
2.88 × 10 ⁻⁵	2.33 × 10 ⁻⁴	8	1.64 × 10 ⁻¹
2.88 × 10 ⁻⁵	4.67 × 10 ⁻⁴	16	3.33 × 10 ⁻¹
2.88 × 10 ⁻⁵	7.00 × 10 ⁻⁴	24	4.91 × 10 ⁻¹
2.88 × 10 ⁻⁵	9.33 × 10 ⁻⁴	32	6.59 × 10 ⁻¹
2.88 × 10 ⁻⁵	1.17 × 10 ⁻³	40	8.20 × 10 ⁻¹

$$k_2 = 7.00 \times 10^2 \text{ L mol}^{-1} \text{ s}^{-1}$$

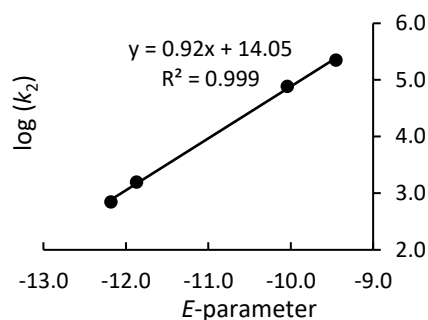


Determination of the Reactivity Parameters *N* and *s_N* for the enamine **2a** in CH₃CN

Table 5.35. Rate constants for the reaction of **2a** with different electrophiles (20 °C)

Electrophile	<i>E</i>	<i>k</i> ₂ / L mol ⁻¹ s ⁻¹	log <i>k</i> ₂
3m	-9.45	2.23 × 10 ⁵	4.64
3o	-10.04	7.73 × 10 ⁴	4.24
3p	-11.87	1.57 × 10 ³	3.95
3q	-12.18	7.00 × 10 ²	3.48

$$N = 15.27, s_N = 0.92$$



5.5.4.6 Reactions of the Enamine **2b**

Table 5.36. Kinetics of the reaction of **2b** with **3j** in CH₃CN (stopped-flow, 20 °C, at 605 nm)

[3j] / mol L ⁻¹	[2b] / mol L ⁻¹	[2b] / [3j]	<i>k</i> _{obs} / s ⁻¹
8.79 × 10 ⁻⁶	4.87 × 10 ⁻⁴	55	2.15 × 10 ¹
8.72 × 10 ⁻⁶	7.31 × 10 ⁻⁴	84	3.31 × 10 ¹
8.51 × 10 ⁻⁶	9.74 × 10 ⁻⁴	114	4.42 × 10 ¹
8.51 × 10 ⁻⁶	1.22 × 10 ⁻³	143	5.38 × 10 ¹
8.37 × 10 ⁻⁶	1.46 × 10 ⁻³	175	6.40 × 10 ¹

$$k_2 = 4.34 \times 10^4 \text{ L mol}^{-1} \text{ s}^{-1}$$

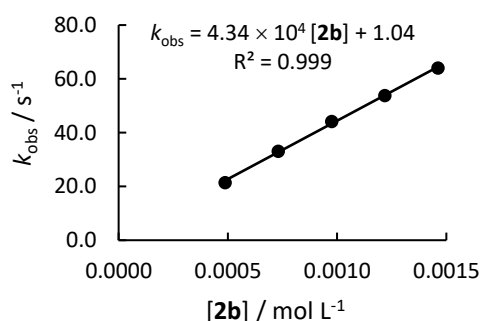
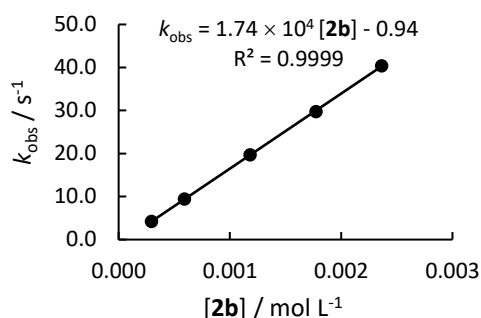


Table 5.37. Kinetics of the reaction of **2b** with **3k** in CH₃CN (stopped-flow, 20 °C, at 612 nm)

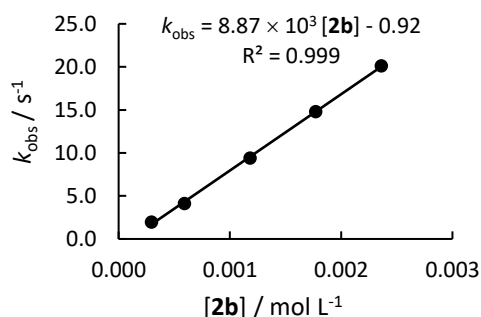
[3k] / mol L ⁻¹	[2b] / mol L ⁻¹	[2b] / [3k]	<i>k</i> _{obs} / s ⁻¹
1.03 × 10 ⁻⁵	2.95 × 10 ⁻⁴	29	4.19
1.03 × 10 ⁻⁵	5.91 × 10 ⁻⁴	57	9.43
1.01 × 10 ⁻⁵	1.18 × 10 ⁻³	116	1.97 × 10 ¹
1.01 × 10 ⁻⁵	1.77 × 10 ⁻³	175	2.97 × 10 ¹
9.85 × 10 ⁻⁶	2.36 × 10 ⁻³	240	4.04 × 10 ¹

$$k_2 = 1.74 \times 10^4 \text{ L mol}^{-1} \text{ s}^{-1}$$

**Table 5.38.** Kinetics of the reaction of **2b** with **3l** in CH₃CN (stopped-flow, 20 °C, at 620 nm)

[3l] / mol L ⁻¹	[2b] / mol L ⁻¹	[2b] / [3l]	<i>k</i> _{obs} / s ⁻¹
9.80 × 10 ⁻⁶	2.95 × 10 ⁻⁴	30	1.95
9.90 × 10 ⁻⁶	5.91 × 10 ⁻⁴	60	4.13
9.80 × 10 ⁻⁶	1.18 × 10 ⁻³	121	9.40
9.70 × 10 ⁻⁶	1.77 × 10 ⁻³	183	1.48 × 10 ¹
9.60 × 10 ⁻⁶	2.36 × 10 ⁻³	246	2.01 × 10 ¹

$$k_2 = 8.87 \times 10^3 \text{ L mol}^{-1} \text{ s}^{-1}$$

**Table 5.39.** Kinetics of the reaction of **2b** with **3m** in CH₃CN (stopped-flow, 20 °C, at 616 nm)

[3m] / mol L ⁻¹	[2b] / mol L ⁻¹	[2b] / [3m]	<i>k</i> _{obs} / s ⁻¹
9.31 × 10 ⁻⁶	2.95 × 10 ⁻⁴	32	6.86 × 10 ⁻¹
9.31 × 10 ⁻⁶	5.91 × 10 ⁻⁴	63	1.45
9.31 × 10 ⁻⁶	1.18 × 10 ⁻³	127	3.17
9.31 × 10 ⁻⁶	1.77 × 10 ⁻³	190	5.07
9.31 × 10 ⁻⁶	2.36 × 10 ⁻³	253	6.89

$$k_2 = 3.03 \times 10^3 \text{ L mol}^{-1} \text{ s}^{-1}$$

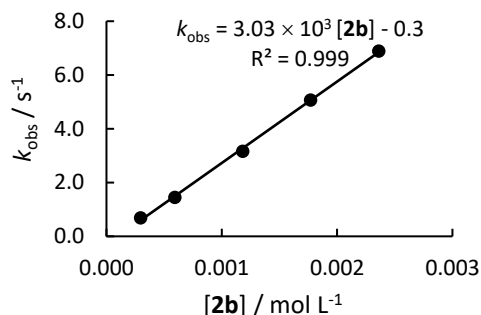
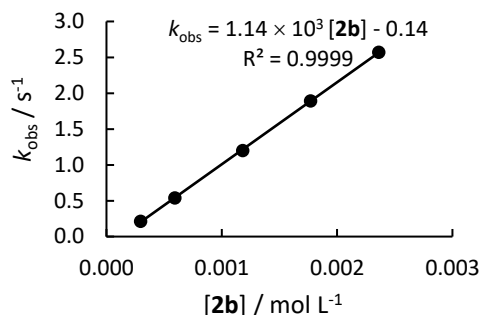


Table 5.40. Kinetics of the reaction of **2b** with **3n** in CH₃CN (stopped-flow, 20 °C, at 635 nm)

[3n] / mol L ⁻¹	[2b] / mol L ⁻¹	[2b] / [3n]	<i>k</i> _{obs} / s ⁻¹
7.77 × 10 ⁻⁶	2.95 × 10 ⁻⁴	38	2.11 × 10 ⁻¹
7.77 × 10 ⁻⁶	5.91 × 10 ⁻⁴	76	5.40 × 10 ⁻¹
7.77 × 10 ⁻⁶	1.18 × 10 ⁻³	152	1.20
7.77 × 10 ⁻⁶	1.77 × 10 ⁻³	228	1.89
7.77 × 10 ⁻⁶	2.36 × 10 ⁻³	304	2.57

$$k_2 = 1.14 \times 10^3 \text{ L mol}^{-1} \text{ s}^{-1}$$

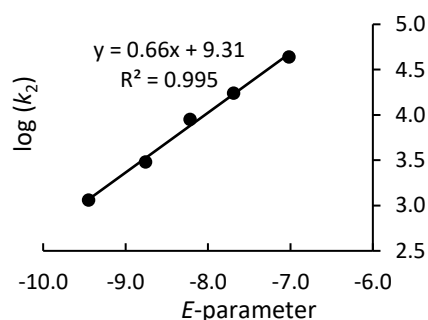


Determination of the Reactivity Parameters *N* and *s_N* for the enamine **2b** in CH₃CN

Table 5.41. Rate constants for the reaction of **2b** with different electrophiles (20 °C)

Electrophile	<i>E</i>	<i>k</i> ₂ / L mol ⁻¹ s ⁻¹	log <i>k</i> ₂
3j	-7.02	4.34 × 10 ⁴	4.64
3k	-7.69	1.74 × 10 ⁴	4.24
3l	-8.22	8.87 × 10 ³	3.95
3m	-8.76	3.03 × 10 ³	3.48
3n	-9.45	1.14 × 10 ³	3.06

$$N = 14.11, s_N = 0.66$$



5.5.4.7 Kinetic investigation for silyl enol ethers **15a-c**

Table 5.42. Kinetics of the reaction of **15a** with **3c** in CH₂Cl₂ (stopped-flow, 20 °C, at 413 nm)

[3c] / mol L ⁻¹	[15a] / mol L ⁻¹	[15a] / [3c]	<i>k</i> _{obs} / s ⁻¹
4.38 × 10 ⁻⁵	9.20 × 10 ⁻⁴	21	6.30 × 10 ⁻²
4.38 × 10 ⁻⁵	2.76 × 10 ⁻³	63	1.20 × 10 ⁻¹
4.38 × 10 ⁻⁵	6.44 × 10 ⁻³	147	2.32 × 10 ⁻¹
4.38 × 10 ⁻⁵	9.20 × 10 ⁻³	210	2.75 × 10 ⁻¹

$$k_2 = 2.62 \times 10^1 \text{ L mol}^{-1} \text{ s}^{-1}$$

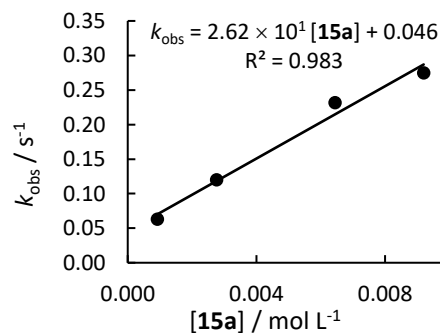
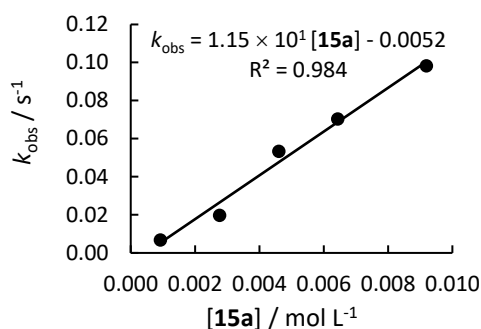


Table 5.43. Kinetics of the reaction of **15a** with **3d** in CH₂Cl₂ (stopped-flow, 20 °C, at 431 nm)

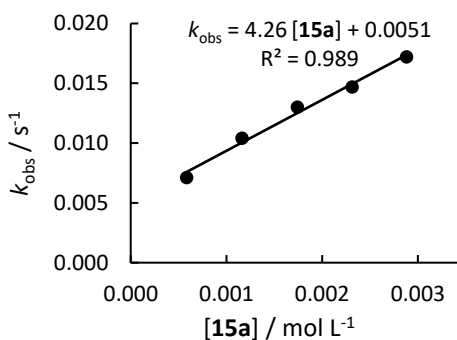
[3d] / mol L ⁻¹	[15a] / mol L ⁻¹	[15a] / [3d]	<i>k</i> _{obs} / s ⁻¹
3.36 × 10 ⁻⁵	9.19 × 10 ⁻⁴	27	6.78 × 10 ⁻³
3.36 × 10 ⁻⁵	2.76 × 10 ⁻³	82	1.98 × 10 ⁻³
3.36 × 10 ⁻⁵	4.60 × 10 ⁻³	137	5.33 × 10 ⁻²
3.36 × 10 ⁻⁵	6.43 × 10 ⁻³	191	7.04 × 10 ⁻²
3.36 × 10 ⁻⁵	9.19 × 10 ⁻³	273	9.82 × 10 ⁻²

$$k_2 = 1.15 \times 10^1 \text{ L mol}^{-1} \text{ s}^{-1}$$

**Table 5.44.** Kinetics of the reaction of **15a** with **3f** in CH₂Cl₂ (diode array spectrophotometer, 20 °C, at 601 nm)

[3f] / mol L ⁻¹	[15a] / mol L ⁻¹	[15a] / [3f]	<i>k</i> _{obs} / s ⁻¹
2.67 × 10 ⁻⁵	5.83 × 10 ⁻⁴	22	7.12 × 10 ⁻³
2.67 × 10 ⁻⁵	1.16 × 10 ⁻³	44	1.04 × 10 ⁻²
2.67 × 10 ⁻⁵	1.74 × 10 ⁻³	65	1.30 × 10 ⁻²
2.67 × 10 ⁻⁵	2.31 × 10 ⁻³	87	1.47 × 10 ⁻²
2.67 × 10 ⁻⁵	2.88 × 10 ⁻³	109	1.72 × 10 ⁻²

$$k_2 = 4.26 \text{ L mol}^{-1} \text{ s}^{-1}$$

**Table 5.45.** Kinetics of the reaction of **15a** with **3f** in CH₃CN (stopped-flow, 20 °C, at 601 nm)

[3f] / mol L ⁻¹	[15a] / mol L ⁻¹	[15a] / [3f]	<i>k</i> _{obs} / s ⁻¹
5.88 × 10 ⁻⁵	9.89 × 10 ⁻⁴	17	2.43 × 10 ⁻¹
5.88 × 10 ⁻⁵	1.98 × 10 ⁻³	34	3.00 × 10 ⁻¹
5.88 × 10 ⁻⁵	3.96 × 10 ⁻³	67	4.62 × 10 ⁻¹
5.88 × 10 ⁻⁵	4.94 × 10 ⁻³	84	5.16 × 10 ⁻¹

$$k_2 = 7.17 \times 10^1 \text{ L mol}^{-1} \text{ s}^{-1}$$

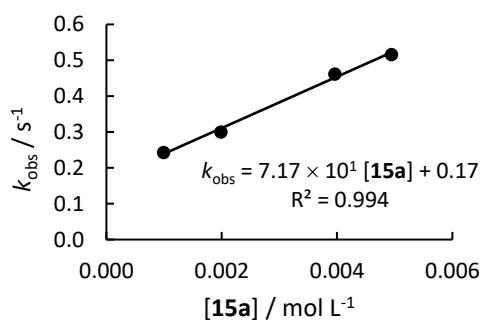
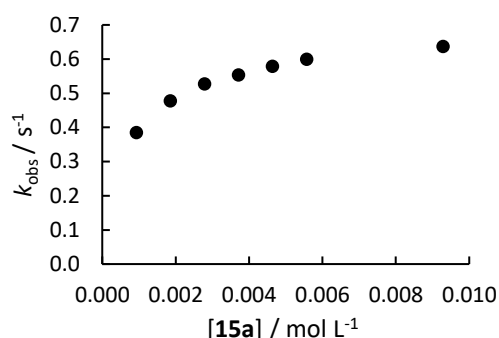
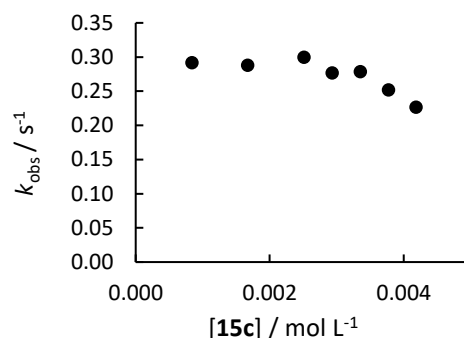


Table 5.46. Kinetics of the reaction of **15a** with **3g** in CH₂Cl₂ (stopped-flow, 20 °C, at 586 nm)

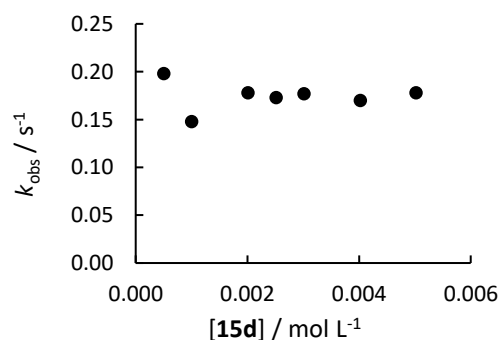
[3g] / mol L ⁻¹	[15a] / mol L ⁻¹	[15a] / [3g]	<i>k</i> _{obs} / s ⁻¹
4.84 × 10 ⁻⁵	9.29 × 10 ⁻⁴	19	3.84 × 10 ⁻¹
4.84 × 10 ⁻⁵	1.86 × 10 ⁻³	38	4.77 × 10 ⁻¹
4.84 × 10 ⁻⁵	2.79 × 10 ⁻³	58	5.27 × 10 ⁻¹
4.84 × 10 ⁻⁵	3.71 × 10 ⁻³	77	5.53 × 10 ⁻¹
4.84 × 10 ⁻⁵	4.64 × 10 ⁻³	96	5.78 × 10 ⁻¹
4.84 × 10 ⁻⁵	5.57 × 10 ⁻³	115	5.99 × 10 ⁻¹
4.84 × 10 ⁻⁵	9.29 × 10 ⁻³	192	6.36 × 10 ⁻¹

**Table 5.48.** Kinetics of the reaction of **15c** with **3d** in CH₂Cl₂ (stopped-flow, 20 °C, at 431 nm)

[3d] / mol L ⁻¹	[15c] / mol L ⁻¹	[15c] / [3d]	<i>k</i> _{obs} / s ⁻¹
6.38 × 10 ⁻⁵	8.37 × 10 ⁻⁴	13	2.92 × 10 ⁻¹
6.38 × 10 ⁻⁵	1.67 × 10 ⁻³	26	2.88 × 10 ⁻¹
6.38 × 10 ⁻⁵	2.51 × 10 ⁻³	39	3.00 × 10 ⁻¹
6.38 × 10 ⁻⁵	2.93 × 10 ⁻³	46	2.77 × 10 ⁻¹
6.38 × 10 ⁻⁵	3.35 × 10 ⁻³	52	2.79 × 10 ⁻¹
6.38 × 10 ⁻⁵	3.77 × 10 ⁻³	59	2.52 × 10 ⁻¹
6.38 × 10 ⁻⁵	4.18 × 10 ⁻³	66	2.27 × 10 ⁻¹

**Table 5.47.** Kinetics of the reaction of **15d** with **3d** in CH₂Cl₂ (stopped-flow, 20 °C, at 431 nm)

[3d] / mol L ⁻¹	[15d] / mol L ⁻¹	[15d] / [3d]	<i>k</i> _{obs} / s ⁻¹
3.18 × 10 ⁻⁵	5.02 × 10 ⁻⁴	16	1.98 × 10 ⁻¹
3.18 × 10 ⁻⁵	1.00 × 10 ⁻³	32	1.48 × 10 ⁻¹
3.18 × 10 ⁻⁵	2.01 × 10 ⁻³	63	1.78 × 10 ⁻¹
3.18 × 10 ⁻⁵	2.51 × 10 ⁻³	79	1.73 × 10 ⁻¹
3.18 × 10 ⁻⁵	3.01 × 10 ⁻³	95	1.77 × 10 ⁻¹
3.18 × 10 ⁻⁵	4.02 × 10 ⁻³	126	1.70 × 10 ⁻¹
3.18 × 10 ⁻⁵	5.02 × 10 ⁻³	158	1.78 × 10 ⁻¹



5.6 Appendix

Selected examples of kinetic measurements for enol ethers 15

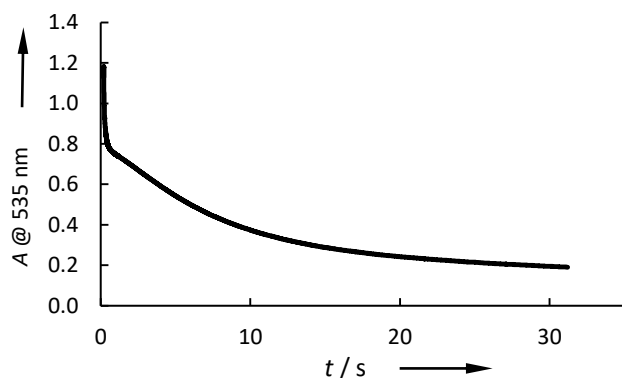


Figure 5.10. Plot of absorbance A (at 535 nm) versus time of the reaction of **15a** ($7.53 \times 10^{-4} \text{ mol L}^{-1}$) with **3b-GaCl₄** ($2.26 \times 10^{-5} \text{ mol L}^{-1}$), generated from (fur)₂CHCl ($2.26 \times 10^{-5} \text{ mol L}^{-1}$) and GaCl₃ ($3.11 \times 10^{-4} \text{ mol L}^{-1}$), in CH₂Cl₂ at 20 °C (stopped-flow). (fur) = 2,3-Dihydrobenzofuran-5-yl.

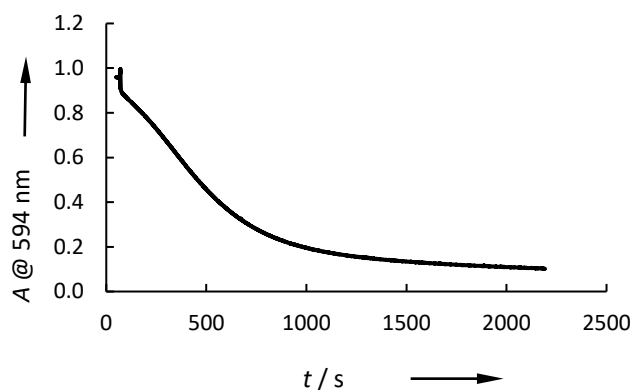


Figure 5.11. Plot of absorbance A (at 594 nm) versus time of the reaction of **15a** ($1.16 \times 10^{-3} \text{ mol L}^{-1}$) with **3e** ($3.36 \times 10^{-5} \text{ mol L}^{-1}$) in CH₂Cl₂ at 20 °C (diode array spectrophotometer).

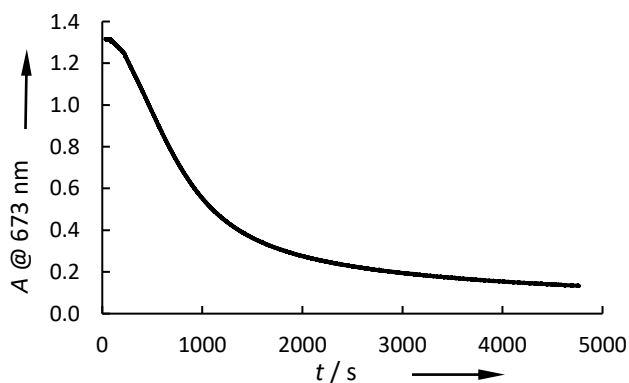


Figure 5.12. Plot of absorbance A (at 673 nm) versus time of the reaction of **15a** ($1.16 \times 10^{-3} \text{ mol L}^{-1}$) with **3h** ($2.67 \times 10^{-5} \text{ mol L}^{-1}$) in CH₂Cl₂ at 20 °C (diode array spectrophotometer).

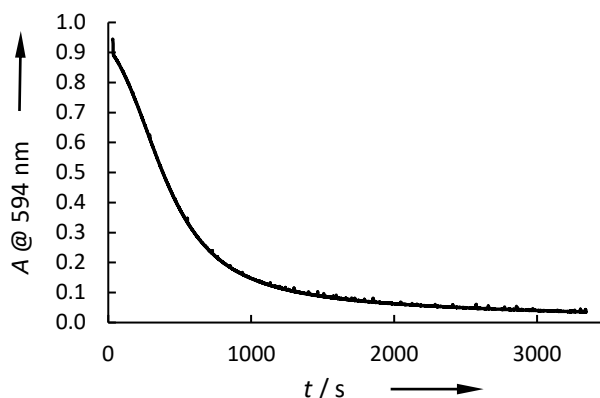


Figure 5.13. Plot of absorbance A (at 594 nm) versus time of the reaction of **15b** ($3.13 \times 10^{-4} \text{ mol L}^{-1}$) with **3i** ($9.93 \times 10^{-6} \text{ mol L}^{-1}$) in CH_2Cl_2 at 20°C (diode array spectrophotometer).

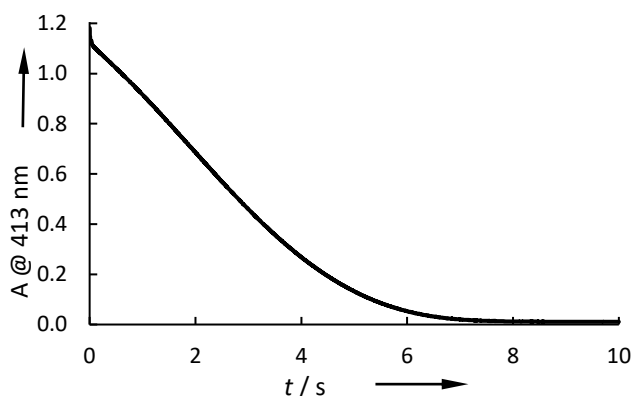


Figure 5.14. Plot of absorbance A (at 413 nm) versus time of the reaction of **15b** ($3.33 \times 10^{-3} \text{ mol L}^{-1}$) with **3c** ($7.68 \times 10^{-6} \text{ mol L}^{-1}$) in CH_2Cl_2 at 20°C (diode array spectrophotometer).

5.7 References

- [1] a) P. W. Hickmott, *Tetrahedron* **1982**, 38, 1975-2050; b) G. G. Vladimir, *Russ. Chem. Rev.* **1984**, 53, 383; c) P. W. Hickmott in *The chemistry of enamines* (Ed. Z. Rappoport), Wiley, Chichester, **1994**, pp. 727-871.
- [2] a) T. Mukaiyama, M. Murakami, *Synthesis* **1987**, 1043-1054; b) R. Mahrwald, *Chem. Rev.* **1999**, 99, 1095-1120.
- [3] J. Baudoux, D. Cahard in *Electrophilic Fluorination with N-F Reagents*, (Ed. S. E. Denmark), Wiley, Hoboken, **2007**, pp. 347-672.
- [4] S. Rossi, A. Puglisi, L. Raimondi, M. Benaglia, *ChemCatChem* 10.1002/cctc.201800170.
- [5] a) A. Prieto, O. Baudoin, D. Bouyssi, N. Monteiro, *Chem. Comm.* **2016**, 52, 869-881; b) T. Umemoto, S. Ishihara, *J. Am. Chem. Soc.* **1993**, 115, 2156-2164.
- [6] a) M. Teruaki, N. Koichi, B. Kazuo, *Chem. Lett.* **1973**, 2, 1011-1014; b) T. Mukaiyama, K. Banno, K. Narasaka, *J. Am. Chem. Soc.* **1974**, 96, 7503-7509.

- [7] S. B. J. Kan, K. K.-H. Ng, I. Paterson, *Angew. Chem. Int. Ed.* **2013**, *52*, 9097-9108.
- [8] a) B. List, R. A. Lerner, C. F. Barbas, *J. Am. Chem. Soc.* **2000**, *122*, 2395-2396; b) N. Zotova, A. Franzke, A. Armstrong, D. G. Blackmond, *J. Am. Chem. Soc.* **2007**, *129*, 15100-15101; c) S. Bahmanyar, K. N. Houk, *J. Am. Chem. Soc.* **2001**, *123*, 12911-12912.
- [9] a) I. Ismail, Z. Weibiao, E. Magnus, X. Yongmei, C. Armando, *Chem. Eur. J.* **2005**, *11*, 7024-7029; b) A. Cordova, W. Zou, I. Ibrahim, E. Reyes, M. Engqvist, W.-W. Liao, *Chem. Commun.* **2005**, 3586-3588.
- [10] S. B. Tsogoeva, S. Wei, *Chem. Comm.* **2006**, 1451-1453.
- [11] H. Huang, E. N. Jacobsen, *J. Am. Chem. Soc.* **2006**, *128*, 7170-7171.
- [12] a) H. Mayr, T. Bug, M. F. Gotta, N. Hering, B. Irrgang, B. Janker, B. Kempf, R. Loos, A. R. Ofial, G. Remennikov, H. Schimmel, *J. Am. Chem. Soc.* **2001**, *123*, 9500-9512; b) R. Lucius, R. Loos, H. Mayr, *Angew. Chem. Int. Ed.* **2002**, *41*, 91-95; c) H. Mayr, B. Kempf, A. R. Ofial, *Acc. Chem. Res.* **2003**, *36*, 66-77; d) H. Mayr, A. R. Ofial, *Pure Appl. Chem.* **2005**, *77*, 1807-1821; e) D. Richter, N. Hampel, T. Singer, A. R. Ofial, H. Mayr, *Eur. J. Org. Chem.* **2009**, 3203-3211.
- [13] a) H. A. Laub, D. Gladow, H. U. Reissig, H. Mayr, *Org. Lett.* **2012**, *14*, 3990-3993; b) H. A. Laub, H. Yamamoto, H. Mayr, *Org. Lett.* **2010**, *12*, 5206-5209; c) B. Kempf, N. Hampel, A. R. Ofial, H. Mayr, *Chem. Eur. J.* **2003**, *9*, 2209-2218; d) T. Kanzian, S. Lakhdar, H. Mayr, *Angew. Chem. Int. Edit.* **2010**, *49*, 9526-9529; e) D. S. Timofeeva, R. Mayer, P. Mayer, A. R. Ofial, H. Mayr, *Chem. Eur. J.* **2018**, *24*, 5901-5910; f) J. Burfeindt, M. Patz, M. Muller, H. Mayr, *J. Am. Chem. Soc.* **1998**, *120*, 3629-3634.
- [14] H. Mayr, M. Patz, *Angew. Chem. Int. Ed. Engl.* **1994**, *33*, 938-957.
- [15] a) T. Lemek, H. Mayr, *J. Org. Chem.* **2003**, *68*, 6880-6886; b) E. Follet, G. Berionni, P. Mayer, H. Mayr, *J. Org. Chem.* **2015**, *80*, 8643-8656.
- [16] a) K. C. Brannock, A. Bell, R. D. Burpitt, C. A. Kelly, *J. Org. Chem.* **1964**, *29*, 801-812; b) M. E. Kuehne, L. Foley, *J. Org. Chem.* **1965**, *30*, 4280-4284; c) S. Penades, H. Kisch, K. Tortschanoff, P. Margaretha, O. E. Polansky, *Monatsh. Chem.* **1973**, *104*, 447-456.
- [17] M. M. Mojtahedi, M. S. Abaee, H. Abbassi, *Can. J. Chem.* **2006**, *84*, 429-432.
- [18] F. C. Bautista: *Structural and Ion-Pairing Effects on the Nucleophilic Reactivity of Carbanions and Organometallics*, Dissertation, LMU München, **2014**.
- [19] a) S. Reim, M. Lau, M. Adeel, I. Hussain, M. A. Yawer, A. Riahi, Z. Ahmed, C. Fischer, H. Reinke, P. Langer, *Synthesis* **2009**, 445-463; b) I. Hussain, V. T. H. Nguyen, M. A. Yawer, T. T. Dang, C. Fischer, H. Reinke, P. Langer, *J. Org. Chem.* **2007**, *72*, 6255-6258.
- [20] J. Jullien, J. M. Penchine, F. Perez, J. J. Piade, *Tetrahedron* **1982**, *38*, 1413-1416.
- [21] I. Zenz, H. Mayr, *J. Org. Chem.* **2011**, *76*, 9370-9378.
- [22] H. Kuroda, E. Hanaki, H. Izawa, M. Kano, H. Itahashi, *Tetrahedron* **2004**, *60*, 1913-1920.
- [23] A. Padwa, T. Brookhart, *J. Org. Chem.* **1979**, *44*, 4021-4030.
- [24] O. V. Fedorov, M. D. Kosobokov, V. V. Levin, M. I. Struchkova, A. D. Dilman, *J. Org. Chem.* **2015**, *80*, 5870-5876.

- [25] S. I. Scherbinina, O. V. Fedorov, V. V. Levin, V. A. Kokorekin, M. I. Struchkova, A. D. Dilman, *J. Org. Chem.* **2017**, *82*, 12967-12974.
- [26] M. L. Mussons, C. Raposo, M. F. de la Torre, J. R. Moran, M. C. Caballero, *Tetrahedron* **1999**, *55*, 4077-4094.
- [27] X. Zhao, D. Liu, F. Xie, W. Zhang, *Tetrahedron* **2009**, *65*, 512-517.
- [28] D. T. W. Chu, S. N. Huckin, *Can. J. Chem.* **1980**, *58*, 138-142.
- [29] A. Ungureanu, A. Levens, L. Candish, D. W. Lupton, *Angew. Chem. Int. Ed.* **2015**, *54*, 11780-11784.